Journal of Control Science and Engineering

Distributed Control of Networked Agent Systems: Theory and Applications

Lead Guest Editor: Guanghui Wen
Guest Editors: Haibo Du, Chaojie Li, Qiang Song, and Wenwu Yu

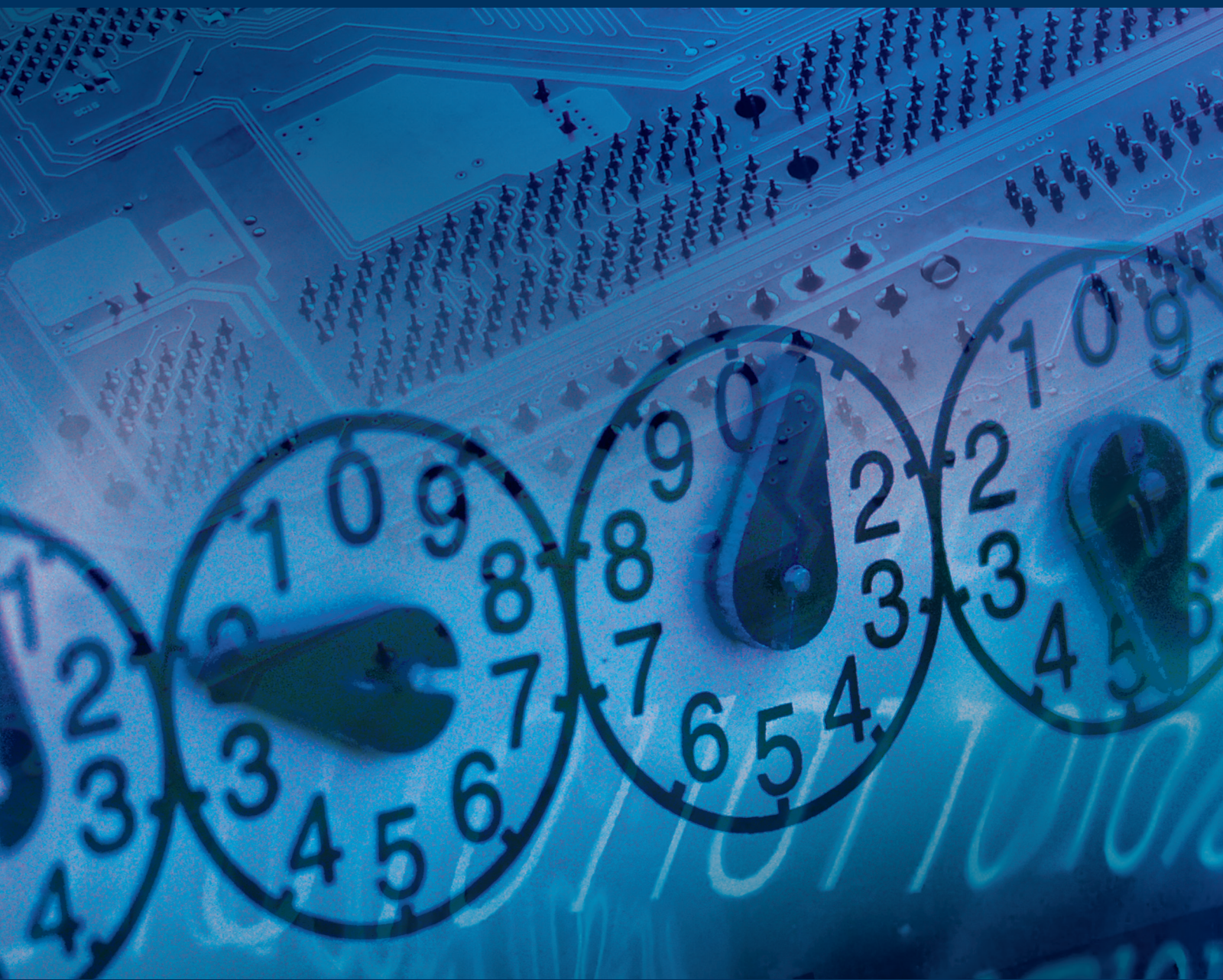

Distributed Control of Networked Agent Systems: Theory and Applications

Journal of Control Science and Engineering

Distributed Control of Networked Agent Systems: Theory and Applications

Lead Guest Editor: Guanghui Wen
Guest Editors: Chaojie Li, Qiang Song, and Wenwu Yu

Editorial Board

Contents

Hindawi
Journal of Control Science and Engineering
Volume 2017, Article ID 3485432, 2 pages
https://doi.org/10.1155/2017/3485432

Editorial

Distributed Control of Networked Agent Systems: Theory and Applications

Guanghui Wen,[1] Haibo Du,[2] Chaojie Li,[3] Qiang Song,[4] and Wenwu Yu[1]

[1]*Research Center for Complex Systems and Network Sciences, School of Mathematics, Southeast University, Nanjing 210096, China*
[2]*School of Electrical Engineering and Automation, Hefei University of Technology, Hefei 230009, China*
[3]*School of Engineering, RMIT University, Melbourne, VIC 3001, Australia*
[4]*College of Electronic Engineering, Henan University of Technology, Zhengzhou 450001, China*

Correspondence should be addressed to Guanghui Wen; wenguanghui@gmail.com

Received 31 May 2017; Accepted 1 June 2017; Published 12 July 2017

A great number of practical complex systems can be modeled as networked agent systems. Typical examples include the distributed satellite systems, a group of robots, wireless sensor networks, and power grids. One critical topic within this context is to understand how globally cooperative behaviors of such systems can be emerged as a result of distributed local interactions which has recently received much attention from various scientific fields.

The present special issue mainly focuses on the new distributed control approaches in networked agent systems as well as their potential engineering applications. It tries to not only explore the underlying mechanisms corresponding to various collective behaviors but also manipulate and even control these fascinating collective behaviors. Call for papers has been carefully prepared by the guest editors and posted on the journal's web page, which has received a lot of attention from researchers in various scientific fields. This special issue has received 30 submissions on networked agent systems. All manuscripts submitted to this special issue went through a thorough peer-refereeing process. Based on the reviewers' reports and the guest editors' comments, 10 original research articles are finally accepted. The contents of accepted papers are summarized below.

(a) Distributed Control and Optimization of Networked Agent Systems. The paper "On Couple-Group Consensus of Multiagent Networks with Communication and Input Time Delays" by L. Ji and X. Zhao investigates couple-group consensus/synchronization of multiagent systems. Some new sufficient criteria for reaching couple-group consensus have been presented. The work of "Distributed Optimization of Multiagent Systems in Directed Networks with Time-Varying Delay" by J. Yan and H. Yu designs a continuous-time distributed optimization algorithm to solve the distributed optimization problem of first-order multiagent systems. In "Synchronization of Coupled Harmonic Oscillators Using Quantized Sampled Position Data" by X. Wang and P. He, the synchronization problem of networked harmonic oscillators with quantized current sampled position data is studied. In "Plug and Play Robust Distributed Control with Ellipsoidal Parametric Uncertainty System" by W. Hong and Y. Wang, distributed control of a continuous linear time invariant system with ellipsoidal parametric uncertainty structured into subsystems is studied.

(b) Analysis and Synthesis of Complex Dynamical Systems. In "Iterative Learning Control with Forgetting Factor for Urban Road Network" by T. Lan et al., to improve the traffic condition, a new iterative learning control (ILC) algorithm with forgetting factor for urban road network is proposed by using the repeat characteristics of traffic flow. The paper "Parameters Design for Logarithmic Quantizer Based on Zoom Strategy" by J. Yan investigates the problem of designing suitable parameters for logarithmic quantizer such that the closed-loop linear time-invariant discrete system is asymptotically convergent. In "A Novel Measurement Matrix

Optimization Approach for Hyperspectral Unmixing" by S. Xu and X. He a novel approach for the optimization of measurement matrix in compressive sensing theory for hyperspectral unmixing is proposed. In "An Out Space Accelerating Algorithm for Generalized Affine Multiplicative Programs Problem" by L. Cai et al., an out space branch-and-bound algorithm is designed for solving generalized affine multiplicative programs problem. The paper "An Effective Algorithm for Globally Solving Sum of Linear Ratios Problems" by H. Jiao et al. proposes an effective algorithm for globally solving the sum of linear ratios problems. In "DCA-Based Real-Time Residual Useful Life Prediction for Critical Faulty Component" by F. Zhou et al., to predict the residual useful life effectively, wavelet filtering based method is developed for early detection of slowly varying fault of dynamical systems.

Acknowledgments

We would like to thank the authors for their contributions and acknowledge all the reviewers for their time and effort in assessing the manuscripts. Special thanks to the Editorial Office of this journal for their kind support.

Guanghui Wen
Haibo Du
Chaojie Li
Qiang Song
Wenwu Yu

Hindawi
Journal of Control Science and Engineering
Volume 2017, Article ID 3949428, 8 pages
https://doi.org/10.1155/2017/3949428

Research Article

Synchronization of Coupled Harmonic Oscillators Using Quantized Sampled Position Data

Xinjing Wang and Peipei He

The School of Resources and Environment, North China University of Water Resource and Electric Power, Zhengzhou 450045, China

Correspondence should be addressed to Xinjing Wang; wangxinjing888@163.com

Received 27 February 2017; Revised 25 April 2017; Accepted 29 May 2017; Published 3 July 2017

Academic Editor: Wenwu Yu

For coupled harmonic oscillators (CHO), the paper studies the synchronization problem by using the quantized current sampled position data. The logarithmic quantizer is adopted here to quantize the information transmitted; thus the quantization error of the sampled position data can be illustrated as the uncertainty according to the sector bound property. On the basis of that, the synchronization problem is converted into the asymptotical stability of the subsystems and even the solving problem of characteristic equation. Some sufficient conditions ensuring the synchronization of CHO are obtained relating to coupling strength, sampling period, and quantizer parameter. The usefulness of the theoretical result is shown by an example at the end.

1. Introduction

Recently, as a special multiagent system, CHO has gotten much attention. By assuming that the undirected network is not connectivity, literature [1] shows that the CHO is also able to achieve synchronization. When the CHO is affected by controller loss and communication time-delays, an algorithm is proposed in [2] to ensure the synchronization of the system and a brief procedure of the convergence analysis for such algorithm is given. By using some special analysis tools, literature [3] shows that the CHO can be synchronized under the conditions of mild connectivity for the directed graph. A frequency dependent topology condition is given in [4] to synchronize the CHO. With the measurement noise, literature [5] gives an effective algorithm and the convergence analysis of the CHO for the directed network topologies with or without leaders. A sufficient condition for the synchronized oscillatory motions of CHO is given by the influence of noise for the strongly connected directed graph.

The control algorithms proposed in the above literature use both velocity information and position information. In some cases, each oscillator exchanges just the velocity information or the position information with its neighbors. The relating papers which design control algorithms just use velocity information or position information include [6–9]. Assuming that the network is connected, the sufficient conditions are given for the synchronized oscillatory motions by just using velocity information in brief [6]. The results of [6] are generalized to the sampled-data CHO affected by input signals loss in [7]. Literature [8] proposes a distributed control method just using the outdated position states. For both positive and negative coupling strengths, it derives some necessary and sufficient conditions (NSCs) for the synchronization of CHO. In [9], by adopting current and outdated position data, respectively, two distributed protocols are adopted for the synchronization of CHO.

On the other hand, as an important issue, data quantization has received extensive attention in multiagent systems. Theoretical results in the past two years include [10–16]. The consensus of multiagent systems is studied according to the robust learning control approach in [10]. For the undirected connected graphs, literature [11] obtains some strong results for the problem of expected time to convergence for quantized consensus. Under the influence of quantized input and disturbances, the distributed quantized H_∞ consensus is investigated in [12]. For the high-order multiagent systems, the quantized consensus is studied in [13], in which it assumed that only the first state can be measured. By adopting both uniform and logarithmic quantizers, some quantized consensus results are achieved

for heterogeneous systems in [14]. By using probabilistic versus deterministic quantizers, the quantized consensus problem for multiagent systems is studied in [15]. Moreover, event-triggered consensus [16], averaging consensus [17], consensus tracking [18], metropolis consensus [19], containment control [20], and other consensus problems [21–23] affected by data quantization are discussed in recent papers.

Summarized above, the synchronization of CHO and quantized consensus for the general multiagent systems have received enough attention, respectively. However, there are few results relating to the synchronization of CHO affected by data quantization, which is the problem studied in our paper. In fact, this paper's main contribution is to extend the results of literature [9] to the synchronization problem for CHO by using the quantized position data. By adopting the logarithmic quantizer, the quantization error of the sampled position data can be illustrated as the uncertainty according to the sector bound property. With this setup, some sufficient conditions relating to coupling strength, sampling period, and quantizer parameter are obtained for synchronized CHO.

The organizational structure of the paper is as follows. Section 2 demonstrates the problem discussed and the CHO network; distributed protocol and logarithmic quantizer are illustrated there in detail. Some sufficient conditions for synchronization of CHO and the detailed proving process are shown in Section 3. The usefulness of the theoretical results is illustrated by a simulation example in Section 4. Section 5 gives some conclusions.

Notation. The n-dimensional Euclidean space is denoted by $\mathbb{R}^n$. $\mathbb{N}$ ($\mathbb{R}^+$) indicates the positive integers (real numbers) set. We denote by $|c|$ the module of complex number c. A^{-1} and A^T are the inverse and the transpose of matrix A, respectively. $\mathbf{0}_n$ and 1_n denote the vectors with dimension $n \times 1$ whose elements are all zeros or ones, respectively. For a multiagent system, especially for CHO, information exchange between agents can be modeled by a network or graph [24]. Let graph $\mathcal{G}$ be with node set $\Omega = \{1, \ldots, M\}$ and edge set $\Upsilon \subseteq \Omega \times \Omega$. If there exists at least one node having a directed path to every other node, the digraph $\mathcal{G}$ is called containing a directed spanning tree (DST). The adjacency matrix $\mathcal{A} = (a_{ij})_{M\times M}$ satisfies $a_{ij} > 0$ if $(j,i) \in \Upsilon$ and $a_{ij} = 0$ if $(j,i) \notin \Upsilon$. $\mathcal{M}_i = \{j \mid a_{ij} > 0, j \notin i\}$, $\forall i \in \{1, \ldots, M\}$ is a set including all the neighbor nodes of node i. We use $L = (l_{ij})_{M\times M}$ to denote the Laplacian matrix, whose elements satisfy $l_{ij} = -a_{ij}$ $(i \neq j)$ and $l_{ii} = \sum_{k=1,k\neq i}^{M} a_{ik}$ [25]. $0 = |\eta_1| \leq |\eta_2| \leq \cdots \leq |\eta_M|$ represent the eigenvalues of L when the digraph $\mathcal{G}$ contains a DST. $\mathrm{diag}(a_1, \ldots, a_M)$ indicates the diagonal matrix with diagonal elements $a_1, \ldots, a_M$.

2. Problem Formulation

For continuous-time CHO, we illustrate the synchronization problem and protocol by using the quantized sampled position data in this section.

For a positive constant h, the synchronization problem of the following CHO network composed by M nodes is discussed:

$$\begin{aligned} \dot{x}_i(t) &= v_i(t), \\ \dot{v}_i(t) &= -hx_i(t) + u_i(t), \quad i \in \{1, \ldots, M\} \end{aligned} \tag{1}$$

with position states $x_i(t)$, velocity states $v_i(t)$, and control input $u_i(t)$ for node i.

Assuming that the information between nodes is transmitted over the network, then it must be quantized before transmission. A protocol using the quantized value of the current relative sampled position data is adopted in this paper:

$$\begin{aligned} u_i(t) = \gamma \sum_{j\in\mathcal{M}_i} a_{ij} \left(q\left(x_i(t_k)\right) - q\left(x_j(t_k)\right)\right), \\ t \in [t_k, t_{k+1}),\ i \in \{1, \ldots, M\},\ k \in \mathbb{N}, \end{aligned} \tag{2}$$

in which coupling strength $\gamma > 0$ is to be designed and $x_i(t_k)$, $i \in \{1, \ldots, M\}$, denote the sampled position at time instants $t_k = kT, k \in \mathbb{N}$, with $t_0 = 0$. The quantizer used here is a general logarithmic one defined as [26, 27]

$$q(\chi) = \begin{cases} \kappa_w & \text{if } \chi \in \left[\frac{1}{1+\delta}\kappa_w, \frac{1}{1-\delta}\kappa_w\right),\ \chi > 0 \\ 0 & \text{if } \chi = 0 \\ -q(-\chi) & \text{if } \chi < 0 \end{cases} \tag{3}$$

for any $\chi \in \mathbb{R}$, with $w \in \mathbb{N} \cup \{0\}$, $\delta \in (0,1)$, $\kappa_{w+1} = \rho\kappa_w$, $v_0 > 0$, and $\rho = (1-\delta)/(1+\delta) \in (0,1)$.

The aim of our paper is designing suitable γ and T such that the CHO (1) under the control input (2) achieves synchronization; that is,

$$\begin{aligned} \lim_{t\to\infty} \left\| x_i(t) - x_j(t) \right\| = 0, \\ \lim_{t\to\infty} \left\| v_i(t) - v_j(t) \right\| = 0 \end{aligned} \tag{4}$$

for any $i, j \in \{1, \ldots, M\}$ $(i \neq j)$.

3. The Sufficient Conditions for Synchronization

For CHO (1) with protocol (2), the synchronization problem is studied in this section. The sufficient conditions for synchronization are pursued on the basis of the following two lemmas.

Lemma 1 (see [28]). *The fact that the graph $\mathcal{G}$ contains a DST is equal to the fact that the matrix L has a simple zero eigenvalue and other eigenvalues having positive real parts. Furthermore, 1_M is the right eigenvector relating to zero eigenvalue of L. Moreover, we can always get a suitable ϕ, which is left eigenvector relating to zero eigenvalue of L, satisfying $\phi^T L = 0$ and $\phi^T 1_M = 1$.*

Lemma 2 (see [29]). *Let $p(s) = s^2 + (\varpi_1 + \mathbf{i}\sigma_1)s + \varpi_0 + \mathbf{i}\sigma_0$ be a complex-coefficient polynomial with real constants $\varpi_0, \sigma_0, \varpi_1$, and σ_1, and then the asymptotical stability of $p(s)$ is equivalent to $\varpi_1 > 0$ and $\varpi_1\sigma_1\sigma_0 + \varpi_1^2\varpi_0 - \sigma_0^2 > 0$.*

By using the above lemmas, the following theorem is given to discuss the synchronization of CHO (1) under protocol (2), which is the main result of this paper.

Theorem 3. *If the graph $\mathcal{G}$ contains a DST and the initial states satisfy $\phi^T x(0) = \phi^T v(0) = 0$ with ϕ defined in Lemma 1, then network (1) under protocol (2) can achieve synchronization if γ and T are selected satisfying*

$$\gamma \notin \left[\frac{h}{\max_{i\in\{2,\ldots,M\}} \mathrm{Re}\left(\widetilde{\xi}_i\right)}, \frac{h}{\min_{i\in\{2,\ldots,M\}} \mathrm{Re}\left(\overline{\xi}_i\right)} \right], \tag{5a}$$

$$T \notin \left\{ \frac{l\pi}{\sqrt{h}} \mid l \in \mathbb{N} \right\}, \tag{5b}$$

$$\gamma < \frac{h\,\mathrm{Re}\left(\widetilde{\xi}_{i_{\max}}\right)}{\left|\widetilde{\xi}_{i_{\max}}\right|^2}, \tag{5c}$$

$$T \in \Gamma_T\left(\max_{i\in\{2,\ldots,M\}, l\in\mathbb{N}} \arctan\sqrt{e_{il}} \right), \tag{5d}$$

where $\widetilde{\xi}_i$ and $\overline{\xi}_i, i \in \{2,\ldots,M\}$ are, respectively, the nonzero eigenvalues of $L(I_M + \overline{\Lambda})$ and $L(I_M - \overline{\Lambda})$ with $\overline{\Lambda} = \delta I_M$, $i_{\max} = \arg\max_{i\in\{2,\ldots,M\}} |\widetilde{\xi}_i|$, $\Gamma_T(\varphi) \triangleq \{T \mid \tan^2(\sqrt{h}T/2) > \tan^2\varphi\}$, for any $\varphi \in [0, \pi/2)$, and

$$e_{il} = \frac{\left|h - \gamma\xi_i^l\right|^2 b_{il}^2}{a_{il}b_{il}^2 + a_{il}^2 c_{il}} \tag{6}$$

for any $i \in \{2,\ldots,M\}, l \in \mathbb{N}$ with $a_{il} = h\gamma\mathrm{Re}(\xi_i^l) - \gamma^2|\xi_i^l|^2$, $b_{il} = h\gamma\mathrm{Im}(\xi_i^l)$, and $c_{il} = h^2 - h\gamma\mathrm{Re}(\xi_i^l)$, in which ξ_i^l denote possible values for $\xi_i(t_k), k \in \mathbb{N}$, defined by (10). Moreover, let $x(t) = (x_1(t),\ldots,x_M(t))^T$ and $v(t) = (v_1(t),\ldots,v_M(t))^T$, and we obtain

$$\begin{aligned} \lim_{t\to\infty} x_i(t) &= \cos\left(\sqrt{h}t\right)\phi^T x(0) \\ &\quad + \frac{1}{\sqrt{h}}\sin\left(\sqrt{h}t\right)\phi^T v(0) = 0, \\ \lim_{t\to\infty} v_i(t) &= -\sqrt{h}\sin\left(\sqrt{h}t\right)\phi^T x(0) \\ &\quad + \cos\left(\sqrt{h}t\right)\phi^T v(0) = 0 \end{aligned} \tag{7}$$

for all $i \in \{1,\ldots,M\}$.

Proof. By the property of logarithmic quantizer, we get $q(x_i(t_k)) = (1+\varepsilon_i(t_k))x_i(t_k)$ with $|\varepsilon_i(t_k)| \le \delta, \forall k \in \mathbb{N}\cup\{0\}, i \in \{1,\ldots,M\}$. For any $t \in \mathbb{R}^+ \cup \{0\}$, let $z_i(t) = (x_i(t), v_i(t))^T$, $i \in \{1,\ldots,M\}$ and $z(t) = (z_1^T(t),\ldots,z_M^T(t))^T$; then network (1) under protocol (2) can be rewritten as

$$\begin{aligned} \dot{z}(t) &= \left(I_M \otimes A\right) z(t) + \gamma\left(L\otimes B\right) \begin{bmatrix} q\left(x_1\left(t_k\right)\right) \\ 0 \\ q\left(x_2\left(t_k\right)\right) \\ 0 \\ \vdots \\ q\left(x_M\left(t_k\right)\right) \\ 0 \end{bmatrix} \\ &= \left(I_M \otimes A\right) z(t) + \gamma\left(L\otimes B\right) \\ &\quad \cdot \begin{bmatrix} 1 & & & & \\ & 0 & & & \\ & & \ddots & & \\ & & & 1 & \\ & & & & 0 \end{bmatrix} \begin{bmatrix} \left(1+\varepsilon_1\left(t_k\right)\right)x_1\left(t_k\right) \\ \left(1+\varepsilon_1\left(t_k\right)\right)v_1\left(t_k\right) \\ \vdots \\ \left(1+\varepsilon_M\left(t_k\right)\right)x_M\left(t_k\right) \\ \left(1+\varepsilon_M\left(t_k\right)\right)v_M\left(t_k\right) \end{bmatrix} \\ &= \left(I_M \otimes A\right) z(t) + \gamma\left(L\otimes B\right)\left(I_M\otimes D\right) \\ &\quad \cdot \left(\left(I_M + \Lambda\left(t_k\right)\right)\otimes I_2\right) z\left(t_k\right) = \left(I_M\otimes A\right) z(t) \\ &\quad + \gamma\left(L\left(I_M + \Lambda\left(t_k\right)\right)\otimes B\right) z\left(t_k\right), \\ &\qquad t \in \left[t_k, t_{k+1}\right),\ k \in \mathbb{N}\cup\{0\}, \end{aligned} \tag{8}$$

where $A = \left[\begin{smallmatrix} 0 & 1 \\ -h & 0 \end{smallmatrix}\right]$, $B = \left[\begin{smallmatrix} 0 & 0 \\ 1 & 0 \end{smallmatrix}\right]$, $D = \left[\begin{smallmatrix} 1 & 0 \\ 0 & 0 \end{smallmatrix}\right]$, and $\Lambda(t_k) = \mathrm{diag}\{\varepsilon_1(t_k),\ldots,\varepsilon_M(t_k)\}$.

For the matrix $L(I_M + \Lambda(t_k)), \forall k \in \mathbb{N}\cup\{0\}$, the following claim holds by Lemma 1.

Claim. If the graph $\mathcal{G}$ contains a DST, then the matrix $L(I_M + \Lambda(t_k)), \forall k \in \mathbb{N}\cup\{0\}$, has a simple zero eigenvalue and other eigenvalues having positive real parts. Furthermore, $[1/(1+\varepsilon_1(t_k)), 1/(1+\varepsilon_1(t_k)),\ldots,1/(1+\varepsilon_M(t_k))]^T$ and ϕ defined in Lemma 1 are the right eigenvector and left eigenvector, respectively, relating to zero eigenvalue of $L(I_M + \Lambda(t_k))$.

Based on the above claim, for any $k \in \mathbb{N}\cup\{0\}$, there must exist matrices $Q(t_k) = (p_1(t_k),\ldots,p_M(t_k)) \in \mathbb{R}^{M\times M}$ and $Q^{-1}(t_k) = (q_1(t_k),\ldots,q_M(t_k))^T \in \mathbb{R}^{M\times M}$ with $p_1(t_k) = [1/(1+\varepsilon_1(t_k)), 1/(1+\varepsilon_1(t_k)),\ldots,1/(1+\varepsilon_M(t_k))]^T$ and $q_1(t_k) = \phi$ such that

$$\begin{aligned} J\left(t_k\right) &= Q^{-1}\left(t_k\right) L\left(I_M + \Lambda\left(t_k\right)\right) Q\left(t_k\right) \\ &= \begin{pmatrix} 0 & 0_{M-1}^T \\ 0_{M-1} & \widehat{L}\left(t_k\right) \end{pmatrix} \end{aligned} \tag{9}$$

with Jordan canonical form $J(t_k)$ and block upper triangular matrix $\widehat{L}(t_k)$ represented as

$$\widehat{L}(t_k) = \begin{pmatrix} \xi_2(t_k) & \tau & 0 & \cdots & 0 \\ 0 & \xi_3(t_k) & \tau & \cdots & 0 \\ & & & \ddots & \\ 0 & 0 & 0 & \cdots & \xi_M(t_k) \end{pmatrix} \tag{10}$$

in which $\xi_i(t_k)$, $i \in \{2,\ldots,M\}$ satisfying $\mathrm{Re}(\xi_2(t_k)) \le \cdots \le \mathrm{Re}(\xi_M(t_k))$ are the nonzero eigenvalues of $L(I_M + \Lambda(t_k))$, and τ is equal to 1 or 0.

Let $m(t) = (m_1^T(t),\ldots,m_M^T(t))^T = (Q^{-1}(t_k)\otimes I_2)z(t)$, $\forall t \in [t_k, t_{k+1})$ and $m_i(t) \in \mathbb{R}^2$, and then (8) gives that

$$\begin{aligned} \dot{m}(t) &= \left(Q^{-1}(t_k)\otimes I_2\right)(I_M\otimes A)\left(Q(t_k)\otimes I_2\right)m(t) \\ &\quad + \gamma\left(Q^{-1}(t_k)\otimes I_2\right)\left(L(I_M+\Lambda(t_k))\otimes B\right) \\ &\quad \cdot\left(Q(t_k)\otimes I_2\right)m(t_k) = \left(I_M\otimes A\right)m(t) \\ &\quad + \gamma\left(J(t_k)\otimes B\right)m(t_k), \quad t\in[t_k,t_{k+1}),\ k\in\mathbb{N}\cup\{0\} \end{aligned} \tag{11}$$

indicating

$$\dot{m}_1(t) = Am_1(t), \tag{12a}$$

$$\begin{aligned} \dot{M}_2(t) &= \left(I_{M-1}\otimes A\right)M_2(t) \\ &\quad + \gamma\left(\widehat{L}(t_k)\otimes B\right)M_2(t_k), \end{aligned} \tag{12b}$$

for any $t \in [t_k, t_{k+1})$, $k \in \mathbb{N}\cup\{0\}$, with $M_2(t) = (m_2^T(t),\ldots, m_M^T(t))^T$.

Next, we will verify that the asymptotic stability of subsystem (12b) is equivalent to the synchronization of (8) if the initial states satisfy $\phi^T x(0) = \phi^T v(0) = 0$. On one hand, if $\lim_{t\to\infty} m_i(t) = \mathbf{0}_2, i \in \{2,\ldots,M\}$, combining with $z(t) = (Q(t_k)\otimes I_2)m(t), t \in [t_k, t_{k+1})$ and $p_1(t_k) = [1/(1+\varepsilon_1(t_k)), 1/(1+\varepsilon_1(t_k)),\ldots, 1/(1+\varepsilon_M(t_k))]^T$ gives $z_i(t) \to (1/(1+\varepsilon_i(t_k)))m_1(t), t \in [t_k, t_{k+1}), i \in \{1,\ldots,M\}$. Moreover, by defining

$$E(t) = \begin{bmatrix} \cos\left(\sqrt{h}(t)\right) & \frac{1}{\sqrt{h}}\sin\left(\sqrt{h}(t)\right) \\ -\sqrt{h}\sin\left(\sqrt{h}(t)\right) & \cos\left(\sqrt{h}(t)\right) \end{bmatrix}, \tag{13}$$

the equalities $\dot{m}_1(t) = Am_1(t)$ and $\phi^T x(0) = \phi^T v(0) = 0$ tell us that

$$\begin{aligned} m_1(t) &= e^{At}m(0) = E(t)\left(\phi^T\otimes I_2\right)z(0) \\ &= \begin{bmatrix} \cos\left(\sqrt{h}t\right)\phi^T x(0) + \frac{1}{\sqrt{h}}\sin\left(\sqrt{h}t\right)\phi^T v(0) \\ -\sqrt{h}\sin\left(\sqrt{h}t\right)\phi^T x(0) + \cos\left(\sqrt{h}t\right)\phi^T v(0) \end{bmatrix} \\ &= \mathbf{0}_2 \end{aligned} \tag{14}$$

for any $t \in \mathbb{R}^+\cup\{0\}$. Thus we get $\lim_{t\to\infty} z_i(t) = \mathbf{0}_2, i \in \{1,\ldots,M\}$ which means that the synchronization of (8) is guaranteed with synchronization state $\mathbf{0}_2$. On the other hand, if the synchronization of (8) is ensured, by letting the synchronization state as $z^*(t) = (x^*(t), v^*(t))^T \in \mathbb{R}^2$, we will show $(x^*(t), v^*(t))^T = \mathbf{0}_2$. In fact, it holds that $m_1(t) = (\phi^T\otimes I_2)z(t) = \sum_{i=1}^M \phi_i z_i(t)$ according to $m(t) = (Q^{-1}\otimes I_2)z(t)$. Based on $\phi^T 1_M = 1$, we get $z^*(t) = m_1(t)$. Combined with (14), it gives $x^*(t) = v^*(t) = 0$, and thus $\lim_{t\to\infty} z(t) = \mathbf{0}_{2M}$. Taking $m(t) = (Q^{-1}(t_k)\otimes I_2)z(t), \forall t \in [t_k, t_{k+1})$, into consideration, we get $\lim_{t\to\infty} m_i(t) = \mathbf{0}_2, i \in \{1,\ldots,M\}$, which ensures the asymptotic stability of subsystem (12b).

By the claim above and (10), we know that the asymptotic stability of (12b) is equal to that of the following subsystems:

$$\dot{m}_i(t) = Am_i(t) + \gamma\xi_i(t_k)Bm_i(t_k), \quad i\in\{2,\ldots,M\}, \tag{15}$$

the solution of which is as

$$\begin{aligned} m_i(t) &= e^{A(t-t_k)}m_i(t_k) + \gamma\xi_i(t_k)\int_{t_k}^{t} e^{A(t-s)}dsBm_i(t_k) \\ &= e^{A(t-t_k)}m_i(t_k) + \gamma\xi_i(t_k)\int_0^{t-t_k} e^{As}dsBm_i(t_k) \\ &= E_i(t-t_k)m_i(t_k) + F_i(\xi_i(t_k), t-t_k)m_i(t_k) \end{aligned} \tag{16}$$

for any $t \in [t_k, t_{k+1})$, $k \in \mathbb{N}\cup\{0\}$, $i \in \{1,\ldots,M\}$, where

$$\begin{aligned} &E_i(t-t_k) \\ &= \begin{pmatrix} \cos\left(\sqrt{h}(t-t_k)\right) & \frac{1}{\sqrt{h}}\sin\left(\sqrt{h}(t-t_k)\right) \\ -\sqrt{h}\sin\left(\sqrt{h}(t-t_k)\right) & \cos\left(\sqrt{h}(t-t_k)\right) \end{pmatrix} \\ &F_i(\xi_i(t_k), t-t_k) \\ &= \begin{pmatrix} \frac{\gamma\xi_i(t_k)\left(1-\cos\left(\sqrt{h}(t-t_k)\right)\right)}{h} & 0 \\ \frac{\gamma\xi_i(t_k)\sin\left(\sqrt{h}(t-t_k)\right)}{\sqrt{h}} & 0 \end{pmatrix}. \end{aligned} \tag{17}$$

Let $S_i(\xi_i(t_k), t-t_k) = E_i(t-t_k) + F_i(\xi_i(t_k), t-t_k)$; then equality (16) gives

$$\begin{aligned} m_i(t) &= S_i(\xi_i(t_k), t-t_k)S_i(\xi_i(t_{k-1}), T) \\ &\quad \cdot S_i(\xi_i(t_{k-2}), T),\ldots, S_i(\xi_i(0), T)m_i(0), \\ &\qquad i\in\{2,\ldots,M\} \end{aligned} \tag{18}$$

for any $t \in [t_k, t_{k+1}), k \in \mathbb{N}\cup\{0\}$.

The boundedness of $S_i(\xi_i(t_k), t-t_k)$ results in that $m_i(t)$ tends to $\mathbf{0}_2$ if $\rho(S_i(\xi_i(t_k), T)) < 1, k \in \mathbb{N}\cup\{0\}, i \in \{2,\ldots,M\}$. Denoting the possible values for $\xi_i(t_k), k \in \mathbb{N}\cup\{0\}, i \in \{2,\ldots,M\}$ by $\xi_i^l, l \in \mathbb{N}$, then $\rho(S_i(\xi_i(t_k), T)) < 1$ is ensured by

$\rho(S_i(\xi_i^l, T)) < 1$ which is equal to the fact that the following equation's solutions satisfy $|\lambda| < 1$:

$$\begin{aligned} f_{il}(\lambda, T) &= \det\left(\lambda I_2 - S_i\left(\xi_i^l, T\right)\right) \\ &= \lambda^2 \\ &\quad - \left(2\cos\left(\sqrt{h}T\right) + \frac{1-\cos\left(\sqrt{h}T\right)}{h}\gamma\xi_i^l\right)\lambda \\ &\quad + \left(1 + \frac{\cos\left(\sqrt{h}T\right)-1}{h}\gamma\xi_i^l\right) = 0. \end{aligned} \tag{19}$$

If we set $\lambda = (s+1)/(s-1)$, characteristic equation (19) is rewritten as

$$\begin{aligned} &2\left(1-\cos\left(\sqrt{h}T\right)\right)\left(1-\frac{\gamma\xi_i^l}{h}\right)s^2 \\ &\quad + 2\left(1-\cos\left(\sqrt{h}T\right)\right)\frac{\gamma\xi_i^l}{h}s + 2\left(1+\cos\left(\sqrt{h}T\right)\right) \\ &= 0 \end{aligned} \tag{20}$$

for any $i \in \{2, \ldots, M\}$, $l \in \mathbb{N}$. According to the property of bilinear transformation, $|\lambda| < 1$ achieves if and only if $\mathrm{Re}(s) < 0$. Moreover, if we define $\overline{\Lambda} = \delta I_M$ and denote the nonzero eigenvalues of $L(I_M + \overline{\Lambda})$ and $L(I_M - \overline{\Lambda})$ as $\widetilde{\xi}_i$ and $\overline{\xi}_i, i \in \{2, \ldots, M\}$, respectively, according to the relationship between the eigenvalues and the parameters $\varepsilon_i, i \in \{1, \ldots, M\}$, we get

$$\min_{i\in\{2,\ldots,M\}} \mathrm{Re}\left(\overline{\xi}_i\right) \le \mathrm{Re}\left(\xi_i^l\right) \le \max_{i\in\{2,\ldots,M\}} \mathrm{Re}\left(\widetilde{\xi}_i\right) \tag{21}$$

which ensures that $h \neq \gamma\xi_i^l, i \in \{2, \ldots, M\}, l \in \mathbb{N}$, if (5a) is satisfied. Combining with (5b) gives that equality (20) can be transferred into, $\forall i \in \{2, \ldots, M\}, l \in \mathbb{N}$,

$$s^2 + \frac{\gamma\xi_i^l}{h-\gamma\xi_i^l}s + \frac{1+\cos\left(\sqrt{h}T\right)}{1-\cos\left(\sqrt{h}T\right)}\frac{h}{h-\gamma\xi_i^l} = 0. \tag{22}$$

Considering $(1+\cos(\sqrt{h}T))/(1-\cos(\sqrt{h}T)) > 0$, Lemma 2 tells us that the roots of (22) located in the left-half plane are equal to

$$\frac{a_{il}}{\left|h-\gamma\xi_i^l\right|^2} > 0, \tag{23}$$

$$\frac{a_{il}b_{il}^2 + a_{il}^2c_{il}}{\left|h-\gamma\xi_i^l\right|^2} - \frac{1+\cos\left(\sqrt{h}T\right)}{1-\cos\left(\sqrt{h}T\right)}b_{il}^2 > 0, \tag{24}$$

where

$$\begin{aligned} a_{il} &= h\gamma\mathrm{Re}\left(\xi_i^l\right) - \gamma^2\left|\xi_i^l\right|^2, \\ b_{il} &= h\gamma\mathrm{Im}\left(\xi_i^l\right), \\ c_{il} &= h^2 - h\gamma\mathrm{Re}\left(\xi_i^l\right) \end{aligned} \tag{25}$$

for all $i \in \{2, \ldots, M\}$, $l \in \mathbb{N}$. Recalling (5a), we have that condition (23) is equivalent to

$$\gamma < \frac{h\mathrm{Re}\left(\xi_i^l\right)}{\left|\xi_i^l\right|^2}, \quad i \in \{2, \ldots, M\}, \ l \in \mathbb{N}, \tag{26}$$

which is guaranteed by

$$\gamma < \min_{i\in\{2,\ldots,M\}, l\in\mathbb{N}} \left\{\frac{h\mathrm{Re}\left(\xi_i^l\right)}{\left|\xi_i^l\right|^2}\right\}. \tag{27}$$

Based on the relationship between the eigenvalues and the parameters $\varepsilon_i, i \in \{1, \ldots, M\}$ and inequality (21), we know that

$$\min_{i\in\{2,\ldots,M\}, l\in\mathbb{N}} \left\{\frac{h\mathrm{Re}\left(\xi_i^l\right)}{\left|\xi_i^l\right|^2}\right\} = \frac{h\mathrm{Re}\left(\widetilde{\xi}_{i_{\max}}\right)}{\left|\widetilde{\xi}_{i_{\max}}\right|^2} \tag{28}$$

with $i_{\max} = \arg\max_{i\in\{2,\ldots,M\}}|\widetilde{\xi}_i|$.

Moreover, (26) gives $\gamma < h/\mathrm{Re}(\xi_i^l)$ indicating $a_{il} > 0$ and $c_{il} > 0$. By defining

$$e_{il} = \frac{\left|h-\gamma\xi_i^l\right|^2 b_{il}^2}{a_{il}b_{il}^2 + a_{il}^2c_{il}}, \tag{29}$$

we get that (24) holds if

$$T \in \Gamma_T\left(\max_{i\in\{2,\ldots,M\}, l\in\mathbb{N}} \arctan\sqrt{e_{il}}\right) \tag{30}$$

with $\Gamma_T(\varphi), \varphi \in [0, \pi/2)$ defined by $\Gamma_T(\varphi) = \{T \mid \tan^2(\sqrt{h}T/2) > \tan^2\varphi\}$. Therefore, if (5a) and (5b) are satisfied, we obtain that the roots of (20) hold negative real part if (5c) and (5d) hold which means that $|\lambda| < 1$, where λ denotes the eigenvalues of $S_i(\xi_i^l, T)$. Thus $\rho(S_i(\xi_i^l, T)) < 1$ is guaranteed which gives $\lim_{t\to\infty} m_i(t) = \mathbf{0}_2$ indicating $\lim_{t\to\infty} z(t) = \mathbf{0}_{2M}$. Up to now, it shows that the synchronization of network (1) under protocol (2) is obtained when (5a), (5b), (5c), and (5d) are satisfied. This completes the proof. □

Remark 4. In this paper, the constraint on the initial state, $\phi^T x(0) = \phi^T v(0) = 0$, is a necessary condition to ensure the synchronization of (8) according to $z_i(t) \to (1/(1+\varepsilon_i(t_k)))m_1(t), t \in [t_k, t_{k+1}), i \in \{1, \ldots, M\}$, in which ε_i and ε_j, $(i \neq j)$ are different from each other. How to relax the constraint on the initial state is one of our further research directions, which will need completely different proof line.

Remark 5. When we design parameters based on the above theorem, it is obvious that the difficulty lies in ascertaining the value of $\varphi = \max_{i\in\{2,\ldots,M\}, l\in\mathbb{N}} \arctan\sqrt{e_{il}}$. In fact, it can always increase or decrease the value of $\varepsilon_i, i \in \{1, \ldots, M\}$ to study the proportional relationship between ε_i and e_{il} and thus determine the value of φ and the feasible interval for T.

Remark 6. It is worth mentioning that the synchronization expression of CHO (1) under protocol (2) is the same as the one under protocol [9]

$$u_i(t) = \gamma \sum_{l \in \mathcal{M}_i} a_{il} \left(x_i(t_k) - x_j(t_k) \right), \quad t \in [t_k, t_{k+1}),\ i \in \{1, \ldots, M\},\ k \in \mathbb{N}, \tag{31}$$

where the current relative sampled position data has not been quantized. This is due to the fact that $E(t)$ defined in (13), which determines the synchronization state, is not influenced by quantization.

4. Simulation

A simulation example is given in this section to show the usefulness of the result. The CHO network composed of four nodes and the adjacency matrix $\mathcal{A}$ is given as

$$\mathcal{A} = \begin{bmatrix} 0 & 1 & 0 & 1 \\ 1 & 0 & 0 & 1 \\ 1 & 1 & 0 & 0 \\ 0 & 1 & 1 & 0 \end{bmatrix}. \tag{32}$$

Select parameters as $h = 0.8$, $\delta = 0.1$, and γ satisfying

$$\begin{aligned} \gamma &= 0.2 \\ &\notin \left[\frac{h}{\max_{i \in \{2,\ldots,M\}} \mathrm{Re}\left(\widetilde{\xi}_i\right)}, \frac{h}{\min_{i \in \{2,\ldots,M\}} \mathrm{Re}\left(\widetilde{\xi}_i\right)} \right] \\ &= [0.2424, 0.3556], \\ \gamma &= 0.2 < \frac{h \mathrm{Re}\left(\widetilde{\xi}_{i_{\max}}\right)}{\left|\widetilde{\xi}_{i_{\max}}\right|^2} = 0.2424. \end{aligned} \tag{33}$$

Based on $\varphi = \max_{i \in \{2,\ldots,M\}, l \in \mathbb{N}} \arctan \sqrt{e_{il}} = 0.6255$ and [9]

$$\begin{aligned} \Gamma_T(\varphi) &= \left\{ T \mid \tan^2\left(\frac{\sqrt{h}T}{2} \right) > \tan^2 \varphi \right\} \\ &= \left(\bigcup_{l=0}^{\infty} \left(\frac{2(\varsigma\pi + \varphi)}{\sqrt{h}}, \frac{(2\varsigma + 1)\pi}{\sqrt{h}} \right) \right) \\ &\cup \left(\bigcup_{l=1}^{\infty} \left(\frac{(2\varsigma - 1)\pi}{\sqrt{h}} \right), \frac{2(\varsigma\pi - \varphi)}{\sqrt{h}} \right) \end{aligned} \tag{34}$$

we know $T \in (1.3987, 3.5124)$ by setting $\varsigma = 0$. Selecting $T = 3 \in \Gamma_T(\varphi)$ and the initial states as $z(0) = [-1, 0, 2, 0, -1, 2, -1, -1]^T$ satisfying $\phi^T x(0) = \phi^T v(0) = 0$ with $\phi = [5/21, 7/21, 3/21, 6/21]^T$, the synchronization states can be shown in Figure 1, from which we see that the CHO network reaches synchronization. If the initial state is set as $z(0) = [1, 0, 2, 0, -1, 2, -1, 1]^T$ which violates $\phi^T x(0) = \phi^T v(0) = 0$, Figure 2 shows that the synchronization errors do not tend to zeros, which means that the synchronization for CHO network is not reached.

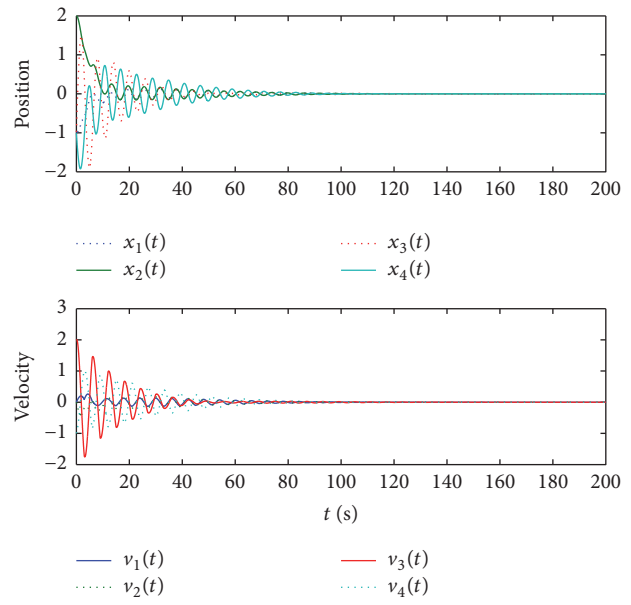

Figure 1: Synchronization with initial states $z(0) = [-1, 0, 2, 0, -1, 2, -1, -1]^T$.

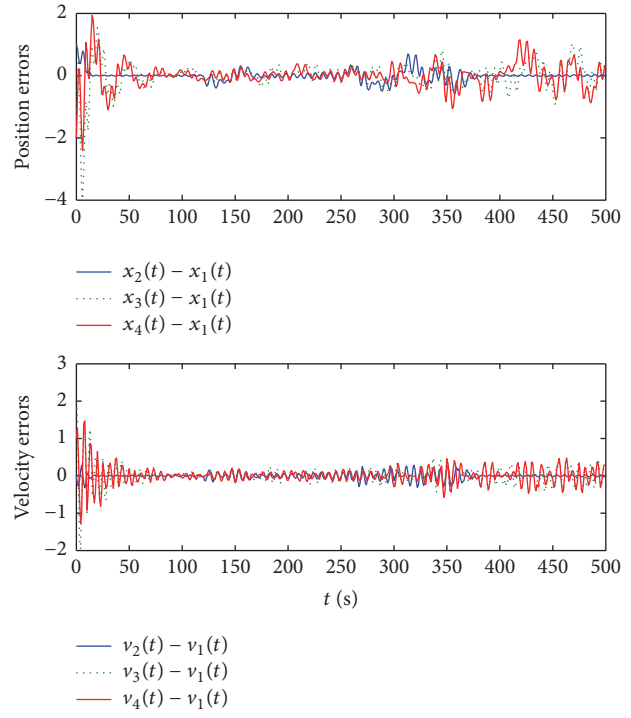

Figure 2: Synchronization errors with initial states $z(0) = [1, 0, 2, 0, -1, 2, -1, 1]^T$.

5. Conclusion

By using the quantized current sampled position data, the sufficient conditions for synchronization of CHO are given according to coupling strength, sampling period, and quantizer parameter. It is worth mentioning that the results here need some restrictions on initial states. How to obtain the

synchronization for CHO network without these restrictions holds some challenges, and it is one of our further research directions.

Conflicts of Interest

The authors declare that they have no conflicts of interest.

Acknowledgments

The work was supported by the National Natural Science Foundation of China (41501562, 61403125, and 61603108) and the State Key Laboratory of Coal Resources and Safe Mining (China University of Mining and Technology) (SKLCRSM16KFD02).

References

[1] H. Su, X. Wang, and Z. Lin, "Synchronization of coupled harmonic oscillators in a dynamic proximity network," *Automatica*, vol. 45, no. 10, pp. 2286–2291, 2009.

[2] J. Zhou, H. Zhang, L. Xiang, and Q. Wu, "Sampled-data synchronization of coupled harmonic oscillators with controller failure and communication delays," *Theoretical and Applied Mechanics Letters*, vol. 3, no. 6, Article ID 063002, 2013.

[3] W. Ren, "Synchronization of coupled harmonic oscillators with local interaction," *Automatica*, vol. 44, no. 12, pp. 3195–3200, 2008.

[4] X. Wang and Z. Cheng, "Synchronization of coupled discrete-time harmonic oscillators with rational frequency," *Institute of Electrical and Electronics Engineers. Transactions on Automatic Control*, vol. 58, no. 6, pp. 1573–1579, 2013.

[5] J. Wang, J. Feng, C. Xu, M. Z. Q. Chen, Y. Zhao, and J. Feng, "The synchronization of instantaneously coupled harmonic oscillators using sampled data with measurement noise," *Automatica*, vol. 66, pp. 155–162, 2016.

[6] J. Zhou, H. Zhang, L. Xiang, and Q. Wu, "Synchronization of coupled harmonic oscillators with local instantaneous interaction," *Automatica*, vol. 48, no. 8, pp. 1715–1721, 2012.

[7] H. Zhang and J. Zhou, "Synchronization of sampled-data coupled harmonic oscillators with control inputs missing," *Systems & Control Letters*, vol. 61, no. 12, pp. 1277–1285, 2012.

[8] Q. Song, W. Yu, J. Cao, and F. Liu, "Reaching Synchronization in Networked Harmonic Oscillators with Outdated Position Data," *IEEE Transactions on Cybernetics*, vol. 46, no. 7, pp. 1566–1578, 2016.

[9] Q. Song, F. Liu, G. Wen, J. Cao, and Y. Tang, "Synchronization of coupled harmonic oscillators via sampled position data control," *IEEE Transactions on Circuits and Systems. I. Regular Papers*, vol. 63, no. 7, pp. 1079–1088, 2016.

[10] T. Zhang and J. Li, "Robust iterative learning control of multi-agent systems with logarithmic quantizer," in *Proceedings of the 34th Chinese Control Conference, CCC 2015*, pp. 7033–7038, chn, July 2015.

[11] S. R. Etesami and T. Başar, "Convergence Time for Unbiased Quantized Consensus over Static and Dynamic Networks," *IEEE Transactions on Automatic Control*, vol. 61, no. 2, pp. 443–455, 2016.

[12] X. Guo, J. Wang, F. Liao, and D. Wang, "Quantized H∞ consensus of multi-Agent systems with quantization mismatch under switching weighted topologies," *IEEE Transactions on Control of Network Systems*, vol. PP, no. 99, 2015.

[13] Z. Qiu, L. Xie, and Y. Hong, "Quantized leaderless and leader-following consensus of high-order multi-agent systems with limited data rate," *Institute of Electrical and Electronics Engineers. Transactions on Automatic Control*, vol. 61, no. 9, pp. 2432–2447, 2016.

[14] Y. Zhu, Y. Zheng, and L. Wang, "Quantised consensus of heterogeneous multi-agent systems," *IET Control Theory & Applications*, vol. 9, no. 17, pp. 2553–2560, 2015.

[15] S. Zhu and B. Chen, "Quantized consensus by the ADMM: probabilistic versus deterministic quantizers," *IEEE Transactions on Signal Processing*, vol. 64, no. 7, pp. 1700–1713, 2016.

[16] Z. Zhang, L. Zhang, F. Hao, and L. Wang, "Periodic Event-Triggered Consensus with Quantization," *IEEE Transactions on Circuits and Systems II: Express Briefs*, vol. 63, no. 4, pp. 406–410, 2016.

[17] M. El Chamie, J. Liu, and T. Basar, "Design and analysis of distributed averaging with quantized communication," *Institute of Electrical and Electronics Engineers. Transactions on Automatic Control*, vol. 61, no. 12, pp. 3870–3884, 2016.

[18] W. Xiong, X. Yu, Y. Chen, and J. Gao, "Quantized Iterative Learning Consensus Tracking of Digital Networks With Limited Information Communication," *IEEE Transactions on Neural Networks and Learning Systems*, 2016.

[19] T. Basar, S. R. Etesami, and A. Olshevsky, "Convergence time of quantized Metropolis consensus over time-varying networks," *Institute of Electrical and Electronics Engineers. Transactions on Automatic Control*, vol. 61, no. 12, pp. 4048–4054, 2016.

[20] X. Mu and K. Liu, "Containment control of single-integrator network with limited communication data rate," *Institute of Electrical and Electronics Engineers. Transactions on Automatic Control*, vol. 61, no. 8, pp. 2232–2238, 2016.

[21] L. Rong, H. Shen, and J. Li, "Distributed quantised consensus in groups of agents with acceleration-like inputs: a reference model-based scheme," *IET Control Theory & Applications*, vol. 10, no. 5, pp. 590–598, 2016.

[22] Z. Zhang, L. Zhang, F. Hao, and L. Wang, "Leader-Following consensus for linear and lipschitz nonlinear multiagent systems with quantized communication," *IEEE Transactions on Cybernetics*, 2016.

[23] Z. Zeng, X. Wang, Z. Zheng, and L. Zhao, "Edge agreement of second-order multi-agent system with dynamic quantization via the directed edge Laplacian," *Nonlinear Analysis. Hybrid Systems*, vol. 23, pp. 1–10, 2017.

[24] H.-X. Hu, Q. Xuan, W. Yu, C.-G. Zhang, and G. Xie, "Second-order consensus for heterogeneous multi-agent systems in the cooperation-competition network: a hybrid adaptive and pinning control approach," *Nonlinear Analysis. Hybrid Systems*, vol. 20, pp. 21–36, 2016.

[25] H.-X. Hu, W. Yu, G. Wen, Q. Xuan, and J. Cao, "Reverse group consensus of multi-agent systems in the cooperation-competition network," *IEEE Transactions on Circuits and Systems I: Regular Papers*, vol. 63, no. 11, pp. 2036–2047, 2016.

[26] N. Elia and S. K. Mitter, "Stabilization of linear systems with limited information," *Institute of Electrical and Electronics Engineers. Transactions on Automatic Control*, vol. 46, no. 9, pp. 1384–1400, 2001.

[27] M. Fu and L. Xie, "The sector bound approach to quantized feedback control," *Institute of Electrical and Electronics Engineers. Transactions on Automatic Control*, vol. 50, no. 11, pp. 1698–1711, 2005.

[28] W. Ren and R. W. Beard, "Consensus seeking in multiagent systems under dynamically changing interaction topologies," *Institute of Electrical and Electronics Engineers. Transactions on Automatic Control*, vol. 50, no. 5, pp. 655–661, 2005.

[29] P. C. Parks and V. Hahn, *Stability Theory*, Qrentice-Hall, NY, USA, 1993.

Hindawi
Journal of Control Science and Engineering
Volume 2017, Article ID 8471024, 13 pages
https://doi.org/10.1155/2017/8471024

Research Article

A Novel Measurement Matrix Optimization Approach for Hyperspectral Unmixing

Su Xu[1,2] and Xiping He[1,2]

[1] *College of Computer Science and Information Engineering, Chongqing Technology and Business University, Chongqing 400067, China*
[2] *Chongqing Engineering Laboratory for Detection, Control and Integrated System, Chongqing Technology and Business University, Chongqing 400067, China*

Correspondence should be addressed to Su Xu; xusu44@163.com

Received 25 January 2017; Revised 25 February 2017; Accepted 16 March 2017; Published 3 July 2017

Academic Editor: Qiang Song

Each pixel in the hyperspectral unmixing process is modeled as a linear combination of endmembers, which can be expressed in the form of linear combinations of a number of pure spectral signatures that are known in advance. However, the limitation of Gaussian random variables on its computational complexity or sparsity affects the efficiency and accuracy. This paper proposes a novel approach for the optimization of measurement matrix in compressive sensing (CS) theory for hyperspectral unmixing. Firstly, a new Toeplitz-structured chaotic measurement matrix (TSCMM) is formed by pseudo-random chaotic elements, which can be implemented by a simple hardware; secondly, rank revealing QR factorization with eigenvalue decomposition is presented to speed up the measurement time; finally, orthogonal gradient descent method for measurement matrix optimization is used to achieve optimal incoherence. Experimental results demonstrate that the proposed approach can lead to better CS reconstruction performance with low extra computational cost in hyperspectral unmixing.

1. Introduction

Compressive sensing (CS) theory [1, 2] is a new developed theoretical framework on signal sampling and data compression, which indicates that if a signal is sparse or compressible in a certain transform domain, the transformed higher-dimensional signal can be projected onto a lower dimensional space by a measurement matrix. It leads to nonadaptive measurement encoding on the signal at a rate far below the Nyquist sampling rate, converting from sampling the signal itself to sampling the information contained in the signal. Therefore it has recently gained more and more attention in various areas of applied mathematics, computer science, and electrical engineering.

Design of measurement matrix is a research hotspot in CS, and measurement matrix optimization has become an inevitable trend to construct a new measurement matrix system. In recent years, scholars have yielded many optimization methods [3–22] to design measurement matrix to reduce the minimum coherence of Gram matrix. These are typically fallen into three categories: iterative thresholding method [3–14], gradient iteration process [15–19], and Tensor product [20–22].

Zhang et al. [6] proposed that the Kronecker product measurement matrix based on orthogonal basis can maintain nonlinear correlation between columns' vector from high-dimensional data. But Kronecker product [5, 6] leads to low sampling efficiency and poor computational complexity, which limit the deep study for measurement matrix.

By using iterative thresholding method, Elad [7] iteratively reduces the average mutual coherence using a shrinkage operation followed by singular value decomposition (SVD) step and shrinks the elements of Gram matrix. Lustig et al. [8] defined an incoherence criterion and proposed a Monte Carlo scheme for random incoherent sampling. Abolghasemi et al. [9] attempted a kind of nonuniform sampling by segmenting the input signal and taking samples with different rates from each segment. Duarte-Carvajalino and Sapiro [10] take advantage of an eigenvalue decomposition process

followed by a KSVD-based algorithm to optimize measurement matrix and learn dictionary basis, respectively. Wang et al. [11] propose to generate colored random projections using an adaptive scheme. Next they [12] propose a variable density sampling strategy by exploiting the prior information about the statistical distributions of natural images in the wavelet domain. Although the algorithm is simple and easy to understand, the research [13, 14] found that iterative thresholding method has slow convergence speed and is easy to fall into local minimum problems in practical application. Meanwhile it damages Restricted Isometric Property (RIP) and eventually may cause the collapse of the BP algorithm.

By using gradient iteration process, Xu et al.'s algorithm [15] first shrinks and updates elements in Gram matrix with Equiangular Tight Frame (ETF). Li et al. [18] constructs the dimensional orthogonal matrix in SVD; Abolghasemi et al.'s algorithm [16] lies in the innovation of the gradient iteration process to obtain measurement matrix. Zhang et al.'s algorithm [17] adopts the spherical search steepest descent method. Tian et al.'s algorithm [19] shrinks Gram matrix with the orthogonal gradient factor matrix to reduce the maximum and average mutual coherence of measurement matrix. The appearance of different pursuit rates brings about the saddle-point steady-state solution, which only guarantees a local minimum solution.

Unfortunately, most algorithms neglect intrasensor correlations between the samples of high-dimensional data like 3D color image, video, and hyperspectral image; it may affect the multispectral features excessively and destroy the original structure of high-dimensional data and it ultimately affects the precision of hyperspectral unmixing.

Toeplitz-structured chaotic measurement matrix is one of deterministic measurement matrices in CS, which requires only $O(M)$ independent variables and $O(M \log 2M)$ operations. But it still has three attractive weaknesses: optimal incoherence being unachieved, reconstruction precision being insufficient, and measurement time being unbearable.

To eliminate the weaknesses, we are inspired to work on optimizing the Toeplitz-structured chaotic measurement matrix to obtain better results from high-dimensional signals. Meanwhile, the possibility of fusing these two attractive optimized methods is certain: rank revealing QR factorization with eigenvalue decomposition from Xu et al.'s algorithm [15] and orthogonal gradient descent approach from Tian et al.'s algorithm [19] to obtain a new optimized method to overcome the computational complexity. This is my intuitive idea of this paper.

The key contribution of this work can be elaborated as follows:

(1) In the domain of designing the measurement matrix, it is crucial to achieve high quality with implementing effective hardware. In this work, some pseudorandom chaotic elements can approximate the random structure component, which satisfies RIP property with overwhelming probability. So these pseudorandom chaotic elements are applied to Toeplitz-structured chaotic measurement matrix, which forms a new measurement matrix (TSCMM). Compared with the others, we attempt to prove that it satisfies RIP conditions.

(2) According to the properties of the separated contents, Gram matrix is improved by a rank revealing QR factorization with eigenvalue decomposition to speed up convergence rate. The results of experiments show that the proposed methods can greatly reduce computation complexity building on the convergence and robustness.

(3) From a practical point of view, high computational complexity imposes restrictions on achieving optimal incoherence; orthogonal gradient descent approach is proposed to acquire measurement matrix optimization. The improved scheme can effectively reduce the reconstruction error and acquire satisfied image quality compared to other conventional methods.

The rest of this paper is organized as follows. The main part of this paper starts with review of some measuring coherence criteria and develops to RIP in Section 2. Based on the previous analysis, the proposed approach for measurement matrix optimization in Section 3 is developed. Particularly motivated by TSCMM, QR factorization with eigenvalue decomposition and improved gradient descent approach is then suggested in the following three subsections, starting with Toeplitz-structured chaotic measurement matrix in Section 3.1, followed by QR factorization algorithm in Section 3.2 and an orthogonal gradient descent approach for measurement matrix optimization in Section 3.3. Experimental results in Section 4 and conclusions in Section 5 are presented.

2. Problem Formulation and Analysis

From the viewpoint of mathematics, CS sample procession is approximated by recovering x from far incomplete measurements:

$$y = \Phi x = \Phi \Psi \theta, \tag{1}$$

where θ in some basis Ψ is sparse or compressible representation, while $\Phi \in \Re^{K \times N}$ is so-called CS measurement matrix. Because of $K \ll N$, the signal is measured through the projection by the measurement matrix Φ which leads to being highly underdetermined.

If the D-dimensional sample signal $X = [x_1^T, x_2^T, \ldots, x_D^T]$ and independent measurements result $Y = [y_1^T, y_2^T, \ldots, y_D^T]$ are unknown, the Kronecker product measurement matrix [5] can be expressed as $\overline{\Phi} = \Phi_1 \otimes \Phi_2 \otimes \cdots \otimes \Phi_D$. When each sensor obtaining its independent measurements is the same measurement matrix $\Phi_D = \Phi'$, the joint measurement matrix can be expressed as $\overline{\Phi} = I_D \otimes \Phi'$, where I_D denotes the $D \times D$ identity matrix, as shown in Figure 1.

The constants δ_K for the matrix Φ are intrinsically tied to the singular values of all column submatrices of a certain size. If $\Phi_1, \Phi_2, \ldots, \Phi_D$ are matrices with restricted isometry constants (RIP) $\delta_K(\Phi_1), \delta_K(\Phi_2), \ldots, \delta_K(\Phi_D)$, the structure of

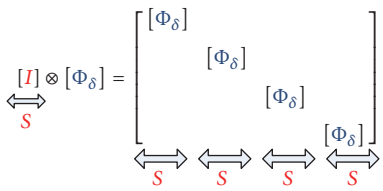

FIGURE 1: The diagram of the joint measurement matrix in Duarte's method.

Kronecker product matrices yields simple bounds for their RIP that can be expressed as

$$\delta_K\left(\Phi_1 \otimes \Phi_2 \otimes \cdots \otimes \Phi_D\right) \leq \prod_{d=1}^{D}\left(1+\delta_K\left(\Phi_d\right)\right) - 1. \quad (2)$$

Considering the D-dimensional Kronecker sparsifying basis $\overline{\Psi} = \Psi_1 \otimes \Psi_2 \otimes \cdots \otimes \Psi_D$ and a global measurement basis or frames obtained through a Kronecker product of individual measurement bases, the definition of mutual coherence is presented as

$$\begin{aligned}&\mu\left(\Phi_1 \otimes \Phi_2 \otimes \cdots \otimes \Phi_D, \Psi_1 \otimes \Psi_2 \otimes \cdots \otimes \Psi_D\right)\\ &\quad = \prod_{d=1}^{D} \mu\left(\Phi_d, \Psi_d\right).\end{aligned} \quad (3)$$

High-dimensional Kronecker compressive sensing (HKCS) [6] proposed the optimal synthetic sensing matrix by taking Kronecker products of individual optimal sensing matrix in each dimension. The optimal sensing matrix that minimizes the mutual coherence of the projection matrix can be expressed as

$$\overline{\Phi}' = \Phi_t \otimes \Phi_s. \quad (4)$$

With the same sampling rate, matrices of HKCS have relatively smaller mutual coherence. It can be written as

$$\mu\left(\overline{\Phi}, \overline{\Psi}\right) \leq \mu\left(\overline{\Phi}', \overline{\Psi}\right). \quad (5)$$

It also indicates that the optimization process is dividable, which preserves the block feature of Kronecker product matrix and enables fast low-scale matrix computation. The overall video acquisition is decomposed as shown in Figure 2.

The high-dimensional Kronecker products measurement matrix is our optimization goal, as shown in Figure 3.

If $A^{cs} = \Psi_t \otimes \Phi_s$ is defined as Gram matrix and minimum square error cost function is defined as E, the optimization problem can be written as

$$\begin{aligned}&E \triangleq \text{MSE} = \left\|\left(A^{cs}\right)^T A^{cs} - I\right\|_F^2\\ &\text{s.t.} \quad A^{cs} = \Psi_t \otimes \Phi_s.\end{aligned} \quad (6)$$

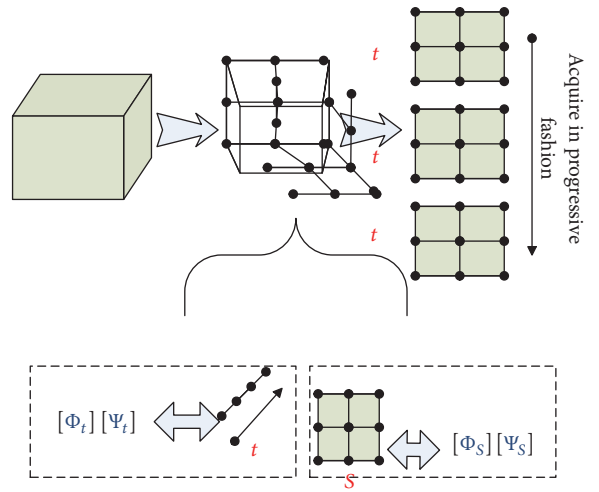

FIGURE 2: The proposed multidimensional compressive sensing for video acquisition.

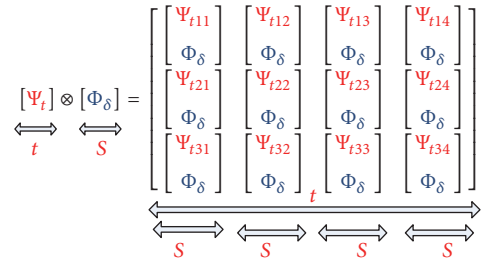

FIGURE 3: The diagram of the joint measurement matrix in HKCS.

The goal of eliminating the correlation is to minimize the difference between Gram matrix and identity matrix in the form of Frobenius norm. Considering Kronecker product properties,

$$E \triangleq \text{MSE} = \left\|\left(\Psi_t^T \Psi_t\right) \otimes \left(\Phi_t^T \Phi_t\right) - I\right\|_F^2. \quad (7)$$

If the value $\Theta^T\Theta = V^T \Lambda V$ can be replaced with its corresponding eigenvalue decomposition and $\Phi_t^T \Phi_t = (8/m)\sum_{i=0}^{n}[x(i)]^T x(n-i)$, (7) can then become as follows:

$$E \triangleq \text{MSE} = \left\|\wedge - \wedge V^T \frac{8}{m}\sum_{i=0}^{n}\left[x\left(i\right)\right]^T x\left(n-i\right) V \wedge\right\|_F^2. \quad (8)$$

Because $\wedge$ is real diagonal matrices, $\wedge V^T V \wedge = (V\wedge)^T V \wedge$. If $B = V\wedge$, then $\overline{B} \coloneqq [|B_{ij}{}^2|]$.

Here, (8) can be reduced to

$$E \triangleq \text{MSE} = \left\|\wedge - B^T \frac{8}{m}\sum_{i=0}^{n}\left[x\left(i\right)\right]^T x\left(n-i\right) B\right\|_F^2. \quad (9)$$

Supposing that B_{ij} is the elements in B, gradient decrease iteration method is used to minimize mean square error (MSE). $B_{ij} \leftarrow B_{ij} - \rho \nabla E$, where ρ is step size and $\rho > 0$.

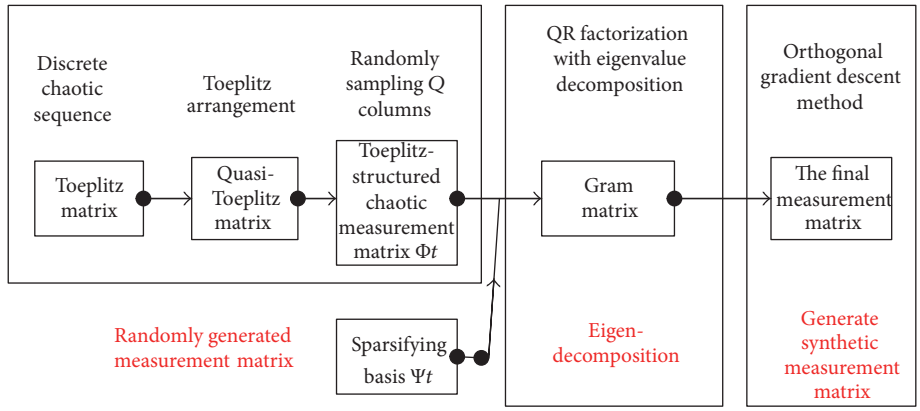

FIGURE 4: The improved scheme by different methods.

$\nabla E \equiv \partial E/\partial B_{ij}$ is gradient value of E; then $B_{(i+1)} = B_i - \eta B_i (B_i^T (8/m) \sum_{i=0}^{n} [x(i)]^T x(n-i) B_i)$. According to Gerschgorin theorem, the column coherence of φ_i can be deduced as follows:

$$\mu = \max_{1 \le i,j \le N, i \ne j} \left| \left\langle \varphi_i, \Psi_j \right\rangle \right|. \tag{10}$$

If $N \le M(M+1)/2$, the infimum of the column coherence is called Welch bound:

$$\mu \ge \mu_w = N - M(N-1)M. \tag{11}$$

Equiangular Tight Frame (ETF) is derived from (11) if the constraints are equality.

3. The Proposed Approach

Based on previous conclusions, the proposed algorithm aims to optimize the Toeplitz-structured chaotic measurement matrix to obtain better results from hyperspectral unmixing. Therefore, the research content in this paper mainly consists of three parts: designed TSCMM, optimized Gram matrix, and orthogonal gradient descent approach, as shown in Figure 4.

The study is given by taking the following methods: firstly, to obtain easy hardware implemented, pseudo-random chaotic elements are used to form a new Toeplitz-structured chaotic measurement matrix (TSCMM), as discussed in Section 3.1; to overcome unbearable Cost Time, Gram matrix is improved by a rank revealing QR factorization with eigenvalue decomposition as discussed in Section 3.2; to achieve optimal incoherence, orthogonal gradient descent method for measurement matrix optimization is presented in Section 3.3. Finally, the improved scheme is presented through explicit analysis and discussion.

3.1. Xu-TSCMM. Recently, [23] is written by myself completely and probed into its initial theory and research. Discrete chaotic system function is proposed to generate a series of pseudo-random numbers. Based on those elements, Toeplitz-structured chaotic measurement matrix (TSCMM) is produced to guarantee the incoherence criterion. To reduce the building time of TSCMM, Circulant/block-diagonal splitting structure is attached on TSCMM. Although about one-third of matrix values are eliminated, the measurement matrix is proved to satisfy Johnson-Lindenstrauss (J-L) lemma and achieves the goal of satisfying RIP. Logistic map [24], as the simplest dynamic systems evidencing chaotic behavior, is described as follows:

$$x_{n+1} = \mu x_n (1 - x_n), \quad \mu \in [0,4], \; x_n \in [0,1] \subset R, \tag{12}$$

where $\mu \in (3.5699, 4] \subset R$ is the discrete state. While parameter μ is 4, the sequence $x_n(t)$ satisfies beta distribution with $\alpha = 0.5$ and $\beta = 0.5$, and the next probability density function $f(x; 0.5, 0.5) = (1/\pi)(x - x^2)^{-1/2}$ has been used for simulation.

Set $z_i(t)$ as the output sequence generated by (12) with initial condition $z_i(0)$, and let $x_i(t)$ denote the regularization of $z_i(t)$ as the following form: $x_i(t) = z_i(t) - 0.5$ $i = 0, 1, 2, \ldots$.

Approximately, $x_i(t)$ can be considered as random variable, and it satisfies the following distribution: $f(x) = (1/\pi)(0.25 - x^2)^{-1/2}$. Then, by selecting m different initial conditions $z(0) \in [0,1]^m \subset R^m$, one can obtain m vectors with dimension R, which enables us to construct the following matrix Φ scaled by $\sqrt{8/m}$:

$$\Phi = \sqrt{\frac{8}{m}} \begin{pmatrix} x_0(0) & \cdots & x_0(n-1) \\ \vdots & \ddots & \vdots \\ x_m(0) & \cdots & x_m(n-1) \end{pmatrix}. \tag{13}$$

Here, (13) is called the beta-like matrix.

According to (13), set one initial condition $z \in (0) \in \Re$, and generate a sequence $x \in \Re^n$ in the chaotic system. Then, Toeplitz-structured matrix $\Phi = \Re^{m \times n}$ is constructed in the following form:

$$\Phi = \sqrt{\frac{8}{m}} \begin{pmatrix} x(n-1) & x(n-2) & \cdots & x(0) \\ x(0) & x(n-1) & & x(1) \\ \vdots & \vdots & \ddots & \vdots \\ x(m-2) & x(m-3) & \cdots & x(m-1) \end{pmatrix}. \tag{14}$$

Here, $\sqrt{8/m}$ is for normalization and Φ is called Toeplitz-structured chaotic measurement matrix (TSCMM), which meets J-L theorem.

3.2. Duarte-ETF Method. Minimum coherence property of ETF has been the main target to find a feasible solution. It is impossible to solve the problem exactly because of the complexity, while the structure of Gram matrix has changed so much that the selection of new units in the following step is very difficult.

To minimize (14), an optimization approach is adopted to reduce the maximum and average mutual coherence of measurement matrix. It shrinks Gram matrix based on ETF theory. The method can minimize the global mutual coherent coefficient of TSCMM by adjusting the eigenvalues above zero to the average value of the sum of these eigenvalues without changing the sum. After performing alternating minimization, the optimized measurement matrix can be constructed from the output Gram matrix with a rank revealing QR factorization with eigenvalue decomposition.

Theorem 1. *Given a measurement matrix $\Phi = \Re^{m\times L}$ and representing matrix $\Theta = \Re^{n\times m}$, there exists a matrix $D = \Theta\Phi$ and Gram matrix $G = \widehat{D}^T\widehat{D}$, where $\widehat{D}$ is the column normalization from D. If the real positive definite matrix G has $\lambda_k > 0$ $(k = 1 \sim m)$, the following equality $\sum_{k=1}^{m}\lambda_k = n$ and $\sum_{k=1}^{m}(\lambda_k)^2 = \sum_{i,j=1}^{n}(\langle\widetilde{d}_i, \widetilde{d}_j\rangle)^2$, where $\widetilde{d}_i$ $(i = 1 \sim n)$ is the column of $\widehat{D}$ which is obtained.*

Based on Theorem 1, to minimize the largest absolute values of the off-diagonals in the corresponding Gram matrix, we can determine the eigenvalues of Gram matrix by solving the following optimization problems:

$$\begin{aligned} \min \quad & \sum_{i\neq j}\left(g_{ij}\right)^2 = \sum_{k=1}^{m}(\lambda_k)^2 - \sum_{i=1}^{n}\left(g_{ij}\right)^2 \\ \text{s.t.} \quad & \sum_{k=1}^{m}\lambda_k = n, \end{aligned} \tag{15}$$

where g_{ij} is the element of Gram matrix. The optimization problem (15) is to minimize the square sum of the element of Gram matrix if the sum of the characteristic value λ_k remains constant. Though the eigenvalue decomposition of Gram matrix has $\lambda_k > 0$, the value n/m has been gradually approaching to minimize the square sum of $\sum_{k=1}^{m}(\lambda_k)^2$. Because real symmetric matrix eigenvalue decomposition is orthogonal, the square sum of nondiagonal elements from Gram matrix gradually decreases and further it attains the effect as follows:

$$\min \quad \sum_{i\neq j}\left(g_{ij}\right)^2 = \sum_{k=1}^{m}\left(\frac{n}{m}\right)^2 = n. \tag{16}$$

Finally, $\widehat{D}$ is obtained after several iterations, which is also the optimal Gram matrix G_{best}.

3.3. The Orthogonal Gradient Descent Approach. According to the definition of Gram matrix, Gram matrix is the product of measurement matrix and sparse matrix. Therefore, the optimal measurement matrix can be directly derived from the optimal Gram matrix. However, as for overcomplete sparse representation based on redundant dictionary, it is very hard to design an effective algorithm to construct measurement matrix. In order to solve this problem, orthogonal gradient descent method is employed to get the optimal measurement matrix Θ_{best}.

If the optimal Gram matrix G_{best} is obtained, the optimal measurement matrix Θ_{best} is as follows:

$$\Theta_{\text{best}} = \arg\min \left\|G_{\text{best}} - \Theta^T\Theta\right\|_F \triangleq F(\Theta). \tag{17}$$

And then the complex problem from optimal Gram matrix G_{best} is transformed into simple minimum of $F(\Theta)$. By determining the derivative of $F(\Theta)$, a skew-symmetric matrix W with the measurement matrix Θ and the gradient matrix ∇F is used to obtain revision factor:

$$\begin{aligned} \nabla F(\Theta) &= \Theta\left(\Theta^T\Theta - G_{\text{best}}\right), \\ W(\Theta, \nabla F) &= \Theta^T(\nabla F) - (\nabla F)^T\Theta. \end{aligned} \tag{18}$$

Next, if I is identity matrix, the orthogonal matrix S can be expressed through the Cayley transform to ensure the positive definiteness of the revision factor:

$$S = (I - W)(I + W)^{-1}. \tag{19}$$

The orthogonal gradient factor matrix Δ can be obtained to update the gradient direction:

$$\Delta = \nabla F + (\nabla F)S = \nabla F(S + I). \tag{20}$$

Combining (19) and (20), (21) can be rewritten as follows:

$$\Delta = \nabla F\left(I + (I - W)(I + W)^{-1}\right), \tag{21}$$

$$\Delta = 2\nabla F(I + W)^{-1}. \tag{22}$$

Finally, update measurement matrix Θ with the orthogonal gradient factor matrix Δ:

$$\Theta \longleftarrow \Theta - \eta\Delta. \tag{23}$$

Because η is updating ratio, $F(\Theta)$ gradually converges at the minimum value. Then the optimal measurement matrix Θ is the goal of our pursuit. According to the linearity property of Toeplitz measurement matrix [25], Θ satisfies J-L property with overwhelming probability. From Theorem 1, it has been proven that J-L condition can replace RIP condition. So Θ also satisfies RIP property with overwhelming probability.

The flow diagram of the proposed method will be given as shown in Algorithm 1.

4. Experiments and Result Analysis

To illustrate the effectiveness of the proposed approach, the most widely used hyperspectral images in unmixing, such

Input: number of measurements M, dictionary $\Psi^{L\times N}$, threshold $\xi = \sqrt{(L-N)/N(L-1)}$
updating ratio η, number of iterations Iter_1, Iter_2
Initialization: Set $\Phi^{M\times N}$ to be TSCMM.
Update: (1) Set the initial value of iteration $k_1 = 0$.
(2) Optimize Gram matrix
(a) Compute Gram matrix: $G = \Theta^T\Theta = \Psi^T\Phi_{k_1}^T\Phi_{k_1}\Psi$;
(b) Normalize: $\widehat{G} = \text{diag}(1/\sqrt{\text{diag}(G)}) * G * \text{diag}(1/\sqrt{\text{diag}(G)})$;
(c) Update the elements of Gram matrix $\widehat{G}$;
(3) Optimize measurement matrix
(a) Set the initial value of iteration $k_2 = 0$;
(b) Compute the orthogonal gradient factor matrix Δ_{k_2};
(c) Update measurement matrix: $\Theta_{k_2} : \Theta_{k_2} = \Theta_{k_2} - \eta\Delta_{k_2}$;
(d) $k_2 = k_2 + 1$, if $k_2 = \text{Iter}_2$, stop; else, return to Step 3.2);
(4) Compute measurement matrix Φ_{k_1};
(5) $k_1 = k_1 + 1$, if $k_1 = \text{Iter}_1$, stop; else, return to Step (2).
Output: Φ_{best} is the optimal measurement matrix Φ_{Iter_1-1}.
Further, SNR and reconstructed signal.

Algorithm 1: The flow diagram of the proposed method. Optimization of TSCMM.

as Cuprite, Urban, and Jasper Ridge, were selected in the spectral range from 380 nm to 2500 nm; each channel band width is up to 9.46 nm. All high-dimensional data is provided by the standard hyperspectral library of 224 bands which comes from [26]. To reduce complexity, there are only 128 × 128 pixel blocks of original image which starts from the $(0, 0)$th pixel. Further, only 8 channels (from 11 to 81 bands every 10 bands) were remained due to dense water vapor and atmospheric effects.

In the course of the experiment, the signal sparsity method is Fourier basis and reconstruction algorithm is Stagewise Orthogonal Matching Pursuit (StOMP) [27]. Various kinds of measurement matrix (Circulant, Toeplitz, Toeplitz-structured chaotic measurement matrix (TSCMM) [23], Elad-Optimization Method (EOM) [7], and Duarte-Carvajalino and Sapiro's Method (Duarte-ETF) [10]) are employed to illustrate the effectiveness of proposed approach for hyperspectral unmixing.

To demonstrate the efficiency of these methods, traditional evaluation methods can generally be divided into two categories: (1) subjective assessment and (2) objective evaluation. Mean Squared Error (MSE) and Peak-Signal-to-Noise Ratio (PSNR) as one of the most important indices from objective evaluation determine the quality of recovery image, while Cost Time (CT) verifies the efficiency of the proposed approach. They all testify experiment results of recovery signals, built on laptop with AthlonTM Processor 1.60 G HZ, 1 GB RAM, Matlab 7.0, and Windows XP operation platform.

4.1. Cuprite. To illustrate the use of the hyperspectral analysis process, a sample scene covers the Cuprite mining district in western Nevada, USA, from NASA's Airborne Visible/Infrared Imaging Spectrometer (AVIRIS) is provided. The data provided here is one of the most widely used hyperspectral images in unmixing study. There are 210 wavelengths ranging from 400 nm to 2500 nm, resulting in a spectral resolution of 10 nm.

In Figure 5, the first image (Top) was taken in blue light, the second image (middle) was taken in red light, and the third image (bottom) was taken in near infrared light centered at a wavelength of 750 nanometers.

Figure 5 presents the subjective evaluation by Circulant, Toeplitz, TSCMM, EOM, Duarte-ETF, and proposed method. Compared with other results, the performance from Figure 5(b) is the worst. The reason is that the elements from Circulant measurement matrix follow periodic repetition permutation, which does not satisfy RIP property with overwhelming probability. Figure 5(c) clearly demonstrates that Toeplitz measurement matrix can avoid the problem well. Because of the property of pseudo-random of chaotic sequence, the performance from TSCMM has further improved, as shown in Figure 5(d). The result from Figures 5(e)–5(g) shows that there is a significant impact on different bands using different optimization methods. Near infrared image is less affected by dust and gas. Visible blue channel has strong capability to penetrate water and visible red channel can reflect the health status of plants. Therefore, the sorted off-diagonal entries of the measurement matrix from EOM are likely more sparse and diagonal entries are more concentrated. The results are clearly shown in Figure 5(g) that the proposed approach had a significant performance compared to any others and closely resembles original image. Furthermore, the objective evaluations, which include Mean Squared Error (MSE), Peak-Signal-to-Noise Ratio (PSNR), and Cost Time (CT), can avoid artificial error and draw compelling conclusion. The results can be clearly seen from different methods on recovery Cuprite, as shown in Table 1.

Figure 5 and Table 1 report the recovery quality of the proposed method on recovery Cuprite. The following observations are summarized: (1) of all evaluating indicators considered here, traditional Circulant had the worst performance in both subjective and objective evaluations; (2) since the introduction of Toeplitz, the performance gets major

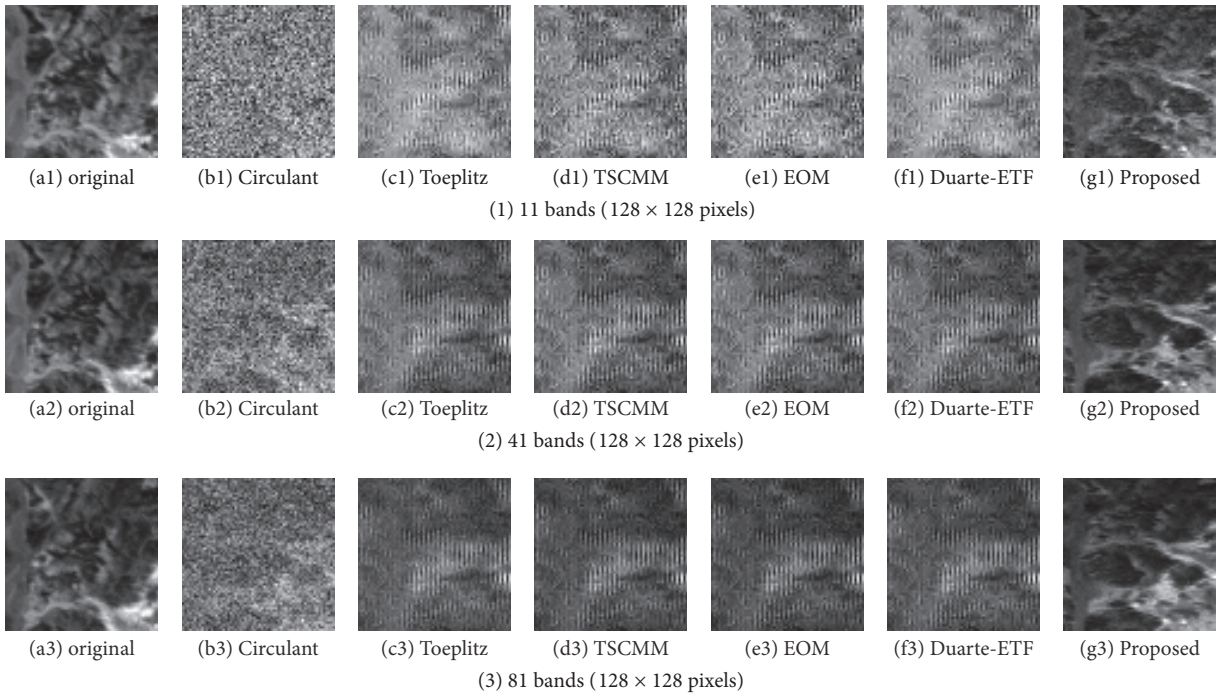

Figure 5: The subjective quality of different CS measurement matrices, from left to right: (a) original, (b) Circulant, (c) Toeplitz, (d) TSCMM, (e) EOM, (f) Duarte-ETF, and (g) proposed method.

Table 1: MSE and PSNR of different matrixes of recovery Cuprite.

Algorithm	11 bands (64 × 64 pixels)		41 bands (64 × 64 pixels)		81 bands (64 × 64 pixels)		
	PSNR	MSE	PSNR	MSE	PSNR	MSE	CT
Circulate	59.9634	0.0656	60.9680	0.0520	61.5821	0.0452	5.1070
Toeplitz	59.9634	0.0656	61.9375	0.0416	63.3173	0.0303	3.5506
TSCMM	60.0696	0.0640	61.9783	0.0412	63.3462	0.0301	**1.7624**
EOM	60.2806	0.0610	62.2337	0.0389	63.3962	0.0297	245.4345
Duarte-ETF	60.6304	0.0562	62.3788	0.0376	63.4082	0.0297	116.5994
Proposed	**64.3532**	**0.0239**	**63.8856**	**0.0266**	**63.7179**	**0.0276**	51.6191

improvement on image quality while improved Toeplitz-structured matrix method (TSCMM) is slightly better than classical Toeplitz matrix method; (3) EOM has significant performance in image quality; however, the optimization process is usually an iterative process, which is also a very complicated and time-consuming process; (4) Duarte-ETF has better contrast and lower computational complexity; (5) the proposed method takes advantage of improved Toeplitz-structured matrix to speed up the convergence speed and improve traditional optimization method to better recovery high-dimensional image. Experimental results show that the proposed method has a better overall performance.

4.2. Urban. University of California Santa Barbara (UCSB) built an urban spectral library for the Goleta/Santa Barbara area. The hyperspectral data of Urban were acquired between late May and early June, 2001, using an ASD full range instrument on loan from the Jet Propulsion Laboratory. These spectra of Urban are characterized by 499 roofs, 179 roads, 66 sidewalks, 56 parking lots, 40 road paints, 37 types of vegetation, 47 types of nonphotosynthetic vegetation, 88 bare soil and beach spectra, 27 acquired from tennis courts, and 50 more from miscellaneous surfaces.

Experiments on the hyperspectral data of Urban demonstrate that the proposed scheme substantially improves the reconstruction accuracy. Clearly it comes to the same conclusion from Figure 6 that, compared with the previous five methods, the effect of proposed approach is obviously superior to any other methods and is the most similar to original image.

To evaluate and compare the proposed method, the following performance indices, such as Average Gradient (AG), Edge-Intensity (EI), Figure Definition (FD), Gray Mean (GM), Standard Deviation (SD), Space Frequency (SF), Variance (VAR), and Structural Similarity (SSIM), were used. It shows that the objective evaluation indices enhance the experiment rigor and convincing. The results are shown in Table 2.

Table 2: Objective evaluation of typical methods and proposed method from recovery Urban.

Bands	Algorithm	The objective evaluation indices										
		AG	EI	FD	GM	SD	MSE	PSNR	SF	SSI	VAR	CT
11	Circulate	0.070476	0.48360	0.12231	0.4106	0.1197	0.0929	58.4508	0.2034	0.98826	0.11972	1.7379
	Toeplitz	0.047687	0.34172	0.10125	0.32796	0.1137	0.0610	60.2804	0.18949	0.99361	0.11366	1.8706
	TSCMM	0.054635	0.38647	0.11414	0.35344	0.1162	0.0686	59.7658	0.19866	0.99254	0.11624	**1.5146**
	EOM	0.056608	0.40032	0.11519	0.35809	0.1172	0.0708	59.6279	0.20025	0.99226	0.11720	305.1965
	Duarte-ETF	0.047687	0.34172	0.10125	0.32796	0.1137	0.0610	60.2804	0.18949	0.99361	0.11366	136.6804
	Proposed	**0.046138**	**0.29123**	**0.06690**	**0.23194**	**0.1197**	**0.0434**	**61.7586**	**0.11956**	**0.99537**	**0.11980**	16.5975
41	Circulate	0.072566	0.51888	0.12438	0.37371	0.1363	0.0631	60.1316	0.20690	0.99349	0.13626	1.6382
	Toeplitz	0.058448	0.41868	0.12772	0.40138	0.1390	0.0786	59.1767	0.22932	0.99207	0.13897	1.8069
	TSCMM	0.061306	0.43672	0.13128	0.39347	0.1362	0.0744	59.4172	0.22736	0.99259	0.13620	**1.5381**
	EOM	0.060340	0.43408	0.12941	0.40222	0.1353	0.0771	59.2609	0.22536	0.99215	0.13529	81.3160
	Duarte-ETF	0.062241	0.44182	0.13123	0.42482	0.1402	0.0873	58.7190	0.23610	0.99089	0.14018	59.7419
	Proposed	**0.050626**	**0.40358**	**0.07196**	**0.24426**	**0.1307**	**0.0452**	**61.5816**	**0.12782**	**0.99561**	**0.13068**	24.3532
81	Circulate	0.082530	0.6279	0.13639	0.49357	0.1449	0.0635	60.1019	0.22630	0.99397	0.14492	1.5829
	Toeplitz	0.077269	0.47993	0.14082	0.44812	0.1390	0.0535	60.8442	0.23904	0.99484	0.13905	1.8284
	TSCMM	0.070612	0.50737	0.14828	0.51106	0.1496	0.0716	59.5790	0.25291	0.99353	0.14958	**1.5702**
	EOM	0.070821	0.51006	0.14940	0.50827	0.1503	0.0707	59.6361	0.25447	0.99369	0.15030	97.3153
	Duarte-ETF	0.074147	0.52535	0.14946	0.48963	0.1499	0.0652	59.9890	0.25959	0.99450	0.14986	59.0915
	Proposed	**0.068955**	**0.42678**	**0.09339**	**0.40915**	**0.1571**	**0.0484**	**61.2814**	**0.16485**	**0.99580**	**0.15708**	28.7426

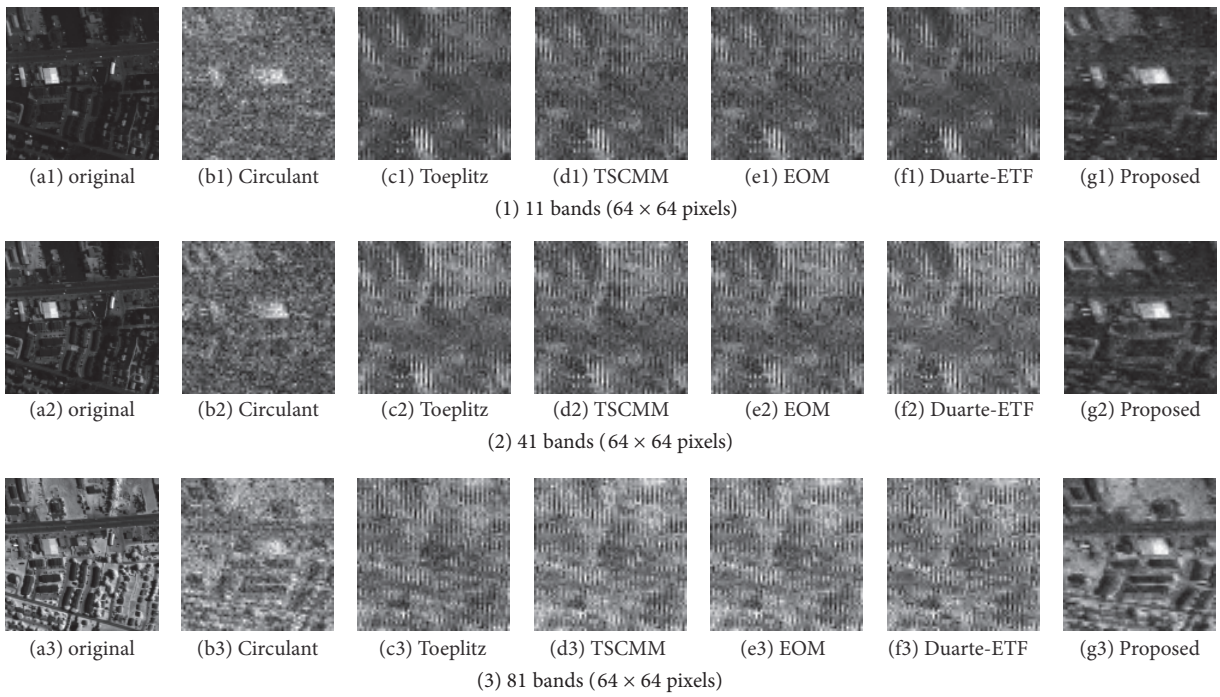

Figure 6: The subjective quality of different CS measurement matrices, from left to right: (a) original, (b) Circulant, (c) Toeplitz, (d) TSCMM, (e) EOM, (f) Duarte-ETF, and (g) proposed method.

The results of Table 2 show that the method has a higher performance than traditional Toeplitz or Circulant matrix method. Although improved Toeplitz-structured matrix method (TSCMM) is slightly better than classical Toeplitz, both classical optimization measurement matrix method (EOM) and proposed method have significant performance in image quality. Furthermore, the proposed method takes advantage of improved Toeplitz-structured matrix to speed up the convergence speed and improve traditional optimization method to recover better high-dimensional image. Experimental results show that the proposed method has a better overall performance.

4.3. Jasper Ridge. The hyperspectral image of Jasper Ridge was obtained on June 2, September 4, and October 6, 1992, which was calibrated to surface reflectance. The image was the most popular source to analyze with spectral mixture analysis using library endmembers representing green foliage, nonphotosynthetic vegetation, and soils characteristic of the site. Field-based vegetation was obtained from US Geological Service.

From Figure 7, it is obvious that the worst effects from traditional Circulant have reached being almost intolerable. While the results from TSCMM and Toeplitz are almost similar, the former has only slight improvement compared to the latter. On the other hand, the performance of the proposed approach was significantly improved compared to that of EOM or Duarte-ETF. The study concluded that the proposed approach had a significant performance compared to that of others. Furthermore, the objective evaluations are shown in Table 3. The results can be clearly seen from different methods on recovery Jasper Ridge.

The results of Table 3 show that the proposed method has a higher performance than traditional Toeplitz or Circulant matrix method. TSCMM takes advantage of improved Toeplitz-structured matrix to speed up the convergence speed and improve traditional Toeplitz or Circulant matrix method to recover better high-dimensional data. Although EOM has the lower column coherence and faster convergence, it weakens RIP condition and causes recovery performance degradation. While the absolute values from Duarte-ETF concentrate around mutual coherence, this can make the equivalent dictionary as close as possible to an ETF. But this algorithm has high computational complexity. Furthermore, experimental results from the proposed method show that the proposed method has a better overall performance.

4.4. Hyperspectral Unmixing. The fourth experiment performs an experimental evaluation of the accuracy of the standard hyperspectral unmixing districts known as Cuprite [28]. To reduce complexity, there are only 188 channels (3–103, 114–147, and 168–220 bands) that were remained due to dense water vapor and atmospheric effects. In the course of the experiment, the signal sparsity method is Fourier basis and reconstruction algorithm is StOMP.

The results are shown in Figure 8 for hyperspectral unmixing and closely resemble those obtained from hyperspectral data. Figure 8 compares the unmixing performance of the proposed method with different endmembers and the abundance from different endmembers is totally dissimilar.

Table 3: The objective evaluations of different matrixes of recovery Jasper Ridge.

Algorithm	11 bands (64 × 64)			81 bands (64 × 64)			151 bands (64 × 64)			
	SNR	PSNR	MSE	SNR	PSNR	MSE	SNR	PSNR	MSE	CT
Circulate	−6.0698	57.3412	0.1199	11.6699	60.0402	0.0644	3.3299	60.3823	0.0595	1.5304
Toeplitz	**24.7566**	**70.7289**	**0.0055**	29.4215	67.7497	0.0109	15.7386	65.7714	0.0172	1.5519
TSCMM	15.3473	66.6425	0.0141	33.9793	69.7291	0.0069	20.0693	67.6521	0.0112	**1.4869**
EOM	4.4853	61.9252	0.0417	35.0894	70.2112	0.0062	21.6750	68.3495	0.0095	78.8838
Duarte-ETF	**24.7566**	**70.7289**	**0.0055**	33.3205	69.4430	0.0074	17.2452	66.4257	0.0148	66.5711
Proposed	21.0504	69.1193	0.0080	**54.9719**	**78.8460**	**8.48e − 04**	**42.2277**	**77.2754**	**0.0012**	34.5743

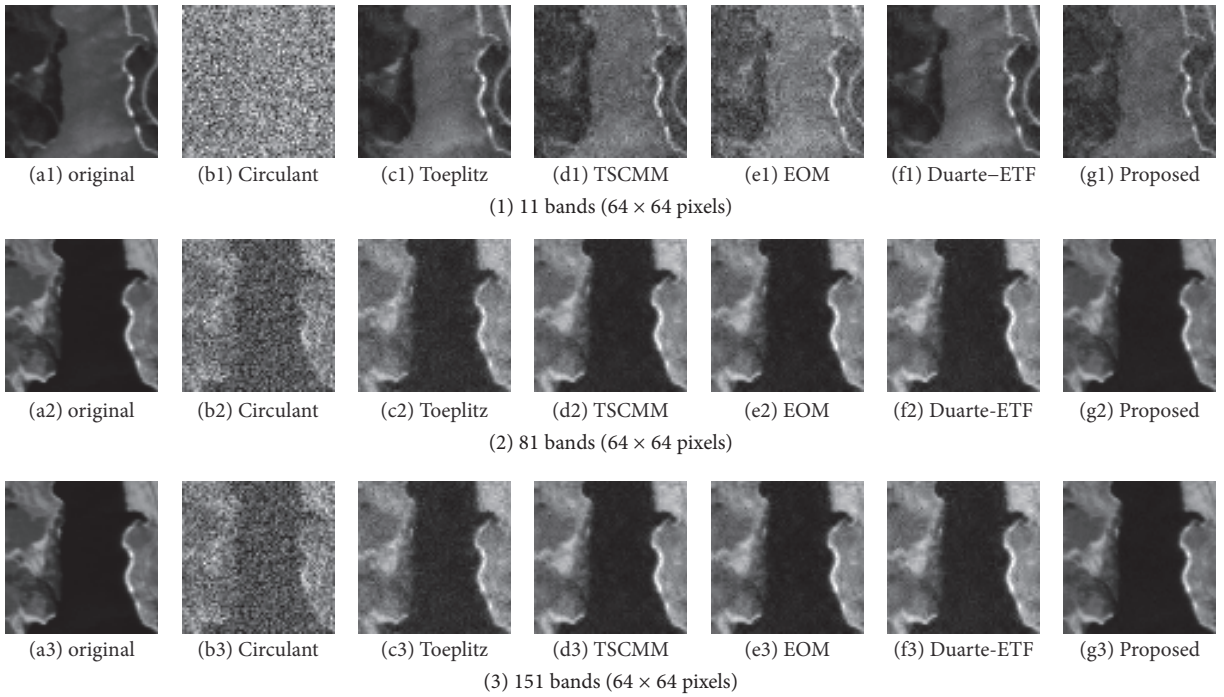

Figure 7: The subjective quality of different CS measurement matrices, from left to right: (a) original, (b) Circulant, (c) Toeplitz, (d) TSCMM, (e) EOM, (f) Duarte-ETF, and (g) proposed method.

These features from the proposed method ensure clear and accurate the abundances.

By accessing information from USGS Digital Spectral Library [29], the unmixing performance has been almost correct. Furthermore, different endmembers from USGS_1995_Library [30] are used to verify that the prediction model of hyperspectral unmixing scheme is accurate in Figure 8.

Apparently, the proposed unmixing results (blue thin thread) have a strong correlation with these endmembers (red thin thread) from USGS_1995_Library. From Figure 9(a), a steep sloping line from Alunite suggests that the unmixing endmember (blue thin thread) has remarkable similarity. This same conclusion has been made in studies from Figures 9(d)–9(h). On the other hand, the unsatisfied results from Figures 9(b) and 9(c) have been caused by smooth curve. The proposed method has good accuracy and is robust to traditional filtering, compression, cutting, and noise attack.

5. Conclusions

In this paper, to overcome the limitation of Toeplitz-structured chaotic measurement matrix, an improved measurement matrix has been carried out in the hyperspectral unmixing process to achieve multiple endmembers of hyperspectral image. And in theory, it proves that this matrix has retained the RIP property with overwhelming probability. Experimental results demonstrate that the proposed method to design of measurement matrix leads to better CS reconstruction performance with low extra computational cost. Compared with some traditional measurement matrix, an improved method has highest technical feasibility, lowest computational complexity, and least computation time consumption in the same recovery quality. The proposed method can take the special advantage in hyperspectral unmixing process and explore the practical satellite system to remote sensing.

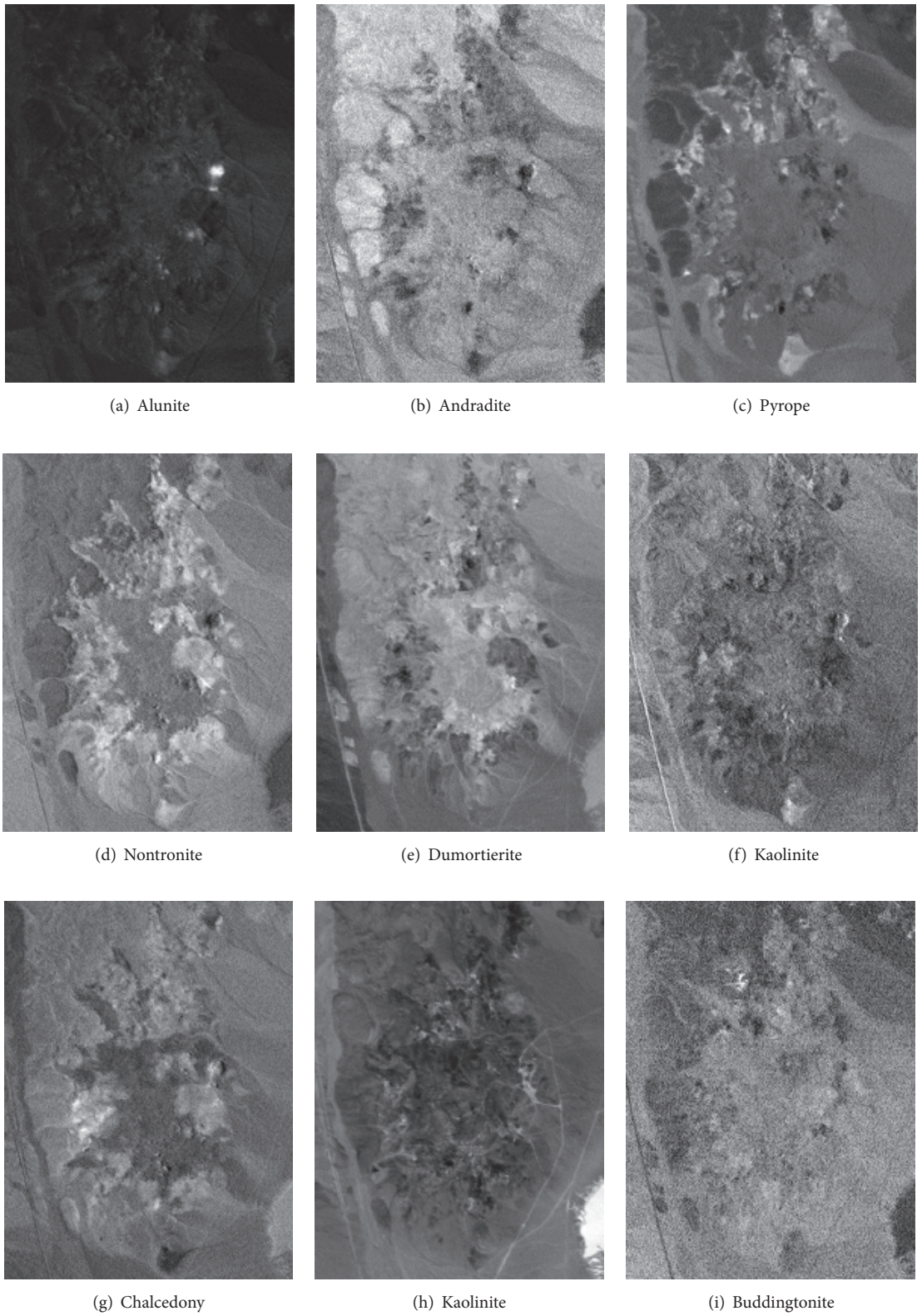

(a) Alunite (b) Andradite (c) Pyrope

(d) Nontronite (e) Dumortierite (f) Kaolinite

(g) Chalcedony (h) Kaolinite (i) Buddingtonite

Figure 8: The results from different elements abundance in hyperspectral unmixing schemes.

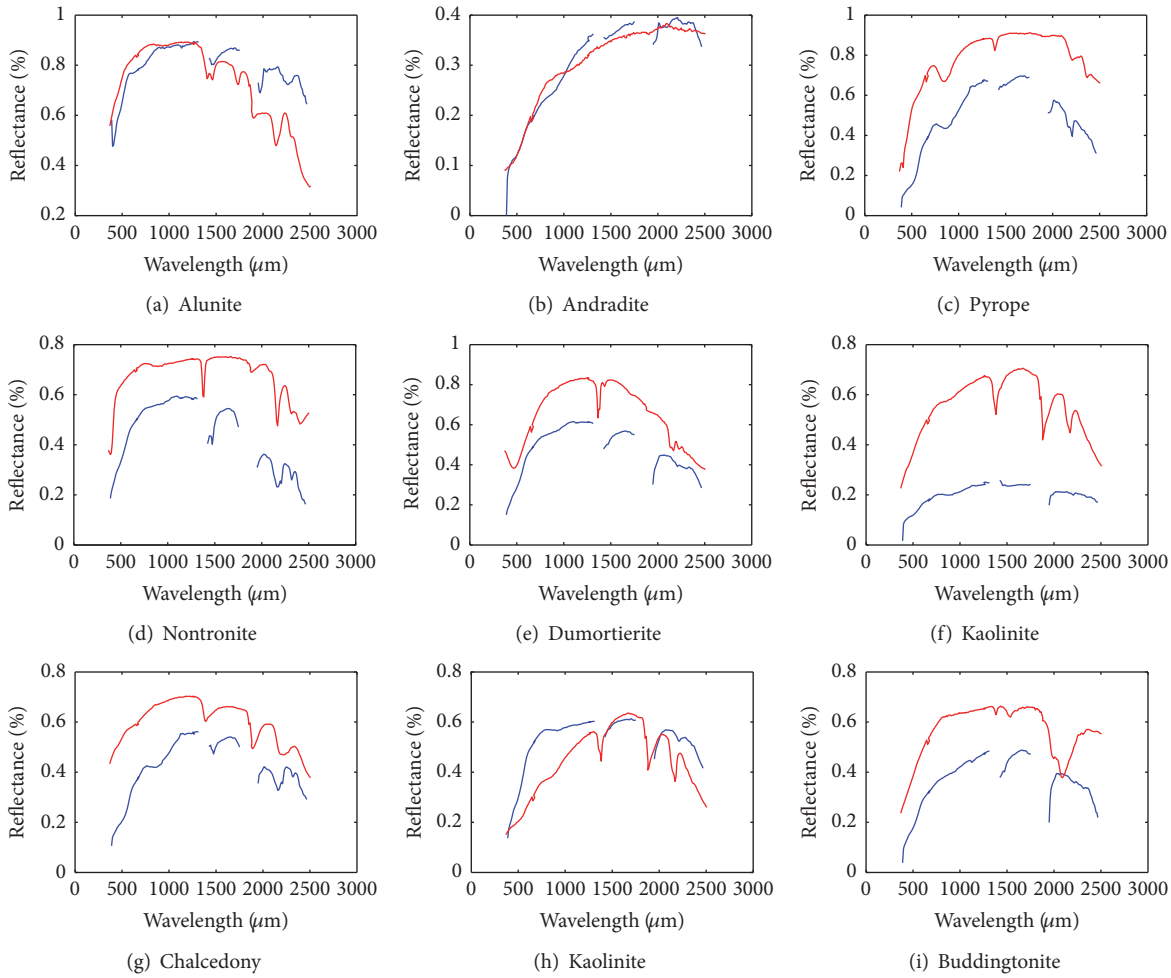

Figure 9: The comparison map between actual unmixing effect and endmember library.

Conflicts of Interest

The authors declare that they have no conflicts of interest.

Acknowledgments

This research is supported by Chongqing Engineering Laboratory for Detection, Control and Integrated System. The project is also funded by Key Technology Research and Industrialization of Fire Monitoring and Early Warning Sensor Network for High Voltage Transmission Line (KJZH17124). This research is funded by Chongqing Education Commission Foundation (KJ1400612). This project is also granted financial support from a Cooperative Project of Chongqing Technology and Business University (990516001).

References

[1] D. L. Donoho, "Compressed sensing," *Institute of Electrical and Electronics Engineers. Transactions on Information Theory*, vol. 52, no. 4, pp. 1289–1306, 2006.

[2] E. J. Candes, J. Romberg, and T. Tao, "Robust uncertainty principles: exact signal reconstruction from highly incomplete frequency information," *Institute of Electrical and Electronics Engineers. Transactions on Information Theory*, vol. 52, no. 2, pp. 489–509, 2006.

[3] T. N. Canh, K. D. Quoc, and B. Jeon, "Multi-resolution kronecker compressive sensing," *Transactions on Smart Processing & Computing*, vol. 3, no. 1, pp. 19–27, 2014.

[4] K. Q. Dinh, H. J. Shim, and B. Jeon, "Measurement coding for compressive imaging using a structural measuremnet matrix," in *2013 20th IEEE International Conference on Image Processing, ICIP 2013*, pp. 10–13, aus, September 2013.

[5] M. F. Duarte and R. G. Baraniuk, "Kronecker compressive sensing," *IEEE Transactions on Image Processing*, vol. 21, no. 2, pp. 494–504, 2012.

[6] B. Zhang, X. Tong, W. Wang, and J. Xie, "The research of Kronecker product-based measurement matrix of compressive sensing," *EURASIP Journal on Wireless Communications and Networking*, vol. 2013, article 161, pp. 1–5, 2013.

[7] M. Elad, "Optimized projections for compressed sensing," *IEEE Transactions on Signal Processing*, vol. 55, no. 12, pp. 5695–5702, 2007.

[8] M. Lustig, D. Donoho, and J. M. Pauly, "Sparse MRI: the application of compressed sensing for rapid MR imaging," *Magnetic Resonance in Medicine*, vol. 58, no. 6, pp. 1182–1195, 2007.

[9] V. Abolghasemi, S. Sanei, S. Ferdowsi, F. Ghaderi, and A. Belcher, "Segmented compressive sensing," in *Proceedings of the IEEE/SP 15th Workshop on Statistical Signal Processing (SSP '09)*, pp. 630–633, September 2009.

[10] J. M. Duarte-Carvajalino and G. Sapiro, "Learning to sense sparse signals: simultaneous sensing matrix and sparsifying dictionary optimization," *IEEE Transactions on Image Processing*, vol. 18, no. 7, pp. 1395–1408, 2009.

[11] Z. Wang, G. R. Arce, and J. L. Paredes, "Colored random projections for compressed sensing," in *2007 IEEE International Conference on Acoustics, Speech and Signal Processing, ICASSP '07*, pp. III873–III876, usa, April 2007.

[12] Z. Wang and G. R. Arce, "Variable density compressed image sampling," *IEEE Transactions on Image Processing*, vol. 19, no. 1, pp. 264–270, 2010.

[13] M. Elad and M. Aharon, "Image denoising via learned dictionaries and sparse representation," in *2006 IEEE Computer Society Conference on Computer Vision and Pattern Recognition, CVPR 2006*, pp. 895–900, usa, June 2006.

[14] M. Aharon, M. Elad, and A. Bruckstein, "K-SVD: an algorithm for designing overcomplete dictionaries for sparse representation," *IEEE Transactions on Signal Processing*, vol. 54, no. 11, pp. 4311–4322, 2006.

[15] J. Xu, Y. Pi, and Z. Cao, "Optimized projection matrix for compressive sensing," *EURASIP Journal on Advances in Signal Processing*, vol. 2010, Article ID 560349, 2010.

[16] V. Abolghasemi, S. Ferdowsi, and S. Sanei, "A gradient-based alternating minimization approach for optimization of the measurement matrix in compressive sensing," *Signal Processing*, vol. 92, no. 4, pp. 999–1009, 2012.

[17] Q. Zhang, Y. Fu, H. Li, and R. Rong, "Optimized projection matrix for compressed sensing," *Circuits, Systems, and Signal Processing*, vol. 33, no. 5, pp. 1627–1636, 2014.

[18] G. Li, Z. Zhu, D. Yang, L. Chang, and H. Bai, "On projection matrix optimization for compressive sensing systems," *IEEE Transactions on Signal Processing*, vol. 61, no. 11, pp. 2887–2898, 2013.

[19] S. Tian, X. Fan, and L. I. Zhetao, "Orthogonal-gradient measurement matrix construction algorithm," *Chinese Journal of Electronics*, vol. 25, no. 1, pp. 81–87, 2016.

[20] V. Abolghasemi, S. Ferdowsi, and B. Makkiabadi, "On optimization of the measurement matrix for compressive sensing," in *Signal Processing Conference*, European IEEE, Ed., pp. 427–431, August 2010.

[21] Q. Li, D. Schonfeld, and S. Friedland, "Generalized tensor compressive sensing," in *2013 IEEE International Conference on Multimedia and Expo, ICME 2013*, usa, July 2013.

[22] S. Friedland, Q. Li, and D. Schonfeld, "Compressive sensing of sparse tensors," *IEEE Transactions on Image Processing*, vol. 23, no. 10, pp. 4438–4447, 2014.

[23] S. u. Xu, H. Yin, C. Yi, Y. Xiong, and T. Xue, "An Improved Toeplitz Measurement Matrix for Compressive Sensing," *International Journal of Distributed Sensor Networks*, vol. 8, pp. 1–8, 2014.

[24] R. L. Devaney, in *Practical Numerical Algorithms for Chaotic Systems*, T. S. Parker and L. O. Chua, Eds., vol. 32, pp. 501–503, Siam Review, 3 edition, 2006.

[25] R. Baraniuk, M. Davenport, R. DeVore, and M. Wakin, "A simple proof of the restricted isometry property for random matrices," *Constructive Approximation. An International Journal for Approximations and Expansions*, vol. 28, no. 3, pp. 253–263, 2008.

[26] Available, http://www.escience.cn/people/feiyunZHU/Dataset_GT.html.

[27] D. L. Donoho, Y. Tsaig, I. Drori, and J.-L. Starck, "Sparse solution of underdetermined systems of linear equations by stagewise orthogonal matching pursuit," *Institute of Electrical and Electronics Engineers. Transactions on Information Theory*, vol. 58, no. 2, pp. 1094–1121, 2012.

[28] K. Lang, "NewsWeeder: Learning to Filter Netnews," in *International Machine Learning Conference*, vol. 1995, pp. 331–339.

[29] Available, http://featureselection.asu.edu/datasets.php.

[30] Available, http://clopinet.com/isabelle/Projects/NIPS/.

Hindawi
Journal of Control Science and Engineering
Volume 2017, Article ID 5249160, 7 pages
https://doi.org/10.1155/2017/5249160

Research Article

An Out Space Accelerating Algorithm for Generalized Affine Multiplicative Programs Problem

Lei Cai,[1] Shuai Tang,[2] Jingben Yin,[3] Zhisong Hou,[1] and Hongwei Jiao[3]

[1]*School of Information Engineering, Henan Institute of Science and Technology, Xinxiang 453003, China*
[2]*Jiyuan Vocational and Technical College, Jiyuan 459000, China*
[3]*School of Mathematical Sciences, Henan Institute of Science and Technology, Xinxiang 453003, China*

Correspondence should be addressed to Lei Cai; cailei2014@126.com and Jingben Yin; jingbenyin@163.com

Received 18 February 2017; Accepted 4 May 2017

Academic Editor: Qiang Song

This paper presents an out space branch-and-bound algorithm for solving generalized affine multiplicative programs problem. Firstly, by introducing new variables and constraints, we transform the original problem into an equivalent nonconvex programs problem. Secondly, by utilizing new linear relaxation technique, we establish the linear relaxation programs problem of the equivalent problem. Thirdly, based on the out space partition and the linear relaxation programs problem, we construct an out space branch-and-bound algorithm. Fourthly, to improve the computational efficiency of the algorithm, an out space reduction operation is employed as an accelerating device for deleting a large part of the investigated out space region. Finally, the global convergence of the algorithm is proved, and numerical results demonstrate the feasibility and effectiveness of the proposed algorithm.

1. Introduction

The generalized affine multiplicative programs problem (GAMP) arises naturally in many practical applications including management science, engineering optimization design, optimal control, Euclidean geometry, economic planning, production planning, and combinatorial mathematics [1, 2]. The problem (GAMP) usually contains many local optimum points which are not global optimum solution, so that important theoretical difficulties and computational complexities exist. Therefore, it is very necessary to establish an effective algorithm for globally solving the problem (GAMP).

The mathematical modelling of the generalized affine multiplicative programs problem is given as follows:

$$\begin{aligned} v = \max \quad & f(y) = \sum_{i=1}^{p} \left(\sum_{j=1}^{n} c_{ij} y_j + d_i \right) \left(\sum_{j=1}^{n} e_{ij} y_j + f_i \right) \\ \text{s.t.} \quad & y \in Y = \{ y \mid Ay \le b \}, \end{aligned} \tag{GAMP}$$

where $p \ge 2$, $c_{ij}, e_{ij}, d_i, f_i \in R$, $i = 1, \ldots, p$, $j = 1, \ldots, n$.

In the last decades, many algorithms have been intended for solving the generalized linear multiplicative programming problem, such as parametric simplex algorithms [3, 4], quadratic programming algorithms [5–9], rectangle branch-and-bound algorithms [10, 11], approximate algorithms [12, 13], finite algorithm [14], outcome space algorithm [15], cutting plane algorithm [16], heuristic algorithm [17], monotonic

optimization algorithms [18, 19], and simplicial branch-and-bound algorithm [20]. Although there exist some algorithms which can be used to solve the generalized linear multiplicative programming problem, as far as we know, it is still necessary to propose a more efficient algorithm for globally solving (GAMP).

In this paper, we shall present an effective algorithm for globally solving (GAMP). First of all, we transform (GAMP) into an equivalent problem (EQ). Secondly, by utilizing the new linear relaxation technique, we systematically convert (EQ) into a series of linear relaxation programs problems, which can infinitely approximate the global optimal solution of (EQ) by a successive partition. Thirdly, based on the out space partition and the linear relaxation programs problem, we construct an out space branch-and-bound algorithm. In this algorithm, the proposed branching operation takes place in R^p, rather than R^n or R^{2p}; this economizes the required computation. Fourthly, to improve the computational efficiency of the algorithm, an out space reduction operation is employed as an accelerating device for deleting a large part of the investigated out space region. Finally, the global convergence of the algorithm is proved, and numerical experimental results demonstrate the feasibility and effectiveness of the proposed algorithm.

This paper is organized as follows. In Section 2, by introducing new variables and constraints, we establish the equivalent problem (EQ) of the initial problem (GAMP). Next, by utilizing the linearization technique, we derive the linear relaxation programming problem of (EQ), which can provide a reliable upper bound for the global optimal value of the (EQ). In Section 3, an out space region reduction operation is introduced, and by combining this operation with bounding technique, an out space accelerating branch-and-bound algorithm is established and its global convergence is proved. Section 4 presents the numerical experimental results obtained by solving some test examples. Finally, the some concluding remarks of this paper are elaborated.

2. Equivalent Problem and Its Linear Relaxation

In this section, we will convert the problem (GAMP) into an equivalent nonconvex problem (EQ). Since $\sum_{j=1}^{n} c_{ij}y_j + d_i$ and $\sum_{j=1}^{n} e_{ij}y_j + f_i$ are all finite affine functions defined in Y, there exist positive constant numbers M_i and N_i such that $\sum_{j=1}^{n} c_{ij}y_j + d_i + M_i > 0$ and $\sum_{j=1}^{n} e_{ij}y_j + f_i + N_i > 0$ for any $y \in Y$. Therefore, in the following, without loss of generality, we can assume that $\sum_{j=1}^{n} c_{ij}y_j + d_i \geq 0$ and $\sum_{j=1}^{n} e_{ij}y_j + f_i \geq 0$ for all $y \in Y$.

Without loss of generality, we let

$$L_i^0 = \min_{y\in Y}\left(\sum_{j=1}^{n} e_{ij}y_j + f_i\right),$$
$$U_i^0 = \max_{y\in Y}\left(\sum_{j=1}^{n} e_{ij}y_j + f_i\right), \quad i = 1,\ldots,p. \tag{1}$$

Define the set $Z^0 = \{z \in R^p \mid L_i^0 \leq z_i \leq U_i^0,\ i = 1,\ldots,p\}$. For any $y \in Y$ and $z \in Z^0$, define the function $g(y,z) = \sum_{i=1}^{p}[z_i(\sum_{j=1}^{n} c_{ij}y_j + d_i)]$, and consider the following equivalent problem:

$$\begin{aligned} \max \quad & g(y,z) = \sum_{i=1}^{p}\left[z_i\left(\sum_{j=1}^{n} c_{ij}y_j + d_i\right)\right] \\ \text{s.t.} \quad & \sum_{j=1}^{n} e_{ij}y_j + f_i - z_i \geq 0, \quad i = 1,\ldots,p, \\ & y \in Y, \\ & z \in Z^0. \end{aligned} \tag{EQ}$$

Obviously, if (y^*, z^*) is a global optimal solution for (EQ), then y^* is a global optimal solution for (GAMP), and $z_i^* = \sum_{j=1}^{n} e_{ij}y_j^* + f_i, i = 1,\ldots,p$. If y^* is a global optimal solution for (GAMP), then (y^*, z^*) is a global optimal solution for (EQ), where $z_i^* = \sum_{j=1}^{n} e_{ij}y_j^* + f_i, i = 1,\ldots,p$.

In the following, the main computation is to globally solve (EQ). Next, we will construct the linear relaxation programs problem of (EQ), which can provide the upper bounds for (EQ) in the proposed branch-and-bound algorithm. Assume that $Z = \{z \in R^p \mid L_i \leq z_i \leq U_i,\ i = 1,\ldots,p\} \subseteq Z^0$. And without loss of generality, let

$$\begin{aligned} T_i^+ &= \left\{j \mid c_{ij} \geq 0,\ j = 1,\ldots,n\right\}, \\ T_i^- &= \left\{j \mid c_{ij} < 0,\ j = 1,\ldots,n\right\}, \\ D_i^+ &= \left\{i \mid d_i \geq 0,\ i = 1,\ldots,p\right\}, \\ D_i^- &= \left\{i \mid d_i < 0,\ i = 1,\ldots,p\right\}. \end{aligned} \tag{2}$$

Then the linear relaxation programs (U_Z) of (EQ) in Z can be given as follows:

$$\begin{aligned} u_Z = \max \quad & \sum_{i=1}^{p}\left(\sum_{T_i^+} U_i c_{ij}y_j + \sum_{T_i^-} L_i c_{ij}y_j\right) + \sum_{D_i^+} U_i d_i \\ & + \sum_{D_i^-} L_i d_i \\ \text{s.t.} \quad & L_i - \left(\sum_{j=1}^{n} e_{ij}y_j + f_i\right) \leq 0, \quad i = 1,\ldots,p, \\ & y \in Y, \end{aligned} \tag{U_Z}$$

where (EQ) in Z is defined by

$$\begin{aligned} v_Z = \max \quad & g(y,z) = \sum_{i=1}^{p} z_i\left(\sum_{j=1}^{n} c_{ij}y_j + d_i\right) \\ \text{s.t.} \quad & \left(\sum_{j=1}^{n} e_{ij}y_j + f_i\right) - z_i \geq 0, \\ & \qquad i = 1,\ldots,p, \\ & y \in Y, \\ & z \in Z \subseteq Z^0. \end{aligned} \tag{EQ_Z}$$

Theorem 1. *(i) For any $Z \subseteq Z^0$, one has $u_Z \geq v_Z$. (ii) If $\overline{Z} = \{z \in R^p \mid \overline{L} \leq z \leq \overline{U}\} \subseteq Z$ and $\overline{Z} \neq \emptyset$, then $u_{\overline{Z}} \leq u_Z$.*

Proof. (i) If $v_Z = -\infty$, then we can easily obtain $u_Z = -\infty$; it is obvious that $u_Z \geq v_Z$, if v_Z is finite and achieved. Denote by $(\overline{y}, \overline{z})$ a global optimal solution for (EQ_Z). Then $\overline{y} \in Y, \overline{z} \in Z$. For each $i \in \{1, \ldots, p\}$, we have $L_i \leq \overline{z}_i \leq U_i$. Therefore, we have

$$\sum_{i=1}^{p} \overline{z}_i \left(\sum_{j=1}^{n} c_{ij} \overline{y}_j + d_i \right) \leq \sum_{i=1}^{p} \left(\sum_{T_i^+} U_i c_{ij} \overline{y}_j + \sum_{T_i^-} L_i c_{ij} \overline{y}_j \right) + \sum_{D_i^+} U_i d_i + \sum_{D_i^-} L_i d_i. \tag{3}$$

Since $(\overline{y}, \overline{z})$ is a global optimal solution for (EQ_Z), it follows that

$$v_Z = \sum_{i=1}^{p} \overline{z}_i \left(\sum_{j=1}^{n} c_{ij} \overline{y}_j + d_i \right). \tag{4}$$

Since $\overline{y}$ is a feasible solution for (U_Z),

$$u_Z \geq \sum_{i=1}^{p} \left(\sum_{T_i^+} U_i c_{ij} \overline{y}_j + \sum_{T_i^-} L_i c_{ij} \overline{y}_j \right) + \sum_{D_i^+} U_i d_i + \sum_{D_i^-} L_i d_i. \tag{5}$$

By the above discussions, we have $u_Z \geq v_Z$.

(ii) Let $\overline{Z} = \{z \in R^p \mid \overline{L} \leq z \leq \overline{U}\} \subseteq Z$ and $\overline{Z} \neq \emptyset$; we have the following conclusions.

If (U_Z) is infeasible, then we can easily prove that $(U_{\overline{Z}})$ is also infeasible; the conclusion is obvious.

If (U_Z) is feasible, since Y is compact set, then u_Z is finite. If $(U_{\overline{Z}})$ is infeasible, then $u_{\overline{Z}} = -\infty < u_Z$. Thus, in the following, we assume that $(U_{\overline{Z}})$ is feasible, then $u_{\overline{Z}}$ is finite, and there exists a point $\overline{y} \in Y$ such that $\overline{L}_i \leq \sum_{j=1}^{n} e_{ij} \overline{y}_j + f_i$, $i = 1, \ldots, p$. And

$$u_{\overline{Z}} = \sum_{i=1}^{p} \left(\sum_{T_i^+} \overline{U}_i c_{ij} \overline{y}_j + \sum_{T_i^-} \overline{L}_i c_{ij} \overline{y}_j \right) + \sum_{D_i^+} \overline{U}_i d_i + \sum_{D_i^-} \overline{L}_i d_i. \tag{6}$$

By $\overline{Z} \subseteq Z$, we have $0 < L_i \leq \overline{L}_i \leq \overline{U}_i \leq U_i$, $i = 1, \ldots, p$. It follows that $\overline{y}$ is a feasible solution of problem (U_Z) and

$$u_{\overline{Z}} \leq \sum_{i=1}^{p} \left(\sum_{T_i^+} U_i c_{ij} \overline{y}_j + \sum_{T_i^-} L_i c_{ij} \overline{y}_j \right) + \sum_{D_i^+} U_i d_i + \sum_{D_i^-} L_i d_i. \tag{7}$$

Since $\overline{y}$ is a feasible solution of (U_Z), we have

$$u_Z \geq \sum_{i=1}^{p} \left(\sum_{T_i^+} U_i c_{ij} \overline{y}_j + \sum_{T_i^-} L_i c_{ij} \overline{y}_j \right) + \sum_{D_i^+} U_i d_i + \sum_{D_i^-} L_i d_i. \tag{8}$$

By the above discussions, we have $u_Z \geq u_{\overline{Z}}$, and the proof is completed. □

By Theorem 1, (U_Z) can provide the valid upper bound for (EQ_Z).

3. Algorithm and Its Convergence

In this section, we shall present a branch-and-bound algorithm for solving (EQ). The critical operation in guaranteeing the global convergence of the proposed algorithm is the selection of a suitable branching technique. In this paper, we choose a simple bisection method. For any selected rectangle $\widehat{Z} = \{z \in R^p \mid \widehat{L}_i \leq z_i \leq \widehat{U}_i,\ i = 1, \ldots, p\} \subseteq Z^0$, this branching rule is given as follows:

(1) Let $\widehat{U}_k - \widehat{L}_k = \max\{\widehat{U}_i - \widehat{L}_i \mid i = 1, \ldots, p\}$.

(2) Let

$$\begin{aligned} \widehat{Z}_1 &= \left\{ z \in R^p \mid \widehat{L}_i \leq z_i \leq \widehat{U}_i,\ i = 1, \ldots, p,\ i \neq k;\ \widehat{L}_k \leq z_k \leq \frac{1}{2}\left(\widehat{L}_k + \widehat{U}_k\right) \right\}, \\ \widehat{Z}_2 &= \left\{ z \in R^p \mid \widehat{L}_i \leq z_i \leq \widehat{U}_i,\ i = 1, \ldots, p,\ i \neq k;\ \frac{1}{2}\left(\widehat{L}_k + \widehat{U}_k\right) \leq z_k \leq \widehat{U}_k \right\}. \end{aligned} \tag{9}$$

3.1. New Region Reduction Operation. For any rectangle $Z^k \subseteq Z^0$, during the process of iteration, we want to recognize whether or not Z^k contains a global optimal solution of (EQ). The proposed new reduction operation aims at replacing the rectangle $Z^k = [L^k, U^k]$ with a smaller rectangle $Z' = [L', U']$ without deleting any global optimal solution of (EQ).

Without loss of generality, we can assume that LB^k is a known lower bound of the optimal value for $\mathrm{EQ}(Z^0)$ and that $v(Z)$ is the maximum value of $g(y, z)$ over Z and Y, and let

$$\begin{aligned} l_i^0 &= \min_{y \in Y} \left(\sum_{j=1}^{n} c_{ij} y_j + d_i \right), \quad i = 1, 2, \ldots, p, \\ u_i^0 &= \max_{y \in Y} \left(\sum_{j=1}^{n} c_{ij} y_j + d_i \right), \quad i = 1, 2, \ldots, p, \\ RUB^k &= \sum_{i=1}^{p} u_i^0 U_i^k, \\ \rho_i^k &= \frac{LB^k - RUB^k + u_i^0 U_i^k}{u_i^0}, \quad i = 1, 2, \ldots, p. \end{aligned} \tag{10}$$

Theorem 2. *For any subrectangle $Z^k = (Z_i^k)_{p \times 1} = [L_i^k, U_i^k]_{p \times 1} \subseteq Z^0$, the following conclusions hold:*

(i) *If $RUB^k < LB^k$, then there is no global optimal solution of $EQ(Z^0)$ over Z^k.*

(ii) *If* $RUB^k \geq LB^k$*, then, for each* $s \in \{1, 2, \ldots, p\}$*, there is no global optimal solution of the* EQ(Z^0) *over* $\underline{Z}^k$*, where*

$$\underline{Z}^k = \left(\underline{Z}_i^k\right)_{p\times 1} \subseteq Z^0$$

$$\text{with } \underline{Z}_i^k = \begin{cases} Z_i^k, & i \neq s,\ i = 1, 2, \ldots, p, \\ \left[L_i^k, \rho_i^k\right) \cap Z_i^k & i = s \in \{1, 2, \ldots, p\}. \end{cases} \tag{11}$$

Proof. (i) If $RUB^k < LB^k$, then we have

$$\begin{aligned} v\left(Z^k\right) &= \max_{z\in Z^k, y\in Y} \sum_{i=1}^{p} \left(\sum_{j=1}^{n} c_{ij} y_j + d_i\right) z_i \\ &\leq \sum_{i=1}^{p} \max_{z\in Z^k, y\in Y} \left[\left(\sum_{j=1}^{n} c_{ij} y_j + d_i\right) z_i\right] = \sum_{i=1}^{p} u_i^0 U_i^k \\ &= RUB^k < LB^k. \end{aligned} \tag{12}$$

Therefore, there exists no global optimal solution of the problem EQ(Z^0) over Z^k.

(ii) If $RUB^{\mathrm{k}} \geq LB^k$, then we have the following conclusions.

For each $s \in \{1, 2, \ldots, p\}$, for any $y \in Y$ and $z \in \underline{Z}^k$, and for each $i = 1, 2, \ldots, p$, since

$$\begin{aligned} &0 \leq l_i^0 \leq \sum_{j=1}^{n} c_{ij} y_j + d_i \leq u_i^0, \\ &0 \leq L_i^k \leq z_i \leq U_i^k, \qquad i \neq s, \\ &0 \leq L_s^k \leq z_s \leq \rho_s^k, \quad i = s, \end{aligned} \tag{13}$$

we have

$$\begin{aligned} v\left(\underline{Z}^k\right) &= \max_{z\in \underline{Z}^k, y\in Y} \left[\sum_{i=1}^{p} \left(\sum_{j=1}^{n} c_{ij} y_j + d_i\right) z_i\right] \\ &\leq \max_{z\in \underline{Z}^k, y\in Y} \left[\sum_{i=1, i\neq s}^{p} \left(\sum_{j=1}^{n} c_{ij} y_j + d_i\right) z_i\right] \\ &\quad + \max_{z\in \underline{Z}^k, y\in Y} \left[\left(\sum_{j=1}^{n} c_{sj} y_j + d_s\right) z_s\right] \\ &< \sum_{i=1, i\neq s}^{p} u_i^0 U_i^k + u_s^0 \rho_s^k \\ &= RUB^k - u_s^0 U_s^k + LB^k - \left(RUB^k - u_s^0 U_s^k\right) \\ &= LB^k. \end{aligned} \tag{14}$$

Therefore, there exists no global optimization solution of EQ(Z^0) over $\underline{Z}^k$. □

By Theorem 2, we can construct a new reduction operation to cut away a part of region in which the global optimal solution of (EQ) does not exist. Assuming that a subrectangle

$$Z^k = \left(Z_i^k\right)_{p\times 1} \subseteq Z^0 \quad \text{with } Z_i^k = \left[L_i^k, U_i^k\right] \tag{15}$$

will be compressed, then, according to Theorem 2, the original rectangle Z^k should be replaced with a new subrectangle:

$$\begin{aligned} &Z' = \left(Z_i'\right)_{p\times 1} \\ &\text{with } Z_i' = \left[\rho_i^k, U_i^k\right] \cap Z_i^k,\ i \in \{1, 2, \ldots, p\}. \end{aligned} \tag{16}$$

Let $UB(Z^k)$ be the optimal value of (U_Z) in Z^k; the basic steps of the proposed algorithm are summarized as follows.

3.2. Algorithm Steps

Step 0. Initialize the iteration counter $k = 0$, the active node set $\Omega_0 = \{Z^0\}$, the lower bound $LB_0 = -\infty$, and the feasible points set $F = \emptyset$.

Solve (U_{Z^0}); obtain u_{Z^0} and $y(Z^0)$. Set $UB_0 = UB(Z^0) = u_{Z^0}$, $y^c = y(Z^0)$, and set $z_i^c = \sum_{j=1}^{n} e_{ij} y_j^c + f_i$ $(i = 1, 2, \ldots, p)$, $LB_0 = g(y^c, z^c)$. Update $F = F \cup \{(y^c, z^c)\}$.

If $UB_0 - LB_0 \leq \epsilon$, then the algorithm stops with (y^c, z^c) and y^c as global optimal solutions of (EQ) and (GAMP), respectively. Otherwise, proceed to next step.

Step 1. Use the proposed reduction operation to compress the investigated rectangle Z^k, and still represent remaining part of the rectangle as Z^k.

Step 2. Subdivide Z^k into two subrectangles; denote by Θ_k its partitioning set.

For each $Z \in \Theta_k$, solve (U_Z) to obtain $UB(Z) = u_Z$ and $y(Z)$. If $UB(Z) < LB_k$, then remove the subrectangle Z from Θ_k, that is, $\Theta_k := \Theta_k \setminus Z$, and skip to next element of Θ_k.

If $\Theta_k = \emptyset$, set $LB_{k+1} = LB_k$, and go to Step 3. Otherwise, set $z_i^c = z_i(Z) = \sum_{j=1}^{n} e_{ij} y_j(Z) + f_i$, $i = 1, 2, \ldots, p$, update $F = F \cup \{(y(Z), z(Z))\}$, set $LB_{k+1} = \max_{(y,z)\in F} g(y, z)$, and denote by $(y^c, z^c) = \operatorname{argmax}_{(y,z)\in F} g(y, z)$ the best known feasible point.

Step 3. Denote by $\Omega_{k+1} = (\Omega_k \setminus Z^k) \cup \Theta_k$ the remaining partition set. We can obtain a new upper bound $UB_k := \inf_{Z\in\Omega_{k+1}} UB(Z)$.

Step 4. Fathom any nonimproving nodes by setting $\Omega_{k+1} = \Omega_k \setminus \{Z : UB(Z) - LB \leq \epsilon,\ Z \in \Omega_k\}$. If $\Omega_{k+1} = \emptyset$, then stop: LB is the optimal value of (EQ), and y^c is a global ϵ-optimal solutions for (GAMP). Otherwise, set $k = k + 1$ and return to Step 1.

3.3. Convergence of the Algorithm. In this subsection, the convergence of the algorithm is given.

Theorem 3. *If the algorithm is finite, upon termination, we can obtain the* ϵ*-global optimal solutions for the problems* (EQ) *and*

(GAMP), *respectively. If the algorithm is infinite, for each* $k \geq 0$, *denote by* y^k *the incumbent solution of* (GAMP), *which is found at the end of iteration* k. *Then,* $\lim_{k\to\infty} y^k = y^*$ *will a global optimal solution for* (GAMP).

Proof. If the algorithm is finite, then the algorithm terminates at iteration k, $k \geq 0$. By the termination condition of the algorithm and the updating method of the upper bound, it can follow easily that the conclusion is obvious.

If the algorithm is infinite, then, it generates a sequence of incumbent solutions for problem (EQ), which may be denoted by $\{(y^k, z^k)\}$. For each $k \geq 1$, (y^k, z^k) is found by solving problem (U_{Z^k}), for some rectangle $Z^k \subseteq Z^0$, for an optimal solution $y^k \in Y$, and setting $z_i^k = \sum_{j=1}^n e_{ij} y_j^k + f_i$, $i = 1, \ldots, p$. Therefore, the sequence $\{y^k\}$ consists of feasible solutions for problem (GAMP). Let y^* be an accumulation point of $\{y^k\}$, and without loss of generality we assume that $\lim_{k\to\infty} y^k = y^*$. Then, since Y is a compact set, $y^* \in Y$. Furthermore, since $\{y^k\}$ is infinite, we may assume without loss of generality that, for each k, $Z^{k+1} \subseteq Z^k$. Since the rectangles Z^k, $k \geq 1$, are formed by rectangular bisection, this implies that, for some point $z^* \in R^p$, we have

$$\lim_{k\to\infty} Z^k = \bigcap_k Z^k = \{z^*\}. \tag{17}$$

Let $Z^* = \{z^*\}$ and, for each k, let Z^k be given by

$$Z^k = \left\{z \in R^p \mid L^k \leq z \leq U^k\right\}. \tag{18}$$

For each k, from Step 2 of the algorithm,

$$UB\left(Z^k\right) = u_{Z^k}. \tag{19}$$

Since $Z^{k+1} \subset Z^k \subseteq Z^0$, for each k, by Theorem 1 and Step 4, this implies that $\{UB(Z^k)\}$ is a nonincreasing sequence bounded by v. Therefore, $\lim_{k\to\infty} UB(Z^k)$ is a finite number and satisfies

$$\lim_{k\to\infty} UB\left(Z^k\right) \geq v. \tag{20}$$

For each k, from Step 1, $UB(Z^k)$ is equal to the optimal value of problem (U_{Z^k}) given by

$$\begin{aligned} \max \quad & \sum_{i=1}^p \left(\sum_{T_i^+} U_i^k c_{ij} y_j + \sum_{T_i^-} L_i^k c_{ij} y_j \right) + \sum_{D_i^+} U_i^k d_i \\ & + \sum_{D_i^-} L_i^k d_i \\ \text{s.t.} \quad & L_i^k - \left(\sum_{j=1}^n e_{ij} y_j + f_i \right) \leq 0, \quad i = 1, \ldots, p, \\ & y \in Y, \end{aligned} \tag{U_{Z^k}}$$

and y^k is an optimal solution for this problem. By the branching technique, we have

$$\lim_{k\to\infty} L^k = \lim_{k\to\infty} U^k = \{z^*\} = Z^*. \tag{21}$$

Since $\lim_{k\to\infty} y^k = y^*$, $L_i^k \leq \sum_{j=1}^n e_{ij} y_j^k + f_i \leq U_i^k$ and the continuity of $(\sum_{j=1}^n e_{ij} y_j + f_i)$, for each $i = 1, \ldots, p$, $\sum_{j=1}^n e_{ij} y_j^* + f_i = z_i^*$. This implies that (y^*, z^*) is a feasible solution for (EQ). Therefore, $g(y^*, z^*) \leq v$. Combing (20), we obtain that

$$g\left(y^*, z^*\right) \leq v \leq \lim_{k\to\infty} UB\left(Z^k\right), \tag{22}$$

since

$$\begin{aligned} \lim_{k\to\infty} UB\left(Z^k\right) &= \lim_{k\to\infty} \left(\sum_{i=1}^p \left(\sum_{T_i^+} U_i^k c_{ij} y_j^k + \sum_{T_i^-} L_i^k c_{ij} y_j^k \right) \right. \\ &\quad \left. + \sum_{D_i^+} U_i^k d_i + \sum_{D_i^-} L_i^k d_i \right) = \sum_{i=1}^p z_i^* \left(\sum_{j=1}^n c_{ij} y_j^* + d_i \right) \\ &= g\left(y^*, z^*\right). \end{aligned} \tag{23}$$

From (22) and (23), since $UB(Z^k) = UB_k$, we have $\lim_{k\to\infty} UB_k = v = g(y^*, z^*)$. Therefore, (y^*, z^*) is a global optimal solution for (EQ). By Theorem 1, this implies that y^* is a global optimal solution for (GAMP). The proof is complete. □

4. Numerical Experiments

To verify the performance of the proposed algorithm, some test problems are implemented on an Intel(R) Core(TM)2 Duo CPU (1.58 GHZ) microcomputer. The algorithm is coded in C++, and each linear programs problem is solved by simplex method in our experiments. These test problems are given in the following, and their numerical results are listed in Tables 1 and 2.

Example 1 (see [14]). One has

$$\begin{aligned} \max \quad & (3y_1 + 5y_2 + 3y_3 + 50) \\ & \times (3y_1 + 4y_2 + 5y_3 + 50) + (3y_1 + 4y_2 + 50) \\ & \times (4y_1 + 3y_2 + 2y_3 + 50) \\ & + (4y_1 + 2y_2 + 4y_3 + 50) \\ & \times (5y_1 + 4y_2 + 3y_3 + 50) \\ \text{s.t.} \quad & 6y_1 + 3y_2 + 3y_3 \leq 10, \\ & 10y_1 + 3y_2 + 8y_3 \leq 10, \\ & y_1, y_2, y_3 \geq 0. \end{aligned} \tag{24}$$

Table 1: Computational results of Examples 1 and 2.

Example	Ref.	Optimal solution	Optimal value	Iteration	ϵ	Time(s)
Example 1	This paper	(0, 3.33333, 0)	11611.1	2	10^{-6}	0.0065
	[14]	(0, 3.33333, 0)	11611.1	2	10^{-6}	0.0074
Example 2	This paper	(0, 0.625, 1.875)	14214.8	1	10^{-6}	0.0198
	[14]	(0, 0.625, 1.875)	14214.8	2	10^{-6}	0.0228

Table 2: Numerical results for Example 3.

n	p	Time(s)
10	10	0.0285
20	10	0.0192
30	10	0.0279
30	30	0.0590
30	40	0.1102
30	50	0.0945
35	50	0.1283
40	50	0.2423
50	50	0.2899

Example 2 (see [14]). One has

$$\begin{aligned}
\max\quad & (4y_1 + 3y_2 + 3y_3 + 50) \times (3y_2 + 3y_3 + 50) \\
& + (3y_1 + 4y_3 + 50) \times (4y_1 + 4y_2 + 5y_3 + 50) \\
& + (y_1 + 2y_2 + 5y_3 + 50) \\
& \times (y_1 + 5y_2 + 5y_3 + 50) \\
& + (y_1 + 2y_2 + 4y_3 + 50) \times (5y_2 + 4y_3 + 50) \\
\text{s.t.}\quad & 2y_1 + y_2 + 5y_3 \le 10, \\
& y_1 + 6y_2 + 3y_3 \le 10, \\
& 5y_1 + 9y_2 + 2y_3 \le 10, \\
& 9y_1 + 7y_2 + 3y_3 \le 10, \\
& y_1, y_2, y_3 \ge 0.
\end{aligned} \tag{25}$$

In Table 1, the notations have been used for column headers: iteration, number of iterations; time: execution time(s) of the algorithm in seconds.

Example 3. One has

$$\begin{aligned}
\max\quad & \sum_{i=1}^{p} \left(\sum_{j=1}^{n} c_{ij} y_j + d_i \right) \left(\sum_{j=1}^{n} e_{ij} y_j + f_i \right) \\
\text{s.t.}\quad & 0 \le y_j \le \gamma_j, \quad j = 1, \ldots, n,
\end{aligned} \tag{26}$$

where c_{ij}, e_{ij}, d_i, f_i, $i = 1, \ldots, p$, $j = 0, 1, \ldots, n$ are randomly generated between 0 and 1; γ_j $(j = 1, \ldots, n)$ were randomly generated between 0 and 16.

Numerical results for Example 3 are given in Table 2, where the convergence tolerance is set to $\epsilon = 10^{-6}$.

From Tables 1 and 2, it is seen that the proposed algorithm in this paper can be used to globally solve the problem (GAMP) with the effectiveness and robustness.

5. Concluding Remarks

In this article, an out space accelerating branch-and-bound algorithm is presented for globally solving the generalized affine multiplicative programs problem (GAMP). First of all, we transform the (GAMP) into an equivalent problem (EQ). By utilizing the new linear relaxation technique, we systematically convert (EQ) into a series of linear relaxation programs problems, which can infinitely approximate the global optimal solution of (EQ) by a successive partition. To improve the computational efficiency of the algorithm, we introduce an out space reduction operation, which offers a theoretical possibility of reducing a large part of the investigated out space region and which can be seen as an accelerating device for improving the convergent speed of the proposed algorithm. By combining the established linear relaxed programs problem with the new reduction operation in a branch-and-bound framework, we design an out space accelerating algorithm for effectively solving (GAMP). By subsequently dividing the initial rectangle and subsequently solving a series of linear relaxed programs problems, the presented algorithm is convergent to the global minimum of (GAMP). Compared with the known algorithms, numerical results demonstrate that the proposed algorithm has higher computational efficiency.

Conflicts of Interest

The authors declare that they have no conflicts of interest.

Acknowledgments

This paper is supported by the Basic and Advanced Technology Research Project of Henan Province (152300410097), the Key Scientific Research Project of Universities in Henan Province (17B413002, 16A110014, and 17A110021), the Major Scientific Research Projects of Henan Institute of Science and Technology (2015ZD07), the National Natural Science Foundation of Henan Province (152300410097), and Science and Technology Project of Henan Province (162102210294).

References

[1] H. Konno, P. T. Thach, and H. Tuy, *Optimization on Low Rank Nonconvex Structures*, vol. 15 of *Nonconvex Optimization and its Applications*, Kluwer Academic Publishers, Dordrecht, The Netherlands, 1997.

[2] J. M. Henderson and R. E. Quandt, *Microeconomic Theorey*, McGraw-Hill, New York, NY, USA, 2nd edition, 1971.

[3] K. Swarup, "Programming with indefinite quadratic function with linear constraints," *Cahier du Coutre d'Etudes de Recherche Operationelle*, vol. 8, pp. 223–234, 1966.

[4] H.-M. Li and K.-C. Zhang, "A decomposition algorithm for solving large-scale quadratic programming problems," *Applied Mathematics and Computation*, vol. 173, no. 1, pp. 394–403, 2006.

[5] H. Wu and K. Zhang, "A new accelerating method for global non-convex quadratic optimization with non-convex quadratic constraints," *Applied Mathematics and Computation*, vol. 197, no. 2, pp. 810–818, 2008.

[6] S.-T. Liu and R.-T. Wang, "A numerical solution method to interval quadratic programming," *Applied Mathematics and Computation*, vol. 189, no. 2, pp. 1274–1281, 2007.

[7] P. Shen and M. Gu, "A duality-bounds algorithm for non-convex quadratic programs with additional multiplicative constraints," *Applied Mathematics and Computation*, vol. 198, no. 1, pp. 1–11, 2008.

[8] P. Shen, Y. Duan, and Y. Ma, "A robust solution approach for nonconvex quadratic programs with additional multiplicative constraints," *Applied Mathematics and Computation*, vol. 201, no. 1-2, pp. 514–526, 2008.

[9] H. Konno and K. Fukaishi, "A branch and bound algorithm for solving low rank linear multiplicative and fractional programming problems," *Journal of Global Optimization*, vol. 18, no. 3, pp. 283–299, 2000.

[10] H.-S. Ryoo and N. V. Sahinidis, "Global optimization of multiplicative programs," *Journal of Global Optimization*, vol. 26, no. 4, pp. 387–418, 2003.

[11] C. Xue, H. Jiao et al., "An approximate algorithm for solving generalized linear multiplicative programming," *Journal of Henan Normal University (Natural Science)*, vol. 36, no. 5, pp. 13–15, 2008.

[12] H. Tuy and N. Duc, "Reverse polyblock approximation for generalized multiplicative/fractional programming," *Vietnam Journal of Mathematics*, vol. 31, no. 4, pp. 391–402, 2003.

[13] S. Schaible and C. Sodini, "Finite algorithm for generalized linear multiplicative programming," *Journal of Optimization Theory and Applications*, vol. 87, no. 2, pp. 441–455, 1995.

[14] H. Jiao, S. Liu, and Y. Chen, "Global optimization algorithm for a generalized linear multiplicative programming," *Journal of Applied Mathematics and Computing*, vol. 40, no. 1-2, pp. 551–568, 2012.

[15] H. P. Benson and G. M. Boger, "Outcome-space cutting-plane algorithm for linear multiplicative programming," *Journal of Optimization Theory and Applications*, vol. 104, no. 2, pp. 301–322, 2000.

[16] X. J. Liu, T. Umegaki, and Y. Yamamoto, "Heuristic methods for linear multiplicative programming," *Journal of Global Optimization*, vol. 15, no. 4, pp. 433–447, 1999.

[17] N. Thi and H. Tuy, "A unified monotonic approach to generalized linear fractional programming," *Journal of Global Optimization*, vol. 26, no. 3, pp. 229–259, 2003.

[18] Y. Chen and H. Jiao, "A nonisolated optimal solution of general linear multiplicative programming problems," *Computers and Operations Research*, vol. 36, no. 9, pp. 2573–2579, 2009.

[19] C.-F. Wang, S.-Y. Liu, and P.-P. Shen, "Global minimization of a generalized linear multiplicative programming," *Applied Mathematical Modelling*, vol. 36, no. 6, pp. 2446–2451, 2012.

[20] H.-W. Jiao, S.-Y. Liu, and Y.-F. Zhao, "Effective algorithm for solving the generalized linear multiplicative problem with generalized polynomial constraints," *Applied Mathematical Modelling*, vol. 39, no. 23-24, pp. 7568–7582, 2015.

Hindawi
Journal of Control Science and Engineering
Volume 2017, Article ID 8138975, 7 pages
https://doi.org/10.1155/2017/8138975

Research Article

An Effective Algorithm for Globally Solving Sum of Linear Ratios Problems

Hongwei Jiao,[1] Lei Cai,[2] Zhisong Hou,[2] and Chunyang Bai[1]

[1]*School of Mathematical Sciences, Henan Institute of Science and Technology, Xinxiang 453003, China*
[2]*School of Information Engineering, Henan Institute of Science and Technology, Xinxiang 453003, China*

Correspondence should be addressed to Hongwei Jiao; jiaohongwei@126.com and Lei Cai; cailei2014@126.com

Received 21 February 2017; Accepted 13 April 2017

Academic Editor: Haibo Du

In this study, we propose an effective algorithm for globally solving the sum of linear ratios problems. Firstly, by introducing new variables, we transform the initial problem into an equivalent nonconvex programming problem. Secondly, by utilizing direct relaxation, the linear relaxation programming problem of the equivalent problem can be constructed. Thirdly, in order to improve the computational efficiency of the algorithm, an out space pruning technique is derived, which offers a possibility of pruning a large part of the out space region which does not contain the optimal solution of the equivalent problem. Fourthly, based on out space partition, by combining bounding technique and pruning technique, a new out space branch-and-bound algorithm for globally solving the sum of linear ratios problems (SLRP) is designed. Finally, numerical experimental results are presented to demonstrate both computational efficiency and solution quality of the proposed algorithm.

1. Introduction

Sum of linear ratios problems (SLRP) have broad wide applications in information technology, control science and engineering, transportation design, government plan, economy and finance [1–5], and so on. In these applications, especially, the number of linear ratios is usually less than four or five. In addition, due to the fact that the sum of linear ratios problems (SLRP) possess generally multiple local optimal solutions that are not globally optimal, the kinds of problems pose significant theoretical difficulty and computational complexity. Therefore, they have attracted interest of many researchers and practitioners.

In this paper, we will investigate the following sum of linear ratios problems:

$$\begin{aligned} (\mathrm{SLRP}): \quad & v = \max G(y) = \sum_{i=1}^{p} \frac{\varphi_i(y)}{\phi_i(y)} \\ \text{s.t.} \quad & y \in \Lambda \triangleq \{y \in R^n \mid Ay \le b,\ y \ge 0\}, \end{aligned} \tag{1}$$

where $A \in R^{m\times n}$, $b \in R^m$, $\varphi_i(y)$, and $\phi_i(y)$ are all affine functions, Λ is a nonempty bounded constraint set, and for any $y \in \Lambda$, $\phi_i(y) \neq 0$, $i = 1, 2, \ldots, p$.

During the past two decades, with the assumption that the denominator $\varphi_i(y) \ge 0$ and the numerator $\phi_i(y) > 0$ for any $y \in \Lambda$, many optimization algorithms have been developed for globally solving the sum of linear ratios problems (SLRP), for example, simplex algorithms, image space algorithm, branch-and-bound algorithms, and monotonic algorithm (see [6–17]). Recently, Jiao et al. [18–20] presented three branch-and-bound algorithms for sum of linear ratios problem by constructing different linear relaxation technique; Jiao et al. [21] presented a new two-level relaxation algorithm for generalized linear multiplicative programming with generalized polynomial constraints, which can be also used to globally solve the sum of linear ratios problem (SLRP) investigated in this paper. In addition, several new algorithms [22–25] have been also proposed for solving linear sum-of-ratios and nonlinear sum-of-ratios problems.

In this paper, we shall present a new out space branch-and-bound algorithm for the sum of linear ratios problems (SLRP) using out space pruning technique. Firstly, we transform the initial problem into the equivalent nonconvex programming problem by introducing new variables. Next, the linear relaxation programming problem of the equivalent problem can be constructed by utilizing direct relaxation.

Secondly, by making full use of the special structure of the equivalent problem and the branch-and-bound algorithm, an out space pruning technique is derived to improve the computational efficiency of the proposed algorithm, which offers a possibility of pruning a large part of the investigated out space region which does not contain the global optimal solution of the equivalent problem. Thirdly, by combining bounding technique and pruning technique, a new out space branch-and-bound algorithm is designed for globally solving the sum of linear ratios problems (SLR). Finally, numerical experimental results are presented to demonstrate both computational efficiency and solution quality of the proposed algorithm.

The remaining sections of this paper are organized as follows. At first, in Section 2, by introducing new variables the equivalent nonconvex programming problem of the initial problem is introduced. Next, by utilizing direct relaxation the linear relaxation programming problem of the equivalent problem is constructed. Second, an out space pruning technique is derived by making full use of the special structure of the equivalent problem and the branch-and-bound algorithm in Section 3. Third, a new out space branch-and-bound algorithm and its global convergence are described in Section 4. Fourth, numerical experiments and their computational results are presented in Section 5. Finally, the concluding remarks of this paper are drawn.

2. Equivalent Problem and Its Linear Relaxation

In this section, to globally solve the problem (SLRP), by the continuity of the linear ratio $\varphi_i(y)/\phi_i(y)$, we know that $\phi_i(y) > 0$ or $\phi_i(y) < 0$. Here, without loss of generality, we can assume that

$$\begin{aligned} &\phi_i(y) > 0, \quad i = 1, 2, \ldots, T; \\ &\phi_i(y) < 0, \quad i = T+1, T+2, \ldots, p \end{aligned} \tag{2}$$

except for the above assumptions, for each $i \in \{1, 2, \ldots, p\}$, since

$$\frac{\varphi_i(y)}{\phi_i(y)} = \frac{\varphi_i(y) + M_i\phi_i(y)}{\phi_i(y)} - M_i, \tag{3}$$

where M_i is an appropriate real number such that $\varphi_i(y) + M_i\phi_i(y) \geq 0$. Thus, without loss of generality, by some proper transformation we can always guarantee that the numerator of each ratio is greater than or equal to 0.

Let

$$U_i^0 = \begin{cases} \dfrac{1}{\min_{y\in\Lambda}\phi_i(y)}, & i = 1, 2, \ldots, T, \\ \dfrac{1}{-\max_{y\in\Lambda}\phi_i(y)}, & i = T+1, \ldots, p; \end{cases}$$

$$L_i^0 = \begin{cases} \dfrac{1}{\max_{y\in\Lambda}\phi_i(y)}, & i = 1, 2, \ldots, T, \\ \dfrac{1}{-\min_{y\in\Lambda}\phi_i(y)}, & i = T+1, \ldots, p. \end{cases} \tag{4}$$

And construct the initial box

$$Z^0 = \left\{ z \in R^p \mid L_i^0 \leq z_i \leq U_i^0,\ i = 1, 2, \ldots, p \right\}; \tag{5}$$

then the problem (SLRP) can be converted into the equivalent problem (EQ) as follows.

$$\begin{aligned} \mathrm{EQ}\left(Z^0\right): \quad & v\left(Z^0\right) = \max H_0(y, z) \\ & = \sum_{i=1}^{T} z_i\varphi_i(y) - \sum_{i=T+1}^{p} z_i\varphi_i(y) \\ \text{s.t.} \quad & H_i(y, z) = z_i\phi_i(y) \leq 1, \quad i = 1, 2, \ldots, T, \\ & H_i(y, z) = z_i\phi_i(y) \leq -1, \\ & \qquad i = T+1,\ T+2, \ldots, p, \\ & y \in \Lambda, \quad z \in Z^0. \end{aligned} \tag{6}$$

The key equivalence theorem for the problem (SLRP) and the EQ(Z^0) is described as follows.

Theorem 1. *If $(y^*, z_1^*, \ldots, z_p^*)$ is a global optimum point of the problem EQ(Z^0), then y^* is a global optimum point of the problem (SLRP). On the contrary, if y^* is a global optimum point of the problem (SLRP), then $(y^*, z_1^*, \ldots, z_p^*)$ is a global optimum point of the problem EQ(Z^0) with $z_i^* = 1/\phi_i(y^*)$, $i = 1, 2, \ldots, T$, $z_i^* = 1/-\phi_i(y^*)$, $i = T+1, T+2, \ldots, p$.*

Proof. The conclusion can be easily drawn, so the proof is omitted. □

From Theorem 1, to solve the problem (SLRP), we may globally solve its equivalent nonconvex programming problem EQ(Z^0) instead.

For each box $Z^k = \{z \in R^p \mid L_i^k \leq z_i \leq U_i^k,\ i = 1, 2, \ldots, p\} \subseteq Z^0$, some notations and functions of this paper are listed as follows:

$$\begin{aligned} H_0^U(y) &= \sum_{i=1}^{T} U_i^k\varphi_i(y) - \sum_{i=T+1}^{p} L_i^k\varphi_i(y); \\ H_0^L(y) &= \sum_{i=1}^{T} L_i^k\varphi_i(y) - \sum_{i=T+1}^{p} U_i^k\varphi_i(y); \\ H_i^U(y) &= U_i^k\phi_i(y), \quad i = 1, 2, \ldots, p; \\ H_i^L(y) &= L_i^k\phi_i(y), \quad i = 1, 2, \ldots, p. \end{aligned} \tag{7}$$

Theorem 2. *For the functions $H_i^U(y)$, $H_i^L(y)$, $H_i(y, z)$, $i = 0, 1, 2, \ldots, p$, where $y \in \Lambda$, $z \in Z^k \subseteq Z^0$, we have the following two conclusions:*

(i) $H_i^U(y) \geq H_i(y, z) \geq H_i^L(y)$, $i = 0, 1, 2, \ldots, p$.

(ii) $\lim_{\|U^k - L^k\| \to 0}[H_i^U(y) - H_i(y, z)] = \lim_{\|U^k - L^k\| \to 0}[H_i(y, z) - H_i^L(y)] = 0$.

Proof. The proof can be easily followed, therefore here it is omitted. □

From the above Theorem 2, for any $Z^k \subseteq Z^0$, the corresponding linear relaxation programming problem LRP(Z^k) of the problem EQ(Z^k) can be established as follows, which can offer a reliable upper bound for the global optimum of EQ(Z^k).

$$\begin{aligned}
\mathrm{LRP}\left(Z^k\right): \quad & \mathrm{UB}\left(Z^k\right) = \max H_0^U(y) \\
& = \sum_{i=1}^{T} U_i^k \varphi_i(y) - \sum_{i=T+1}^{p} L_i^k \varphi_i(y) \\
\text{s.t.} \quad & H_i^L(y) = L_i^k \phi_i(y) \le 1, \quad i = 1, 2, \ldots, T, \\
& H_i^L(y) = L_i^k \phi_i(y) \le -1, \\
& \qquad i = T+1, T+2, \ldots, p, \\
& y \in \Lambda.
\end{aligned} \tag{8}$$

3. Out Space Pruning Technique

For any box $Z^k \subseteq Z^0$, we need to recognize whether or not Z^k contains global optimum point of the problem (EQ). Thus, in this section, we shall construct an out space pruning technique for pruning a part of the investigated out space region which does not contain the global optimum point of the problem (SLRP) and use the technique to improve the computational efficiency of the proposed algorithm. The proposed new out space pruning technique aims at replacing the box $Z^k = [L^k, U^k]$ with a smaller box $Z' = [L', U']$ without pruning any global optimum point of the problem (EQ).

We assume, without loss of generality, that LB is a currently known lower bound of the global optimum value of the EQ(Z^0) and that $v(Z^k)$ denote the maximum value of the problem $H_0(y, z)$ over Z^k and D and set

$$\begin{aligned}
& l_i^0 = \min_{y \in \Lambda} \varphi_i(y), \quad i = 1, 2, \ldots, p, \\
& u_i^0 = \max_{y \in \Lambda} \varphi_i(y), \quad i = 1, 2, \ldots, p, \\
& \mathrm{RUB}^k = \sum_{i=1}^{T} U_i^k u_i^0 - \sum_{i=T+1}^{p} L_i^k l_i^0, \\
& \rho_i^k = \frac{\mathrm{LB} - \mathrm{RUB}^k + U_i^k u_i^0}{u_i^0}, \quad i = 1, 2, \ldots, T, \\
& \rho_i^k = \frac{-\mathrm{LB} + \mathrm{RUB}^k + L_i^k l_i^0}{l_i^0}, \\
& \qquad i = T+1, T+2, \ldots, p.
\end{aligned} \tag{9}$$

Theorem 3. *For any subbox $Z^k = (Z_i^k)_{p\times 1} = [L_i^k, U_i^k]_{p\times 1} \subseteq Z^0$, we have the following two conclusions:*

(i) *Suppose that $\mathrm{RUB}^k < \mathrm{LB}$; then there does not exist any global optimum point of EQ(Z^k) over Z^k.*

(ii) *Suppose that $\mathrm{RUB}^k \ge \mathrm{LB}$; then, when $j \in \{1, 2, \ldots, T\}$, there does not exist any global optimum point of EQ(Z^0) over Z_a^k; and when $j \in \{T+1, T+2, \ldots, p\}$, there does not exist any global optimum point of EQ(Z^0) over Z_b^k, where*

$$\begin{aligned}
& Z_a^k = \left(Z_{ai}^k\right)_{p\times 1} \subseteq Z^0 \\
& \qquad \text{with } Z_{ai}^k = \begin{cases} Z_i^k, & i \ne j,\ i = 1, 2, \ldots, p, \\ \left[L_i^k, \rho_i^k\right) \cap Z_i^k, & i = j \in \{1, 2, \ldots, T\}. \end{cases} \\
& Z_b^k = \left(Z_{bi}^k\right)_{p\times 1} \subseteq Z^0 \\
& \qquad \text{with } Z_{bi}^k = \begin{cases} Z_i^k, & i \ne j,\ i = 1, 2, \ldots, p, \\ \left(\rho_i^k, U_i^k\right] \cap Z_i^k, & i = j \in \{T+1, T+2, \ldots, p\}, \end{cases}
\end{aligned} \tag{10}$$

Proof. (i) Suppose that $\mathrm{RUB}^k < \mathrm{LB}$; then we have

$$\begin{aligned}
v\left(Z^k\right) &= \max_{z \in Z^k, y \in \Lambda} \sum_{i=1}^{p} z_i \varphi_i(y) \le \sum_{i=1}^{p} \max_{z \in Z^k, y \in \Lambda} z_i \varphi_i(y) \\
&= \sum_{i=1}^{T} U_i^k u_i^0 - \sum_{i=T+1}^{p} L_i^k l_i^0 = \mathrm{RUB}^k < \mathrm{LB};
\end{aligned} \tag{11}$$

therefore, there does not exist any global optimum point of the problem EQ(Z^k) over Z^k.

(ii) Suppose that $\mathrm{RUB}^k \ge \mathrm{LB}$; then we can get the following several conclusions.

When $j \in \{1, 2, \ldots, T\}$, for any $y \in \Lambda$ and $z \in Z_a^k$, since

$$\begin{aligned}
& 0 \le l_i^0 \le \varphi_i(y) \le u_i^0, \\
& 0 \le L_i^k \le z_i \le U_i^k, \\
& \qquad i = 1, 2, \ldots, p,\ i \ne j; \\
& 0 \le L_j^k \le z_j < \rho_j^k, \quad i = j,
\end{aligned} \tag{12}$$

we can get

$$\begin{aligned}
v\left(Z_a^k\right) &= \max_{z \in Z_a^k, y \in \Lambda} \left(\sum_{i=1}^{T} z_i \varphi_i(y) - \sum_{i=T+1}^{p} z_i z_i \varphi_i(y) \right) \\
&\le \max_{z \in Z_a^k, y \in \Lambda} \sum_{i=1, i \ne j}^{T} z_i \varphi_i(y) \\
&\quad - \min_{z \in Z_a^k, y \in \Lambda} \sum_{i=T+1}^{p} z_i \varphi_i(y) + \max_{z \in Z_a^k, y \in \Lambda} z_i \varphi_i(y) \\
&< \sum_{i=1, i \ne j}^{T} U_i^k u_i^0 - \sum_{i=T+1}^{p} L_i^k l_i^0 + \rho_j^k u_j^0 \\
&= \mathrm{RUB}^k - U_j^k u_j^0 + \rho_j^k u_j^0 < \mathrm{LB}.
\end{aligned} \tag{13}$$

Therefore, there does not exist any global optimum point of EQ(Z^k) over Z_a^k.

Similarly, when $j \in \{T+1, T+2, \ldots, p\}$, and for any $y \in \Lambda$ and $z \in Z_b^k$, since

$$\begin{aligned} &0 \le l_i^0 \le \varphi_i(y) \le u_i^0, \\ &0 \le L_i^k \le z_i \le U_i^k, \\ &\qquad\qquad i = 1, 2, \ldots, p,\ i \ne j, \\ &0 \le \rho_j^k < z_j \le U_j^k, \quad i = j, \end{aligned} \tag{14}$$

we have

$$\begin{aligned} v\left(Z_b^k\right) &= \max_{z \in Z_b^k, y \in \Lambda} \left(\sum_{i=1}^{T} z_i \varphi_i(y) - \sum_{i=T+1}^{p} z_i \varphi_i(y) \right) \\ &\le \max_{z \in Z_b^k, y \in \Lambda} \sum_{i=1}^{T} z_i \varphi_i(y) \\ &\quad - \min_{z \in Z_b^k, y \in \Lambda} \sum_{i=T+1, i \ne j}^{p} z_i \varphi_i(y) - \min_{z \in Z_b^k, y \in \Lambda} z_i \varphi_i(y) \\ &< \sum_{i=1}^{T} U_i^k u_i^0 - \sum_{i=T+1, i \ne j}^{p} L_i^k l_i^0 - \rho_j^k l_j^0 \\ &= \mathrm{RUB}^k + L_j^k l_j^0 - \rho_j^k l_j^0 < \mathrm{LB}. \end{aligned} \tag{15}$$

Therefore, there does not exist any global optimum point of EQ(Z^k) over Z_b^k. □

By the above Theorem 3, we can construct an out space pruning technique to prune a part of the investigated out space region which does not contain the global optimum point of the problem (EQ). Assume that a subbox

$$Z^k = \left(Z_i^k\right)_{p \times 1} \subseteq Z^0 \quad \text{with } Z_i^k = \left[L_i^k, U_i^k\right] \tag{16}$$

will be pruned; then from the Theorem 3, the investigated box Z^k can be renewed by a subbox

$$\begin{aligned} &Z' = \left(Z_i'\right)_{p \times 1} \\ &\text{with } Z_i' = \begin{cases} \left[\rho_i^k, U_i^k\right] \cap Z_i^k, & i \in \{1, 2, \ldots, T\}, \\ \left[L_i^k, \rho_i^k\right] \cap Z_i^k, & i \in \{T+1, T+2, \ldots, p\}. \end{cases} \end{aligned} \tag{17}$$

4. Algorithm and Its Convergence

In this section, by utilizing the above new pruning technique, we will present a new out space branch-and-bound algorithm for globally solving the problem (SLRP). In the algorithm, the branching operation is performed in out space R^p. Assume that $Z = \{z \in R^p \mid L_i \le z_i \le U_i,\ i = 1, 2, \ldots, p\}$ is Z^0 or a subbox of it, which will be partitioned, the branching rule is selected as follows.

Set

$$\begin{aligned} &q \in \arg\max \{U_i - L_i \mid i = 1, 2, \ldots, p\}, \\ &Z^1 = \left\{ z \in R^p \mid L_i \le z_i \le \frac{L_q + U_q}{2},\ i = q,\ L_i \le z_i \right. \\ &\qquad \left. \le U_i,\ i = 1, 2, \ldots, p,\ i \ne q \right\}, \\ &Z^2 = \left\{ z \in R^p \mid \frac{L_q + U_q}{2} \le z_i \le U_i,\ i = q,\ L_i \le z_i \right. \\ &\qquad \left. \le U_i,\ i = 1, 2, \ldots, p,\ i \ne q \right\}. \end{aligned} \tag{18}$$

Obviously, from [26] we can get that this branching rule is exhaustive; that is, if $\{Z^k\}$ represents a nested subsequence of boxes (i.e., $Z^{k+1} \subseteq Z^k$, for all k) formed by partitioning process, then there exists a unique point $z^* \in R^p$ satisfying $\bigcap_k Z^k = \{z^*\}$.

4.1. Out Space Branch-and-Bound Algorithm. Based upon the above linear relaxation bounding problem, the new out space pruning technique, and bisection method, an out space branch-and-bound algorithm is proposed for globally solving the (SLRP) as follows.

Step 1. Let $k = 0$, $\Delta_0 = \{Z^0\}$, $\varepsilon \ge 0$, $l_i^0 = \min_{y \in \Lambda} \varphi_i(y)$, and $u_i^0 = \max_{y \in \Lambda} \varphi_i(y)$, $i = 1, 2, \ldots, p$. And let

$$\begin{aligned} U_i^0 &= \begin{cases} \dfrac{1}{\min_{y \in \Lambda} \phi_i(y)}, & i = 1, 2, \ldots, T, \\ \dfrac{1}{-\max_{y \in \Lambda} \phi_i(y)}, & i = T+1, \ldots, p, \end{cases} \\ L_i^0 &= \begin{cases} \dfrac{1}{\max_{y \in \Lambda} \phi_i(y)}, & i = 1, 2, \ldots, T, \\ \dfrac{1}{-\min_{y \in \Lambda} \phi_i(y)}, & i = T+1, \ldots, p, \end{cases} \end{aligned} \tag{19}$$

and construct the initial box

$$Z^0 = \left\{ z \in R^p \mid L_i^0 \le z_i \le U_i^0,\ i = 1, 2, \ldots, p \right\}. \tag{20}$$

Using simplex method to solve LRP(Z^0), set its optimum solution y^0 and optimum value UB(Z^0), respectively. Let $\mathrm{UB}_0 = \mathrm{UB}(Z^0)$, $z_i^0 = \phi_i(y^0)$ ($i = 1, 2, \ldots, p$), $\mathrm{LB}_0 = H_0(y^0, z^0)$. If $\mathrm{UB}_0 - \mathrm{LB}_0 \le \varepsilon$, then (y^0, z^0) and y^0 are global optimum solutions of EQ(Z^0) and the (SLRP), respectively. Otherwise, let $F = \emptyset$, $k = 1$ and continue to the following Step 2.

Step 2. Set $\mathrm{LB} = \mathrm{LB}_{k-1}$. For each investigated subbox Z^{k-1}, use the former out space pruning technique to prune the investigated subbox Z^{k-1}, let the remaining box be Z', and set $Z^{k-1} = Z'$, $\mathrm{LB}_k = \mathrm{LB}_{k-1}$.

Step 3. Partition Z^{k-1} into two subboxes $Z^{k,1}, Z^{k,2} \subseteq Z^{k-1}$ using the bisection technique. Let the new partitioned subboxes set be $\overline{Z}^k$. Set $F = F \cup \{Z^{k-1}\}$. For each $Z^{k,t} \in \overline{Z}^k$, solve the (LRP) using simplex method to get $\mathrm{UB}(Z^{k,t})$ and $y^{k,t}$, and set $z_i^{k,t} = \phi_i(y^{k,t})$, $i = 1, 2, \ldots, p$. If $\mathrm{UB}(Z^{k,t}) < \mathrm{LB}_k$, then let $\overline{Z}^k := \overline{Z}^k \setminus Z^{k,t}$, $F = F \cup \{Z^{k,t}\}$; otherwise, update $\mathrm{LB}_k = \min\{\mathrm{LB}_k, H_0(y^{k,t}, z^{k,t})\}$, if necessary.

Step 4. Let the remaining partitioned set $\Delta_{k-1} := (\Delta_{k-1} \setminus Z^{k-1}) \cup \{\overline{Z}^k\}$, and let the new upper bound $\mathrm{UB}_k = \max_{Z \in \Delta_{k-1}} \mathrm{UB}(Z)$. Let $\Delta_k = \{Z \mid Z \in (\Delta_{k-1} \cup \{Z^{k,1}, Z^{k,2}\}), Z \notin F\}$ and $\mathrm{UB}_k = \min\{\mathrm{UB}(Z) \mid Z \in \Delta_k\}$. If $\mathrm{UB}_k - \mathrm{LB}_k \le \varepsilon$, then we get that (y^k, z^k) and y^k are global optimum points of the $\mathrm{EQ}(Z^0)$ and the (SLRP), respectively. Otherwise, let $k = k + 1$ and return to Step 2.

4.2. Convergence Analysis. In the following, we describe the global convergence of the above algorithm.

Theorem 4. *The above algorithm either stops finitely to obtain the global optimum point of the (SLRP) or produces an infinite sequence $\{y^k\}$ whose accumulation point y^* must be the global optimum point of the (SLRP).*

Proof. If the proposed algorithm stops finitely at k_{th} iteration, where $k \ge 0$, obviously, when the algorithm stops, we can get y^k and (y^k, z^k) by solving the $\mathrm{LRP}(Z^k)$, which are the feasible points of the (SLRP) and the (EQ), where

$$\begin{aligned} z_i^k &= \frac{1}{\phi_i(y^k)}, \quad i = 1, 2, \ldots, T; \\ z_i^k &= \frac{1}{-\phi_i(y^k)}, \quad i = T+1, T+2, \ldots, p; \end{aligned} \tag{21}$$

and by terminating step of the algorithm, the updating operations of the lower bound and upper bound, and Theorems 1 and 2, we can easily follow that

$$\begin{aligned} H_0(y^k, z^k) &\ge \mathrm{UB}_k - \varepsilon, \\ \mathrm{UB}_k &\ge v, \\ v &\ge H_0(y^k, z^k), \\ G(y^k) &= H_0(y^k, z^k). \end{aligned} \tag{22}$$

By combining the above all inequalities and equality, we can easily get that

$$v - \epsilon \le G(y^k) \le v. \tag{23}$$

Therefore, if the algorithm stops finitely at k_{th} iteration, then y^k is the global ϵ–optimal solution of the (SLRP).

If the above algorithm generates an infinite sequence $\{y^k\}$ of incumbent solutions by solving the $\mathrm{LRP}(Z^k)$, let

$$\begin{aligned} z_i^k &= \frac{1}{\phi_i(y^k)}, \quad i = 1, 2, \ldots, T, \\ z_i^k &= \frac{1}{-\phi_i(y^k)}, \quad i = T+1, T+2, \ldots, p; \end{aligned} \tag{24}$$

then we can get an infinite sequence $\{y^k, z^k\}$ of incumbent solutions for $\mathrm{EQ}(Z^k)$. By the continuity character of the function $\phi_i(y^k)$ and $1/\phi_i(y^k) = z_i^k \in [L_i^k, U_i^k]$ $(i = 1, \ldots, T)$ and $1/-\phi_i(y^k) = z_i^k \in [L_i^k, U_i^k]$ $(i = T+1, \ldots, p)$, and the exhaustiveness of the bisection rule, we can get the following conclusions, for each $i \in \{1, 2, \ldots, T\}$:

$$\begin{aligned} \frac{1}{\phi_i(y^*)} &= \lim_{k\to\infty} \frac{1}{\phi_i(y^k)} = \lim_{k\to\infty} L_i^k = \lim_{k\to\infty} U_i^k \\ &= \lim_{k\to\infty} \left[L_i^k, U_i^k\right] = \bigcap_k \left[L_i^k, U_i^k\right] = \{z_i^*\}; \end{aligned} \tag{25}$$

for each $i \in \{T+1, T+2, \ldots, p\}$,

$$\begin{aligned} \frac{1}{-\phi_i(y^*)} &= \lim_{k\to\infty} \frac{1}{-\phi_i(y^k)} = \lim_{k\to\infty} L_i^k = \lim_{k\to\infty} U_i^k \\ &= \lim_{k\to\infty} \left[L_i^k, U_i^k\right] = \bigcap_k \left[L_i^k, U_i^k\right] = \{z_i^*\}. \end{aligned} \tag{26}$$

Therefore, (y^*, z^*) is a feasible point of the $\mathrm{EQ}(Z^0)$, also since $\{\mathrm{UB}(Z^k)\}$ is a decreasing real number sequence bounded by v, we can follow that

$$\begin{aligned} H_0(y^*, z^*) &\le v \le \lim_{k\to\infty} \mathrm{UB}\left(Z^k\right) \\ &= \lim_{k\to\infty} \left(\sum_{i=1}^{T} U_i^k \varphi_i\left(y^k\right) - \sum_{i=T+1}^{p} L_i^k \varphi_i\left(y^k\right) \right) \\ &= H_0(y^*, z^*). \end{aligned} \tag{27}$$

Thus, from the updating method of the lower bound and the continuity character of the $G(y)$, we can get that

$$\begin{aligned} \lim_{k\to\infty} \mathrm{LB}\left(Z^k\right) &= v = H_0(y^*, z^*) = G(y^*) \\ &= \lim_{k\to\infty} G\left(y^k\right) = \lim_{k\to\infty} \mathrm{UB}\left(Z^k\right). \end{aligned} \tag{28}$$

Hence, y^* is the global optimum point of the (SLRP); the conclusion is proved. □

4.3. Numerical Example. In this subsection, some well-known test problems are implemented on Intel(R) Core(TM)2 Duo CPU microcomputer to verify the performance of the proposed out space branch-and-bound algorithm. The proposed out space branch-and-bound algorithm is coded in C++ program, and the simplex method is used to solve each linear relaxation programming problem.

Table 1: Numerical results for test problem.

Number	(m, n, p, c)	Ref.	Ave. Iter.	Ave. L.	Ave. Time (s)	ϵ
(1)	(2, 3, 3, 2)	This paper	3.2	3.1	0.015	10^{-6}
	(2, 3, 3, 2)	[15]	38.3	7.8	0.05	10^{-6}
	(2, 3, 3, 2)	[16]	4.6	1.0	0	10^{-5}
(2)	(4, 3, 4, 2)	This paper	5.2	4.6	0.05	10^{-6}
	(4, 3, 4, 2)	[15]	46	8.2	0.1	10^{-6}
	(4, 3, 4, 2)	[16]	5.6	1.1	0	10^{-5}
(3)	(5, 10, 3, 2)	This paper	6.2	3.8	0.073	10^{-6}
	(5, 10, 3, 2)	[15]	414.3	60.2	1.9	10^{-6}
	(5, 10, 3, 2)	[16]	6.3	1.4	0	10^{-5}
(4)	(10, 20, 3, 2)	This paper	7.3	4.4	0.087	10^{-6}
	(10, 20, 3, 2)	[15]	402.7	56.8	10.1	10^{-6}
	(10, 20, 3, 2)	[16]	7.4	2.0	0.023	10^{-5}
(5)	(15, 30, 3, 2)	This paper	6.5	4.5	0.130	10^{-6}
	(15, 30, 3, 2)	[15]	424.3	61.6	35.1	10^{-6}
	(15, 30, 3, 2)	[16]	7.0	2.0	3.1	10^{-5}

Numerical problems and their computational results are summarized in Table 1. Some notations have been also used for column headers in Table 1 as follows. Ave. Iter. represents the average number of iterations of the algorithm; Ave. L. represents the average number of the necessary maximum nodes of the algorithm; Ave. Time (s) stands for the execution time of algorithm in seconds.

Problem (see [15, 16]).

$$\begin{aligned} \max \quad & \sum_{j=1}^{p} \frac{\sum_{i=1}^{n} d_{ji} y_i + c}{\sum_{i=1}^{n} \sigma_{ji} y_i + c} \\ \text{s.t.} \quad & \sum_{i=1}^{n} a_{ki} y_i \le b_k, \quad k = 1, \ldots, m, \\ & y_i \ge 0.0, \quad i = 1, 2, \ldots, n, \end{aligned} \tag{29}$$

where $d_{ji}, \sigma_{ji}, a_{ki}, j = 1, \ldots, p, k = 1, \ldots, m, i = 1, \ldots, n$, are randomly generated in $[0.0, 1.0]$; c are generated in $[1.0, 100.0]$; $b_k = 1.0, k = 1, 2, \ldots, m$. In the investigated problem, m denotes the number of the constraints, n denotes the dimension of the problem, and p denotes the number of ratios.

From Table 1, compared with the known algorithms, numerical results indicate that the proposed algorithm can be used to globally solve the problems (SLRP) with the higher computational efficiency.

5. Concluding Remarks

In this paper, we present an effective algorithm for globally solving the sum of linear ratios problem (SLRP). By introducing new variables, we transform the initial sum of linear ratios problems (SLRP) into the equivalent nonconvex programming problem. Next, the linear relaxation programming problem of the equivalent problem is established by utilizing direct relaxation. To improve the computational efficiency of the algorithm, an out space pruning technique is derived, which offers a possibility of pruning a large part of the investigated out space region which does not contain the optimal solution of the equivalent problem. Based on out space partition, by combining bounding technique and reduction technique, a new outcome space branch-and-bound algorithm for globally solving the sum of linear ratios problem (SLRP) is constructed. Finally, numerical problems and their computational results are presented to demonstrate both computational efficiency and solution quality of the proposed algorithm.

In future research, we can extend the proposed algorithm and reduction technique to solve nonlinear fractional problems, like concave-convex sum-of-ratios problem, convex-convex sum-of-ratios problem, linear fractional multiplicative problem, generalized linear fractional programming problem, and so on.

Conflicts of Interest

The authors declare that they have no conflicts of interest.

Acknowledgments

This paper is supported by the Cultivation Plan of Young Key Teachers in Colleges and Universities of Henan Province (2016GGJS-107), the Basic and Advanced Technology Research Project of Henan Province (152300410097), the Key Scientific Research Project of Universities in Henan Province (17B413002, 16A110014, and 17A110021), the Major Scientific Research Projects of Henan Institute of Science and Technology (2015ZD07), the National Natural Science Foundation of Henan Province (152300410097), and Science and Technology Project of Henan Province (162102210294).

References

[1] Y. Almogy and O. Levin, *Parametric Analysis of a Multistage Stochastic Shipping Problem, Operational Research 69*, Tavistock Publications, London, England, UK, 1970.

[2] H. P. Benson, "A simplicial branch and bound duality-bounds algorithm for the linear sum-of-ratios problem," *European Journal of Operational Research*, vol. 182, no. 2, pp. 597–611, 2007.

[3] C. S. Colantoni, R. P. Manes, and A. Whinston, "Programming, profit rates, and pricing decisions, accounting review," vol. 44, pp. 467–481, 1969.

[4] M. R. Rao, "Cluster analysis and mathematical programming," *Journal of the American Statistical Association*, vol. 66, no. 335, pp. 622–626, 1971.

[5] H. Konno and H. Watanabe, "Bond portfolio optimization problems and their applications to index tracking: a partial optimization approach," *Journal of the Operations Research Society of Japan*, vol. 39, no. 3, pp. 295–306, 1996.

[6] A. Charnes and W. W. Cooper, "Programming with linear fractional functionals," *Naval Research Logistics Quarterly*, vol. 9, pp. 181–186, 1962.

[7] H. Konno, Y. Yajima, and T. Matsui, "Parametric simplex algorithms for solving a special class of nonconvex minimization problem," *Journal of Global Optimization*, vol. 1, pp. 65–81, 1991.

[8] J. E. Falk and S. W. Palocsay, "Image space analysis of generalized fractional programs," *Journal of Global Optimization*, vol. 4, pp. 63–88, 1994.

[9] Y. Ji, K.-C. Zhang, and S.-J. Qu, "A deterministic global optimization algorithm," *Applied Mathematics and Computation*, vol. 185, no. 1, pp. 382–387, 2007.

[10] H. Konno and K. Fukaishi, "A branch and bound algorithm for solving low rank linear multiplicative and fractional programming problems," *Journal of Global Optimization*, vol. 18, pp. 283–299, 2000.

[11] P.-P. Shen and C.-F. Wang, "Global optimization for sum of linear ratios problem with coefficients," *Applied Mathematics and Computation*, vol. 176, no. 1, pp. 219–229, 2006.

[12] C.-F. Wang and P.-P. Shen, "A global optimization algorithm for linear fractional programming," *Applied Mathematics and Computation*, vol. 204, no. 1, pp. 281–287, 2008.

[13] H. Jiao, "A branch and bound algorithm for globally solving a class of nonconvex programming problems," *Nonlinear Analysis*, vol. 70, no. 2, pp. 1113–1123, 2009.

[14] H. P. Benson, "On the global optimization of sums of linear fractional functions over a convex set," *Journal of Optimization Theory and Applications*, vol. 121, no. 1, pp. 19–39, 2004.

[15] W. Yanjun, S. Peiping, and L. Zhian, "A branch-and-bound algorithm to globally solve the sum of several linear ratios," *Applied Mathematics and Computation*, vol. 168, no. 1, pp. 89–101, 2005.

[16] Y. Shi, *Global optimization for sum of ratios problems, Dissertation of master degree for Henan Normal University*, Henan Normal University, 2011.

[17] N. T. H. Phuong and H. Tuy, "A unified monotonic approach to generalized linear fractional programming," *Journal of Global Optimization*, vol. 26, no. 3, pp. 229–259, 2003.

[18] H.-W. Jiao and S.-Y. Liu, "A practicable branch and bound algorithm for sum of linear ratios problem," *European Journal of Operational Research*, vol. 243, no. 3, pp. 723–730, 2015.

[19] H. Jiao, S. Liu, J. Yin, and Y. Zhao, "Outcome space range reduction method for global optimization of sum of affine ratios problem," *Open Mathematics*, vol. 14, pp. 736–746, 2016.

[20] H. Jiao, C. Bai, and X. Wang, "Reduction-branch-bound algorithm for solving sum of linear ratios problems," *Mathematica Applicata*, vol. 29, no. 3, pp. 625–631, 2016.

[21] H.-W. Jiao, S.-Y. Liu, and Y.-F. Zhao, "Effective algorithm for solving the generalized linear multiplicative problem with generalized polynomial constraints," *Applied Mathematical Modelling. Simulation and Computation for Engineering and Environmental Systems*, vol. 39, no. 23-24, pp. 7568–7582, 2015.

[22] B. L. Gorissen, "Robust fractional programming," *Journal of Optimization Theory and Applications*, vol. 166, no. 2, pp. 508–528, 2015.

[23] A. Aubry, V. Carotenuto, and A. De Maio, "New Results on Generalized Fractional Programming Problems With Toeplitz Quadratics," *IEEE Signal Processing Letters*, vol. 23, no. 6, pp. 848–852, 2016.

[24] N. Ruan and D. Y. Gao, "Global solutions to fractional programming problem with ratio of nonconvex functions," *Applied Mathematics and Computation*, vol. 255, pp. 66–72, 2015.

[25] H. Li, "A genetic algorithm using a finite search space for solving nonlinear/linear fractional bilevel programming problems," *Annals of Operations Research*, vol. 235, pp. 543–558, 2015.

[26] R. Horst and H. Tuy, *Global Optimization: Deterministic Approaches*, Springer, Berline, Germany, 2nd edition, 1993.

Hindawi
Journal of Control Science and Engineering
Volume 2017, Article ID 8492139, 11 pages
https://doi.org/10.1155/2017/8492139

Research Article

DCA-Based Real-Time Residual Useful Life Prediction for Critical Faulty Component

Funa Zhou, Jiayu Wang, and Yulin Gao

School of Computer and Information Engineering, Henan University, Kaifeng, China

Correspondence should be addressed to Jiayu Wang; wangjiayu11115@163.com and Yulin Gao; gaoyulinhn@163.com

Received 28 February 2017; Accepted 26 April 2017; Published 21 May 2017

Academic Editor: Chaojie Li

Residual useful life (RUL) prediction is significant for condition-based maintenance. Traditional data-driven RUL prediction method can only predict fault trend of the system rather than RUL of a specific system component. Thus it cannot tell the operator which component should be maintained. The innovation of this paper is as follows: (1) Wavelet filtering based method is developed for early detection of slowly varying fault. (2) Designated component analysis is introduced as a feature extraction tool to define the fault precursor of a specific component. (3) Exponential life prediction model is established by nonlinear fitting of the historical RUL and the fault size characterized by the statistics used. Once online detection statistics is obtained, real-time RUL of the critical component can be predicted online. Simulation shows the effectiveness of this algorithm.

1. Introduction

With the rapid development of modern industrial technology, reliability, maintainability, and security of large-scale system have widely received attention [1–4]. Abnormal detection, root cause identification, and RUL prediction are the stages for efficient system monitoring.

Abnormality is expected to be detected as quickly as possible to prevent major accidents and reduce loss of downtime and maintenance. In the past decades, multivariate statistical analysis techniques such as principal component analysis (PCA) and partial least squares (PLS) [5–7] have been widely used in complex system monitoring [8]. However, abnormal detection and fault diagnosis usually answer the question of "having trouble," not "how long it will happen."

Detection and maintenance after system failure are usually too late for system with higher security requirement and expensive downtime loss, such as power station, power transmission, petrochemical industry, large-scale iron, steel enterprise, and other industry fields [9].

If condition-based maintenance rather than breakdown maintenance is used, severe faults leading to shutdown can be avoided, and a lot of maintenance cost can be saved [10]. Fault prediction technology is a critical step of condition-based maintenance. In recent years, fault prediction has become a hot topic in the field of system monitoring [11]. Artificial neural network (ANN) [12–17], autoregressive model (AR) [18, 19], support vector machine (SVM) [20], vector autoregressive model (VAR), and so forth [21] are commonly used fault prediction methods. But these pure data-driven methods without reference to expert experience can only predict fault trend rather than directly predict RUL online.

An important stage of RUL prediction strategy is how to properly assess fault size that reflects the degradation process. If a damage precursor is available, damage precursor based method for RUL prediction is an objective choice [22]. So fault damage precursor as well as the control limits should be determined before online RUL prediction. Existing method for establishing the fault damage precursor can be categorized into 2 classes: data-driven method and model-based method. Accurate fault propagation model to establish fault damage precursor is usually unavailable. However, thanks to the rapid development of sensor technology and condition monitoring technology, large amount of observation data reflecting status of the system can be used to establish damage precursor by using data-driven method [9, 13]. Therefore, data-based method is gradually attracting the attention of researchers. Li et al. use historical normal data to establish PCA model, and 1-norm of the residual vector is used to define the fault damage precursor [23, 24]. RUL can be estimated by multistep

recursive prediction using AR model with forgetting factor [25, 26]. Ma et al. [27] use square prediction error based fault reconstruction method to estimate fault size in the first step. Then RUL can be estimated by multilevel recursive prediction. Li et al. [24] propose a fault prediction method for industry process with performance degradation by using multiscale PCA. Fault size computed by fault reconstruction can be used to establish a prediction model based on exponential smoothing technique. These methods share the same deficiency that fault direction is computed by PCA related method [27]. But pattern compounding problem of PCA makes it impossible to establish 1-1 correspondence between the failure component and the reconstructed fault direction [28]. Thus PCA based RUL prediction cannot tell the operator which critical component should be maintained.

Designated component analysis (DCA) is a knowledge-guided data-driven feature extraction method which can be used to diagnose root cause of the abnormality [29]. In this paper, DCA is introduced as a feature extraction tool for establishing fault damage precursor and life prediction model. Since small fault is usually buried in noise, pretreatment of filtering is developed for early detection of slowly varying small fault.

Remark 1. It is assumed that failure of critical component defined by expert has disastrous impact on the system. So RUL prediction of critical component is much significant in the sense that unnecessary surplus maintenance can be reduced to save maintenance cost.

The remainder of this paper is organized as follows: Section 2 describes principal component analysis and designated component analysis. DCA-based real-time prediction for critical component is developed in Section 3. Simulation analysis in Section 4 shows the efficiency of the method proposed. Conclusions and further research are given in the last section of the paper.

2. Review of PCA and DCA

2.1. PCA Modeling. Assume $Y_0 \in R^{n\times m}$ is the observation data matrix collected in the normal operation conditions, where m is the number of observation variables and n is the number of samples. Firstly, Y_0 is standardized via

$$\overline{Y_0} = \left[Y_0 - \begin{pmatrix}1 & 1 & \cdots & 1\end{pmatrix}^T M\right] \operatorname{diag}\left(\frac{1}{s_1}, \frac{1}{s_2}, \ldots, \frac{1}{s_m}\right), \quad (1)$$

where $M = [Y_0(1)\ Y_0(2)\ \cdots\ Y_0(m)]$ is the mean of Y_0, $Y_0(m)$ is the variable of Y_0, $s = [s_1\ s_2\ \cdots\ s_m]$ is the standard deviation of Y_0.

$\overline{Y_0}$ can be decomposed into two parts as follows [11]:

$$\overline{Y_0} = \sum_{i=1}^{v} t_i {p_i}^T + E, \quad (2)$$

where $t_i \in R^{n\times 1}$ is the score vector, $p_i \in R^{m\times 1}$ is the loading vector, v ($v < m$) is the number of significant principal components, and $E = \sum_{i=v+1}^{m} t_i {p_i}^T$ is the residual error.

After establishing PCA modeling under normal operating conditions, multivariate statistics called squared prediction error (SPE), can be used for fault detection and diagnosis. SPE is described as follows:

$$\mathrm{SPE}(i) = \|E(i)\|^2 = Y_i \left(I - PP^T\right) {Y_i}^T, \quad (3)$$

where Y_i ($i = 1, 2, \ldots, n$) represents a sample of online observation data, and P is a matrix composed of the first v loading vectors.

SPE control limit can be determined via

$$Q_\alpha = \theta_1 \left[\frac{C_\alpha \sqrt{2\theta_2 h_0^2}}{\theta_1} + 1 + \frac{\theta_2 h_0 (h_0 - 1)}{\theta_1^2}\right]^{1/h_0}, \quad (4)$$

$$\theta_t = \sum_{j=k+1}^{m} \lambda_j^t \quad (t = 1, 2, 3), \quad (5)$$

$$h_0 = 1 - \frac{2\theta_1\theta_3}{3\theta_2^2}, \quad (6)$$

where λ_j is the eigenvalues of the covariance matrices and C_α is the threshold of hypothesis testing to normal distribution with confidence level α.

The system is considered to be abnormal if

$$\mathrm{SPE} \geq Q_\alpha. \quad (7)$$

2.2. DCA. DCA is a knowledge-guided multivariate statistical feature extraction method [29]. The basic idea is to define a designated pattern via the fault-symptom relation.

First, different from the loading vector $p_i \in R^{m\times 1}$ of PCA, the definition of designated pattern D_i is defined by a knowledge-guided means via

$$D_i = \begin{bmatrix} d_{i1} \\ d_{i2} \\ \vdots \\ d_{im} \end{bmatrix}, \quad i = 1, 2, \ldots, L, \quad (8)$$

where d_{ir} ($r = 1, 2, \ldots, m$) can be taken as 0 or 1 according to the fault-symptom relation, and $d_{ir} = 1$ means that the symptom r is shown in the ith designated pattern; otherwise $d_{ir} = 0$.

Table 1 lists the typical fault-symptom relation of an air compressor. There are 17 typical faults and 19 observation parameters included in the table. Insufficient supply of lubricating oil or oil blockage, lubricant contamination, motor drive failure, and so on are the typical faults listed in Table 1. First-stage exhaust temperature, intercooler exhaust temperature, two-stage exhaust temperature, oil cooling outlet temperature and motor current, and so forth are the observed parameters [29].

Table 1: Typical fault-symptom relation of air compressor.

	u_1	u_2	u_3	u_4	u_5	u_6	u_7	u_8	u_9	u_{10}	u_{11}	u_{12}	u_{13}	u_{14}	u_{15}	u_{16}	u_{17}	u_{18}	u_{19}	u_{20}
D_1	1	0	0	0	0	0	1	0	0	0	0	0	0	0	0	0	0	0	0	0
D_2	0	1	0	0	0	0	1	0	0	0	0	0	0	0	0	0	0	0	0	0
D_3	0	0	1	0	0	0	1	0	0	0	0	0	0	0	0	0	0	0	0	0
D_4	0	0	0	0	0	0	0	0	0	0	1	0	1	0	0	0	0	0	0	0
D_5	0	0	0	0	0	0	1	0	0	0	0	0	0	1	0	0	0	0	0	0
D_6	1	1	1	0	0	0	1	0	0	0	0	0	0	0	0	0	0	0	0	0
D_7	0	0	0	1	1	1	0	1	1	1	0	0	0	0	0	0	0	0	0	0
D_8	0	0	0	0	1	1	0	0	0	1	0	0	1	0	0	0	0	0	0	0
D_9	0	0	0	1	1	1	0	1	1	1	1	1	0	0	0	0	0	0	0	0
D_{10}	0	0	0	0	0	1	0	0	0	1	0	0	1	0	0	0	0	0	0	0
D_{11}	0	0	0	0	0	0	0	0	0	0	1	1	0	0	0	1	0	0	0	0
D_{12}	0	0	0	0	0	0	0	0	0	0	0	0	1	0	0	0	0	0	0	0
D_{13}	0	0	0	0	0	0	0	0	0	0	0	0	0	0	0	1	1	0	0	0
D_{14}	0	0	0	0	0	0	0	0	0	0	0	0	0	0	0	0	1	0	0	0
D_{15}	0	0	0	0	0	0	0	0	0	0	0	0	0	0	0	0	0	1	0	0
D_{16}	0	0	0	0	0	0	0	0	0	0	0	0	0	0	0	0	0	0	1	0
D_{17}	0	0	0	0	0	0	0	0	0	0	0	0	0	0	0	0	0	0	0	1

From Table 1, the fifth row corresponds to the fault of insufficient supply of lubricating oil, the sixth row corresponds to the fault of lubricant contamination, and these fault patterns can be defined as follows [29]:

$$\begin{aligned} &D_5 \\ &= \left[0\ 0\ 0\ 0\ 0\ 0\ 1\ 0\ 0\ 0\ 0\ 0\ 0\ 1\ 0\ 0\ 0\ 0\ 0\ 0\right]^T, \\ &D_6 \\ &= \left[1\ 1\ 1\ 0\ 0\ 0\ 1\ 0\ 0\ 0\ 0\ 0\ 0\ 1\ 0\ 0\ 0\ 0\ 0\ 0\right]^T. \end{aligned} \tag{9}$$

Then, project the observation variable y to designated patterns D_i to obtain the designated component w_i:

$$w_i = {D_i}^T y. \tag{10}$$

Similarly to (2), the observation matrix Y_0 can be decomposed as

$$Y_0 = \sum_{i=1}^{L} D_i W_i + E, \tag{11}$$

where L is the number of designated patterns, $W_i = [w_i(1), w_i(2), \ldots, w_i(n)] \in R^{1\times n}$, and E is the residual matrix.

Finally, Shewhart chart of each designated component is used to implement fault diagnosis.

3. DCA-Based Real-Time Prediction for Critical Component

DCA-based RUL prediction method needs to determine critical component by expert experience. In this paper, the component corresponding to designated pattern D_1 is assumed to be a critical component.

3.1. Fault Damage Precursor Based on Historical Observation

3.1.1. Knowledge-Guided Data-Driven Feature Extraction. Project historical normal observation data Y_0 to the designated pattern D_i to obtain the designated component vector W_{0i}:

$$W_{0i} = D_i^T Y_0, \quad i = 1, 2, \ldots, L. \tag{12}$$

The designated component W_{0i} is the feature extracted from Y_0. In general, statistical distribution of W_{0i} is normal distribution as long as the observation of each observation variable is normal distribution.

3.1.2. Data-Driven Fault Damage Precursor. In the case when there is no fault damage precursor determined by expert or by physical fault propagation model, it is necessary to establish a data-driven fault damage precursor for describing the fault evolution process. For this purpose, the failure control limit q to determine the failure time and the fault trend control limit l_1 for early detection of slowly varying fault should first be determined. Specific steps are as follows.

Step 1 (failure control limit and fault trend control limit). As it is analyzed in Section 3.1.1, W_{0i} has the normal distribution. By 3σ criteria of hypothesis testing to normal distribution, the critical designated component W_{01} falls into interval $[-3\sigma, 3\sigma]$ with confidence level 99.7% [30, 31]:

$$P\left(-3\sigma \le W_{01} \le 3\sigma\right) = 99.7\%. \tag{13}$$

So the failure control limit q can be determined via

$$q = 3\sigma, \tag{14}$$

where σ is the standard deviation of W_{01}.

For the sake of determining fault trend control limit l_1, wavelet filtering is firstly introduced as a preprocessing tool to historical normal observation data, and then DCA is used to perform feature extraction to the filtered normal observation. The filtering process can be described as follows [32, 33].

First, discrete wavelet transform (DWT) for the observation vector of the ith observation variable $Y_0^{(i)}$ can be depicted via

$$\begin{aligned} a_{(j)}(k) &= \sum_N h(N-2k)\, Y_{0_{(j)}}^{(i)}(k), \\ d_{(j)}(k) &= \sum_N g(N-2k)\, Y_{0_{(j)}}^{(i)}(k), \end{aligned} \tag{15}$$

where $k = 0, 1, 2, \ldots, n-1$; n is the number of discrete sampling points; $a_{(j)}(k)$ is the scaling coefficient for signal on the scale j; $d_{(j)}(k)$ is the wavelet coefficient for signal on the scale j; h is a low-pass filter, g is a high-pass filter, and N is the length of the filter.

After DWT, the next step is filtering. How to select the threshold is the key problem because it will directly affect the result of wavelet filter. In this paper, we choose the soft threshold method shown in

$$\widehat{d}_{(j)}(k) = \begin{cases} \operatorname{sign}\left(d_{(j)}(k)\right)\left(\left|d_{(j)}(k)\right| - T\right), & \left|d_{(j)}(k)\right| \geq T \\ 0, & \left|d_{(j)}(k)\right| < T, \end{cases} \tag{16}$$

where T is the filtering threshold.

Finally, inverse discrete wavelet transform (IDWT) is implemented to obtain the filtered observation:

$$\widetilde{Y}_0^{(i)} = \sum_k a_j(k)\, h(N-2k) + \sum_k \widehat{d}_j(k)\, g(N-2k). \tag{17}$$

Based on the filtered normal observation, fault trend control limit l_1 can be determined via (19):

$$W_{0iF} = D_i^T \widetilde{Y}_0, \quad i = 1, 2, \ldots, L, \tag{18}$$

$$l_1 = 3\sigma_1, \tag{19}$$

where σ_1 is the standard deviation of W_{01F}.

Step 2 (fault trend detection point and the failure point). Project historical faulty observation data Y_1 to the designated pattern D_1 to get the designated component W_1:

$$W_1 = D_1^T Y_1. \tag{20}$$

The extracted feature W_1 can characterize the fault evolution process of the critical component. The failure point t_f can be calculated as follows:

$$t_f = \min\left\{k : W_1(k) \geq q\right\}. \tag{21}$$

Similarly, the filtered designated component can be computed via (22).

$$W_{1F} = D_1^T Y_{1F}. \tag{22}$$

Once W_{1F} and fault trend control limit l_1 have been obtained, the definition of fault trend detection point t_s can be expressed as

$$t_s = \operatorname*{argmin}_k \left\{k : W_{1F}(k) \geq l_1\right\}. \tag{23}$$

Step 3 (fault damage precursor). Smoothing technique descripted in (24) is required to get a more smooth fault damage precursor:

$$\begin{aligned} \overline{W_{1F}}(1) &= W_{1F}(1) \\ \overline{W_{1F}}(2) &= \frac{\left(W_{1F}(1) + W_{1F}(2) + W_{1F}(3)\right)}{3} \\ \overline{W_{1F}}(3) &= \frac{\left(W_{1F}(1) + W_{1F}(2) + W_{1F}(3) + W_{1F}(4) + W_{1F}(5)\right)}{5} \\ &\vdots \\ \overline{W_{1F}}(k) &= \frac{\left(W_{1F}(k-c+1) + W_{1F}(k-c+2) \cdots + W_{1F}(k)\right)}{c} \\ &\vdots, \end{aligned} \tag{24}$$

where c is the size of the smoothing window; $W_{1F}(i)$ $(i = 1, 2, \ldots, n)$ is the element of vector W_{1F}.

The fault evolution process in the period from t_s to t_f can be defined as fault damage precursor, denoted by C:

$$C\left(t - t_s + 1\right) = \overline{W_{1F}}(t), \quad \left(t = t_s, t_s + 1, \ldots, t_f\right). \tag{25}$$

3.1.3. The RUL Prediction Model. The historical RUL is defined by the deviation between t and t_f:

$$\mathrm{RUL}\left(t - t_s + 1\right) = t_f - t, \quad \left(t = t_s, t_s + 1, \ldots, t_f\right), \tag{26}$$

where t is the current sampling time.

Once the fault precursor defined in (26) is established, the algorithm of establishing RUL prediction model can be divided into three steps.

Step 1. Computerize the deviation between fault damage precursor and the control limit denoted by R:

$$R\left(t - t_s + 1\right) = C(t) - l_1. \tag{27}$$

Step 2. Once the deviation R and the historical RUL have been obtained, historical data can be determined as follows:

$$J = \{(R, \mathrm{RUL})\}. \tag{28}$$

Step 3. Exponential life prediction model is established by nonlinear fitting of the historical data. Fitting equation is shown as follows:

$$\mathrm{RUL} = c + a \times e^{bR}. \tag{29}$$

3.2. Online Fault Diagnosis. Firstly, online observation data after pretreatment of wavelet filtering is denoted by Y_z. Project Y_z to the designated patterns D_i to obtain the designated component vector W_{iz}:

$$W_{iz} = D_i^T Y_z, \quad i = 1, 2, \ldots, L. \tag{30}$$

The smoothed designated component is denoted by $\overline{W_{iz}}$. Shewhart charts based method is used in this paper to implement fault diagnosis.

3.3. Online Life Prediction. A key step of online RUL prediction for the critical component is to judge whether $R(k)$ is positive or negative. If $R(k)$ is positive, it means that the system is abnormal. Real-time RUL prediction results can be obtained via exponential life prediction model:

$$\begin{aligned} R(k) &= \overline{W_{1z}}(k) - l_1 > 0, \\ \widehat{\mathrm{RUL}}(k) &= c + a \times e^{bR(k)}, \\ k &= t_s, t_s + 1, \ldots, t_f. \end{aligned} \tag{31}$$

4. Simulation

4.1. Simulation Data. In this section, $m = 20$, $n = 1000$ are used for simulation. Normal observation data is the compound of ten coexisting change patterns:

$$Y_0 = \sum_{i=1}^{L} D_i \overline{W_i}, \tag{32}$$

where $L = 10$ is the number of designated patterns, D_1, D_7 represent fault patterns, and the rest are normal random disturbance patterns. $\overline{W_i}$ is the sample vector of designated component for simulation. In MATLAB, $\overline{W_i}$ can be defined by the function of "randn" and some linear operations. Assuming $\overline{W_i}$ is normally distributed,

$$\begin{aligned} \overline{W_1} &= \mathrm{randn}(1, n), \\ \overline{W_2} &= 0.5\overline{W_1} + 0.8\,\mathrm{randn}(1, n), \\ \overline{W_3} &= 0.5\overline{W_1} + 0.5\overline{W_2}, \\ \overline{W_4} &= 0.5\overline{W_2} + 0.1\,\mathrm{randn}(1, n), \\ \overline{W_5} &= \overline{W_3} + 0.2\overline{W_4}, \\ \overline{W_6} &= 0.2\overline{W_1} + 0.3\overline{W_4}, \\ \overline{W_7} &= 0.3\,\mathrm{randn}(1, n), \\ \overline{W_8} &= 0.2\overline{W_7} + 0.2\,\mathrm{randn}(1, n), \\ \overline{W_9} &= 0.1\overline{W_8} + 0.2\,\mathrm{randn}(1, n), \\ \overline{W_{10}} &= 0.5\,\mathrm{randn}(1, n). \end{aligned} \tag{33}$$

From 130th to 1000th sampling point, the influence of fault patterns D_1 becomes greater

$$f_1 = g_1\left(1 - e^{-t_1/\tau_1}\right), \tag{34}$$

where $g_1 = 6$, $t_1 \in [0, 13]$, $\tau_1 = 8$.

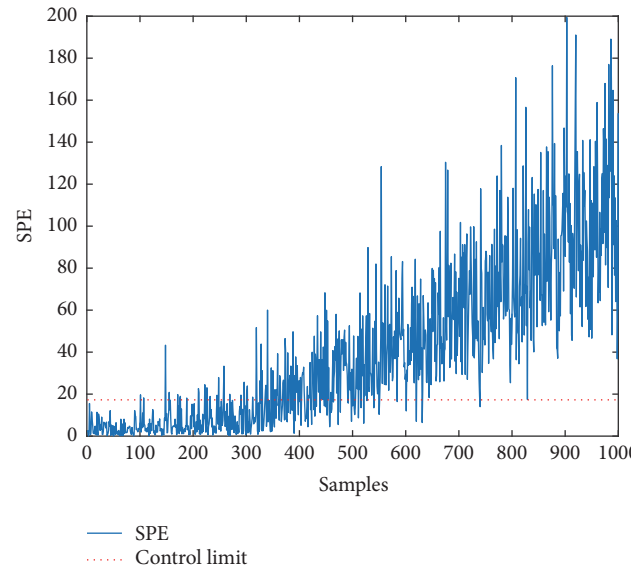

Figure 1: PCA based fault detection.

From 300th to 1000th sampling point, the influence of fault patterns D_7 becomes greater

$$f_7 = g_7\left(1 - e^{-t_7/\tau_7}\right), \tag{35}$$

where $g_7 = 4$, $t_7 \in [1, 8]$, $\tau_7 = 6$.

4.2. Data Feature Extraction Based on DCA. Figure 1 shows SPE chart of PCA. The control limit with confidence level $\alpha = 0.003$, which can be calculated by (4). From Figure 1, the abnormally can be detected from the 411th sample time. It can be concluded from Figure 1 that the detection time using PCA is not consistent with the failure point of any component.

Therefore, DCA is introduced to overcome the pattern compounding deficiency of PCA. DCA-based faults diagnosis results are depicted in Figure 2. The dotted red line is the control limit. As shown in Figure 2, the Shewhart charts correspond to D_1, D_7 beyond the upper control limit from 451 and 501, respectively. The results indicate that DCA is an effective multiple faults diagnosis method for multiple faults diagnosis.

4.3. Early Fault Feature Extraction Based on DCA. In this part, wavelet based denoising technique is used to extract early fault feature. The filtered SPE chart of PCA is shown in Figure 3. The blue line denotes the filtered SPE (abbreviated as F-SPE in the following); the black point line denotes the filtered SPE after smoothing (abbreviated as F-S-SPE in the following). The fault trend can be detected from the 154th sample point.

Figure 4 shows the faults results of DCA preprocessed by wavelet filter (WF-DCA). The blue line denotes the filtered designated components (the F-dcs); the black line denotes the filtered dcs after smoothing (the F-S-dcs). It can be seen from Figure 4 that the fault trend of the 1st dc can be detected at 161. The 7th dc is abnormal from 326.

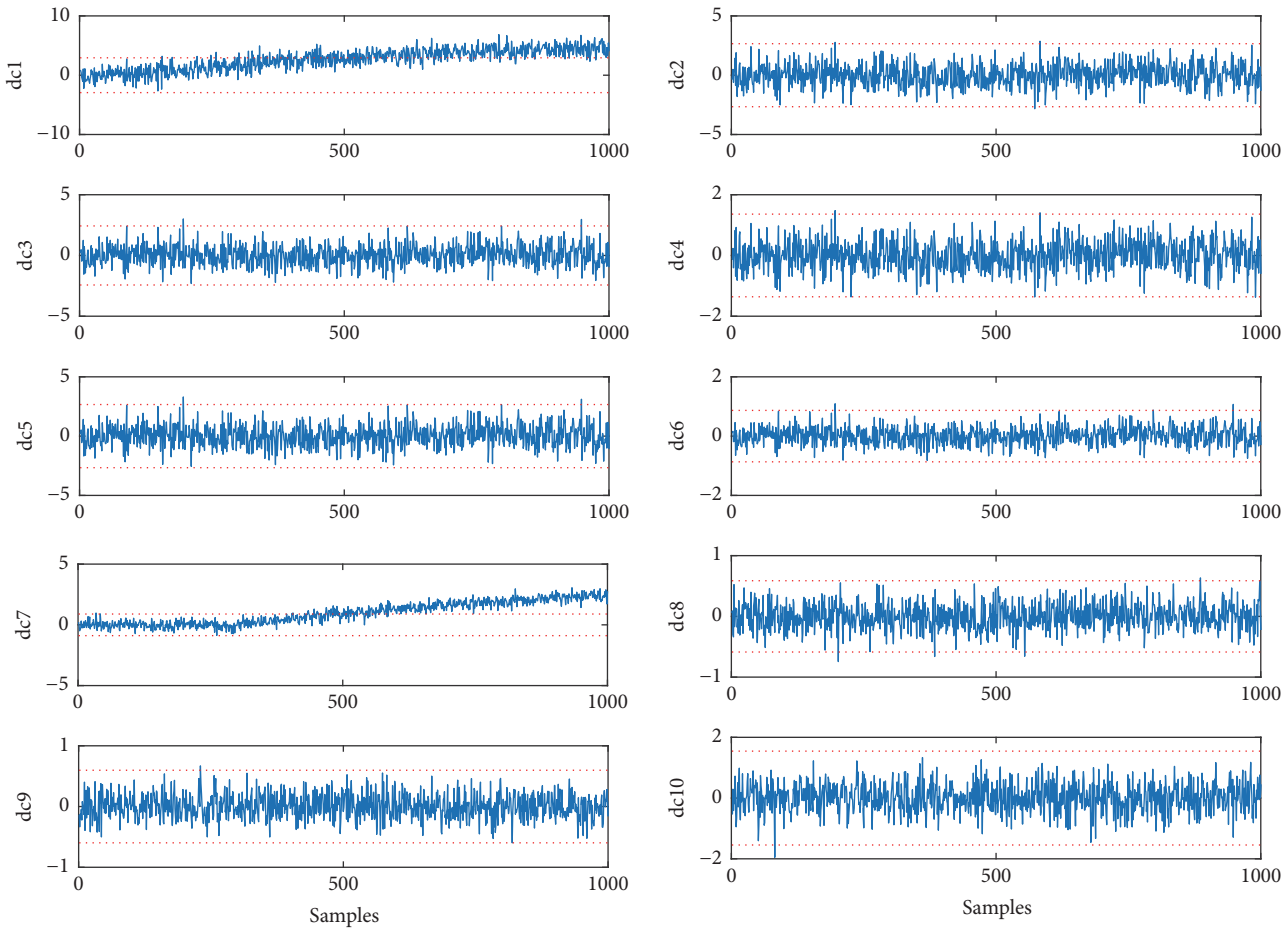

Figure 2: DCA-based faults diagnosis.

These simulation results imply that the early fault detection can be achieved by wavelet filtering which can increase the signal-to-noise ratio (SNR) of the fault signal. This paper determines the fault trend detection point using wavelet filtering technique.

4.4. RUL Prediction Model. In this paper, the system component corresponding to D_1 is assumed to be a critical component. In order to get more precise RUL prediction model, smoothing technique is used to postprocess the fault precursor. The smoothed evolution precursor between fault trend detection point and failure point can be defined as the damage precursor to establish RUL prediction model.

For establishing RUL prediction model based on WF-PCA, the failure time $t_f = 411$ can be determined from Figure 1. The fault trend detection point $t_s = 154$ can be obtained from Figure 3. The F-S-SPE between 154 and 411 can be defined as the fault damage precursor. Use RUL $= a \times e^{bR}$ as the fitting function to establish RUL prediction model, where R is the deviation between the value of F-S-SPE and the control limit. Figure 5 shows the fitted RUL prediction model based on WF-PCA.

Figure 6 shows the fitted RUL prediction model of the critical component based on WF-DCA. The first F-S-dc between 161 and 451 can be defined as fault damage precursor,

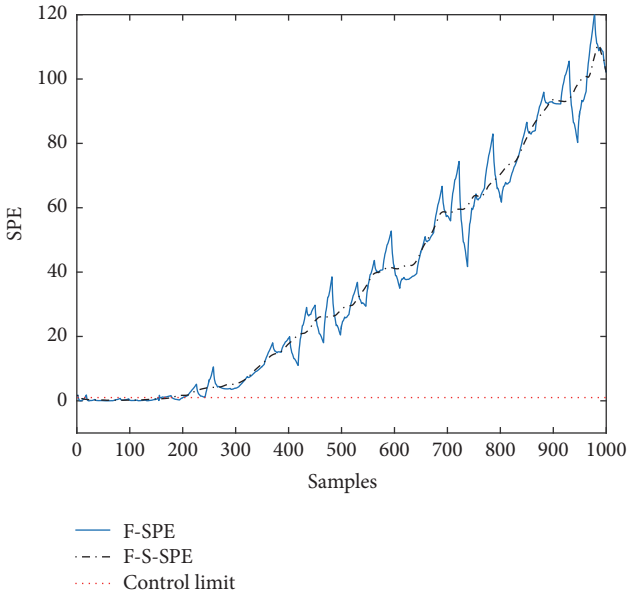

Figure 3: WF-PCA based early fault detection.

where t_f and t_s can be obtained from Figures 2 and 4, respectively.

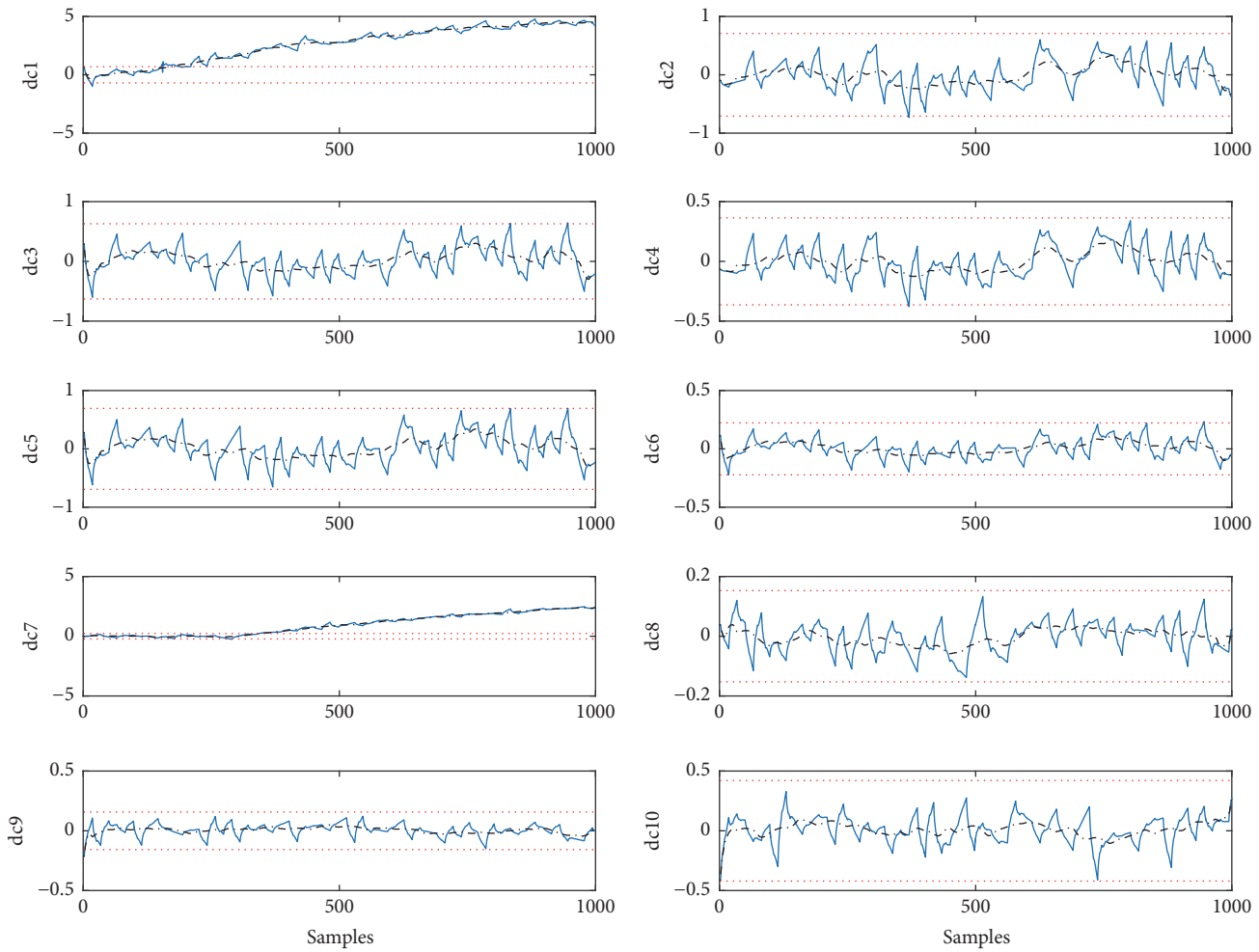

Figure 4: WF-DCA-based early faults diagnosis.

4.5. Online Life Prediction and Fault Diagnosis Based on DCA. Once online data is obtained, we can predict the online RUL based on the aforementioned prediction model. Figure 7 depicts the online fault detection results by online F-S-SPE. It can be seen from Figure 7 that the fault trend can be detected from the 152nd sample point.

To further demonstrate the superiority of the proposed method, two commonly used prediction algorithms are employed for comparison, namely, AR and BPNN. For BPNN and AR, fault trend prediction and recursive RUL prediction are implemented in two separate stages which makes them unavailable to predicting the RUL online. The parameters of BPNN are shown in Table 2. In this paper, the order of AR model is 1, and the regression parameter is φ. The recursive RUL prediction process can be formulated as follows:

$$\overline{W_{1z}}(k+s) = \varphi \overline{W_{1z}}(k+s-1) \geq q, \quad k = t_s, t_s+1, \ldots, t_f, \tag{36}$$

where s is the number of recursive steps and q is the failure control limit.

Figure 8 shows the online RUL prediction result of PCA. The blue line is the real RUL. The dotted red line is the predicted RUL by the method proposed in this paper. The dotted black line is the predicted RUL by AR. The dotted blue line is the predicted RUL by BPNN. As we can see from Figure 8, the prediction accuracy of the dotted red line is higher than that of the dotted black line and the dotted blue line. Extra recursive steps are required for both AR and BPNN based RUL prediction model. The method proposed in this paper can avoid this problem and reduce the prediction error.

Figure 9 depicts the online faults diagnosis results based on WF-DCA. From Figure 9, the fault trends corresponding to D_1 and D_7 can be detected from 165 and 324, respectively. Figure 10 shows the online prediction result of the critical component. The blue line is the real RUL. The dotted red

Table 2: Parameters of BPNN in pretraining.

Parameters	BPNN
Layers	3
Neurons in each layer	[1, 10, 1]
Learning rate	0.0001
Epochs	1000

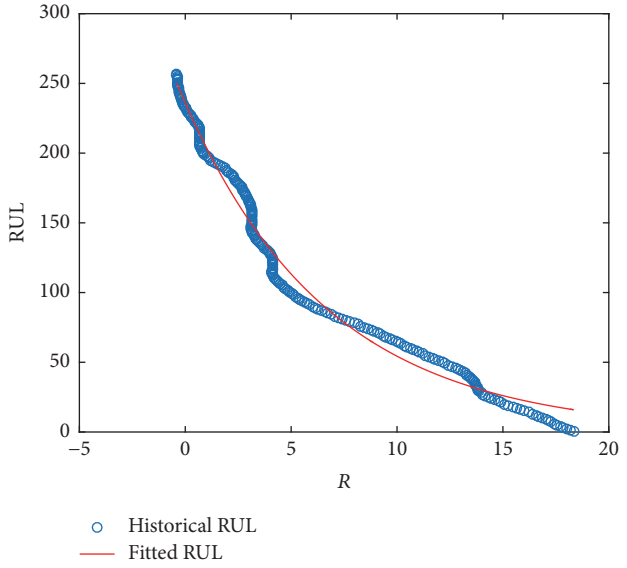

Figure 5: The fitted RUL prediction model based on PCA.

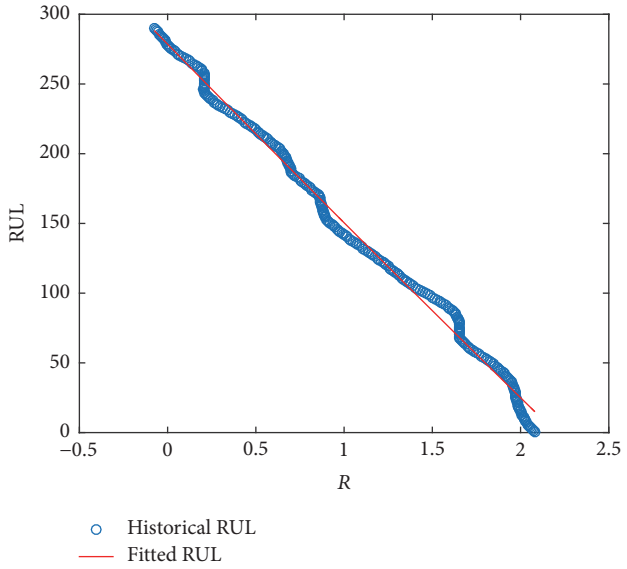

Figure 6: The fitted RUL prediction model of the critical component based on DCA.

Table 3: Mean of RUL prediction error.

Statistics	Fitting	AR	BPNN
SPE	10.536	15.969	14.450
dc1	9.973	24.156	20.035

line is the predicted RUL by nonlinear fitting method. The dotted black line is the predicted RUL by AR. The dotted blue line is the predicted RUL by BPNN. It can be seen from Figure 10 that fitted RUL prediction model is more efficient than other models. The mean of RUL prediction error is listed in Table 3. It can be concluded from Table 3 that the proposed method is a good choice for the RUL prediction of the critical component.

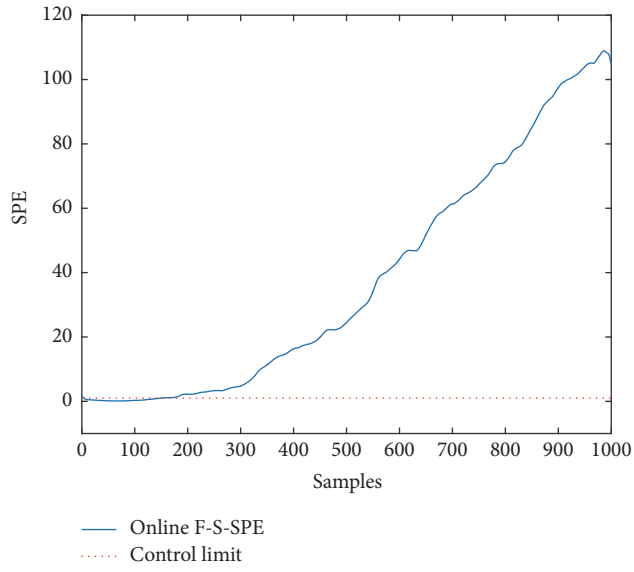

Figure 7: Online early fault detection based on WF-PCA.

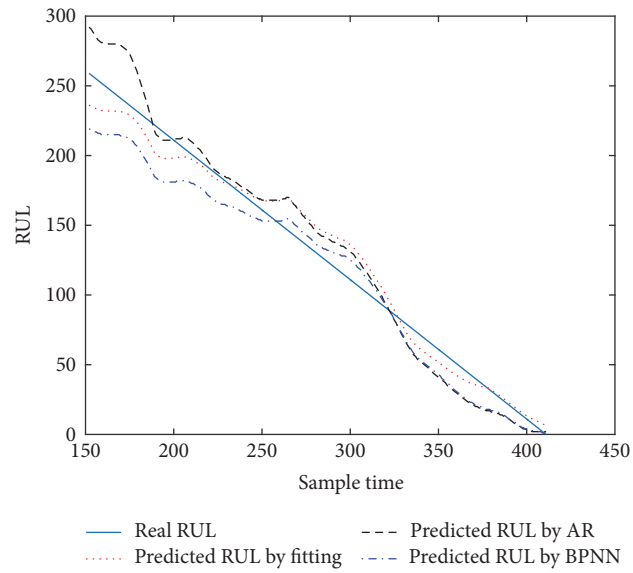

Figure 8: Online RUL prediction based on PCA.

5. Conclusions

Traditional RUL prediction is based on autoregression which cannot ensure a real-time RUL prediction since necessary computation time is required for online recursive prediction. In addition in order to implement RUL prediction for critical component that has disastrous impact on the system, DCA is introduced as a fault feature extraction tool for a certain system component to overcome the pattern compounding problem of PCA. The fault feature extracted by DCA can be used to define the fault precursor. For the sake of establishing RUL prediction model, wavelet filter technology based preprocessing is used for early detection of those slowly varying faults. Finally, exponential fitting based online RUL

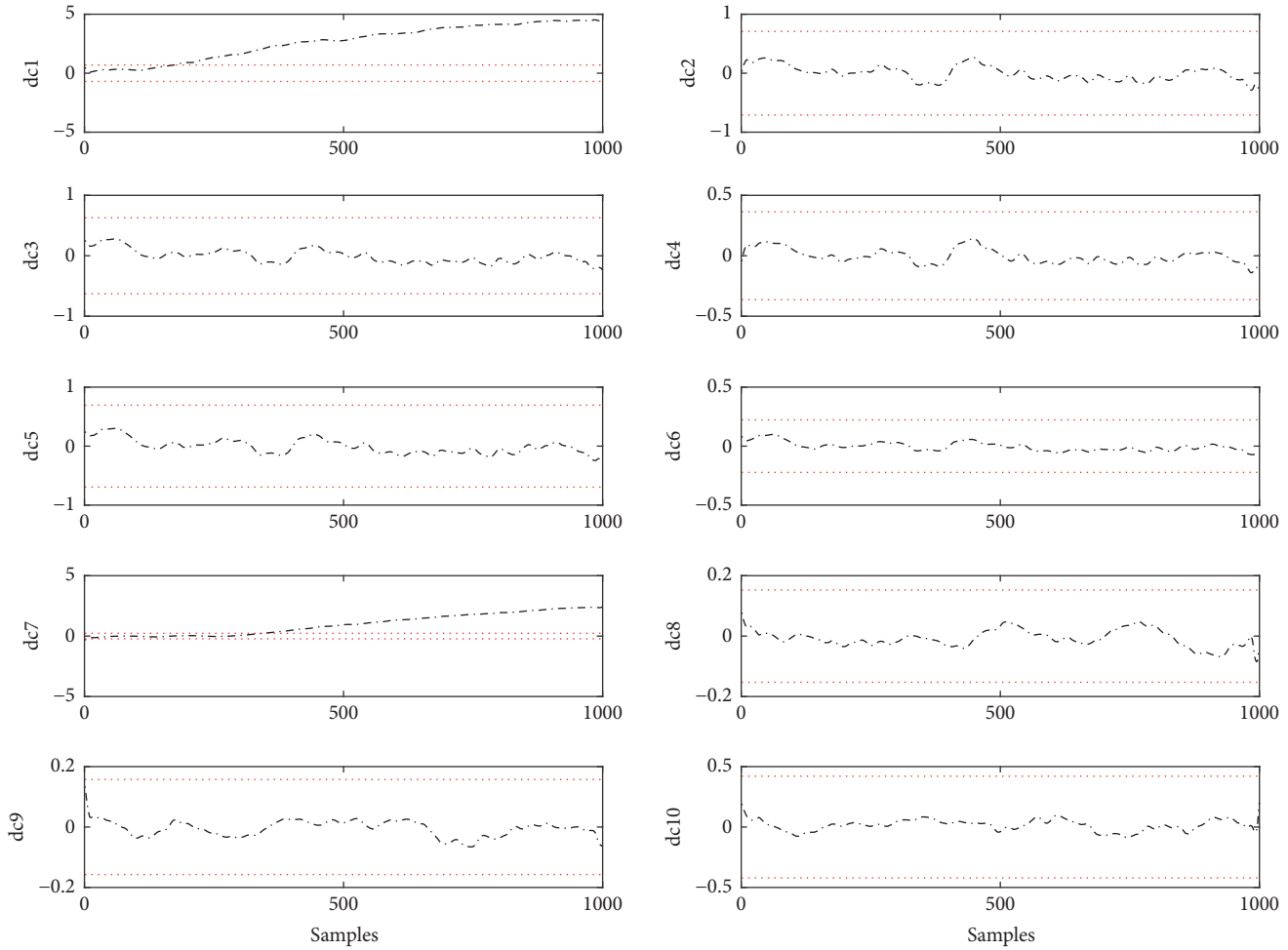

Figure 9: Online early fault diagnosis based on DCA.

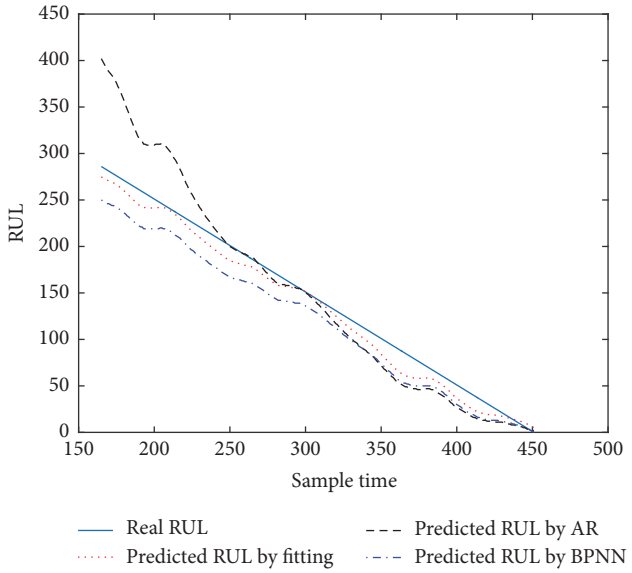

Figure 10: The online prediction result of the critical component.

prediction model is developed to get the real-time online prediction of RUL.

Conflicts of Interest

The authors declare that they have no conflicts of interest.

Acknowledgments

This research was supported in part by the Natural Science Fund of China (Grant no. U1604158) and Technical Innovation Talents Scheme of Henan Province (Grant no. 2012HASTIT005).

References

[1] Y.-T. Hu, C.-H. Hu, X.-Y. Kong, and Z.-J. Zhou, "Real-time lifetime prediction method based on wavelet support vector regression and fuzzy c-means clustering," *Acta Automatica Sinica*, vol. 38, no. 3, pp. 331–340, 2012 (Chinese).

[2] C. Jin-Yin, H. Hui-Hao, Z. Xiao, and Y. Dong-Yong, "Fault diagnosis research for power system based on timing constraint fuzzy directed graph," *International Journal of Control and Automation*, vol. 9, no. 1, pp. 323–346, 2016.

[3] J. Uddin, M. R. Islam, J.-M. Kim, and C.-H. Kim, "A two-dimensional fault diagnosis model of induction motors using a gabor filter on segmented images," *International Journal of Control and Automation*, vol. 9, no. 1, pp. 11–22, 2016.

[4] J. Lou, K. Shan, and J. Xu, "A new condition monitoring method for wind turbines based on power curve model," *International Journal of Control and Automation*, vol. 121, pp. 470–475, 2016.

[5] K. X. Peng, L. MA, and K. Zhang, "Review of quality-related fault detection and diagnosis techniques for complex industrial processes," *Acta Automatica Sinica*, vol. 43, no. 3, pp. 349–365, 2017 (Chinese).

[6] Y. Chen, "Reference-related component analysis: a new method inheriting the advantages of PLS and PCA for separating interesting information and reducing data dimension," *Chemometrics and Intelligent Laboratory Systems*, vol. 156, pp. 196–202, 2016.

[7] Z. He, H. Zhou, J. Wang, and S. Zhai, "A unified framework for contrast research of the latent variable multivariate regression methods," *Chemometrics and Intelligent Laboratory Systems*, vol. 143, pp. 136–145, 2015.

[8] C. Zhao and F. Gao, "Online fault prognosis with relative deviation analysis and vector autoregressive modeling," *Chemical Engineering Science*, vol. 138, pp. 531–543, 2015.

[9] Z. Xu, Y. Ji, and D. Zhou, "A new real-time reliability prediction method for dynamic systems based on on-line fault prediction," *IEEE Transactions on Reliability*, vol. 58, no. 3, pp. 523–538, 2009.

[10] Z. H. Cheng, Z. Y. Yang, J. M. Zhao, Y. B. Wang, and Z. W. Li, "Preventive maintenance strategy optimizing model under two-dimensional warranty policy," *Eksploatacja i Niezawodnosc - Maintenance and Reliability*, vol. 17, no. 3, pp. 365–373, 2015.

[11] L. Kumar, S. Misra, and S. K. Rath, "An empirical analysis of the effectiveness of software metrics and fault prediction model for identifying faulty classes," *Computer Standards Interfaces*, vol. 53, pp. 1–32, 2017.

[12] Z. Sheng, J. Wang, Z. Liu, and L. Dong, "The monitoring of CNC machine processing condition based on the BP neural network," *Advanced Materials Research*, vol. 542-543, pp. 95–98, 2012.

[13] S. Aras and D. K. İpek, "A new model selection strategy in time series forecasting with artificial neural networks: IHTS," *Neurocomputing*, vol. 174, pp. 974–987, 2016.

[14] Z. Tang and P. A. Fishwick, "Feedforward neural nets as models for time series forecasting," *Journal on Computing*, vol. 5, no. 4, pp. 374–385, 1993.

[15] X. Y. Wen, P. C. Li, J. N. Chen, Y. Zhu, and X. F. Wu, "Optimized BP neural network algorithm in predicting camellia oleifera yield," *Journal of Northeast Forestry University*, vol. 10, pp. 56–60, 2016.

[16] P. Poonnoy, A. Tansakul, and M. Chinnan, "Artificial neural network modeling for temperature and moisture content prediction in tomato slices undergoing microwave-vacuum drying," *Journal of Food Science*, vol. 72, no. 1, pp. E42-E47, 2007.

[17] D. Liu, Z. Yu, Z. Hao, C. Zhu, and Q. Ju, "On the development of improved artificial neural network model and its application on hydrological forecasting," in *Proceeding of the 3rd International Conference on Natural Computation, ICNC 2007*, pp. 45–49, August 2007.

[18] W.-F. Yang and F.-L. Zeng, "Parameter estimation of the AR model based on interval analysis," in *Proceeding of the 2nd International Symposium on Intelligent Information Technology Application Workshop, IITA 2008*, pp. 990–993, December 2008.

[19] T. Xu, J. Wu, Z.-S. Wu, and Q. Li, "Long-term sunspot number prediction based on EMD analysis and AR model," *Chinese Journal of Astronomy and Astrophysics*, vol. 8, no. 3, pp. 337–342, 2008 (Chinese).

[20] X. K. Wei, Y. H. Li, P. Zhang, and J. M. Lu, "Analysis and applications of time series forecasting model via support vector machines," in *Systems Engineering and Electronics*, vol. 03, pp. 529–532, 2005.

[21] Y. Y. Ni and J. X. Zhang, "Modeling and forecasting for multivariate time series using a vector autoregression model," *Chinese Journal of Health Statistics*, vol. 31, no. 1, pp. 53–56, 2014 (Chinese).

[22] P. Do Van, E. Levrat, A. Voisin, and B. Iung, "Remaining useful life (RUL) based maintenance decision making for deteriorating systems," in *Proceedings of the IFAC Workshop on Advanced Maintenance Engineering, Services and Technology, (A-MEST '12)*, pp. 66–72, November 2012.

[23] G. Li and D. Zhou, "SPM-based online fault prediction approach for multivariate continuous processes," *Journal of Chemical Industry and Engineering*, vol. 59, no. 7, pp. 1829–1833, 2008 (Chinese).

[24] G. Li, S. J. Qin, Y. Ji, and D. Zhou, "Reconstruction based fault prognosis for continuous processes," *Control Engineering Practice*, vol. 18, no. 10, pp. 1211–1219, 2010.

[25] R. Lewis and G. C. Reinsel, "Prediction of multivariate time series by autoregressive model fitting," *Journal of Multivariate Analysis*, vol. 16, no. 3, pp. 393–411, 1985.

[26] X.-S. Si, W. Wang, C.-H. Hu, and D.-H. Zhou, "Remaining useful life estimation—a review on the statistical data driven approaches," *European Journal of Operational Research*, vol. 213, no. 1, pp. 1–14, 2011.

[27] J. Ma, Q. Y. Wang, and G. Li, "Fault prediction of purbine machine based PCA fault reconstruction method," *Automation and Information Engineering*, vol. 03, pp. 25–28, 2011.

[28] F. N. Zhou, C. L. Wen, Z. G. Chen, and Y. B. Leng, "DCA based multi-level small fault diagnosis method," *Chinese Journal of Electronics*, vol. 38, no. 8, pp. 1874–1879, 2010 (Chinese).

[29] F. N. Zhou, *Multi-Fault Diagnosis Method and Application Based on Statistical Feature Extraction [Ph.D. dissertation]*, Shanghai Maritime University, Shanghai, China, 2009.

[30] M. Panda and P. Khilar, "Distributed self fault diagnosis algorithm for large scale wireless sensor networks using modified three sigma edit test," *Ad Hoc Networks*, vol. 25, pp. 170–184, 2015.

[31] T. A. Brunner, "Relative merits of using maximum error versus 3(sigma) in describing the performance of laser-exposure reticle writing systems," in *The International Society for Optical Engineering*, vol. 2440 of *Proceedings of SPIE*, pp. 550–559, 1995.

[32] R. Ganesan, "Real-time monitoring of complex sensor data using wavelet-based multiresolution analysis," *International Journal of Advanced Manufacturing Technology*, vol. 39, no. 5-6, pp. 543–558, 2008.

[33] H. Li, X. Yang, J. Li, J. Chen, and C. Cheng, "The maximum energy of wavelet decomposition approximation -related adaptive wavelet de-nosing for partial discharge UHF pulse in GIS," *Transactions of China Electrotechnical Society*, vol. 27, no. 5, pp. 84–91, 2012.

Hindawi
Journal of Control Science and Engineering
Volume 2017, Article ID 7937916, 9 pages
https://doi.org/10.1155/2017/7937916

Research Article

Distributed Optimization of Multiagent Systems in Directed Networks with Time-Varying Delay

Junxiu Yan and Hui Yu

College of Science, China Three Gorges University, Yichang 443002, China

Correspondence should be addressed to Hui Yu; yuhui@ctgu.edu.cn

Received 3 January 2017; Revised 19 February 2017; Accepted 16 March 2017; Published 29 March 2017

Academic Editor: Chaojie Li

This paper addresses a distributed consensus optimization problem of a first-order multiagent system with time-varying delay. A continuous-time distributed optimization algorithm is proposed. Different from most ways of solving distributed optimization problem, the Lyapunov-Razumikhin theorem is applied to the convergence analysis instead of the Lyapunov-Krasovskii functionals with LMI conditions. A sufficient condition for the control parameters is obtained to make all the agents converge to the optimal solution of the system. Finally, an example is given to validate the effectiveness of our theoretical result.

1. Introduction

In recent years, the distributed optimization problem of multiagent systems has been investigated by many researchers; researches on distributed optimization and control theorem have been developing rapidly and have been applied to various fields of industry and defense, like smart grid [1, 2], sensor networks [3], social networks [4], and so on. The objective of distributed optimization problem is to solve an optimization problem cooperatively in a distributed way, where the objective function is formed by a sum of local objective functions, and each agent can only know one local objective function. The ultimate goal is to make the states of all the agents converge to optimal solution of the optimization problem via local coordination. Compared with the consensus problem of multiagent systems, which makes all agents achieve a common state [5–8], not only does the optimization problem make all agents achieve the same state, but also at the same time the achieved state minimizes the optimization problem.

The current literatures about distributed optimization problems are more focused on discrete-time algorithms (see [9–12] and references therein). In both papers [9, 11], discrete-time subgradient algorithms are proposed for unconstrained, separable, convex optimization problem and each agent communicates with the other agents over a time-varying network topology. A projected consensus subgradient algorithm is proposed for constrained optimization problem in [10], and, in [12], the authors devise two distributed primal-dual subgradient algorithms over networks with dynamically changing topologies but satisfying a standard connectivity property. But, recently, some continuous-time methods have also been successfully used to solve distributed optimization problem. Based on the gradient algorithm and integral feedback, auxiliary-variables are introduced in continuous-time dynamical system [13–15]. From the control system viewpoint, a continuous-time multiagent system dynamic is proposed with undirected communication topology [13]; the algorithm is further investigated over a strongly connected and weight balanced directed graph [16], and even a modified system is proposed in [14] with auxiliary-variables no longer needing to exchange information. In [17], the authors present a second-order multiagent system for distributed optimization network under bound constraints, and, in [18], a distributed protocol design for the high-order agent-network under a connected communication topology is proposed. In order to avoid using auxiliary-variables, a family of Zero-Gradient-Sum algorithms are proposed over fixed communication topology in [19].

On the other hand, it is common that time-delay exists in practical systems because of the finite speeds of information transmission and spreading as well as traffic

congestions. Therefore, time-delay should be taken into account in algorithm design of multiagent systems. For time-delay systems modelled by delayed differential equations, an effective way to deal with their convergence and stability analysis is based on the Lyapunov-Krasovskii functionals or Lyapunov-Razumikhin functions. Most of the existing works concentrate on Lyapunov functions combining with Linear Matrix Inequality (LMI) techniques to deal with the consensus problem of multiagent systems with time-delay [20, 21]. The methods based on Lyapunov-Krasovskii functionals can be applied to a wide variety of problems and may provide necessary and sufficient conditions of convergence and stability, but it often leads to computational complexity and poor scalability. When the number of the agents is large, it would be difficult to verify the solvability of the LMI conditions. However, based on the Lyapunov-Razumikhin theorem, the authors propose a neighbor-based distributed controller [7, 8] enabling the agents to achieve consensus along with interconnection delays, which can avoid verifying the LMI condition and reducing computational burden. In [15], distributed consensus optimization algorithms are proposed for continuous-time multiagent systems with time-delay, and some sufficiency conditions based on LMI are obtained.

Motivated by the above observations, the distributed consensus optimization problem of continuous-time multiagent systems with time-varying delay is considered. The interconnected graph is assumed to be directed, strongly connected, and weighted-balanced. The Lyapunov-Razumikhin function is used in the stability analysis. The convergence of the proposed algorithm is guaranteed with the model parameters satisfying some conditions. Meanwhile, the conditions can also give an estimate of the upper bound of the time-delay, which can avoid verifying and calculating the complicated LMI conditions. From the results, we can also see clearly the relationship among the parameters in the system.

The outline of this paper is organized as follows. Some basic knowledge on the algebraic graph theory and useful lemmas are presented in Section 2. The convergence results of the algorithm are established under the given communication condition on network topology by applying Lyapunov-Razumikhin Theorem in Section 3. An example is provided to illustrate the result in this paper in Section 4. Finally, the concluding remarks are given in Section 5.

Notations. $\mathcal{R}$ and $\mathcal{R}^n$ represent the set of real numbers and the set of $n \times 1$ real vectors, respectively; $I_n \in \mathcal{R}^{n\times n}$ is the $n \times n$ identity matrix; $\mathbf{1}_n$ (or $\mathbf{0}_n$) denotes an n dimensional column vector whose all entries being 1 (or 0); A^T represents the transpose of a matrix A; for vectors $x_1, x_2, \ldots, x_n$, $\mathrm{col}(x_1, x_2, \ldots, x_n) = [x_1^T, x_2^T, \ldots, x_n^T]^T$; for a vector w, then $\|w\| = \sqrt{w^T w}$ represents the standard Euclidean norm.

2. Preliminaries and Problem Statement

2.1. Preliminaries. Consider a multiagent system consisting of N agents, if each agent is regarded as a node, the communication topology among these agents can be described by a weighted digraph $\mathcal{G} = (\mathcal{V}, \mathcal{E}, \mathcal{A})$ with the finite set of nodes $\mathcal{V} = \{1, 2, \ldots, N\}$ and edge set $\mathcal{E} \subset \mathcal{V} \times \mathcal{V}$. An edge starts from i and ends on j, which means that agent i can send information to agent j. The weighted adjacency matrix $\mathcal{A} = [a_{ij}] \in R^{N\times N}$ is defined as $a_{ij} > 0$ if $(i, j) \in \mathcal{E}$ and $a_{ij} = 0$ otherwise. If $\sum_{j=1}^{N} a_{ij} = \sum_{j=1}^{N} a_{ji}$ for all $i \in \mathcal{V}$, the digraph $\mathcal{G}$ is called weighted-balanced. A path is a sequence of connected edges in a graph. If there is a path between any two nodes of a digraph $\mathcal{G}$, then digraph $\mathcal{G}$ is said to be strongly connected, otherwise disconnected. The degree matrix $\mathcal{D} = \mathrm{diag}\{d_1, d_2, \ldots, d_N\} \in \mathcal{R}^{N\times N}$ of graph $\mathcal{G}$ is a diagonal matrix with the ith diagonal element being $d_i = \sum_{j=1}^{N} a_{ij}$ for $i \in \mathcal{V}$. The Laplacian of graph $\mathcal{G}$ is defined as $L = \mathcal{D} - \mathcal{A}$.

The next lemmas related to the important properties of Laplace L and provide useful mathematical tools.

Lemma 1 (see [22]). *Laplace matrix L has at least one zero eigenvalue with $\mathbf{1}_N = [1, 1, \ldots, 1] \in \mathcal{R}^N$ as its eigenvector, and all the nonzero eigenvalues of L have positive real parts. Laplacian L has a simple zero eigenvalue if and only if $\mathcal{G}$ is strongly connected.*

Lemma 2. *For matrices A, B, C and D with appropriate dimensions, the Kronecker product $\otimes$ satisfies* (1) $(A \otimes B)(C \otimes D) = (AC) \otimes (BD)$; (2) $(A \otimes B)^T = A^T \otimes B^T$; (3) $(A \otimes B)^{-1} = A^{-1} \otimes B^{-1}$.

Lemma 3 (see [23]). *For a given real matrix $S = \begin{pmatrix} X & Y \\ Y^T & Z \end{pmatrix}$ with $X^T = X$ and $Z^T = Z$, then the following conditions are equivalent:*

(1) $S > 0$;
(2) $X > 0$, $Z - Y^T X^{-1} Y > 0$;
(3) $Z > 0$, $X - Y Z^{-1} Y^T > 0$.

2.2. Problem Statement. We consider a multiagent system consisting of N agents. The dynamics of the ith agent, $i \in \mathcal{V}$, is described by

$$\dot{x}_i(t) = u_i(t), \tag{1}$$

where $x_i \in \mathcal{R}^m$ denotes the state of agent i and $u_i \in \mathcal{R}^m$ is the control input.

Consider the multiagent optimization problem, in which the goal is to minimize the sum of local cost functions associated with the individual agent. More specially, it can be expressed as

$$\text{minimize} \quad f(x) = \sum_{i=1}^{N} f_i(x), \quad x \in \mathcal{R}^m. \tag{2}$$

Let $\mathbf{x} = \mathrm{col}(x_1, x_2, \ldots, x_N) \in \mathcal{R}^{Nm}$. Next, we provide an alternative formulation of (2), that is,

$$\begin{aligned} &\text{minimize} \quad f(\mathbf{x}) = \sum_{i=1}^{N} f_i(x_i), \quad x_i \in \mathcal{R}^m, \\ &\text{subject to} \quad (L \otimes I_m)\mathbf{x} = 0_{Nm}. \end{aligned} \tag{3}$$

We can see that the problem (2) on $\mathscr{R}^m$ is equivalent to the problem (3) on $\mathscr{R}^{Nm}$.

In this paper, our goal is to design a distributed controller for each agent such that the states of all the agents converge to the optimal solution of the optimization problem (2) via local communication.

Before proceeding, we give the following assumption on the local cost function f_i based on convex analysis [24].

Assumption 4. (a) For each $i \in \mathscr{V}$, f_i is differentiable and its gradient is Lipschitz with constant $\rho_i > 0$ in $\mathscr{R}^m$:

$$\left\|\nabla f_i(x) - \nabla f_i(y)\right\| \le \rho_i \left\|x - y\right\|, \quad \forall x, y \in \mathscr{R}^m. \tag{4}$$

(b) for $i \in \mathscr{V}$, f_i is m_i-strongly convex with constant $m_i > 0$:

$$(x-y)^T \left(\nabla f_i(x) - \nabla f_i(y)\right) \ge m_i \left\|x - y\right\|^2, \quad \forall x, y \in \mathscr{R}^m. \tag{5}$$

Remark 5. Under Assumption 4(b), we can note that f is strictly convex; then the problem (3) has an unique optimal solution.

Assumption 6. The digraph $\mathscr{G}$ is weighted-balanced and strongly connected.

From Lemma 1 and Assumption 6, there exists a matrix $Q \in \mathscr{R}^{N\times(N-1)}$ with

$$\begin{aligned} \mathbf{1}_N^T Q &= 0, \\ Q^T Q &= I_{N-1}, \\ QQ^T &= I_N - \frac{1}{N}\mathbf{1}_N \mathbf{1}_N^T, \end{aligned} \tag{6}$$

such that the matrix $Q^T L Q = H$, where the real parts of all the eigenvalues of H are positive, and $H + H^T$ is positive definite.

When considering the presence of time-varying communication delay among the information transmission, the continuous-time distributed optimization protocol is proposed for agent i ($i \in \mathscr{V}$) as follows:

$$\begin{aligned} u_i(t) &= -k\sum_{j=1}^{N} a_{ij}\left[x_i(t-\tau(t)) - x_j(t-\tau(t))\right] - w_i(t) \\ &\quad - \gamma \nabla f_i\left(x_i(t)\right), \\ \dot{w}_i(t) &= \alpha \sum_{j=1}^{N} a_{ij}\left[x_i(t-\tau(t)) - x_j(t-\tau(t))\right], \\ w_i(0) &= 0, \end{aligned} \tag{7}$$

where $w_i(t)$ is an auxiliary state of agent i and $\tau(t)$ is a continuously differentiable function satisfying $\tau(t) \in [0, \tau]$ with $\tau > 0$ for all $t > 0$ and k, α, γ are the scalar tuning positive parameters; $-\gamma\nabla f_i(x_i(t))$ is the gradient term to guide the agents for optimization; $-k\sum_{j=1}^{N} a_{ij}[x_i(t-\tau(t)) - x_j(t-\tau(t))]$ is the consensus term with time-delay to make all the agents converge to the same point; $-w_i(t)$ is an integral term to correct the error caused by the consensus term.

Let

$$\begin{aligned} &\mathbf{w}(t) = \operatorname{col}\left(w_1(t), w_2(t), \ldots, w_N(t)\right), \\ &\nabla \overline{f}\left(x(t)\right) \\ &\quad = \operatorname{col}\left(\nabla f_1\left(x_1(t)\right), \nabla f_2\left(x_2(t)\right), \ldots, \nabla f_N\left(x_N(t)\right)\right). \end{aligned} \tag{8}$$

Then the closed-loop system of (1) and (7) can be expressed as a compact form:

$$\begin{aligned} \dot{\mathbf{x}}(t) &= -k\left(L \otimes I_m\right)\mathbf{x}(t-\tau(t)) - \mathbf{w}(t) - \gamma \nabla \overline{f}\left(\mathbf{x}(t)\right), \\ \dot{\mathbf{w}}(t) &= \alpha\left(L \otimes I_m\right)\mathbf{x}(t-\tau(t)). \end{aligned} \tag{9}$$

Let the right-side of closed-loop system (9) be equal to 0; then we can get the equilibrium point $(\mathbf{x}^*, \mathbf{w}^*)$, that is,

$$\begin{aligned} -k\left(L \otimes I_m\right)\mathbf{x}^* - \mathbf{w}^* - \gamma \nabla \overline{f}\left(\mathbf{x}^*\right) &= 0, \\ \alpha\left(L \otimes I_m\right)\mathbf{x}^* &= 0. \end{aligned} \tag{10}$$

According to the properties of Laplacian matrix and from (10), one can obtain

$$\begin{aligned} \mathbf{x}^* &= \mathbf{1}_N \otimes \pi, \quad \pi \in \mathscr{R}^m, \\ \mathbf{w}^* &= -\gamma \nabla \overline{f}\left(\mathbf{x}^*\right). \end{aligned} \tag{11}$$

Under Assumption 6, we have $\mathbf{1}_N^T L = 0$. Left multiplying the second equation of (9) by $\mathbf{1}_N^T \otimes I_m$ and using initial conditions $w_i(0) = 0$, we obtain $\sum_{j=1}^{N} \dot{w}_j(t) = 0$; then

$$\sum_{j=1}^{N} w_j(t) = \sum_{j=1}^{N} w_j(0) = 0, \quad \forall t \ge 0. \tag{12}$$

Left multiplying the second equation of (11) by $\mathbf{1}_N^T \otimes I_m$ again results in

$$\begin{aligned} 0 &= \sum_{j=1}^{N} w_j^* = -\gamma\left(\mathbf{1}_N^T \otimes I_m\right)\nabla \overline{f}\left(\mathbf{x}^*\right) = -\gamma \sum_{j=1}^{N} \nabla f_i(\pi) \\ &= -\gamma \nabla f\left(\mathbf{x}^*\right). \end{aligned} \tag{13}$$

Thus, the optimal condition $\nabla f(\mathbf{x}^*) = 0$ is satisfied, which means $\mathbf{x}^* = \mathbf{1}_N \otimes x^*$, $x^* \in \mathscr{R}^m$ is the optimal solution of the optimization problem (3).

Using the transformation

$$\begin{aligned} \overline{\mathbf{x}}(t) &= \mathbf{x}(t) - \mathbf{x}^*, \\ \overline{\mathbf{w}}(t) &= \mathbf{w}(t) - \mathbf{w}^*, \end{aligned} \tag{14}$$

one can shift the equilibrium point into the origin; then the system (9) can be transformed into the following form:

$$\begin{aligned} \dot{\overline{\mathbf{x}}}(t) &= -k\left(L \otimes I_m\right)\overline{\mathbf{x}}(t-\tau(t)) - \overline{\mathbf{w}}(t) - \gamma \Psi\left(\overline{\mathbf{x}}(t)\right), \\ \dot{\overline{\mathbf{w}}}(t) &= \alpha\left(L \otimes I_m\right)\overline{\mathbf{x}}(t-\tau(t)), \end{aligned} \tag{15}$$

where $\Psi(\overline{\mathbf{x}}(t)) = \nabla \overline{f}(\mathbf{x}(t)) - \nabla \overline{f}(\mathbf{x}^*)$.

3. Main Results

Before analyzing the consensus and optimization problem (9), we introduce the stability of time-delay systems. Consider the following time-delay system:

$$\begin{aligned} \dot{x} &= f\left(t, x_t\right), \quad t > t_0, \\ x\left(\theta\right) &= \varphi\left(\theta\right), \quad \theta \in \left[-\tau, t_0\right], \end{aligned} \tag{16}$$

where $x_t(\theta) = x(t+\theta)$, $\forall\theta \in [-\tau, t_0]$ and $f(t,0) = 0$. In the sequel, suppose that $t_0 = 0$. Let $C([-\tau,0], \mathscr{R}^n)$ be a Banach space of continuous function defined on an interval $[-\tau, 0]$, taking values in $\mathscr{R}^n$ with topology of uniform convergence, and with a norm $\|\varphi\|_c = \max_{\theta\in[-\tau,t_0]}\|\varphi(\theta)\|$.

The definition of the stability of the solution $x = 0$ is given as follows in terms of the solution of the delayed equation (16).

Lemma 7 (see [25]). *Let ϕ_1, ϕ_2, and ϕ_3 be continuous, nonnegative, nondecreasing function with $\phi_1(s) > 0$, $\phi_2(s) > 0$, $\phi_3(s) > 0$ for $s > 0$ and $\phi_1(0) = \phi_2(0) = 0$. For system (16), suppose that the function $f : \mathscr{R} \times C([-\tau,0], \mathscr{R}^n) \to \mathscr{R}$ takes bounded sets of $C([-\tau,0], \mathscr{R}^n)$ in bounded sets of R^n. There is a continuous function $V(t,x)$ such that*

$$\phi_1\left(\|x\|\right) \le V\left(t,x\right) \le \phi_2\left(\|x\|\right), \quad t \in \mathscr{R},\ x \in \mathscr{R}^n. \tag{17}$$

In addition, there exists a continuous nondecreasing function $\phi(s)$ with $\phi(s) > s$, $s > 0$ such that

$$\dot{V}\left(t,x\right)\Big|_{(16)} \le -\phi_3\left(s\right). \tag{18}$$

If

$$V\left(t+\theta, x\left(t+\theta\right)\right) < \phi\left(V\left(t,x\right)\right), \quad \theta \in \left[-\tau, 0\right], \tag{19}$$

then the solution $x = 0$ of system (16) is uniformly asymptotically stable.

Usually, $V(t,x)$ is called Lyapunov-Razumikhin function if it satisfies (17) and (18) in Lemma 7.

Then the main results can be obtained as follows.

Theorem 8. *Suppose Assumptions 4 and 6 hold, satisfy*

$$2\gamma\underline{m} \ge \gamma^2\overline{\rho}^2 + \underline{\lambda}_2 \tag{20}$$

and take

$$k > k^* = \frac{2}{\underline{\lambda}_1} + \alpha \tag{21}$$

and assume that

$$\begin{aligned} \tau &< \tau^* \\ &= \frac{\underline{\lambda}_2}{(k-\alpha)\left[(k+\alpha)\,\overline{\lambda}_1 + k^3\overline{\lambda}_2\right] + \left(2q + \delta\gamma^2\overline{\rho}^2 q\right)\left(\overline{\mu}+1\right)}, \end{aligned} \tag{22}$$

where $q > 1$, $\overline{\mu} = 1 + k/\alpha$, and $\delta = \lambda_{\max}(P_1)/\lambda_{\min}(P)$, and, respectively,

$$\begin{aligned} \underline{\lambda}_1 &= \lambda_{\min}\left(H^T + H\right), \\ \underline{\lambda}_2 &= \lambda_{\min}\left(R - I_{2N-2}\right); \\ \overline{\lambda}_1 &= \lambda_{\max}\left(HH^T\right), \\ \overline{\lambda}_2 &= \lambda_{\max}\left(H^2\left(H^2\right)^T\right), \end{aligned} \tag{23}$$

where $\lambda_{\min}(\cdot)$ and $\lambda_{\max}(\cdot)$ denote the smallest and the largest nonzero eigenvalue of positive semidefinite matrix, respectively.

Then, the optimization problem (3) for multiagent system (1) can be solved by the optimization control (7), where

$$R = \begin{pmatrix} (k-\alpha)\left(H^T + H\right) & I_{N-1} \\ I_{N-1} & 2I_{N-1} \end{pmatrix} \otimes I_m. \tag{24}$$

Proof. Let

$$\begin{aligned} e\left(t\right) &= \left(T^T \otimes I_m\right)\overline{\mathbf{x}}\left(t\right), \\ \vartheta\left(t\right) &= \left(T^T \otimes I_m\right)\overline{\mathbf{w}}\left(t\right), \\ T &= \left[\frac{\mathbf{1}_N}{\sqrt{N}} Q\right]. \end{aligned} \tag{25}$$

Denote $e = \mathrm{col}(e_1, e_2)$, and $\vartheta = \mathrm{col}(\vartheta_1, \vartheta_2)$ with $e_1, \vartheta_1 \in \mathscr{R}^m$, and $e_2, \vartheta_2 \in \mathscr{R}^{m(N-1)}$. By the structure of T and (6), we can know that T is an orthogonal matrix. Then the system (15) can be rewritten as

$$\begin{aligned} \dot{e}_1\left(t\right) &= -\gamma\left(\frac{\mathbf{1}_N^T}{\sqrt{N}} \otimes I_m\right)\Psi\left(\overline{\mathbf{x}}\left(t\right)\right), \\ \dot{e}_2\left(t\right) &= -k\left(H \otimes I_m\right)e_2\left(t-\tau\left(t\right)\right) - \vartheta_2\left(t\right) \\ &\quad - \gamma\left(Q^T \otimes I_m\right)\Psi\left(\overline{\mathbf{x}}\left(t\right)\right), \\ \dot{\vartheta}_1\left(t\right) &= 0, \\ \dot{\vartheta}_2\left(t\right) &= \alpha\left(H \otimes I_m\right)e_2\left(t-\tau\left(t\right)\right). \end{aligned} \tag{26}$$

Let $\boldsymbol{\varepsilon}(t) = \mathrm{col}(e(t), \vartheta(t)) = \mathrm{col}(e_1(t), e_2(t), \vartheta_1(t), \vartheta_2(t))$, and construct the Lyapunov-Razumikhin function as

$$V\left(\boldsymbol{\varepsilon}\left(t\right)\right) = \boldsymbol{\varepsilon}^T\left(t\right)P\boldsymbol{\varepsilon}\left(t\right) \tag{27}$$

with

$$P = \begin{pmatrix} 1 & 0 & 1 & 0 \\ 0 & I_{N-1} & 0 & I_{N-1} \\ 1 & 0 & \dfrac{k}{\alpha} & 0 \\ 0 & I_{N-1} & 0 & \dfrac{k}{\alpha} I_{N-1} \end{pmatrix} \otimes I_m. \tag{28}$$

We can have the fact that $P = \left(\begin{smallmatrix} I_N & I_N \\ I_N & (k/\alpha)I_N \end{smallmatrix}\right) \otimes I_m$ is positive definite since $k > \alpha$.

The derivation of V along the system (26) is given by

$$\begin{aligned}\dot{V}(\boldsymbol{\varepsilon}(t)) &= 2\boldsymbol{\varepsilon}^T(t) P\dot{\boldsymbol{\varepsilon}}(t)\\ &= 2\left[e_1(t)+\vartheta_1(t)\right]^T \dot{e}_1(t)\\ &\quad + 2\left[e_2(t)+\vartheta_2(t)\right]^T \dot{e}_2(t)\\ &\quad + 2\left[e_1(t)+\frac{k}{\alpha}\vartheta_1(t)\right]^T \dot{\vartheta}_1(t)\\ &\quad + 2\left[e_2(t)+\frac{k}{\alpha}\vartheta_2(t)\right]^T \dot{\vartheta}_2(t).\end{aligned} \tag{29}$$

Combining the third equation of (26) and (12) gives $\vartheta_1(t) = 0,\ \forall t \geq 0$; then

$$\begin{aligned}\dot{V}(\boldsymbol{\varepsilon}(t)) &= 2e_1^T(t)\dot{e}_1(t) + 2\left[e_2(t)+\vartheta_2(t)\right]^T \dot{e}_2(t)\\ &\quad + 2\left[e_2(t)+\frac{k}{\alpha}\vartheta_2(t)\right]^T \dot{\vartheta}_2(t)\\ &= 2e_1^T(t)\dot{e}_1(t) + 2\boldsymbol{\varepsilon}_{2:N}^T(t) P_1\dot{\boldsymbol{\varepsilon}}_{2:N}(t),\end{aligned} \tag{30}$$

where $\boldsymbol{\varepsilon}_{2:N}(t) = \mathrm{col}(e_2^T(t), \vartheta_2^T(t))$, $P_1 = \begin{pmatrix} I_{N-1} & I_{N-1} \\ I_{N-1} & (k/\alpha)I_{N-1}\end{pmatrix} \otimes I_m$.

For the second and fourth equalities of system (26), we have a compact form

$$\dot{\boldsymbol{\varepsilon}}_{2:N}(t) = C\boldsymbol{\varepsilon}_{2:N}(t) + E\boldsymbol{\varepsilon}_{2:N}(t-\tau(t)) + F \tag{31}$$

with $C = \begin{pmatrix} 0 & -I_{N-1} \\ 0 & 0\end{pmatrix} \otimes I_m$, $E = \begin{pmatrix} -kH & 0 \\ \alpha H & 0\end{pmatrix} \otimes I_m$, and $F = \begin{pmatrix} -\gamma(Q^T \otimes I_m)\Psi(\bar{\mathbf{x}}(t)) \\ 0\end{pmatrix}$.

By the Leibniz-Newton formula

$$\begin{aligned}\boldsymbol{\varepsilon}_{2:N}(t-\tau(t)) &= \boldsymbol{\varepsilon}_{2:N}(t) - \int_{t-\tau(t)}^{t} \dot{\boldsymbol{\varepsilon}}_{2:N}(s)\,ds\\ &= \boldsymbol{\varepsilon}_{2:N}(t) - C\int_{-\tau(t)}^{0} \boldsymbol{\varepsilon}_{2:N}(t+s)\,ds\\ &\quad - E\int_{-2\tau(t)}^{-\tau(t)} \boldsymbol{\varepsilon}_{2:N}(t+s)\,ds\\ &\quad - \int_{-\tau(t)}^{0} F(t+s)\,ds.\end{aligned} \tag{32}$$

Therefore, the system (31) can be rewritten as

$$\begin{aligned}\dot{\boldsymbol{\varepsilon}}_{2:N}(t) &= \overline{F}\boldsymbol{\varepsilon}_{2:N}(t) - EC\int_{-\tau(t)}^{0} \boldsymbol{\varepsilon}_{2:N}(t+s)\,ds\\ &\quad - E^2\int_{-2\tau(t)}^{-\tau(t)} \boldsymbol{\varepsilon}_{2:N}(t+s)\,ds\\ &\quad - E\int_{-\tau(t)}^{0} F(t+s)\,ds + F,\end{aligned} \tag{33}$$

where $\overline{F} = E + C$.

Thus, we can get

$$\begin{aligned}&2\boldsymbol{\varepsilon}_{2:N}^T(t) P_1\dot{\boldsymbol{\varepsilon}}_{2:N}(t)\\ &\quad = \boldsymbol{\varepsilon}_{2:N}^T(t)\left(\overline{F}^T P_1 + P_1\overline{F}\right)\boldsymbol{\varepsilon}_{2:N}(t)\\ &\qquad - 2\boldsymbol{\varepsilon}_{2:N}^T(t) P_1 EC\int_{-\tau(t)}^{0} \boldsymbol{\varepsilon}_{2:N}(t+s)\,ds\\ &\qquad - 2\boldsymbol{\varepsilon}_{2:N}^T(t) P_1 E^2\int_{-2\tau(t)}^{-\tau(t)} \boldsymbol{\varepsilon}_{2:N}(t+s)\,ds\\ &\qquad - 2\boldsymbol{\varepsilon}_{2:N}^T(t) P_1 E\int_{-\tau(t)}^{0} F(t+s)\,ds\\ &\qquad + 2\boldsymbol{\varepsilon}_{2:N}^T(t) P_1 F.\end{aligned} \tag{34}$$

Combining (30) and (34) gives

$$\begin{aligned}\dot{V}(\boldsymbol{\varepsilon}(t)) &= \boldsymbol{\varepsilon}_{2:N}^T(t)\left(\overline{F}^T P_1 + P_1\overline{F}\right)\boldsymbol{\varepsilon}_{2:N}(t)\\ &\quad - 2\boldsymbol{\varepsilon}_{2:N}^T(t) P_1 EC\int_{-\tau(t)}^{0} \boldsymbol{\varepsilon}_{2:N}(t+s)\,ds\\ &\quad - 2\boldsymbol{\varepsilon}_{2:N}^T(t) P_1 E^2\int_{-2\tau(t)}^{-\tau(t)} \boldsymbol{\varepsilon}_{2:N}(t+s)\,ds\\ &\quad - 2\boldsymbol{\varepsilon}_{2:N}^T(t) P_1 E\int_{-\tau(t)}^{0} F(t+s)\,ds\\ &\quad + 2\boldsymbol{\varepsilon}_{2:N}^T(t) P_1 F + 2e_1^T(t)\dot{e}_1(t).\end{aligned} \tag{35}$$

Note that $2a^Tb \leq a^T\Phi a + b^T\Phi^{-1}b$ holds for any appropriate positive definite matrix Φ; then let $a^T = -\boldsymbol{\varepsilon}_{2:N}^T(t)P_1EC$, $b = \boldsymbol{\varepsilon}_{2:N}(t+s)$, and $\Phi = P_1^{-1}$; one can obtain

$$\begin{aligned}&-2\boldsymbol{\varepsilon}_{2:N}^T(t) P_1 EC\int_{-\tau(t)}^{0} \boldsymbol{\varepsilon}_{2:N}(t+s)\,ds\\ &\quad = \int_{-\tau(t)}^{0} 2\left(-\boldsymbol{\varepsilon}_{2:N}^T(t) P_1 EC\right)\boldsymbol{\varepsilon}_{2:N}(t+s)\,ds\\ &\quad \leq \tau(t)\,\boldsymbol{\varepsilon}_{2:N}^T(t) P_1 EC P_1^{-1}\left(P_1EC\right)^T\boldsymbol{\varepsilon}_{2:N}(t)\\ &\qquad + \int_{-\tau(t)}^{0} \boldsymbol{\varepsilon}_{2:N}^T(t+s) P_1\boldsymbol{\varepsilon}_{2:N}(t+s)\,ds\\ &\quad \leq \tau\boldsymbol{\varepsilon}_{2:N}^T(t) P_1 EC P_1^{-1}\left(P_1EC\right)^T\boldsymbol{\varepsilon}_{2:N}(t)\\ &\qquad + \int_{-\tau(t)}^{0} \boldsymbol{\varepsilon}_{2:N}^T(t+s) P_1\boldsymbol{\varepsilon}_{2:N}(t+s)\,ds.\end{aligned} \tag{36}$$

Similarly, let $a^T = -\boldsymbol{\varepsilon}_{2:N}^T(t)P_1E^2$, $b = \boldsymbol{\varepsilon}_{2:N}(t+s)$, and $\Phi = P_1^{-1}$; we have

$$\begin{aligned}
&-2\boldsymbol{\varepsilon}_{2:N}^T(t)\,P_1E^2\int_{-2\tau(t)}^{-\tau(t)}\boldsymbol{\varepsilon}_{2:N}(t+s)\,ds\\
&\quad=\int_{-2\tau(t)}^{-\tau(t)}2\left(-\boldsymbol{\varepsilon}_{2:N}^T(t)\,P_1E^2\right)\boldsymbol{\varepsilon}_{2:N}(t+s)\,ds\\
&\quad\le\tau(t)\,\boldsymbol{\varepsilon}_{2:N}^T(t)\,P_1E^2P_1^{-1}\left(P_1E^2\right)^T\boldsymbol{\varepsilon}_{2:N}(t)\\
&\qquad+\int_{-2\tau(t)}^{-\tau(t)}\boldsymbol{\varepsilon}_{2:N}^T(t+s)\,P_1\boldsymbol{\varepsilon}_{2:N}(t+s)\,ds\\
&\quad\le\tau\boldsymbol{\varepsilon}_{2:N}^T(t)\,P_1E^2P_1^{-1}\left(P_1E^2\right)^T\boldsymbol{\varepsilon}_{2:N}(t)\\
&\qquad+\int_{-2\tau(t)}^{-\tau(t)}\boldsymbol{\varepsilon}_{2:N}^T(t+s)\,P_1\boldsymbol{\varepsilon}_{2:N}(t+s)\,ds,
\end{aligned}\tag{37}$$

and let $a^T = -\boldsymbol{\varepsilon}_{2:N}^T(t)P_1E$, $b = F(t+s)$, and $\Phi = P_1^{-1}$; there is

$$\begin{aligned}
&-2\boldsymbol{\varepsilon}_{2:N}^T(t)\,P_1E\int_{-\tau(t)}^{0}F(t+s)\,ds\\
&\quad\le\tau(t)\,\boldsymbol{\varepsilon}_{2:N}^T(t)\,P_1EP_1^{-1}\left(P_1E\right)^T\boldsymbol{\varepsilon}_{2:N}(t)\\
&\qquad+\int_{-\tau(t)}^{0}F^T(t+s)\,P_1F(t+s)\,ds\\
&\quad\le\tau\boldsymbol{\varepsilon}_{2:N}^T(t)\,P_1EP_1^{-1}\left(P_1E\right)^T\boldsymbol{\varepsilon}_{2:N}(t)\\
&\qquad+\int_{-\tau(t)}^{0}F^T(t+s)\,P_1F(t+s)\,ds.
\end{aligned}\tag{38}$$

Due to

$$F(t)=\begin{pmatrix}-\gamma\left(Q^T\otimes I_m\right)\Psi\left(\overline{\mathbf{x}}(t)\right)\\0\end{pmatrix},\tag{39}$$

then

$$\begin{aligned}
\|F(t)\|^2&=\gamma^2\left\|\left(Q^T\otimes I_m\right)\Psi\left(\overline{\mathbf{x}}(t)\right)\right\|^2\le\gamma^2\overline{\rho}^2\left\|\overline{\mathbf{x}}(t)\right\|^2\\
&=\gamma^2\overline{\rho}^2\left\|e(t)\right\|^2\le\gamma^2\overline{\rho}^2\left\|\boldsymbol{\varepsilon}(t)\right\|^2,
\end{aligned}\tag{40}$$

with the transformation $e(t) = (T^T \otimes I_m)\overline{\mathbf{x}}(t)$; we have

$$\begin{aligned}
2e_1^T(t)\,\dot{e}_1(t)&=-2\gamma e_1^T(t)\left(\frac{\mathbf{1}_N^T}{\sqrt{N}}\otimes I_m\right)\Psi\left(\overline{\mathbf{x}}(t)\right)\\
&=-2\gamma\overline{\mathbf{x}}^T(t)\,\Psi\left(\overline{\mathbf{x}}(t)\right)\\
&\quad+2\gamma e_2^T(t)\left(Q^T\otimes I_m\right)\Psi\left(\overline{\mathbf{x}}(t)\right);
\end{aligned}\tag{41}$$

then, from Assumption 4, it follows that

$$\begin{aligned}
&2\boldsymbol{\varepsilon}_{2:N}^T(t)\,P_1F+2e_1^T(t)\,\dot{e}_1(t)\\
&\quad=-2\gamma\left(e_2^T(t)+\vartheta_2^T(t)\right)\left(Q^T\otimes I_m\right)\Psi\left(\overline{\mathbf{x}}(t)\right)\\
&\qquad-2\gamma\overline{\mathbf{x}}^T(t)\,\Psi\left(\overline{\mathbf{x}}(t)\right)\\
&\qquad+2\gamma e_2^T(t)\left(Q^T\otimes I_m\right)\Psi\left(\overline{\mathbf{x}}(t)\right)\\
&\quad=-2\gamma\vartheta_2^T(t)\left(Q^T\otimes I_m\right)\Psi\left(\overline{\mathbf{x}}(t)\right)\\
&\qquad-2\gamma\overline{\mathbf{x}}^T(t)\,\Psi\left(\overline{\mathbf{x}}(t)\right)\\
&\quad\le\vartheta_2^T(t)\,\vartheta_2(t)+\gamma^2\left\|\left(Q^T\otimes I_m\right)\Psi\left(\overline{\mathbf{x}}(t)\right)\right\|^2\\
&\qquad-2\gamma\underline{m}\left\|\overline{\mathbf{x}}(t)\right\|^2\\
&\quad\le\vartheta_2^T(t)\,\vartheta_2(t)+\gamma^2\overline{\rho}^2\left\|\overline{\mathbf{x}}(t)\right\|^2-2\gamma\underline{m}\left\|\overline{\mathbf{x}}(t)\right\|^2\\
&\quad\le\boldsymbol{\varepsilon}_{2:N}^T(t)\,\boldsymbol{\varepsilon}_{2:N}(t)-\left(2\gamma\underline{m}-\gamma^2\overline{\rho}^2\right)\left\|\overline{\mathbf{x}}(t)\right\|^2,
\end{aligned}\tag{42}$$

where $\underline{m} = \min\{m_1, m_2, \ldots, m_N\}$ and $\overline{\rho} = \max\{\rho_1, \rho_2, \ldots, \rho_N\}$.

According to the Lyapunov-Razumikhin Theorem, take $\phi(s) = qs$ for some constant $q > 1$. In case that

$$V\left(\boldsymbol{\varepsilon}(t+\theta)\right)<qV\left(\boldsymbol{\varepsilon}(t)\right),\quad\theta\in[-2\tau,0],\tag{43}$$

then

$$\begin{aligned}
&\boldsymbol{\varepsilon}_{2:N}^T(t+s)\,P_1\boldsymbol{\varepsilon}_{2:N}(t+s)\\
&\quad\le e_1^T(t+s)\,e_1(t+s)+\boldsymbol{\varepsilon}_{2:N}^T(t+s)\,P_1\boldsymbol{\varepsilon}_{2:N}(t+s)\\
&\quad=\boldsymbol{\varepsilon}^T(t+s)\,P\boldsymbol{\varepsilon}(t+s)<q\boldsymbol{\varepsilon}^T(t)\,P\boldsymbol{\varepsilon}(t).
\end{aligned}\tag{44}$$

Next, considering the integral term in (38) and according to (40), we can obtain

$$\begin{aligned}
&\int_{-\tau(t)}^{0}F^T(t+s)\,P_1F(t+s)\,ds\\
&\quad\le\lambda_{\max}(P_1)\int_{-\tau(t)}^{0}F^T(t+s)\,F(t+s)\,ds\\
&\quad\le\lambda_{\max}(P_1)\,\gamma^2\overline{\rho}^2\int_{-\tau(t)}^{0}\boldsymbol{\varepsilon}^T(t+s)\,\boldsymbol{\varepsilon}(t+s)\,ds\\
&\quad\le\frac{\lambda_{\max}(P_1)}{\lambda_{\min}(P)}\gamma^2\overline{\rho}^2\int_{-\tau(t)}^{0}\boldsymbol{\varepsilon}^T(t+s)\,P\boldsymbol{\varepsilon}(t+s)\,ds\\
&\quad\le\delta\gamma^2\overline{\rho}^2q\int_{-\tau(t)}^{0}\boldsymbol{\varepsilon}^T(t)\,P\boldsymbol{\varepsilon}(t)\,ds\\
&\quad\le\delta\gamma^2\overline{\rho}^2q\tau\left[e_1^T(t)\,e_1(t)+\boldsymbol{\varepsilon}_{2:N}^T(t)\,P_1\boldsymbol{\varepsilon}_{2:N}(t)\right]\\
&\quad\le\delta\gamma^2\overline{\rho}^2q\tau\overline{\mathbf{x}}^T(t)\,\overline{\mathbf{x}}(t)+\delta\gamma^2\overline{\rho}^2q\tau\boldsymbol{\varepsilon}_{2:N}^T(t)\,P_1\boldsymbol{\varepsilon}_{2:N}(t)\\
&\quad\le\delta\gamma^2\overline{\rho}^2q\tau\boldsymbol{\varepsilon}^T(t)\,\boldsymbol{\varepsilon}(t)+\delta\gamma^2\overline{\rho}^2q\tau\boldsymbol{\varepsilon}_{2:N}^T(t)\,P_1\boldsymbol{\varepsilon}_{2:N}(t),
\end{aligned}\tag{45}$$

and, substituting (44) into the integral term in (36), we can obtain

$$\begin{aligned}
&\int_{-\tau(t)}^{0} \boldsymbol{\varepsilon}_{2:N}^{T}(t+s) P_1 \boldsymbol{\varepsilon}_{2:N}(t+s)\, ds \\
&< \int_{-\tau(t)}^{0} q\boldsymbol{\varepsilon}^{T}(t) P \boldsymbol{\varepsilon}(t)\, ds \\
&< \int_{-\tau(t)}^{0} \left[q e_1^{T}(t) e_1(t) + q\boldsymbol{\varepsilon}_{2:N}^{T}(t) P_1 \boldsymbol{\varepsilon}_{2:N}(t) \right] ds \\
&< q\tau e_1^{T}(t) e_1(t) + q\tau \boldsymbol{\varepsilon}_{2:N}^{T}(t) P_1 \boldsymbol{\varepsilon}_{2:N}(t) \\
&< q\tau \left\| \overline{\mathbf{x}}(t) \right\|^2 + q\tau \boldsymbol{\varepsilon}_{2:N}^{T}(t) P_1 \boldsymbol{\varepsilon}_{2:N}(t) \\
&\le q\tau \boldsymbol{\varepsilon}^{T}(t) \boldsymbol{\varepsilon}(t) + q\tau \boldsymbol{\varepsilon}_{2:N}^{T}(t) P_1 \boldsymbol{\varepsilon}_{2:N}(t).
\end{aligned} \tag{46}$$

Similarly,

$$\begin{aligned}
&\int_{-2\tau(t)}^{-\tau(t)} \boldsymbol{\varepsilon}_{2:N}^{T}(t+s) P_1 \boldsymbol{\varepsilon}_{2:N}(t+s)\, ds \\
&\quad < q\tau \boldsymbol{\varepsilon}^{T}(t) \boldsymbol{\varepsilon}(t) + q\tau \boldsymbol{\varepsilon}_{2:N}^{T}(t) P_1 \boldsymbol{\varepsilon}_{2:N}(t).
\end{aligned} \tag{47}$$

Then from (35) and above inequalities, we have

$$\begin{aligned}
\dot{V}(\boldsymbol{\varepsilon}(t)) \le{}& -\boldsymbol{\varepsilon}_{2:N}^{T}(t) \left(R - I_{2N-2}\right) \boldsymbol{\varepsilon}_{2:N}(t) + \tau \boldsymbol{\varepsilon}_{2:N}^{T}(t) \\
&\cdot \left[P_1 E C P_1^{-1} \left(P_1 E C\right)^{T} + P_1 E^2 P_1^{-1} \left(P_1 E^2\right)^{T} \right. \\
&+ P_1 E P_1^{-1} \left(P_1 E\right)^{T} + \left(2q + \delta\gamma^2\overline{\rho}^2 q\right) P_1 \left. \right] \boldsymbol{\varepsilon}_{2:N}(t) \\
&+ \left(2q\tau + \delta\gamma^2\overline{\rho}^2 q\tau\right) \boldsymbol{\varepsilon}^{T}(t) \boldsymbol{\varepsilon}(t) - \left(2\gamma\underline{m} - \gamma^2\overline{\rho}^2\right) \\
&\cdot \left\| \overline{\mathbf{x}}(t) \right\|^2,
\end{aligned} \tag{48}$$

where

$$\begin{aligned}
R = -\left(\overline{F}^{T} P_1 + P_1 \overline{F}\right) &= \begin{pmatrix} (k-\alpha)\left(H^{T} + H\right) & I_{N-1} \\ I_{N-1} & 2I_{N-1} \end{pmatrix} \\
&\otimes I_m, \\
P_1 E C P_1^{-1} \left(P_1 E C\right)^{T} &+ P_1 E^2 P_1^{-1} \left(P_1 E^2\right)^{T} \\
&+ P_1 E P_1^{-1} \left(P_1 E\right)^{T} \\
&= \begin{pmatrix} (k-\alpha)\left[(k+\alpha) HH^{T} + k^3 H^2 \left(H^2\right)^{T}\right] & 0 \\ 0 & 0 \end{pmatrix} \\
&\otimes I_m.
\end{aligned} \tag{49}$$

According to Lemma 3, if k satisfies condition (21), then $R - I_{2N-2}$ is positive definite; we have

$$\begin{aligned}
&\boldsymbol{\varepsilon}_{2:N}^{T}(t) \left(R - I_{2N-2}\right) \boldsymbol{\varepsilon}_{2:N}(t) \ge \underline{\lambda}_2 \boldsymbol{\varepsilon}_{2:N}^{T}(t) \boldsymbol{\varepsilon}_{2:N}(t) \\
&\quad = \underline{\lambda}_2 \boldsymbol{\varepsilon}_{2:N}^{T}(t) \boldsymbol{\varepsilon}_{2:N}(t) + \underline{\lambda}_2 e_1^{T}(t) e_1(t) \\
&\qquad - \underline{\lambda}_2 e_1^{T}(t) e_1(t) = \underline{\lambda}_2 \boldsymbol{\varepsilon}^{T}(t) \boldsymbol{\varepsilon}(t) - \underline{\lambda}_2 e_1^{T}(t) e_1(t) \\
&\quad \ge \underline{\lambda}_2 \boldsymbol{\varepsilon}^{T}(t) \boldsymbol{\varepsilon}(t) - \underline{\lambda}_2 \left\| \overline{\mathbf{x}}(t) \right\|^2,
\end{aligned} \tag{50}$$

if condition (20) is satisfied and due to the fact that $\boldsymbol{\varepsilon}_{2:N}^{T}(t)\boldsymbol{\varepsilon}_{2:N}(t) \le \boldsymbol{\varepsilon}^{T}(t)\boldsymbol{\varepsilon}(t)$; then

$$\begin{aligned}
\dot{V}(\boldsymbol{\varepsilon}(t)) \le{}& -\underline{\lambda}_2 \boldsymbol{\varepsilon}^{T}(t) \boldsymbol{\varepsilon}(t) + \underline{\lambda}_2 \left\| \overline{\mathbf{x}}(t) \right\|^2 + \tau \boldsymbol{\varepsilon}_{2:N}^{T}(t) \\
&\cdot \left\{ (k-\alpha) \left[(k+\alpha) \overline{\lambda}_1 + k^3 \overline{\lambda}_2 \right] + \left(2q + \delta\gamma^2\overline{\rho}^2 q\right) \overline{\mu} \right\} \\
&\cdot \boldsymbol{\varepsilon}_{2:N}(t) + 2\left(\delta\gamma^2\overline{\rho}^2 q\tau + q\tau\right) \boldsymbol{\varepsilon}^{T}(t) \boldsymbol{\varepsilon}(t) - \left(2\gamma\underline{m} \right. \\
&\left. - \gamma^2\overline{\rho}^2\right) \left\| \overline{\mathbf{x}}(t) \right\|^2 \le -\underline{\lambda}_2 \boldsymbol{\varepsilon}^{T}(t) \boldsymbol{\varepsilon}(t) + \tau \boldsymbol{\varepsilon}^{T}(t) \\
&\cdot \left\{ (k-\alpha) \left[(k+\alpha) \overline{\lambda}_1 + k^3 \overline{\lambda}_2 \right] + \left(2q + \delta\gamma^2\overline{\rho}^2 q\right) \overline{\mu} \right. \\
&\left. + \left(2q + \delta\gamma^2\overline{\rho}^2 q\right) \right\} \boldsymbol{\varepsilon}(t) - \left(2\gamma\underline{m} - \gamma^2\overline{\rho}^2 - \underline{\lambda}_2\right) \\
&\cdot \left\| \overline{\mathbf{x}}(t) \right\|^2 \le -\underline{\lambda}_2 \boldsymbol{\varepsilon}^{T}(t) \boldsymbol{\varepsilon}(t) + \tau \boldsymbol{\varepsilon}^{T}(t) \\
&\cdot \left\{ (k-\alpha) \left[(k+\alpha) \overline{\lambda}_1 + k^3 \overline{\lambda}_2 \right] \right. \\
&\left. + \left(2q + \delta\gamma^2\overline{\rho}^2 q\right) \left(\overline{\mu} + 1\right) \right\} \boldsymbol{\varepsilon}(t)
\end{aligned} \tag{51}$$

and we take τ has the upper bound in (22); then $\dot{V}(\boldsymbol{\varepsilon}(t))$ is negative definite. Thus by the Lyapunov-Razumikhin theorem, we can conclude that $\boldsymbol{\varepsilon}(t) \to 0$; that is, $e(t) \to 0_{mN}$, $\vartheta(t) \to 0_{mN}$ as $t \to \infty$.

With the transformation $\overline{\mathbf{x}}(t) = (T \otimes I_m)e(t)$ and $\overline{\mathbf{w}}(t) = (T \otimes I_m)\vartheta(t)$ and T is a orthogonal matrix, we can obtain $\overline{\mathbf{x}}(t) \to 0_{mN}$, $\overline{\mathbf{w}}(t) \to 0_{mN}$, which means $\mathbf{x}(t) \to \mathbf{x}^*$, $\mathbf{w}(t) \to \mathbf{w}^*$ as $t \to \infty$. As a result, this proof is completed. □

Remark 9. The continuous-time protocol considered in this paper is based on the algorithm proposed in [15], and under the same communication topology, but the conditions of convergence analysis needed by this paper are more relaxed. From (20) and (21), it is clearly shown that k^* is independent of parameters β and γ but dependent on α and communication topology, while τ^* is independent of constant m_i in this paper compared to [15]. We can know when the number of the agents is large, it would be difficult to verify the LMI condition, but, in this paper, it only needs the model parameters to meet some boundary conditions, and when considering the dynamic system with time-varying delay, the Lyapunov function with Razumikhin technique is also an effective method compared to Lyapunov-Krasovskii method.

4. Simulations

In this section, we give an example to validate our theoretical results. In the example, we consider a multiagent system

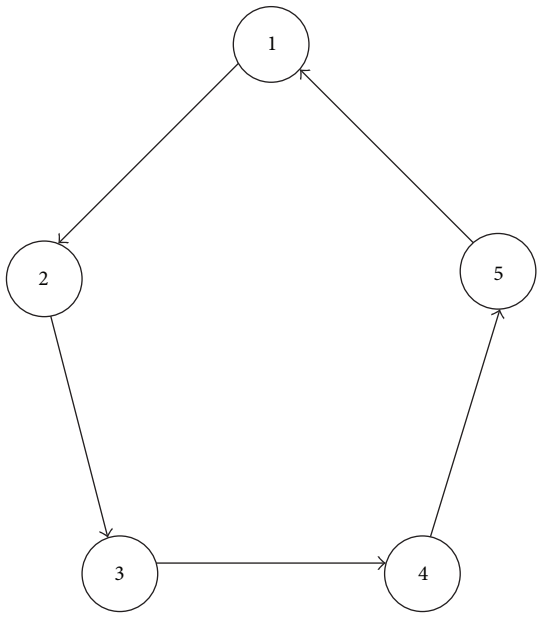

Figure 1: Connected graph.

consisting of five agents. Suppose that the interconnected topology is described as in Figure 1.

Consider the following optimization problem:

$$\text{minimize} \quad f(x) = \sum_{i=1}^{N} f_i(x), \quad x \in \mathcal{R}, \tag{52}$$

where the local objective function is given as follows:

$$\begin{aligned} f_1(x) &= 0.7(x-8)^2, \\ f_2(x) &= 0.6x^2 - 2, \\ f_3(x) &= (x+2)^2, \\ f_4(x) &= 0.8x^2 + 2x, \\ f_5(x) &= \sin\frac{x}{2} + \frac{x^2}{2}. \end{aligned} \tag{53}$$

Obviously, for $i = 1, 2, \ldots, 5$, f_i is differentiable and satisfies Assumption 4. Choosing $\alpha = 0.6$, $k = 2.2$, $\gamma = 0.4$, $q = 1.1$ and time-varying delay $\tau(t) = 0.01|\cos(t)|$, we can obtain $\overline{\rho} = 2$, $\underline{m} = 1$, $k^* = 2.0472$ and $\tau^* = 0.0004$.

Let the initial values $x(0) = [x_1(0), x_2(0), x_3(0), x_4(0), x_5(0)]^T = [-8, -2, 2, 3, 10]^T$, $w(0) = [w_1(0), w_2(0), w_3(0), w_4(0), w_5(0)]^T = [0, 0, 0, 0, 0]^T$. The simulation results are shown in Figures 2 and 3.

We can see that the trajectories x_i of each agent i converge to the global optimal solution $x^* = 0.6565$ of the objective function $f(x) = \sum_{i=1}^{N} f_i(x)$ and all the trajectories w_i converge to a constant, respectively, for $i = 1, 2, \ldots, 5$. The optimal value of $f(x)$ is 45.2602.

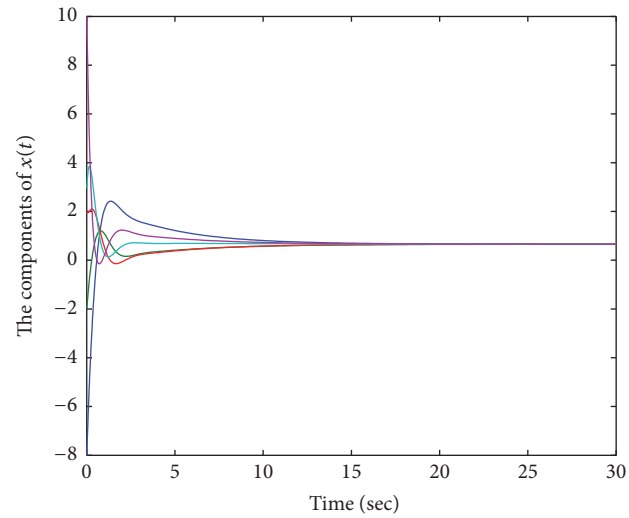

Figure 2: The trajectories of x_i.

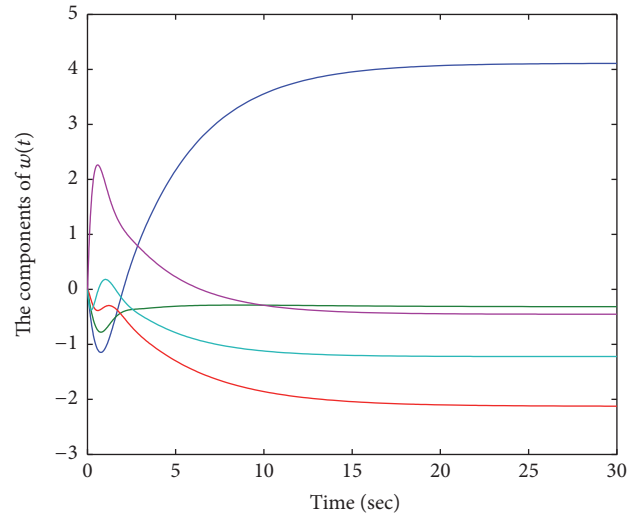

Figure 3: The trajectories of w_i.

5. Conclusion

In this paper, the consensus optimization problem of multiagents with communication delays was considered. By a continuous-time algorithm, consensus and optimization under some parameter bound conditions are ensured. Graph theory is used to describe the interconnection topologies. Lyapunov-Razumikhin theory were employed for stability analysis. The connectivity assumption of directed graph plays a key role in the analysis of algorithm convergence. Numerical examples were given to illustrate the theoretical results.

Conflicts of Interest

The authors declare that they have no conflicts of interest.

Acknowledgments

This work is supported in part by Natural Science Foundation of China (61273183 and 61374028).

References

[1] P. Yi, Y. Hong, and F. Liu, "Distributed gradient algorithm for constrained optimization with application to load sharing in power systems," *Systems & Control Letters*, vol. 83, pp. 45–52, 2015.

[2] T.-H. Chang, A. Nedić, and A. Scaglione, "Distributed constrained optimization by consensus-based primal-dual perturbation method," *IEEE Transactions on Automatic Control*, vol. 59, no. 6, pp. 1524–1538, 2014.

[3] M. Rabbat and R. Nowak, "Distributed optimization in sensor networks," in *Proceedings of the 3rd International Symposium on Information Processing in Sensor Networks (IPSN '04)*, pp. 20–27, IEEE, April 2004.

[4] S. S. Ram, V. V. Veeravalli, and A. Nedić, "Distributed non-autonomous power control through distributed convex optimization," in *Proceedings of the 28th Conference on Computer Communications (IEEE INFOCOM '09)*, pp. 3001–3005, IEEE, Rio de Janeiro, Brazil, April 2009.

[5] R. Olfati-Saber and R. M. Murray, "Consensus problems in networks of agents with switching topology and time-delays," *IEEE Transactions on Automatic Control*, vol. 49, no. 9, pp. 1520–1533, 2004.

[6] R. Olfati-Saber, J. A. Fax, and R. M. Murray, "Consensus and cooperation in networked multi-agent systems," *Proceedings of the IEEE*, vol. 95, no. 1, pp. 215–233, 2007.

[7] J. Hu and Y. S. Lin, "Consensus control for multi-agent systems with double-integrator dynamics and time delays," *IET Control Theory & Applications*, vol. 4, no. 1, pp. 109–118, 2010.

[8] W. X. Li and Z. W. Chen, "Leader-following consensus of second-order multi-agent systems with time-delay and nonlinear dynamics," in *Proceedings of the 31th Chinese Control Conference*, pp. 7251–7256, 2015.

[9] A. Nedić and A. Ozdaglar, "Distributed subgradient methods for multi-agent optimization," *IEEE Transactions on Automatic Control*, vol. 54, no. 1, pp. 48–61, 2009.

[10] A. Nedic, A. Ozdaglar, and P. A. Parrilo, "Constrained consensus and optimization in multi-agent networks," *IEEE Transactions on Automatic Control*, vol. 55, no. 4, pp. 922–938, 2010.

[11] I. Lobel and A. Ozdaglar, "Distributed subgradient methods for convex optimization over random networks," *IEEE Transactions on Automatic Control*, vol. 56, no. 6, pp. 1291–1306, 2011.

[12] M. Zhu and S. Martinez, "On distributed convex optimization under inequality and equality constraints," *IEEE Transactions on Automatic Control*, vol. 57, no. 1, pp. 151–164, 2012.

[13] J. Wang and N. Elia, "A control perspective for centralized and distributed convex optimization," in *Proceedings of the 50th IEEE Conference on Decision and Control and European Control Conference (CDC-ECC '11)*, pp. 3800–3805, IEEE, Orlando, Fla, USA, December 2011.

[14] S. S. Kia, J. Cortés, and S. Martínez, "Distributed convex optimization via continuous-time coordination algorithms with discrete-time communication," *Automatica*, vol. 55, pp. 254–264, 2015.

[15] S. F. Yang, Q. S. Liu, and J. Wang, "Distributed optimization based on a multiagent system in the presence of communication delays," *IEEE Transactions on Systems, Man, and Cybernetics: Systems*, 2016.

[16] B. Gharesifard and J. Cortes, "Distributed continuous-time convex optimization on weight-balanced digraphs," *IEEE Transactions on Automatic Control*, vol. 59, no. 3, pp. 781–786, 2014.

[17] Q. Liu and J. Wang, "A second-order multi-agent network for bound-constrained distributed optimization," *IEEE Transactions on Automatic Control*, vol. 60, no. 12, pp. 3310–3315, 2015.

[18] Y. Zhang and Y. Hong, "Distributed optimization design for high-order multi-agent systems," in *Proceedings of the 34th Chinese Control Conference (CCC '15)*, pp. 7251–7256, IEEE, July 2015.

[19] J. Lu and C. Y. Tang, "Zero-gradient-sum algorithms for distributed convex optimization: the continuous-time case," *IEEE Transactions on Automatic Control*, vol. 57, no. 9, pp. 2348–2354, 2012.

[20] J. W. Wang and J. X. Li, "Exponential consensus of second-order multi-agent systems with time-varying delay under switching network," in *Proceedings of the IEEE International Conference on Information and Automation*, pp. 1058–1063, IEEE, August 2015.

[21] Y. G. Sun, L. Wang, and G. M. Xie, "Average consensus in networks of dynamic agents with switching topologies and multiple time-varying delays," *Systems & Control Letters*, vol. 57, no. 2, pp. 175–183, 2008.

[22] C. Godsil and G. Royle, *Algebraic Graph Theory*, Springer, New York, NY, USA, 2001.

[23] S. Boyd, L. E. Ghaoui, E. Feron, and V. Balakrishnan, *Linear Matrix Inequalities in System and Control Theory*, SIAM, Philadelphia, Pa, USA, 1994.

[24] R. T. Rockafellar, *Convex Analysis*, Princeton University Press, Princeton, NJ, USA, 1972.

[25] J. K. Hale and S. M. V. Lunel, *Introduction to the Theory of Functional Differential Equations*, Springer, New York, NY, USA, 1991.

Hindawi
Journal of Control Science and Engineering
Volume 2017, Article ID 9269187, 7 pages
https://doi.org/10.1155/2017/9269187

Research Article

Iterative Learning Control with Forgetting Factor for Urban Road Network

Tianyi Lan,[1] Fei Yan,[2] and Hui Lin[1]

[1]*School of Automation, Northwestern Polytechnical University, Xi'an, Shaanxi 710072, China*
[2]*College of Information Engineering, Taiyuan University of Technology, Taiyuan, Shanxi 030024, China*

Correspondence should be addressed to Fei Yan; yanfei140222@163.com

Received 13 September 2016; Revised 10 January 2017; Accepted 8 February 2017; Published 28 February 2017

Academic Editor: Qiang Song

In order to improve the traffic condition, a novel iterative learning control (ILC) algorithm with forgetting factor for urban road network is proposed by using the repeat characteristics of traffic flow in this paper. Rigorous analysis shows that the proposed ILC algorithm can guarantee the asymptotic convergence. Through iterative learning control of the traffic signals, the number of vehicles on each road in the network can gradually approach the desired level, thereby preventing oversaturation and traffic congestion. The introduced forgetting factor can effectively adjust the control input according to the states of the system and filter along the direction of the iteration. The results show that the forgetting factor has an important effect on the robustness of the system. The theoretical analysis and experimental simulations are given to verify the validity of the proposed method.

1. Introduction

Urban road intersection is the meeting center of traffic flow in urban network. Whether the vehicles can drive safely and orderly through the intersection or not has an important influence on the patency of the road network. The signal control of the intersection ensures the efficient operation of traffic flow in urban network and prevents traffic congestion.

At present, many signal control methods for urban road intersection have been developed by researchers based on different theories. Some corresponding signal control systems have been developed and put into use, such as SCOOT [1], SCATS [2], UTOPIA/SPOT [3], RHODES [4], OPAC [5], and PRODYN [6]. According to the different theories, there are several methods, for instance, the optimal control [7, 8], model predictive control [9, 10], and agent based method [11]. However, most of them are still in the theoretical research stage. Based on the optimal control theory, Aboudolas et al. proposed a signal control method for urban road intersection, which can calculate the signal timing of large-scale urban road network with the advantages of simple structure and small amount of calculation [7, 8]. But the method performs inappropriately when the traffic state is oversaturated. In [9, 10], Van den Berg et al. introduced a signal control method for urban road intersection based on model predictive control, which can calculate the signal timing online rolling and operate easily; however, tedious calculation is necessary for the large-scale urban road network. Negenborn et al. proposed a signal control method for urban road intersection based on the agent based method, which can work out the urban traffic signal control in distributed manner and avoid the complex calculation of the centralized control [11]. However, this method is difficult to achieve in practice.

From the macro point of view, traffic flow has obvious characteristics of repeatability. Therefore, how to make use of the repetitive nature of traffic flow to control the intersection is important for improving urban traffic conditions. For the system with characteristics of repeatability, iterative learning control, which is proposed by Arimoto et al. [12], can deal with the control problems of complex nonlinear dynamic, time-varying, and unknown system in a simple way, and it has been widely used.

In the field of traffic control, Hou and Xu applied the iterative learning control method to expressway ramp control [13] and further proposed the hybrid ramp control method by combing the iterative learning control and feedback control

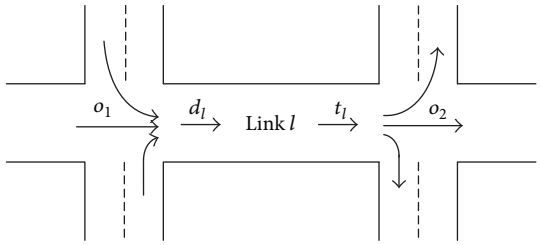

Figure 1: Signalized intersections.

to enhance robustness of the system [14]. However, there is little research on the ILC for urban road intersection control [15–17]. Therefore, the iterative learning control algorithm with forgetting factor for urban road intersection is discussed in this work. The introduced forgetting factor can effectively adjust the control input according to the states of the system and filter along the direction of the iteration. So it can accelerate the speed of convergence, smooth the tracking error curve, track the desired trajectory better, and reduce the impact of internal interference in the system on the convergence. The robustness of iterative learning control with forgetting factor is proven by rigorous analysis. Finally, the effectiveness of the method is verified by numerical simulation.

2. Traffic Flow Modeling

Let o_1 and o_2 be the two adjacent intersections, the corresponding road is l, d_l denotes the input flow of road l, and t_l is the output flow, which is shown in Figure 1.

Then the number of vehicles x_l on road l at time k is

$$x_l(k+1) = x_l(k) + T\left[d_l(k) - t_l(k)\right], \tag{1}$$

where T is the control cycle and $k = 0, 1, 2, \ldots, K$ is the sampling time.

The input flow $d_l(k)$ at road l is the sum of traffic from the upper roads; that is,

$$d_l(k) = \sum_{w \in I_{o_1}} \tau_{w,l} t_w(k), \tag{2}$$

where I_{o_1} is the road collection for traffic into the intersection o_1 and $\tau_{w,l}$ is the rate for traffic flow through road w into road l.

Let $g_l(k)$ be the effective green light time for road l at time k; then the output flow $t_l(k)$ is

$$t_l(k) = \left(\frac{g_l(k)}{C}\right) S_l, \tag{3}$$

where $g_l(k) = \sum_{i \in V_l} u_{o_2,i}(k)$, $u_{o_2,i}(k)$ is the green time for phase i at intersection o_2, and V_l is the phase set with right of way for road l. S_l is the saturated flow for road l; C is the signal cycle.

Submitting (2) and (3) into (1), we can get the state function of road l as follows:

$$\begin{aligned} x_l(k+1) &= x_l(k) \\ &\quad + T\left[\sum_{w \in I_{o_1}} \tau_{w,l} \frac{S_w}{C} \sum_{i \in V_w} u_{o_1,i}(k) - \frac{S_z}{C} \sum_{i \in V_l} u_{o_2,i}(k)\right]. \end{aligned} \tag{4}$$

Therefore, for different phases at intersection o, the green time $u_{o,i}$, the loss time l_o, and signal cycle C should satisfy the following equation:

$$\sum_{i \in F_o} u_{o,i}(k) + l_o = C. \tag{5}$$

Considering the pedestrian crossing time, $u_{o,i}$ should also satisfy

$$u_{o,i}^{\min} \le u_{o,i}(k) \le u_{o,i}^{\max}, \tag{6}$$

where $u_{o,i}^{\min}$ and $u_{o,i}^{\max}$ are the minimum and maximum of $u_{o,i}$, respectively.

3. State Space Model and Assumptions

3.1. State Space Model. Define the state equation (4) for all roads of the urban network, which combines with the output equation. The state space model of urban network is shown as follows:

$$\begin{aligned} \mathbf{x}(k+1) &= A\mathbf{x}(k) + B\mathbf{u}(k), \\ \mathbf{y}(k+1) &= C\mathbf{x}(k+1), \end{aligned} \tag{7}$$

where $\mathbf{x}(k)$ is the state vector, $\mathbf{u}(k)$ is the control vector, $\mathbf{y}(k)$ is the output vector, and state matrix A and output matrix C are the identity matrix, respectively. The elements of input matrix B contain the characteristic parameters of road network such as phase, cycle, turning saturation flow rate, and other parameters.

According to the actual requirement, the control input $\mathbf{u}(k)$ must be in a reasonable range; that is to say, $\mathbf{u}(k)$ must satisfy formula (6) and $\mathbf{u}(k) \in [\mathbf{u}_{\min}(k), \mathbf{u}_{\max}(k)]$; this condition can also be illustrated by the saturation function $\mathbf{u}(k)$, which is shown as follows:

$$\begin{aligned} &\operatorname{sat}[\mathbf{u}(k)] \\ &= \begin{cases} \mathbf{u}_{\min}(k), & \mathbf{u}(k) \le \mathbf{u}_{\min}(k), \\ \mathbf{u}(k), & \mathbf{u}_{\min}(k) < \mathbf{u}(k) < \mathbf{u}_{\max}(k), \\ \mathbf{u}_{\max}(k), & \mathbf{u}(k) \ge \mathbf{u}_{\max}(k). \end{cases} \end{aligned} \tag{8}$$

Therefore, when the input is limited, the state space equation of (7) is

$$\begin{aligned} \mathbf{x}(k+1) &= A\mathbf{x}(k) + B\operatorname{sat}[\mathbf{u}(k)], \\ \mathbf{y}(k+1) &= C\mathbf{x}(k+1). \end{aligned} \tag{9}$$

3.2. Assumptions

Assumption 1. In the process of iteration, the initial condition should be satisfied:

$$\begin{aligned} \mathbf{x}_n(0) &= \mathbf{x}_d(0), \\ \mathbf{y}_n(0) &= \mathbf{y}_d(0), \\ &\forall n, \end{aligned} \tag{10}$$

where $\mathbf{x}_d(0)$ and $\mathbf{y}_d(0)$ are the initial values for the desired state and desired output, respectively. n is the number of iterations.

Assumption 2. For the given desired output $\mathbf{y}_d(k)$ $(k \in [0, K])$, there exists the control input $\mathbf{u}_d(k)$ $(k \in [0, K])$ which satisfies

$$\begin{aligned} \mathbf{x}_d(k+1) &= A\mathbf{x}_d(k) + B\mathbf{u}_d(k), \\ \mathbf{y}_d(k+1) &= C\mathbf{x}_d(k+1), \end{aligned} \tag{11}$$

where $\mathbf{x}_d(k)$ $(k \in [0, K])$ is the corresponding desired state of $y_d(k)$ $(k \in [0, K])$.

3.3. Control Objective. Through the iterative learning control of green time, the number of vehicles on $[0, K]$ can approach the reasonable expectation in the urban network, and then traffic congestion can be avoided by preventing the excessive saturated traffic flow.

4. Iterative Learning Control with Forgetting Factor for Urban Network

The definition of norms used in this paper is given as follows:

$$\left\|\mathbf{g}(k)\right\|_\lambda = \sup_{k\in[0,K]} a^{-\lambda k} \left\|\mathbf{g}(k)\right\|, \tag{12}$$

where $\lambda > 0$ and $a > 1$.

In the paper, $\|\cdot\|$ denotes the infinite norm, thus, for the matrix W with size $s \times t$, whose elements denote $w_{i,j}$,

$$\|W\| = \max_{1\le i\le t} \sum_{j=1}^{s} \left|w_{i,j}\right|. \tag{13}$$

For system (9), the iterative learning control law with forgetting factor in this paper is designed as follows:

$$\begin{aligned} \mathbf{u}_{n+1}(k) = (1-\alpha)\,\mathrm{sat}\left[\mathbf{u}_n(k)\right] + \alpha\mathbf{u}_0(k) \\ + \beta\mathbf{e}_n(k+1), \end{aligned} \tag{14}$$

where $\mathbf{e}_n(k) = y_d(k) - y_n(k)$ is the tracking error for the nth iteration, β is the iterative learning gain matrix, and α is the iterative forgetting factor for the system which satisfies $0 < \alpha < 1$.

Before investigating learning properties under constraints, we first introduce an important Property:

$$\left\|u_d(k) - \mathrm{sat}\left[u_n(k)\right]\right\| \le \left\|u_d(k) - u_n(k)\right\|. \tag{15}$$

Proof. When u is a scalar, we can easily obtain that

$$\begin{aligned} &\left(u_d(k) - \mathrm{sat}\left[u_n(k)\right]\right)^2 - \left(u_d(k) - u_n(k)\right)^2 \\ &\quad = \left(\mathrm{sat}\left[u_n(k)\right] - u_n(k)\right) \\ &\quad \cdot \left(\mathrm{sat}\left[u_n(k)\right] + u_n(k) - 2u_d(k)\right). \end{aligned} \tag{16}$$

For limited u, there are three possible cases:

(1) $u_n(k) \in [u_{\min}(k), u_{\max}(k)]$.

(2) $u_n(k) > u_{\max}(k)$.

(3) $u_n(k) < u_{\min}(k)$.

(1) When $u_n(k) \in [u_{\min}(k), u_{\max}(k)]$, $u_n(k) = \mathrm{sat}[u_n(k)]$; then (15) is equal to zero, so the "=" relationship of Property holds.

(2) When $u_n(k) > u_{\max}(k)$, $\mathrm{sat}[u_n(k)] = u_{\max}(k)$, and

$$\begin{aligned} \mathrm{sat}\left[u_n(k)\right] - u_n(k) &= u_{\max}(k) - u_n(k) < 0, \\ \mathrm{sat}\left[u_n(k)\right] + u_n(k) - 2u_d(k) &> 0. \end{aligned} \tag{17}$$

From (17), it is obvious that (16) is less than zero.

(3) When $u_n(k) < u_{\min}(k)$, $\mathrm{sat}[u_n(k)] = u_{\min}(k)$; thus

$$\begin{aligned} \mathrm{sat}\left[u_n(k)\right] - u_n(k) &= u_{\min}(k) - u_n(k) > 0, \\ \mathrm{sat}\left[u_n(k)\right] + u_n(k) - 2u_d(k) &< 0. \end{aligned} \tag{18}$$

From (18) it can be concluded that (16) is less than zero.

From the above discussions, we can see that the Property holds when u is a scalar. Below we give the proof of the Property for vector-valued u.

$$\begin{aligned} &\left\|u_d(k) - \mathrm{sat}\left[u_n(k)\right]\right\|^2 \\ &\quad = \sum_{j=1}^{N} \left[u_{j,d}(k) - \mathrm{sat}\left[u_{j,n}(k)\right]\right]^2 \\ &\quad \le \sum_{j=1}^{N} \left[u_{j,d}(k) - u_{j,n}(k)\right]^2 = \left\|u_d(k) - u_n(k)\right\|^2. \end{aligned} \tag{19}$$

This means that Property still holds. □

The robustness theorem of iterative learning control is given as follows.

Theorem 3. *For system (9) which satisfies Assumptions 1 and 2, if there exists a matrix β which satisfies $\|(1-\alpha)I - \beta C\mathbf{B}\| < 1$, then the tracking error converges to bounded range for $[0, K]$ with the iterative learning control law (14); that is,*

$$\lim_{n\to\infty} \sup_{k\in[0,K]} \left\|\mathbf{e}_n(k)\right\|_\lambda \le \frac{b_\xi}{1-\rho}. \tag{20}$$

Proof. Define

$$\begin{aligned} \delta x_n(k) &= x_d(k) - x_n(k), \\ \delta u_n(k) &= u_d(k) - u_n(k). \end{aligned} \tag{21}$$

The state equation for the nth iteration is

$$\begin{aligned}\mathbf{x}_n(k+1) &= \mathbf{A}\mathbf{x}_n(k) + \mathbf{B}\,\mathrm{sat}\left[\mathbf{u}_n(k)\right],\\ \mathbf{y}_n(k+1) &= \mathbf{C}\mathbf{x}_n(k+1).\end{aligned} \tag{22}$$

From Assumption 2, we have

$$\begin{aligned}e_n(k+1) &= y_d(k+1) - y_n(k+1)\\ &= C\left\{\mathbf{A}\mathbf{x}_d(k) + \mathbf{B}\mathbf{u}_d(k) - \mathbf{A}\mathbf{x}_n(k) - \mathbf{B}\,\mathrm{sat}\left[\mathbf{u}_n(k)\right]\right\}\\ &= C\left\{\mathbf{A}\left(\mathbf{x}_d(k) - \mathbf{x}_n(k)\right) + \mathbf{B}\left(\mathbf{u}_d(k) - \mathrm{sat}\left[\mathbf{u}_n(k)\right]\right)\right\}\\ &= C\mathbf{A}\left(\mathbf{x}_d(k) - \mathbf{x}_n(k)\right)\\ &\quad + C\mathbf{B}\left(\mathbf{u}_d(k) - \mathrm{sat}\left[\mathbf{u}_n(k)\right]\right).\end{aligned} \tag{23}$$

From formula (14), we have

$$\begin{aligned}\delta\mathbf{u}_{n+1}(k) &= (1-\alpha)\left(\mathbf{u}_d(k) - \mathrm{sat}\left[\mathbf{u}_n(k)\right]\right)\\ &\quad + \alpha\left(\mathbf{u}_d(k) - \mathbf{u}_0(k)\right) - \beta\mathbf{e}_n(k+1).\end{aligned} \tag{24}$$

Submitting (23) into (24), we have

$$\begin{aligned}\delta\mathbf{u}_{n+1}(k) &= (1-\alpha)\left(\mathbf{u}_d(k) - \mathrm{sat}\left[\mathbf{u}_n(k)\right]\right) + \alpha\left(\mathbf{u}_d(k)\right.\\ &\quad \left. - \mathbf{u}_0(k)\right) - \beta\left(C\left\{\mathbf{A}\left(\mathbf{x}_d(k) - \mathbf{x}_n(k)\right)\right.\right.\\ &\quad \left.\left. + \mathbf{B}\left(\mathbf{u}_d(k) - \mathrm{sat}\left[\mathbf{u}_n(k)\right]\right)\right\}\right) = (1-\alpha)\left(\mathbf{u}_d(k)\right.\\ &\quad \left. - \mathrm{sat}\left[\mathbf{u}_n(k)\right]\right) + \alpha\left(\mathbf{u}_d(k) - \mathbf{u}_0(k)\right) - \beta C\mathbf{A}\left(\mathbf{x}_d(k)\right.\\ &\quad \left. - \mathbf{x}_n(k)\right) - \beta C\mathbf{B}\left(\mathbf{u}_d(k) - \mathrm{sat}\left[\mathbf{u}_n(k)\right]\right) = \left((1-\alpha)\right.\\ &\quad \left.\cdot I - \beta C\mathbf{B}\right)\left(\mathbf{u}_d(k) - \mathrm{sat}\left[\mathbf{u}_n(k)\right]\right) + \alpha\delta\mathbf{u}_0(k)\\ &\quad - \beta C\mathbf{A}\delta\mathbf{x}_n(k).\end{aligned} \tag{25}$$

Taking the norm on both sides of formula (25), we have

$$\begin{aligned}&\left\|\delta\mathbf{u}_{n+1}(k)\right\|\\ &\quad \le \left\|(1-\alpha)I - \beta C\mathbf{B}\right\|\left\|\mathbf{u}_d(k) - \mathrm{sat}\left[\mathbf{u}_n(k)\right]\right\|\\ &\qquad + \alpha\left\|\delta\mathbf{u}_0(k)\right\| + \left\|\beta C\mathbf{A}\right\|\left\|\delta\mathbf{x}_n(k)\right\|\\ &\quad \le \left\|(1-\alpha)I - \beta C\mathbf{B}\right\|\left\|\mathbf{u}_d(k) - \mathbf{u}_n(k)\right\|\\ &\qquad + \alpha\left\|\delta\mathbf{u}_0(k)\right\| + \left\|\beta C\mathbf{A}\right\|\left\|\delta\mathbf{x}_n(k)\right\|\\ &\quad \le \left\|(1-\alpha)I - \beta C\mathbf{B}\right\|\left\|\delta\mathbf{u}_n(k)\right\| + \alpha\left\|\delta\mathbf{u}_0(k)\right\|\\ &\qquad + \varepsilon\left\|\delta\mathbf{x}_n(k)\right\|,\end{aligned} \tag{26}$$

where $\varepsilon = \|\beta C\mathbf{A}\|$.

$$\begin{aligned}\delta x_n(k) &= x_d(k) - x_n(k)\\ &= A\mathbf{x}_d(k-1) + B\mathbf{u}_d(k-1) - \mathbf{A}\mathbf{x}_n(k-1)\\ &\quad - \mathbf{B}\,\mathrm{sat}\left[\mathbf{u}_n(k-1)\right]\\ &= A\left(\mathbf{x}_d(k-1) - \mathbf{x}_n(k-1)\right)\\ &\quad + B\left(\mathbf{u}_d(k-1) - \mathrm{sat}\left[\mathbf{u}_n(k-1)\right]\right).\end{aligned} \tag{27}$$

Taking the norm on both sides of formula (27), we have

$$\begin{aligned}\left\|\delta x_n(k)\right\| &\le \|A\|\left\|\delta\mathbf{x}_n(k-1)\right\|\\ &\quad + \|B\|\left\|\mathbf{u}_d(k-1) - \mathrm{sat}\left[\mathbf{u}_n(k-1)\right]\right\|\\ &\le \|A\|\left\|\delta\mathbf{x}_n(k-1)\right\| + \|B\|\left\|\delta\mathbf{u}_n(k-1)\right\|\\ &\le \|A\|^2\left\|\delta\mathbf{x}_n(k-2)\right\|\\ &\quad + \|A\|\|B\|\left\|\delta\mathbf{u}_n(k-2)\right\|\\ &\quad + \|B\|\left\|\delta\mathbf{u}_n(k-1)\right\|\\ &\le \|A\|^3\left\|\delta\mathbf{x}_n(k-3)\right\|\\ &\quad + \|A\|^2\|B\|\left\|\delta\mathbf{u}_n(k-3)\right\|\\ &\quad + \|A\|\|B\|\left\|\delta\mathbf{u}_n(k-2)\right\|\\ &\quad + \|B\|\left\|\delta\mathbf{u}_n(k-1)\right\|\\ &\le \|A\|^k\left\|\delta\mathbf{x}_n(0)\right\|\\ &\quad + \sum_{j=0}^{k-1}\|A\|^{k-j-1}\|B\|\left\|\delta\mathbf{u}_n(j)\right\|.\end{aligned} \tag{28}$$

Taking the λ-norm on both sides of (28) with Assumption 1, we have

$$\left\|\delta x_n(k)\right\| \le \sum_{j=0}^{k-1} a^{k-j-1} b\left\|\delta\mathbf{u}_n(j)\right\|, \tag{29}$$

where $a = \|A\|$ and $b = \|B\|$.

Taking λ-norm on both sides of (29), we have

$$\begin{aligned}\left\|\delta x_n(k)\right\|_\lambda &\le \sup_{k\in[0,K]} a^{-\lambda k}\sum_{j=0}^{k-1} a^{k-j-1} b\left\|\delta\mathbf{u}_n(j)\right\|\\ &\le a^{-1}b\sup_{k\in[0,K]}\sum_{j=0}^{k-1} a^{-\lambda k}a^{\lambda j}a^{k-j}\sup_{k\in[0,K]} a^{-\lambda j}\left\|\delta\mathbf{u}_n(j)\right\|\\ &\le a^{-1}b\left\|\delta\mathbf{u}_n(k)\right\|_\lambda\sup_{k\in[0,K]}\sum_{j=0}^{k-1} a^{(\lambda-1)(j-k)}\\ &\le \left\|\delta\mathbf{u}_n(k)\right\|_\lambda\frac{1-a^{(1-\lambda)K}}{a^\lambda - a}b.\end{aligned} \tag{30}$$

Taking λ-norm on both sides of (26), we have

$$\begin{aligned}\left\|\delta\mathbf{u}_{n+1}(k)\right\|_\lambda &\le \left\|(1-\alpha)I - \beta C\mathbf{B}\right\|\left\|\delta\mathbf{u}_n(k)\right\|_\lambda\\ &\quad + \alpha\left\|\delta\mathbf{u}_0(k)\right\|_\lambda + \varepsilon\left\|\delta\mathbf{x}_n(k)\right\|_\lambda.\end{aligned} \tag{31}$$

Submitting (30) into (31), we have

$$\begin{aligned}&\left\|\delta\mathbf{u}_{n+1}(k)\right\|_\lambda\\ &\le \left(\left\|(1-\alpha)I - \beta C\mathbf{B}\right\| + \frac{1-a^{(1-\lambda)K}}{a^\lambda - a}b\varepsilon\right)\left\|\delta\mathbf{u}_n(k)\right\|_\lambda\\ &\quad + \alpha\left\|\delta\mathbf{u}_0(k)\right\|_\lambda.\end{aligned} \tag{32}$$

From the convergence condition,

$$\left\|(1-\alpha)\, I - \beta C\mathbf{B}\right\| < 1. \tag{33}$$

When λ tends to infinity, we have

$$\left(\left\|(1-\alpha)\, I - \beta C\mathbf{B}\right\| + \frac{1-a^{(1-\lambda)K}}{a^{\lambda}-a} b\varepsilon\right) \le \rho < 1. \tag{34}$$

Form (32), we can also obtain the following result:

$$\begin{aligned}\left\|\delta\mathbf{u}_{n+1}(k)\right\|_{\lambda} &\le \rho \left\|\delta\mathbf{u}_{n}(k)\right\|_{\lambda} + \varepsilon_1 \\ &\le \rho^{n+1} \left\|\delta\mathbf{u}_{0}(k)\right\|_{\lambda} + \frac{\varepsilon_1\left(1+\rho^{n+1}\right)}{1-\rho},\end{aligned} \tag{35}$$

where $\varepsilon_1 = \alpha\|\delta\mathbf{u}_0(k)\|_{\lambda}$.

When $n \to \infty$, the following result is obtained:

$$\lim_{n\to\infty} \left\|\delta u_{n+1}(k)\right\|_{\lambda} \le \frac{\varepsilon_1}{1-\rho}. \tag{36}$$

From (30) and (36), we get

$$\left\|\delta x_{n}(k)\right\|_{\lambda} \le \frac{\varepsilon_1}{1-\rho} \cdot \frac{1-a^{(1-\lambda)K}}{a^{\lambda}-a} b. \tag{37}$$

When λ tends to infinity, we have $\varepsilon_1 \to 0$; therefore

$$\lim_{n\to\infty} \left\|\delta x_{n+1}(k)\right\|_{\lambda} = 0. \tag{38}$$

We can also get the following result:

$$\lim_{n\to\infty} \left\|e_{n+1}(k)\right\|_{\lambda} = 0. \tag{39}$$

Thus, we can complete the proof of the theorem. □

5. Simulation Research

In order to validate the effectiveness of the proposed iterative learning control algorithm with forgetting factor for urban network, the following simulation results are given by using VISSIM. Figure 2 shows the test network, which is composed of 36 links and 9 intersections. Each link has two-way lanes. VISSIM is employed to simulate the real traffic environment for simulations and provides the traffic measurements of the states to MATLAB for calculating the new input signals by the ILC-based control laws. Different from the methods in [15–17], the new input signals are calculated by the proposed iterative learning control law (14) in the simulation.

The input flow of the network for the starting link is shown in Figure 3.

We compare the proposed method with fixed timing (FT) method to verify the effectiveness of the proposed method. The result of fixed timing method is calculated by the classical Webster optimization program. In order to minimize the initial iterative error, the initial input $\mathbf{u}_0(k)$ for (14) is selected as the fixed timing plan.

Selecting the vehicle average delay time (TDT) and the number of stops (AVS) as the evaluation indexes, the simulation results are shown in Table 1.

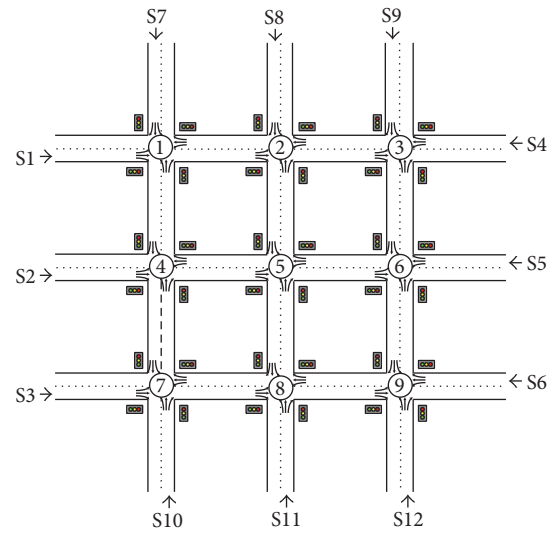

Figure 2: The simulation network.

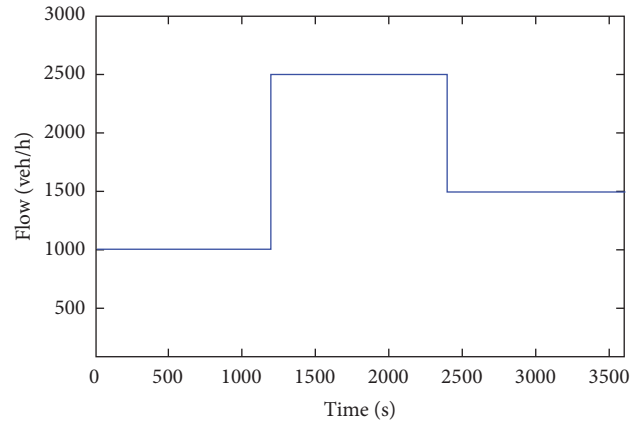

Figure 3: The input flow for the network.

Table 1: Simulation results.

Control strategy	Fixed timing method		Iterative learning control	
Evaluation index	TDT(s)	AVS	TDT(s)	AVS
1	93.06	1.69	82.30	1.56
2	92.73	1.72	80.96	1.59
3	96.15	1.81	83.77	1.65

Table 1 shows that the traffic conditions under iterative learning control algorithm with forgetting factor are obviously improved, compared to the fixed timing control. The maximum total delay time decreases from 96.15 h to 83.77 h, as low as 12.9%. The maximum average vehicle stop time reduces from 1.81 to 1.65; the decrease rate is 8.8%. The result shows that iterative learning control algorithm with forgetting factor has strong robustness.

The variation curves of total network delay time and average number of vehicle stops are illustrated in Figures 4 and 5, respectively.

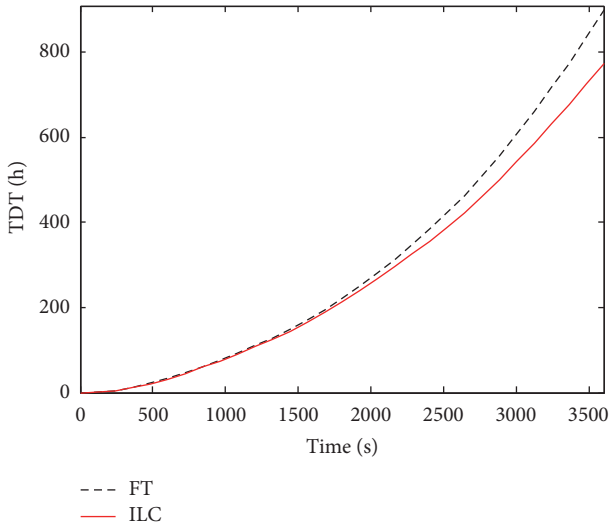

Figure 4: Total delay time for two control strategies.

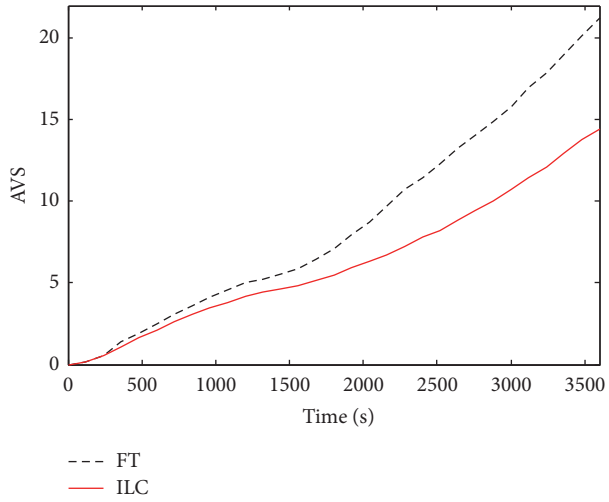

Figure 5: The average number of vehicle stops for two control strategies.

Figures 4 and 5 show that there is no significant change for the total delay time and average vehicle stop times at the initial stages due to the lighter traffic flow. But with the increasing of traffic flow, compared with iterative learning control, the total delay time and average vehicle stop times increase significantly under the fixed timing control strategy after 1200 s. The results show that the iterative learning control algorithm with forgetting factor can control traffic flow by adjusting the green time according to the traffic conditions. Then the traffic conditions can be improved by reducing the total delay time and the number of vehicle stops.

6. Conclusions

This work proposes an iterative learning control algorithm with forgetting factor for urban road intersection. The robustness of iterative learning control algorithm is proven by using mathematical analysis. The number of vehicles on different roads in the network approaches the reasonable expectations by using the iterative learning control of the traffic signal. The result ensures that the green time is used completely and prevents traffic jams. The results show that the forgetting factor has an important effect on the robustness of the system. The effectiveness of the algorithm is verified by the theoretical analysis and numerical simulations.

Competing Interests

The authors declare that they have no competing interests.

Acknowledgments

This study has been supported by National Science Foundation (Grant no. 51407143).

References

[1] D. I. Robertson and R. D. Bretherton, "Optimizing networks of traffic signals in real time—the SCOOT method," *IEEE Transactions on Vehicular Technology*, vol. 40, no. 1, pp. 11–15, 1991.

[2] P. R. Lowrie, "The Sydney coordinated adaptive traffic system-principles, methodology, algorithms," in *Proceedings of the International Conference on Road Traffic Signaling*, pp. 67–70, London, UK, March 1982.

[3] V. Mauro and C. Di Taranto, "UTOPIA," *Control Computers Communications in Transportation*, vol. 20, no. 4, pp. 245–252, 1990.

[4] S. Sen and K. L. Head, "Controlled optimization of phases at an intersection," *Transportation Science*, vol. 31, no. 1, pp. 5–17, 1997.

[5] N. H. Gartner, "Simulation study of OPAC: a demand-responsive strategy for traffic signal control," in *Transportation and Traffic Theory*, pp. 233–250, 1983.

[6] J. L. Farges, J. J. Henry, and J. Tufal, "The PRODYN real-time traffic algorithm," in *Proceedings of the 4th IFAC Symposium of Transportation Systems*, pp. 307–312, Baden-Baden, Germany, April 1983.

[7] K. Aboudolas, M. Papageorgiou, and E. Kosmatopoulos, "Store-and-forward based methods for the signal control problem in large-scale congested urban road networks," *Transportation Research Part C: Emerging Technologies*, vol. 17, no. 2, pp. 163–174, 2009.

[8] C. Diakaki, M. Papageorgiou, and K. Aboudolas, "A multivariable regulator approach to traffic-responsive network-wide signal control," *Control Engineering Practice*, vol. 10, no. 2, pp. 183–195, 2002.

[9] M. Van den Berg, A. Hegyi, B. De Schutter, and J. Hellendoorn, "A Macroscopic traffic flow model for integrated control of freeway and urban traffic networks," in *Proceedings of the 42nd IEEE Conference on Decision and Control*, pp. 2774–2779, December 2003.

[10] M. van den Berg, B. De Schutter, A. Hegyi, and J. Hellendoorn, "Model predictive control for mixed urban and freeway networks," in *Proceedings of the 83rd Annual Meeting of the Transportation Research Board*, pp. 3304–3327, Washington, DC, USA, January 2004.

[11] R. R. Negenborn, B. De Schutter, and H. Hellendoorn, "Multi-agent model predictive control of transportation networks," in *Proceedings of the IEEE International Conference on Networking, Sensing and Control (ICNSC '06)*, pp. 296–301, Ft. Lauderdale, Fla, USA, April 2006.

[12] S. Arimoto, S. Kawamura, and F. Miyazaki, "Bettering operation of Robots by learning," *Journal of Robotic Systems*, vol. 1, no. 2, pp. 123–140, 1984.

[13] Z. S. Hou and J. X. Xu, "Freeway traffic density control using iterative learning control approach," in *Proceedings of the IEEE 6th International Conference on Intelligent Transportation Systems*, pp. 12–15, Shanghai, China, October 2003.

[14] Z. Hou, X. Xu, J. Yan, J.-X. Xu, and G. Xiong, "A complementary modularized ramp metering approach based on iterative learning control and ALINEA," *IEEE Transactions on Intelligent Transportation Systems*, vol. 12, no. 4, pp. 1305–1318, 2011.

[15] F. Yan, F. Tian, and Z. Shi, "An extended signal control strategy for urban network traffic flow," *Physica A*, vol. 445, pp. 117–127, 2016.

[16] F. Yan, F. Tian, and Z. Shi, "Effects of iterative learning based signal control strategies on macroscopic fundamental diagrams of urban road networks," *International Journal of Modern Physics C*, vol. 27, no. 4, 20 pages, 2016.

[17] F. Yan, F.-l. Tian, and Z.-k. Shi, "Iterative learning control approach for signaling split in urban traffic networks with macroscopic fundamental diagrams," *Mathematical Problems in Engineering*, vol. 2015, Article ID 975328, 12 pages, 2015.

Hindawi
Journal of Control Science and Engineering
Volume 2017, Article ID 4028258, 9 pages
https://doi.org/10.1155/2017/4028258

Research Article

Parameters Design for Logarithmic Quantizer Based on Zoom Strategy

Jingjing Yan

College of Electrical Engineering, Henan University of Technology, Zhengzhou 450052, China

Correspondence should be addressed to Jingjing Yan; yanjingjing2009@163.com

Received 30 December 2016; Revised 8 February 2017; Accepted 12 February 2017; Published 27 February 2017

Academic Editor: Haibo Du

This paper is concerned with the problem of designing suitable parameters for logarithmic quantizer such that the closed-loop system is asymptotic convergent. Based on zoom strategy, we propose two methods for quantizer parameters design, under which it ensures that the state of the closed-loop system can load in the invariant sets after some certain moments. Then we obtain that the quantizer is unsaturated, and thus the quantization errors are bounded under the time-varying logarithm quantization strategy. On that basis, we obtain that the closed-loop system is asymptotic convergent. A benchmark example is given to show the usefulness of the proposed methods, and the comparison results are illustrated.

1. Introduction

With the continuous improvement of the communication capability and reliability of the network, the data in the control system is transmitted through the network increasingly. The network bandwidth, although it may be very large, is always limited, so the data quantization is inevitable. At present, zoom strategy proposed in [1, 2] is a popular method in quantized control system.

Based on zoom strategy, literature [3] analyzes the stabilization problem for linear systems with multidimensional state and one-dimensional input. The main contribution of that paper is the trade-off between the quantized controller complexity and the system performance. Literature [4] proposes a unified framework to describe both the network conditions and the state quantization of linear systems. A model describing the nonideal network conditions and input/output state quantization is given by [5], and the problem of the quantized output feedback controller is designed there to asymptotically stabilize the closed-loop system. Hereafter, zoom strategy is widely used in quantized feedback stabilization problem.

As for the system affected by data quantization and time-delay, literature [6] proves that under some conditions, the closed-loop system can be global asymptotically stabilized via a dynamic quantization strategy by integral mean value theorem. Literature [7] designs an optimal dynamic quantizer which is able to minimize the maximum output error between the quantized system and unquantized systems. Supposing that the quantizer is to be saturated, two types of quantizer are discussed in [8] such that the state of the closed-loop system starting from a neighborhood of the origin exponentially converges to a bounded region. If the closed-loop system is affected by data quantization and packet dropout, we study the quantized stabilization of linear discrete-time systems and discrete-time and continuous-time fuzzy systems, respectively, in [9] and [10]. Assuming that the system is relating to quantization and disturbance, the related results can be shown in [11–13]. In literature [11], the authors propose two specific control strategies that yield the input-to-state stability of the closed-loop system based on quantized state. When the sampled state/output can only be obtained by the controller, literature [12] designs the full state feedback controller and the output feedback controller to stabilize the system. We generalize the results of [12] to the case that the system is also affected by packet dropout in [13]. For the stabilization problem of the closed-loop system affected by quantization and saturation, literature [8, 14] gets some results.

Zoom strategy is also combined with other methods to stabilize the closed-loop system, such as sliding-mode control

method [15], Kalman filter [16], scheduling protocol [17], and event-triggered control [18–20]. Furthermore, it is used to stabilize different kinds of systems, such as switched system [21–24], multiagent system [25, 26], and interconnected system [27]. More related works can be seen in review of literature [28, 29].

In summary, zoom strategy is a popular method to adjust the quantizer parameters, especially for uniform quantizer, such that the quantized control system is stable. As we know, logarithmic quantizer is another kind of commonly used quantizer [30, 31]. Compared with uniform quantizer, logarithmic quantizer has better performance near the origin. Consider this advantage, some papers adopt logarithmic quantization method to quantize the system state or output. Recent results include literature [32–36]. However, most of the existing papers assume that the parameters of the logarithmic quantizer are given previously. Few articles study the parameters design for logarithmic quantizer, which is the main research of this paper.

In this paper, we will propose two design methods for the parameters of the logarithmic quantizer. By zoom strategy, we design the logarithmic quantizer parameters including v_0, δ, and quantization density ρ, which determine the saturation boundary, dead zone, and the quantization intervals of the quantizer. Under the parameters designed, we guarantee the unsaturation of the quantizer and the asymptotic convergence of the closed-loop system.

The rest of this paper is organized as follows. We describe the problem discussed here in Section 2. Two design methods for the parameters of the logarithmic quantizer are illustrated in Sections 3 and 4, respectively. A well-known benchmark example is adopted in Section 5 to show the effectiveness of the design methods, and their comparison is also illustrated there. Finally, some conclusions are given in Section 6.

Notation. $\mathbb{R}^n$ denotes the n-dimensional Euclidean space. $\mathbb{R}^+$ and $\mathbb{N}$ denote the set of positive real numbers and positive integers, respectively. We denote by $\|\cdot\|$ the standard Euclidean norm in $\mathbb{R}^n$ and the corresponding induced matrix norm in $\mathbb{R}^{n\times n}$. $\lambda_{\max}(P)$ and $\lambda_{\min}(P)$ denote the maximum and minimum eigenvalue of matrix P, respectively. $A^\top \in \mathbb{R}^{m\times n}$ denotes the transposed of matrix $A \in \mathbb{R}^{n\times m}$. The signal $\lceil y \rceil$ indicates the least integer not less than y. $\mathbf{0}_{n\times 1}$ denotes zero vector with dimension $n \times 1$.

2. Problem Formulation

This paper considers the following linear time-invariant discrete systems:

$$x(k+1) = Ax(k) + Bu(k), \tag{1}$$

where $x \in \mathbb{R}^n$ is the state vector, $u \in \mathbb{R}^m$ is the control input, and A and B are constant matrices with proper dimensions. In the following, we assume that the open-loop system is unstable; that is, $\|A\| > 1$.

Assuming that the network is located at the sensor side, thus the controller can only receive the quantized values of the system states due to the limited bandwidth. Hence the controller can be illustrated as

$$u(k) = KQ(x(k)), \tag{2}$$

where K is the feedback matrix to be designed and $Q(\cdot)$ is a logarithmic quantizer defined as

$$Q(x(k)) = \left[q(x_1(k)), \ldots, q(x_n(k))\right]^\top. \tag{3}$$

Suppose that the quantization level of the quantizer is equal to $2N+1$, $N \in \mathbb{N}$. For any $i \in \{1, 2, \ldots, n\}$, if $k \in [k_j, k_{j+1})$, $j \in \mathbb{N} \cup \{0\}$, where k_j will be designed below, we define

$$q(x_i(k)) = \begin{cases} v_j & \text{if } x_i(k) \in \left[\dfrac{1}{1+\delta}v_j, +\infty\right) \\ v_{j+m} & \text{if } x_i(k) \in \left[\dfrac{1}{1+\delta}v_{j+m}, \dfrac{1}{1-\delta}v_{j+m}\right),\ m \in \{1, 2, \ldots, N-1\} \\ 0 & \text{if } x_i(k) \in \left[0, \dfrac{1}{1+\delta}v_{j+N-1}\right) \\ -q(-x_i(k)) & \text{if } x_i(k) \in (-\infty, 0], \end{cases} \tag{4}$$

with $\delta \in (0,1)$ and $v_{j+1} = \rho v_j$, $v_0 > 0$, in which the quantization density ρ is given by $\rho = (1-\delta)/(1+\delta) \in (0,1)$. Obviously, δ, ρ, and v_0 are the critical parameters of the logarithmic quantizer, which are assumed to be undetermined.

The aim of this paper is to design the quantizer parameters δ, ρ, and v_0 based on zoom strategy to ensure the unsaturation of the quantizer; that is, $\|x(k)\| \le (1/(1-\delta))v_j$, $k \in [k_j, k_{j+1})$, $j \in \mathbb{N} \cup \{0\}$. From which we can see that the quantization errors are bounded and the system state tends to zero when k tends to infinity according to the definition of v_j. The main innovation of this paper is that the zoom strategy, which is always adopted to discuss the properties of the uniform quantizer, is used here to determine the parameters of the logarithmic quantizer.

In what follows, we will propose two methods for quantizer parameters design and compare them in simulation example.

3. First Method for Quantizer Parameters Design

If there exist a positive-definite matrix P and a feedback matrix K such that

$$\Pi \coloneqq P - (A + BK)^{\top} P (A + BK) > 0, \tag{5}$$

that is, the system can be stabilized by standard state feedback, then the asymptotic convergence of the closed-loop system can be guaranteed by the quantizer parameters designed in the following theorem.

Theorem 1. *For any given matrices K, P, and Π defined by (5) and the quantization level $2N + 1$, we select quantizer parameters δ and ρ satisfying*

$$\rho = \sqrt{\frac{\lambda_{\max}(P)}{\lambda_{\min}(P)}}\Upsilon\sqrt{n}\delta(1+\varepsilon) < 1, \tag{6}$$

where ε is an arbitrary given positive constant and Υ is defined by $\Upsilon = 2\|BKP(A + BK)\|/\lambda_{\min}(\Pi)$. Given a constant $\eta \in \mathbb{N}$, if δ and ρ selected above satisfy the inequalities $\delta \geq \rho^N$ and $\rho^\eta < \|A\|^{-1}$, then we have $\|x(k)\| \leq (1/(1-\delta))v_j$ for any $k \in [k_j, k_{j+1})$, $j \in \mathbb{N} \cup \{0\}$, where k_0 and v_0 are determined by (9) below and $k_{j+1} \coloneqq k_j + \tau \coloneqq k_j + \lceil\widetilde{\tau}\rceil$ with

$$\widetilde{\tau} = \frac{\lambda_{\min}(P) - \lambda_{\max}(P)\left(\Upsilon\sqrt{n}(1+\varepsilon)\delta\right)^2}{\lambda_{\min}(\Pi)\left(\Upsilon\sqrt{n}\delta\right)^2\varepsilon(1+\varepsilon)}. \tag{7}$$

Hence we have $\lim_{k\to\infty} x(k) = \mathbf{0}_{n\times 1}$; that is, the closed-loop system is asymptotic convergent.

Remark 2. If the bandwidth of the network is large enough such that $N \geq \ln\delta/\ln\rho$, then the condition $\delta \geq \rho^N$ can always be guaranteed. Moreover, the inequality $\rho^\eta < \|A\|^{-1}$ must be ensured if η is selected large enough based on $\rho < 1$. Comprehensively, if the bandwidth of the network and the constant η are set suitably, we can always find the quantizer parameters satisfying the conditions of the above theorem.

Remark 3. Based on the relationship of ρ and δ, that is, $\rho = (1-\delta)/(1+\delta)$, we can determine their values by the equality (6).

Proof.

Stage 1 (zooming-out). In this stage, the system is as open-mode; that is, $x(k+1) = Ax(k)$. The aim of this stage is to determine the value of v_0 and a moment where the system state is unsaturated.

For any given constants $\widetilde{v}_0 \in \mathbb{R}^+$, $\eta \in \mathbb{N}$, and ρ defined by (6), we set $\widetilde{v}(k)$, $\forall k \in \mathbb{N}$, as

$$\begin{aligned} \widetilde{v}(k+1) &= \frac{1}{\rho^\eta}\widetilde{v}(k), \\ \widetilde{v}(0) &= \widetilde{v}_0. \end{aligned} \tag{8}$$

If ρ satisfies $\rho^\eta < \|A\|^{-1} < 1$, then there must exist a moment k_0 such that

$$\|x(k_0)\| \leq \sqrt{\frac{\lambda_{\min}(P)}{\lambda_{\max}(P)}}\frac{\widetilde{v}(k_0)}{1-\delta} \coloneqq \sqrt{\frac{\lambda_{\min}(P)}{\lambda_{\max}(P)}}\frac{v_0}{1-\delta}, \tag{9}$$

and thus

$$\begin{aligned} &x(k_0) \in R_0 \\ &\quad\coloneqq \left\{x(k) : x^{\top}(k)Px(k) \leq \left(\frac{v_0}{1-\delta}\right)^2\lambda_{\min}(P)\right\}. \end{aligned} \tag{10}$$

Remark 3. The definition of $\widetilde{v}(k)$, $\forall k \in \mathbb{N}\cup\{0\}$, is to ensure that it can be represented as $\widetilde{v}(k) = \rho^m\widetilde{v}_0$, where $m = l\eta, l \in \mathbb{N}\cup\{0\}$. On the basis of that, we can ensure that $\widetilde{v}(k)$, $\forall k \in \mathbb{N} \cup \{0\}$, is the quantized value of the logarithmic quantizer.

Stage 2 (zooming-in). Let the zooming-out stage finish at the moment k_0 and the system is transferred to closed-mode. The purpose of this stage is to design the quantizer parameters and k_j, $j \in \mathbb{N} \cup \{0\}$, such that $\|x(k)\| \leq (1/(1-\delta))v_j$ for any $k \in [k_j, k_{j+1})$. To this end, we first illustrate that R_0 is an invariant set.

If $x(k) \in R_0$, then $\|x(k)\| \leq (1/(1-\delta))v_0$. Thus we obtain $|x_i(k)| \leq (1/(1-\delta))v_0$ which results in that

$$\begin{aligned} &\left|q(x_i(k)) - x_i(k)\right| \\ &\leq \max\left\{\left(\frac{1}{1-\delta} - 1\right)v_0, \left(1 - \frac{1}{1+\delta}\right)v_0, \frac{1}{1+\delta}v_{N-1}\right\} \\ &= \frac{\delta}{1-\delta}v_0, \end{aligned} \tag{11}$$

where the last equality is obtained by $\delta \geq \rho^N$. Hence, we get

$$\|e(k)\| \leq \sqrt{n}\frac{\delta}{1-\delta}v_0, \tag{12}$$

with $e(k) \coloneqq Q(x(k)) - x(k)$.

Let Lyapunov function as $V(k) = x^{\top}(k)Px(k)$, then it is easy to get

$$\begin{aligned} \Delta V(x(k)) &= x^{\top}(k+1)Px(k+1) - x^{\top}(k)Px(k) \\ &= x^{\top}(k)\left[(A+BK)^{\top}P(A+BK) - P\right]x(k) \\ &\quad + 2e^{\top}(k)(BK)^{\top}P(A+BK)x(k) \\ &\leq -\lambda_{\min}(\Pi)\|x(k)\|^2 \\ &\quad + 2\|BKP(A+BK)\|\|x(k)\|\sqrt{n}\frac{\delta}{1-\delta}v_0 \\ &= -\lambda_{\min}(\Pi)\|x(k)\|\left(\|x(k)\| - \Upsilon\sqrt{n}\frac{\delta}{1-\delta}v_0\right). \end{aligned} \tag{13}$$

For an arbitrary given positive constant ε, if

$$\|x(k)\| \geq \Upsilon\sqrt{n}\frac{\delta}{1-\delta}v_0(1+\varepsilon), \tag{14}$$

then we get

$$\Delta V(x(k)) \le -\lambda_{\min}(\Pi)\|x(k)\|\Upsilon\sqrt{n}\frac{\delta}{1-\delta}\nu_0\varepsilon. \tag{15}$$

Moreover, by (13) we know that the set $\mathbf{B}$, defined by

$$\mathbf{B} := \left\{x(k) \mid x(k) \le \Upsilon\sqrt{n}\frac{\delta}{1-\delta}\nu_0\right\}, \tag{16}$$

is an invariant set. Define $\widetilde{\mathbf{B}}$ as

$$\widetilde{\mathbf{B}} := \left\{x(k) \mid x^{\top}(k)Px(k) \le \lambda_{\max}(P)\left(\Upsilon\sqrt{n}\frac{\delta}{1-\delta}\nu_0\right)^2\right\}, \tag{17}$$

and it is obvious that $\widetilde{\mathbf{B}} \supset \mathbf{B}$. If δ selected satisfies the following inequality:

$$\sqrt{\frac{\lambda_{\max}(P)}{\lambda_{\min}(P)}}\Upsilon\sqrt{n}\delta(1+\varepsilon) < 1, \tag{18}$$

we can see that $R_0 \supset \widetilde{\mathbf{B}} \supset \mathbf{B}$, and thus R_0 is an invariant set.

Next, we will show that there exists a moment $k_1 := k_0 + \tau$ such that $\|x(k_1)\| \le (1/(1-\delta))\nu_1$. Let

$$\rho = \sqrt{\frac{\lambda_{\max}(P)}{\lambda_{\min}(P)}}\Upsilon\sqrt{n}\delta(1+\varepsilon), \tag{19}$$

and we can claim that

$$x^{\top}(k_1)Px(k_1) \le \lambda_{\max}(P)\left(\Upsilon\sqrt{n}\frac{\delta}{1-\delta}\nu_0(1+\varepsilon)\right)^2. \tag{20}$$

In fact, if (20) does not hold, we get

$$x^{\top}(k_1)Px(k_1) > \lambda_{\max}(P)\left(\Upsilon\sqrt{n}\frac{\delta}{1-\delta}\nu_0(1+\varepsilon)\right)^2. \tag{21}$$

Consider that the set $\widetilde{R}_1$, defined as

$$\widetilde{R}_1 := \left\{x(k) : x^{\top}(k)Px(k) \le \lambda_{\max}(P)\left(\Upsilon\sqrt{n}\frac{\delta}{1-\delta}\nu_0(1+\varepsilon)\right)^2\right\}, \tag{22}$$

is an invariant set based on $\widetilde{R}_1 \supset \mathbf{B}$. Combined with (21) we know that

$$x^{\top}(k)Px(k) > \lambda_{\max}(P)\left(\Upsilon\sqrt{n}\frac{\delta}{1-\delta}\nu_0(1+\varepsilon)\right)^2 \tag{23}$$

holds for any $k \in [k_0, k_1]$. Hence we get

$$\|x(k)\| > \Upsilon\sqrt{n}\frac{\delta}{1-\delta}\nu_0(1+\varepsilon), \tag{24}$$

for any $k \in [k_0, k_1]$. Similar to the analysis of (13)–(15), we get

$$\begin{aligned}
&\Delta V(x(k_0+\tau-i)) \\
&= x^{\top}(k_0+\tau-i+1)Px(k_0+\tau-i+1) \\
&\quad - x^{\top}(k_0+\tau-i)Px(k_0+\tau-i) \\
&\le -\lambda_{\min}(\Pi)\|x(k_0+\tau-i)\|\Upsilon\sqrt{n}\frac{\delta}{1-\delta}\nu_0\varepsilon \\
&< -\lambda_{\min}(\Pi)\left(\Upsilon\sqrt{n}\frac{\delta}{1-\delta}\nu_0\right)^2\varepsilon(1+\varepsilon),
\end{aligned} \tag{25}$$

for any $i \in \{1, 2, \ldots, \tau\}$. Hence it is obtained that

$$\begin{aligned}
&x^{\top}(k_0+\tau)Px(k_0+\tau) - x^{\top}(k_0)Px(k_0) \\
&< -\lambda_{\min}(\Pi)\left(\Upsilon\sqrt{n}\frac{\delta}{1-\delta}\nu_0\right)^2\varepsilon(1+\varepsilon)\tau \\
&\le -\lambda_{\min}(\Pi)\left(\Upsilon\sqrt{n}\frac{\delta}{1-\delta}\nu_0\right)^2\varepsilon(1+\varepsilon)\widetilde{\tau} \\
&= \lambda_{\max}(P)\left(\Upsilon\sqrt{n}(1+\varepsilon)\delta\right)^2\left(\frac{\nu_0}{1-\delta}\right)^2 \\
&\quad - \lambda_{\min}(P)\left(\frac{\nu_0}{1-\delta}\right)^2.
\end{aligned} \tag{26}$$

However, (10) and (21) give that

$$\begin{aligned}
&x^{\top}(k_0+\tau)Px(k_0+\tau) - x^{\top}(k_0)Px(k_0) \\
&> \lambda_{\max}(P)\left(\Upsilon\sqrt{n}(1+\varepsilon)\delta\right)^2\left(\frac{\nu_0}{1-\delta}\right)^2 \\
&\quad - \lambda_{\min}(P)\left(\frac{\nu_0}{1-\delta}\right)^2,
\end{aligned} \tag{27}$$

which contradicts formula (26). Therefore, the claim (20) holds; that is,

$$\begin{aligned}
x^{\top}(k_1)Px(k_1) &\le \lambda_{\max}(P)\left(\Upsilon\sqrt{n}\frac{\delta}{1-\delta}\nu_0(1+\varepsilon)\right)^2 \\
&= \lambda_{\min}(P)\left(\frac{\rho\nu_0}{1-\delta}\right)^2 \\
&= \lambda_{\min}(P)\left(\frac{\nu_1}{1-\delta}\right)^2.
\end{aligned} \tag{28}$$

We define the set R_1 as

$$R_1 := \left\{x(k) : x^{\top}(k)Px(k) \le \left(\frac{\nu_1}{1-\delta}\right)^2\lambda_{\min}(P)\right\}. \tag{29}$$

Similar to the analysis of R_0, we know that R_1 is an invariant set. Thus it is easy to see that $x(k) \in R_1$, $\forall k \in [k_1, k_2)$. Furthermore, similar analysis gives

$$\begin{aligned}
&x(k) \in R_j \\
&:= \left\{x(k) : x^{\top}(k)Px(k) \le \left(\frac{\nu_j}{1-\delta}\right)^2\lambda_{\min}(P)\right\},
\end{aligned} \tag{30}$$

for any $k \in [k_j, k_{j+1})$, $j \in \mathbb{N} \cup \{0\}$. So far, we know that $\|x(k)\| \leq v_j/(1-\delta)$, $\forall k \in [k_j, k_{j+1})$, $j \in \mathbb{N} \cup \{0\}$; that is, the quantizer is unsaturated for any $k \in [k_0, +\infty)$. Hence, we get $\lim_{k\to\infty}\|x(k)\| = 0$ and thus $\lim_{k\to\infty} x(k) = \mathbf{0}_{n\times 1}$, which completes the proof. □

4. Second Method for Quantizer Parameters Design

If there are matrices P and K such that the following inequality holds

$$\Lambda \coloneqq P - 2(A+BK)^{\top} P (A+BK) > 0, \tag{31}$$

then the asymptotic convergence of the closed-loop system can also be obtained by the quantizer parameters designed in Theorem 4.

Theorem 4. *For any given matrices K, P, and Λ defined by (31) and the quantization level $2N+1$, quantizer parameters δ and ρ are selected satisfying*

$$\rho = \sqrt{\frac{\lambda_{\max}(P)}{\lambda_{\min}(P)}}\sqrt{\Gamma(1+\varepsilon)}\sqrt{n}\delta < 1, \tag{32}$$

where ε is a positive constant and Γ is defined by $\Gamma = \|(BK)^{\top}PBK\|/\lambda_{\min}(\Lambda)$. Given a constant $\eta \in \mathbb{N}$, if δ and ρ selected above satisfy $\delta \geq \rho^N$ and $\rho^{\eta} < \|A\|^{-1}$, then we get $\|x(k)\| \leq (1/(1-\delta))v_j$ for any $k \in [k_j, k_{j+1})$, $j \in \mathbb{N}\cup\{0\}$, where k_0 and v_0 are determined by (9) and $k_{j+1} \coloneqq k_j + \omega \coloneqq k_j + \lceil\widetilde{\omega}\rceil$ with

$$\widetilde{\omega} = \frac{\lambda_{\min}(P) - \lambda_{\max}(P)\Gamma(1+\varepsilon)n\delta^2}{\lambda_{\min}(\Lambda)\Gamma\varepsilon n\delta^2}. \tag{33}$$

Then we have $\lim_{k\to\infty} x(k) = \mathbf{0}_{n\times 1}$.

Proof.

Stage 1 (zooming-out). The same as the proof of Theorem 1, we get a moment k_0 and a positive constant v_0 such that

$$\begin{aligned} x(k_0) &\in \overline{R}_0 \\ &\coloneqq \left\{x(k) : x^{\top}(k)Px(k) \leq \left(\frac{v_0}{1-\delta}\right)^2 \lambda_{\min}(P)\right\}. \end{aligned} \tag{34}$$

Note that the positive-definite matrix P used here is defined by (31) rather than (5); thus the definitions of the sets $\overline{R}_0$ and R_0 are different from each other.

Stage 2 (zooming-in). If δ and ρ selected satisfy $\delta \geq \rho^N$ and $x(k) \in \overline{R}_0$, $\forall k \in \mathbb{N}$, then we know that $\|e(k)\| \leq \sqrt{n}(\delta/(1-\delta))v_0$ holds, and thus

$$\begin{aligned} &\Delta V(x(k)) \\ &\leq x^{\top}(k)\left[2(A+BK)^{\top}P(A+BK) - P\right]x(k) \\ &\quad + e^{\top}(k)(BK)^{\top}PBKe(k) \\ &\leq -\lambda_{\min}(\Lambda)\|x(k)\|^2 \\ &\quad + \left\|(BK)^{\top}PBK\right\|\left(\sqrt{n}\frac{\delta}{1-\delta}v_0\right)^2. \end{aligned} \tag{35}$$

If

$$\|x(k)\| \geq \sqrt{\Gamma(1+\varepsilon)}\sqrt{n}\frac{\delta}{1-\delta}v_0, \tag{36}$$

then we have

$$\Delta V(x(k)) \leq -\lambda_{\min}(\Lambda)\Gamma\varepsilon\left(\sqrt{n}\frac{\delta}{1-\delta}v_0\right)^2. \tag{37}$$

Due to that the set $\overline{\mathbf{B}}$, defined by

$$\overline{\mathbf{B}} \coloneqq \left\{x(k) \mid x(k) \leq \sqrt{\Gamma}\sqrt{n}\frac{\delta}{1-\delta}v_0\right\}, \tag{38}$$

is an invariant one; if we select δ small enough such that

$$\sqrt{\frac{\lambda_{\max}(P)}{\lambda_{\min}(P)}}\sqrt{\Gamma(1+\varepsilon)}\sqrt{n}\delta < 1, \tag{39}$$

then we get $\overline{R}_0 \supset \overline{\mathbf{B}}$ and thus $\overline{R}_0$ is an invariant set. Definition of ρ is as in (32) and $k_1 = k_0 + \omega$; we claim that

$$x^{\top}(k_1)Px(k_1) \leq \lambda_{\max}(P)\Gamma(1+\varepsilon)n\left(\frac{\delta}{1-\delta}v_0\right)^2. \tag{40}$$

In fact, if (40) does not hold, we know that

$$x^{\top}(k)Px(k) > \lambda_{\max}(P)\Gamma(1+\varepsilon)n\left(\frac{\delta}{1-\delta}v_0\right)^2, \tag{41}$$

and thus

$$\|x(k)\| > \sqrt{\Gamma(1+\varepsilon)n}\left(\frac{\delta}{1-\delta}v_0\right) \tag{42}$$

holds for any $k \in [k_0, k_1]$. Based on (37) we get

$$\Delta V\left(x\left(k_0+\omega-i\right)\right) < -\lambda_{\min}(\Lambda)\Gamma\varepsilon\left(\sqrt{n}\frac{\delta}{1-\delta}v_0\right)^2, \tag{43}$$

for any $i \in \{1, 2, \ldots, \omega\}$. Hence, the following inequality can be given

$$\begin{aligned} &x^{\top}(k_0+\tau)Px(k_0+\tau) - x^{\top}(k_0)Px(k_0) \\ &< -\lambda_{\min}(\Lambda)\Gamma\varepsilon\left(\sqrt{n}\frac{\delta}{1-\delta}v_0\right)^2\widetilde{\omega} \\ &= \lambda_{\max}(P)\Gamma(1+\varepsilon)n\delta^2\left(\frac{v_0}{1-\delta}\right)^2 \\ &\quad - \lambda_{\min}(P)\left(\frac{v_0}{1-\delta}\right)^2. \end{aligned} \tag{44}$$

But (34) and (41) give that

$$x^{\top}(k_0+\tau)Px(k_0+\tau)-x^{\top}(k_0)Px(k_0) > \lambda_{\max}(P)\Gamma(1+\varepsilon)n\delta^2\left(\frac{v_0}{1-\delta}\right)^2 - \lambda_{\min}(P)\left(\frac{v_0}{1-\delta}\right)^2 \quad (45)$$

which results in a contradiction. Thus the claim (40) holds, combined with the definition of ρ which results in

$$x^{\top}(k_1)Px(k_1) \le \lambda_{\min}(P)\left(\frac{v_1}{1-\delta}\right)^2. \quad (46)$$

Similar to the proof of Theorem 1, we obtain the unsaturation of the quantizer and the asymptotic convergence of the closed-loop system. This completes the proof. □

5. Simulation

In this section, we adopt a well-known benchmark example to illustrate the effectiveness of the main results. Let discretization interval be 0.2; we convert the continuous-time linearized model of the benchmark to discrete-time one shown as

$$x(k+1) = Ax(k) + Bu(k), \quad (47)$$

with

$$A := \begin{bmatrix} 1.4381 & 0.0864 & 0.9830 & -0.5676 \\ -0.0972 & 0.4477 & -0.0553 & 0.1009 \\ 0.1047 & 0.4929 & 0.2662 & 0.4775 \\ -0.0437 & 0.3930 & -0.1274 & 0.6201 \end{bmatrix},$$
$$B := \begin{bmatrix} 0.0645 & -0.3382 \\ 0.7823 & 0.0132 \\ 0.5413 & -0.3478 \\ 0.4578 & 0.0507 \end{bmatrix}. \quad (48)$$

Case 1 ($N = 11$).

Method I. Obviously, the above system is unstable but stabilizable. Thus we can design a feedback matrix K as

$$K = \begin{bmatrix} 0.2260 & -0.7118 & 0.1752 & -0.7204 \\ 2.6884 & 0.1380 & 2.1328 & -1.1746 \end{bmatrix} \quad (49)$$

and a positive-definite P by LMI toolbox in MATLAB such that the inequality (5) holds. By the definition of matrix Π, direct calculations result in $\Upsilon = 0.9070$, $\delta = 0.1043$, $\rho = 0.8111$, and $\tau = 13$, where ε is selected as 0.5. Let $\eta = 3$; we obtain that $\delta \ge \rho^N$ and $\rho^\eta < \|A\|^{-1}$ hold. Let $x_0 = [9, 0, 10, 20]^{\top}$ and $\tilde{v}_0 = 10$; we get $k_0 = 6$ by Figure 1, where

$$M(k) := \sqrt{\frac{\lambda_{\min}(P)}{\lambda_{\max}(P)}}\frac{\tilde{v}(k)}{1-\delta}. \quad (50)$$

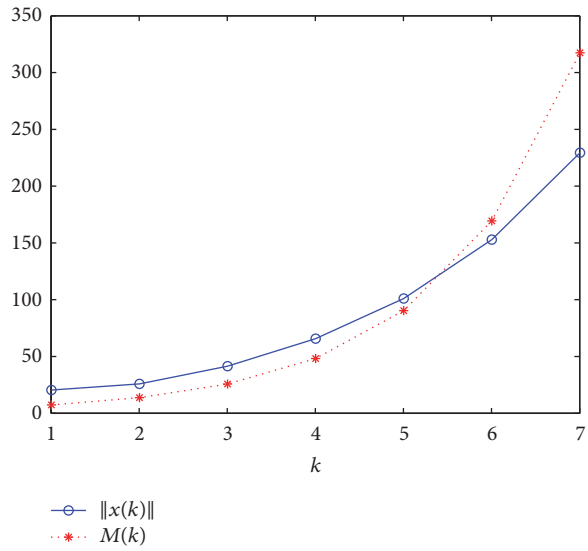

Figure 1: Selection of k_0.

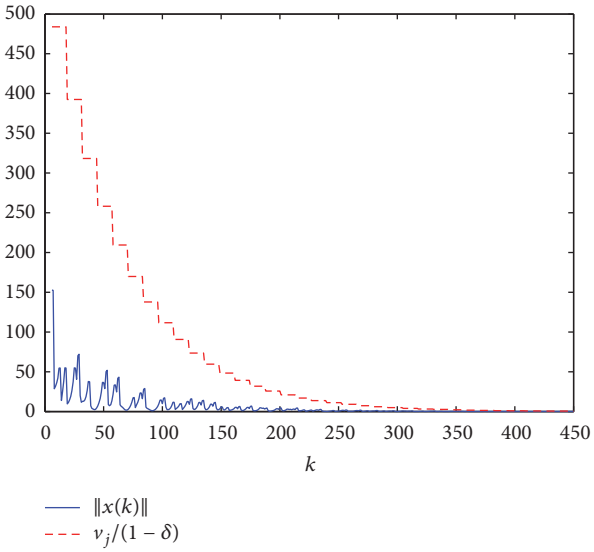

Figure 2: Unsaturation of the quantizer when $N = 11$ under method I.

Let $k_{j+1} := k_j + \tau$, $\forall k \in [k_j, k_{j+1})$, $j \in \mathbb{N} \cup \{0\}$; we obtain that $\|x(k)\| \le (1/(1-\delta))v_j$ for any $k \in [k_j, k_{j+1})$ and $\lim_{k\to\infty} x(k) = \mathbf{0}_{n\times 1}$, which are represented in Figures 2 and 3, respectively.

Method II. In fact, if K and P are selected as the ones in Method I, we know that the matrix Λ defined by (31) is positive-definite. If $\varepsilon = 0.5$ and $\eta = 11$, by simple calculations we get $\Gamma = 20.9343$, $\delta = 0.0294$, and $\rho = 0.9428$. Obviously, the condition $\rho^\eta < \|A\|^{-1}$ is satisfied but $\delta \ge \rho^N$ is violated. Hence, Theorem 4 is invalid when $N = 11$.

Case 2 ($N = 60$).

Method I. If the matrices K and P and the variables ε and η are selected as the ones in Case 1, then the corresponding

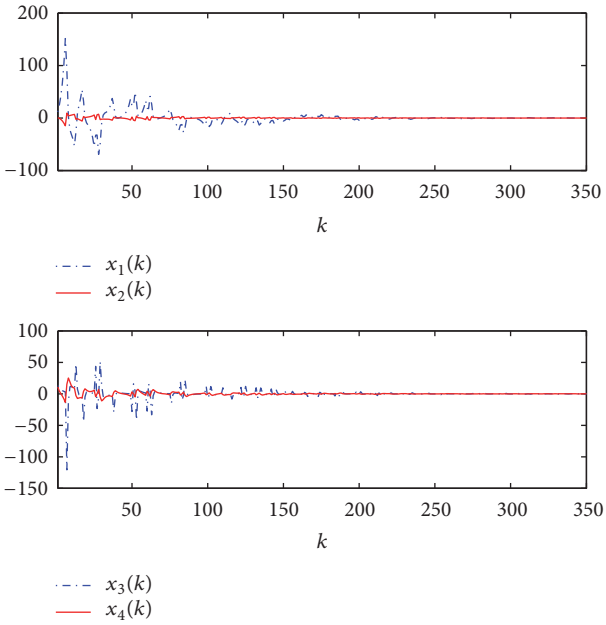

Figure 3: Asymptotic convergence of the system when $N = 11$ under method I.

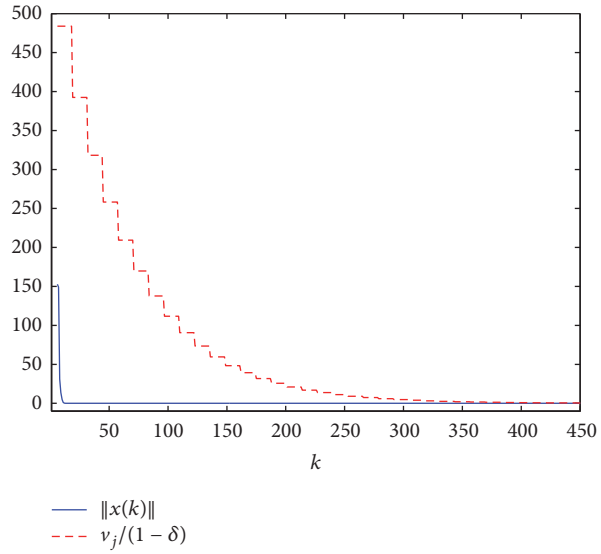

Figure 4: Unsaturation of the quantizer when $N = 60$ under method I.

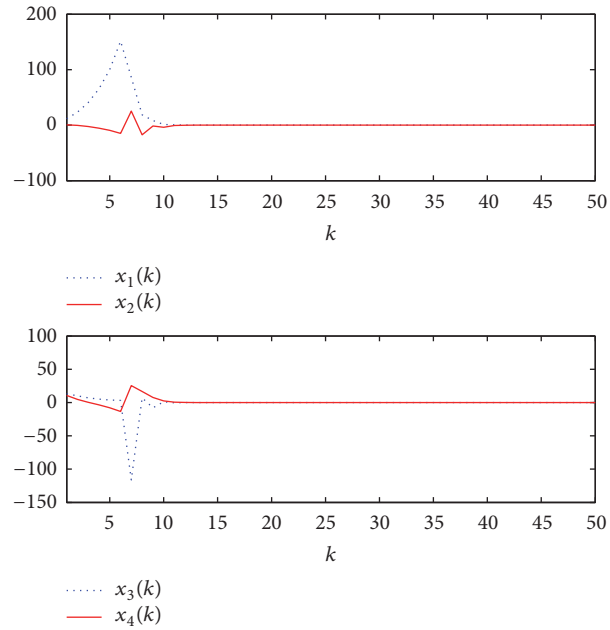

Figure 5: Asymptotic convergence of the system when $N = 60$ under method I.

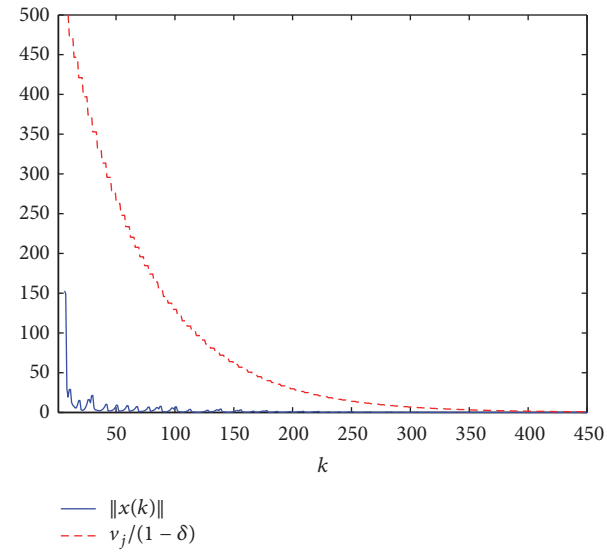

Figure 6: Unsaturation of the quantizer when $N = 60$ under method II.

variables calculated are the same as above. Due to $N = 60 > 11$, the conditions on Theorem 1 are satisfied. If $x_0 = [9, 0, 10, 20]^\top$ and $\tilde{v}_0 = 10$, we also get $k_0 = 6$. The unsaturation of the quantizer and the asymptotic convergence of the closed-loop system are shown in Figures 4 and 5, respectively.

Method II. If K, P, ε, and η are selected as the ones in Case 1, we get that Γ, δ, and ρ are the same as above. If $N = 60$, then the conditions on Theorem 4 are satisfied. If $x_0 = [9, 0, 10, 20]^\top$ and $\tilde{v}_0 = 10$, then we get $k_0 = 6$ and $\omega = 4$. By Figures 6 and 7, we know that the quantizer is unsaturated and the closed-loop system is asymptotic convergent.

Comparison. From Case 1, we obtain that the first design method has a wider applicability than the second one. When N is large enough, two methods proposed here can guarantee the unsaturation of the quantizer and the asymptotic convergence of the closed-loop system according to the discussions of Case 2. Note that the decreasing period ω of the second method is less than the one, that is, τ, of the first method. However, the decreasing rate ρ of the second method is

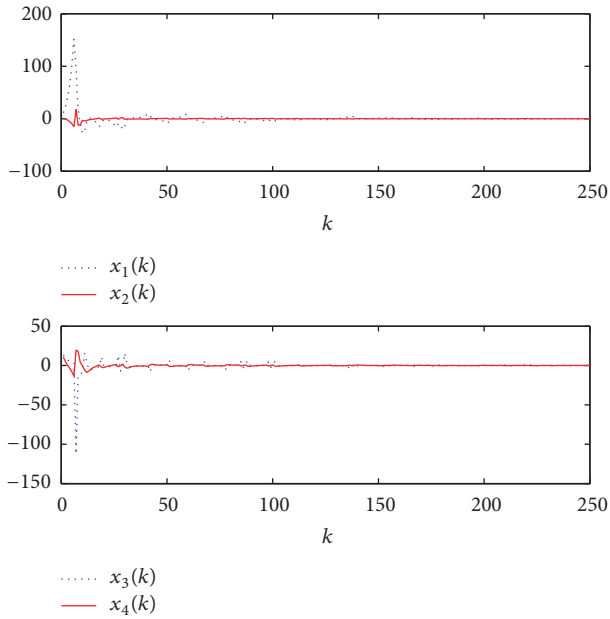

FIGURE 7: Asymptotic convergence of the system when $N = 60$ under method II.

larger than the one of the first method. Comprehensively, the convergence speed of the closed-loop system under the second method is slower than the one under the first method. The reason of this is that the second method adopts the following inequality:

$$E^T PF + F^T PE \leq E^T PE + F^T PF, \tag{51}$$

with positive-definite matrix P and matrices E and F to amplify the formula, but the first method avoids it.

6. Conclusion

This paper proposed two design methods for logarithmic quantizer parameters. Under both methods, we ensured the unsaturation of the quantizer and the asymptotic convergence of the closed-loop system. Further research includes designing the logarithmic quantizer parameters when the system is affected by network-induced imperfection, like time-delay, packet dropout, and so on.

Competing Interests

The author declares that he has no competing interests.

Acknowledgments

The work was supported by the National Natural Science Foundation of China (61403125, 6150020851, and U150410292) and the Natural Science Foundation of Henan Province Education Department (15A413012).

References

[1] R. W. Brockett and D. Liberzon, "Quantized feedback stabilization of linear systems," *Institute of Electrical and Electronics Engineers. Transactions on Automatic Control*, vol. 45, no. 7, pp. 1279–1289, 2000.

[2] D. Liberzon, "Hybrid feedback stabilization of systems with quantized signals," *Automatica*, vol. 39, no. 9, pp. 1543–1554, 2003.

[3] F. Fagnani and S. Zampieri, "Quantized stabilization of linear systems: complexity versus performance," *Institute of Electrical and Electronics Engineers. Transactions on Automatic Control*, vol. 49, no. 9, pp. 1534–1548, 2004.

[4] C. Peng and Y.-C. Tian, "Networked H_∞ control of linear systems with state quantization," *Information Sciences*, vol. 177, no. 24, pp. 5763–5774, 2007.

[5] E. Tian, D. Yue, and C. Peng, "Quantized output feedback control for networked control systems," *Information Sciences. An International Journal*, vol. 178, no. 12, pp. 2734–2749, 2008.

[6] D. Liberzon, "Quantization, time delays, and nonlinear stabilization," *IEEE Transactions on Automatic Control*, vol. 51, no. 7, pp. 1190–1195, 2006.

[7] M. Li, J. Sun, and L. Dou, "Stability of an improved dynamic quantised system with time-varying delay and packet losses," *IET Control Theory and Applications*, vol. 9, no. 6, pp. 988–995, 2015.

[8] E. Fridman and M. Dambrine, "Control under quantization, saturation and delay: an LMI approach," *Automatica. A Journal of IFAC, the International Federation of Automatic Control*, vol. 45, no. 10, pp. 2258–2264, 2009.

[9] J. Yan, Y. Xia, B. Liu, and M. Fu, "Stabilisation of quantised linear systems with packet dropout," *IET Control Theory & Applications*, vol. 5, no. 8, pp. 982–989, 2011.

[10] J. Yan, Y. Xia, and L. Li, "Stabilization of fuzzy systems with quantization and packet dropout," *International Journal of Robust and Nonlinear Control*, vol. 24, no. 10, pp. 1563–1583, 2014.

[11] D. Liberzon and D. Nesic, "Input-to-state stabilization of linear systems with quantized state measurements," *IEEE Transactions on Automatic Control*, vol. 52, no. 5, pp. 767–781, 2007.

[12] Y. Sharon and D. Liberzon, "Input to state stabilizing controller for systems with coarse quantization," *IEEE Transactions on Automatic Control*, vol. 57, no. 4, pp. 830–844, 2012.

[13] J. Yan and Y. Xia, "Quantized control for networked control systems with packet dropout and unknown disturbances," *Information Sciences*, vol. 354, pp. 86–100, 2016.

[14] H. Yang, Y. Xia, H. Yuan, and J. Yan, "Quantized stabilization of networked control systems with actuator saturation," *International Journal of Robust and Nonlinear Control*, vol. 26, no. 16, pp. 3595–3610, 2016.

[15] B. Andrievsky, A. Andrievsky, and I. Zaitceva, "Adaptive zooming strategy in discrete-time implementation of sliding-mode control," in *Proceedings of the 1st IFAC Conference on Modelling, Identification and Control of Nonlinear Systems (MICNON '15)*, pp. 319–326, Saint Petersburg, Russia, June 2015.

[16] Y. Xia, J. Yan, J. Shang, M. Fu, and B. Liu, "Stabilization of quantized systems based on Kalman filter," *Control Engineering Practice*, vol. 20, no. 10, pp. 954–962, 2012.

[17] K. Liu, E. Fridman, K. H. Johansson, and Y. Xia, "Quantized Control under round-robin communication protocol," *IEEE Transactions on Industrial Electronics*, vol. 63, no. 7, pp. 4461–4471, 2016.

[18] P. Tallapragada and J. Cortes, "Event-triggered stabilization of linear systems under bounded bit rates," *IEEE Transactions on Automatic Control*, vol. 61, no. 6, pp. 1575–1589, 2016.

[19] Y. Guan, Q.-L. Han, and C. Peng, "Event-triggered quantized-data feedback control for linear systems," in *Proceedings of the IEEE International Symposium on Industrial Electronics (ISIE '13)*, pp. 1–6, IEEE, Taipei, Taiwan, May 2013.

[20] T. Sun and L. Zhou, "Model-based event-triggered quantized control for linear discrete-time systems," in *Proceedings of the 27th Chinese Control and Decision Conference (CCDC '15)*, pp. 5281–5286, May 2015.

[21] D. Liberzon, "Finite data-rate feedback stabilization of switched and hybrid linear systems," *Automatica. A Journal of IFAC, the International Federation of Automatic Control*, vol. 50, no. 2, pp. 409–420, 2014.

[22] M. Wakaiki and Y. Yamamoto, "Stability analysis of sampled-data switched systems with quantization," *Automatica*, vol. 69, pp. 157–168, 2016.

[23] M. Wakaiki and Y. Yamamoto, "Stabilization of switched linear systems with quantized output and switching delays," *IEEE Transactions on Automatic Control*, 2016.

[24] G. Yang and D. Liberzon, "Finite data-rate stabilization of a switched linear system with unknown disturbance," *IFAC-PapersOnLine*, vol. 49, no. 18, pp. 1085–1090, 2016.

[25] Z. Zeng, X. Wang, Z. Zheng, and L. Zhao, "Edge agreement of second-order multi-agent system with dynamic quantization via the directed edge Laplacian," *Nonlinear Analysis. Hybrid Systems*, vol. 23, pp. 1–10, 2017.

[26] P. Yi and Y. Hong, "Quantized subgradient algorithm and data-rate analysis for distributed optimization," *IEEE Transactions on Control of Network Systems*, vol. 1, no. 4, pp. 380–392, 2014.

[27] S. Dashkovskiy and L. Naujok, "Quasi-ISS/ISDS observers for interconnected systems and applications," *Systems & Control Letters*, vol. 77, pp. 11–21, 2015.

[28] Z.-P. Jiang and T.-F. Liu, "Quantized nonlinear control—a survey," *Acta Automatica Sinica*, vol. 39, no. 11, pp. 1820–1830, 2013.

[29] D. Zhang, P. Shi, Q. Wang, and L. Yu, "Analysis and synthesis of networked control systems: a survey of recent advances and challenges," *ISA Transactions*, vol. 66, pp. 376–392, 2017.

[30] N. Elia and S. K. Mitter, "Stabilization of linear systems with limited information," *Institute of Electrical and Electronics Engineers. Transactions on Automatic Control*, vol. 46, no. 9, pp. 1384–1400, 2001.

[31] M. Fu and L. Xie, "The sector bound approach to quantized feedback control," *IEEE Transactions on Automatic Control*, vol. 50, no. 11, pp. 1698–1711, 2005.

[32] D. Du, B. Qi, M. Fei, and Z. Wang, "Quantized control of distributed event-triggered networked control systems with hybrid wired-wireless networks communication constraints," *Information Sciences*, vol. 380, pp. 74–91, 2017.

[33] W. Liu, C. Lim, P. Shi, and S. Xu, "Backstepping fuzzy adaptive control for a class of quantized nonlinear systems," *IEEE Transactions on Fuzzy Systems*, p. 1, 2017.

[34] Y. Wang, W. Ren, and Y. Lu, "Nonfragile H_∞ filtering for nonlinear markovian jumping systems with mode-dependent time delays and quantization," *Journal of Control Science and Engineering*, vol. 2016, Article ID 7167692, 11 pages, 2016.

[35] Y. He, Y.-E. Wang, and X.-M. Li, "Quadratic stabilization for linear time-delay systems with a logarithmic quantizer," *Neurocomputing*, vol. 173, pp. 1995–2000, 2016.

[36] L. Xing, C. Wen, Y. Zhu, H. Su, and Z. Liu, "Output feedback control for uncertain nonlinear systems with input quantization," *Automatica*, vol. 65, pp. 191–202, 2016.

Hindawi Publishing Corporation
Journal of Control Science and Engineering
Volume 2016, Article ID 8753657, 8 pages
http://dx.doi.org/10.1155/2016/8753657

Research Article

Plug and Play Robust Distributed Control with Ellipsoidal Parametric Uncertainty System

Hong Wang-jian[1] and Wang Yan-xiang[2]

[1]*Dipartimento di Elettronica, Informazione, Politecnico di Milano, Piazza Leonardo da Vinci 32, 20133 Milano, Italy*
[2]*School of Mechanical and Electronic Engineering, Jingdezhen Ceramic Institute, Jingdezhen 333403, China*

Correspondence should be addressed to Wang Yan-xiang; wangyanxiang1@jci.edu.cn

Received 4 August 2016; Revised 10 October 2016; Accepted 31 October 2016

Academic Editor: Haibo Du

We consider a continuous linear time invariant system with ellipsoidal parametric uncertainty structured into subsystems. Since the design of a local controller uses only information on a subsystem and its neighbours, we combine the plug and play idea and robust distributed control to propose one distributed control strategy for linear system with ellipsoidal parametric uncertainty. Firstly for linear system with ellipsoidal parametric uncertainty, a necessary and sufficient condition for robust state feedback control is proposed by means of linear matrix inequality. If this necessary and sufficient condition is satisfied, this robust state feedback gain matrix can be easily derived to guarantee robust stability and prescribed closed loop performance. Secondly the plug and play idea is introduced in the design process. Finally by one example of aircraft flutter model parameter identification, the efficiency of the proposed control strategy can be easily realized.

1. Introduction

Modern engineering system offers many examples of man-made systems characterized by a large numbers of states and inputs. One concept about large-scale systems is always thought as the result of many subsystems interacting through the coupling of physical variables or the transmission of information over one communication network. Complexity of these large-scale systems brings some challenges such as the application of simulation, analysis, and control design algorithms.

Consider the problem of control design algorithms for large-scale systems; two common used algorithms are centralized control scheme and distributed control scheme. In centralized control scheme, all control variables are computed by a single regulator. Therefore all subsystems transmit their outputs to the central controller in order to design the control inputs which will be sent back to actuators collocated with subsystems. But a centralized control scheme for the large-scale systems will suffer from many problems such as (1) computational complexity, a centralized regulator needs a considerable amount of computing power and memory in order to compute control inputs within a sampling interval, (2) communication network, a centralized control requires a star-like topology of the communication network that impacts the cost of the control system, and (3) reliability, a failure in a single subsystem or in a link could comprise the proper functioning of the overall controlled large-scale system. In order to remedy the above drawbacks, each subsystem in distributed control scheme is equipped with a local controller that receives the outputs from the corresponding subsystem and computes the control inputs. It means that each subsystem is equipped with a local controller, but controllers can transmit and receive quantities from other subsystems. Therefore if these pieces of information are properly used, the goal of stabilizing the closed loop large-scale system and guaranteeing prescribed level of performance can be achieved.

Now one new idea of distributed control scheme is proposed to design the local controller in large-scale systems in reference [1], where the design of a local controller uses only information from parent subsystems. This new

approach has several advantages. First, the communication flow at the design stage has the same topology of the coupling graph that is usually sparse. Second, after each parent subsystem has sent required quantities to its children, the design of local controllers can be finished in parallel. Third, the complexity of synthesizing a local controller for a subsystem scales only with the number of its parents rather than the total number of subsystems. Fourth, if a subsystem joins an existing network, at most, subsystems that are influenced by it can retune their controllers. In a similar way, if a subsystem leaves the network, at most, its children can retune their controllers. In [1], this kind of distributed control scheme is named as the plug and play distributed control. The main essence of plug and play distributed control scheme is that, when a subsystem joins or leaves an existing network of subsystems, there is a procedure for automatically assessing if the operation does not spoil stability and constraint satisfaction for the overall large-scale system. In these years, research on plug and play distributed control is being untaken. In [2], a linear system structured into physically coupled subsystem was considered, further one plug and play distributed model predictive control was proposed to guarantee asymptotic stability and satisfaction of constraints on system inputs and states. Reference [3] considered the problem of designing distributed controllers for large-scale linear constrained systems composed by a number of interacting subsystems. Several aspects of plug and play distributed control were improved in [4], and based on the computation of robust control invariant sets, all critical steps in the design of a local controller could be solved through linear programming strategy. Reference [5] considered the control of a large-scale system composed of state coupled linear subsystems that could be added or removed offline; the possibility of coping with constraints on system variables was studied in [6], while guaranteeing stability, robustness, and global optimality. Plug and play distributed methods span from cooperative to noncooperative, which requires limited computational load in [7]. A review about architectures for distributed model predictive control can be seen in [8]. Generally plug and play distributed control procedures are very attractive for large-scale systems where the number of subsystems varies with time [9]. And the plug and play idea provides a scalable procedure for the addition and removal of new generation units [10]. Furthermore, plug and play distributed controllers can facilitate the revamping of control systems and allow one to automatically assess feasibility of the whole process.

Using above descriptions and advantages of plug and play distributed control, in this short note, we apply this new plug and play idea into the robust control scheme to propose one new method (plug and play robust distributed control method). The goal of the robust control scheme is to guarantee that one $H\infty$ norm with respect to one transfer function from external noise to system output is less than one given upper bound [11]. Here the controller is the common stable state feedback controller, and under the condition that the assumed model structure is given previously, we solve the problem of how to design one robust distributed controller with ellipsoidal parametric uncertainty system. First, we derive one necessary and sufficient condition under which the robust distributed controller exists by using the linear matrix inequality tool for each subsystem. This necessary and sufficient condition of linear matrix inequality form can guarantee the robust stability and performance requirement. Then the distributed state feedback controller is chosen as one matrix from the state space matrix form directly [12]. Second, the idea of plug and play is merged into the robust distributed control and one plug and play robust distributed control algorithm is formulated. Finally, some simulation examples are used to illustrate the efficiency of our new method.

2. Model Description

Consider a continuous time linear invariant system.

$$\begin{aligned} \dot{x}(t) &= Ax(t) + B_1 u(t), \\ y(t) &= C(\theta)\, x(t) + B_2 u(t), \end{aligned} \tag{1}$$

where $x(t) \in R^n$ and $u(t) \in R^m$ are state and input, respectively, at time t and $y(t) \in R^p$ is output. Then the above four matrices satisfy

$$\begin{aligned} A &\in R^{n\times n}, \\ B_1 &\in R^{n\times m}, \\ C(\theta) &\in R^{p\times n}, \\ B_2 &\in R^{p\times m}. \end{aligned} \tag{2}$$

As one unknown parameter vector $\theta \in R^n$ lies in matrix $C(\theta)$, (1) is a parameterized model. Assume all matrices are known a priori except for matrix $C(\theta)$, this assumption signifies that (1) has uncertain zeros [13]. Assume that the unknown parameter vector θ is in one given ellipsoidal parametric set U_θ.

$$U_\theta = \left\{\theta : (\theta - \theta_0)^T R (\theta - \theta_0) \le 1\right\}, \tag{3}$$

where variables θ_0 and R are used to express the center and volume corresponding to the above given ellipsoidal parametric set U_θ. The state $x(t) = \left(x_1(t) \;\; x_2(t) \;\; \cdots \;\; x_M(t)\right)$ is partitioned into M vector $x_i(t) \in R^{n_i}$, where $i \in M = 1 : M$ and $n = \sum_{i\in M} n_i$. Similarly the input and the output are composed by M vector $u_i(t) \in R^{m_i}$, $y_i(t) \in R^{p_i}$ such that

$$\begin{aligned} u(t) &= \left(u_1(t) \;\; u_2(t) \;\; \cdots \;\; u_M(t)\right), \quad m = \sum_{i\in M} m_i \\ y(t) &= \left(y_1(t) \;\; y_2(t) \;\; \cdots \;\; y_M(t)\right), \quad p = \sum_{i\in M} p_i. \end{aligned} \tag{4}$$

Assume that (1) can be equivalently described by the ith subsystem (Σ_i), $i \in M$, given by

$$\begin{aligned} (\Sigma_i)& \\ \dot{x}_i(t) &= A_{ii} x_i(t) + B_{1i} u_i(t) + \sum_{i\in N_i} A_{ij} x_j(t) \\ y_i(t) &= C_i(\theta_i)\, x_i(t) + B_{2i} u_i(t), \end{aligned} \tag{5}$$

where

$$\begin{aligned} A_{ii} &\in R^{n_i \times n_i}, \\ B_{1i} &\in R^{n_i \times m_i}, \\ C_i(\theta_i) &\in R^{p_i \times n_i}, \\ B_{2i} &\in R^{p_i \times m_i}, \\ A_{ij} &\in R^{n_i \times n_j}, \\ & i, j \in M. \end{aligned} \tag{6}$$

N_i is the set of parents of subsystem i, and it is defined as

$$N_i = \left\{ j \in M : A_{ij} \neq 0,\ i \neq j \right\}. \tag{7}$$

Further since $y_i(t)$ depends on the local state $x_i(t)$ only, subsystems (Σ_i), $i \in M$ are output-decoupled and $C = \operatorname{diag}(C_1 \ C_2 \ \cdots \ C_M)$. Also the unknown parameter vector $\theta \in R^n$ is partitioned into the M vector $\theta_i \in R^{n_i}$, where $i \in M = 1 : M$ and $n = \sum_{i \in M} n_i$.

We treat $w_i(t) = \sum_{i \in N_i} A_{ij} x_j(t)$ as a disturbance and reformulate (5) as follows:

$$\begin{aligned} (\Sigma_i) \\ \dot{x}_i(t) &= A_{ii} x_i(t) + B_{1i} u_i(t) + B_{3i} w_i(t) \\ y_i(t) &= C_i(\theta_i) x_i(t) + B_{2i} u_i(t), \end{aligned} \tag{8}$$

where $w_i(t) \in R^{n_i}$, $B_{3i} \in R^{n_i \times n_i}$ and vector $\theta_i \in R^{n_i}$ is also in one given ellipsoidal parametric set U_{θ_i}.

$$U_{\theta_i} = \left\{ \theta_i : (\theta_i - \theta_{i0})^T R_i (\theta_i - \theta_{i0}) \leq 1 \right\}, \tag{9}$$

where variables θ_{i0} and R_i are all similar to above definitions. After combining (8) and (9), the problem of our paper is to design one stable distributed state feedback controller $u_i(t) = K_i x_i(t)$ under the condition of disturbance $w_i(t)$ and ellipsoidal parametric set U_{θ_i}. The state feedback matrix K_i satisfies that $K_i \in R^{m_i \times n_i}$.

For the convergence of next analysis, we need the following two assumptions to express that subsystems (Σ_i), $i \in M$ are state coupled and input decoupled.

Assumption 1. Matrix A is composed by blocks A_{ij}, $\forall i, j \in M$ and $B = \operatorname{diag}(B_1 \ B_2 \ \cdots \ B_M)$.

The physical meaning of assumption 1 is that each subsystem is coupled through state variables only. In reference [14], this type of coupling is sometimes called dynamic coupling. This dynamic coupling exists in many communication networks.

Assumption 2. The matrix pairs (A_{ii}, B_i), $\forall i \in M$ are controllable.

Under these two assumptions, if one stable distributed state feedback controller $u_i(t) = K_i x_i(t)$ is obtained, then the controller

$$\begin{aligned} u(t) &= (u_1(t) \ \ u_2(t) \ \ \cdots \ \ u_M(t)) \\ &= (K_1 x_1(t) \ \ K_2 x_2(t) \ \ \cdots \ \ K_M x_M(t)) \end{aligned} \tag{10}$$

can be used to control system (1), while guaranteeing stability and robustness [15]. By observing (8) again, we obtain one closed loop transfer function $T_i(q, \theta_i)$ from external disturbance to system output $y_i(t)$.

$$T_i(q, \theta_i) = (C_i + B_{2i} K_i)(qI - A_{ii} - B_{1i} K_i)^{-1} B_{3i}. \tag{11}$$

The goal of robust distributed control is to find one stable feedback controller K_i to satisfy the following inequality.

$$\left\| T_i(q, \theta_i) \right\|_\infty < \gamma, \quad \forall \theta_i \in U_{\theta_i}, \tag{12}$$

where γ is a given upper bound, and $H\infty$ norm is defined as.

$$\begin{aligned} \left\| T_i(q, \theta_i) \right\|_\infty &= \sup_{w \in [0, 2\pi]} \left\| T_i\left(e^{jw}, \theta_i\right) \right\| \\ &= \sup_{w \in [0, 2\pi]} \sigma\left[T_i\left(e^{jw}, \theta_i\right) \right], \end{aligned} \tag{13}$$

where $\| \cdot \|$ denotes the maximal singular value; the existence of that stable state feedback controller K_i satisfying inequality (12) can be verified by a linear matrix inequality condition [16]. Further this linear matrix inequality condition is a necessary and sufficient condition in the robust control theory.

3. One Necessary and Sufficient Condition

In this section, we derive one linear matrix inequality condition in one state feedback $H\infty$ problem. Further in this problem, the unknown parameter vector θ_i is known in one given ellipsoidal parametric set U_{θ_i}. This linear matrix inequality condition can be formulated as the following Theorem 3.

Theorem 3. *Assume the following equality holds*

$$B_{2i}^T [C_i \ \ B_{2i}] = [0 \ \ I]. \tag{14}$$

Then the following two statements are equivalent to each other:

(1) *There exists one state feedback controller*

$$u_i(t) = K_i x_i(t) \tag{15}$$

which satisfies $\|T_i(q, \theta_i)\|_\infty < \gamma$.

(2) *There exists a symmetric matrix* $X_i \in R^{n_i \times n_i}$ *such that*

$$\begin{bmatrix} A_{ii} X_i + X_i A_{ii}^T - \gamma^2 \left(B_{1i} B_{1i}^T - B_{3i} B_{3i}^T \right) & X_i C_i^T(\theta_i) \\ C_i(\theta_i) X_i & -I \end{bmatrix} < 0. \tag{16}$$

Proof. From the results in [17], we see that the $L2$ gain of one linear time invariant system is equivalent to the $H\infty$ norm of its transfer matrix function. Then the condition that $H\infty$ norm of one transfer matrix function is less than scalar γ can be transformed to that its $L2$ gain is less than scalar γ. Furthermore the necessary and sufficient condition that the $L2$ gain is less than scalar γ can be reformulated as follows.

Taking one quadratic function as that,

$$V_i\left(x_i\left(t\right)\right) = x_i^T\left(t\right) P_i x_i\left(t\right), \quad P_i > 0, \tag{17}$$

such that, for all variables t, we have

$$\frac{dV_i\left(x_i\left(t\right)\right)}{dt} + y_i^T\left(t\right) y_i\left(t\right) - \gamma^2 w_i^T\left(t\right) w_i\left(t\right) < 0. \tag{18}$$

Substituting $u_i(t) = K_i x_i(t)$ into (8), we obtain.

$$\left(\Sigma_i\right)$$

$$\begin{aligned} \dot{x}_i\left(t\right) &= \left[A_{ii} + B_{1i}K_i\right] x_i\left(t\right) + B_{3i} w_i\left(t\right), \\ y_i\left(t\right) &= \left[C_i\left(\theta_i\right) + B_{2i}K_i\right] x_i\left(t\right). \end{aligned} \tag{19}$$

Substituting equation (19) into (18), we see that

$$\begin{aligned} &\dot{x}_i^T\left(t\right) P_i x_i\left(t\right) + x_i^T\left(t\right) P_i \dot{x}_i^T\left(t\right) + y_i^T\left(t\right) y_i\left(t\right) \\ &\quad - \gamma^2 w_i^T\left(t\right) w_i\left(t\right) < 0. \end{aligned} \tag{20}$$

Through complex mathematical operations, one linear matrix inequality is obtained.

$$\begin{bmatrix} \left[A_{ii} + B_{1i}K_i\right]^T P_i + P_i\left[A_{ii} + B_{1i}K_i\right] + \left[C_i\left(\theta_i\right) + B_{2i}K_i\right]^T \left[C_i\left(\theta_i\right) + B_{2i}K_i\right] & P_i B_{3i} \\ B_{3i}^T P_i & -\gamma^2 I \end{bmatrix} < 0. \tag{21}$$

Equation (21) is equivalent to the notion that there exists K_i and $Q_i = P_i^{-1}$ such that

$$\begin{bmatrix} \left[A_{ii} + B_{1i}K_i\right]^T Q_i + Q_i\left[A_{ii} + B_{1i}K_i\right] + B_{3i}B_{3i}^T & Q_i\left[C_i\left(\theta_i\right) + B_{2i}K_i\right]^T \\ \left[C_i\left(\theta_i\right) + B_{2i}K_i\right] Q_i & -\gamma^2 I \end{bmatrix} < 0. \tag{22}$$

Introduce one new variable $Y_i = K_i Q_i$, and then (22) can be rewritten as

$$\begin{bmatrix} A_{ii}Q_i + Q_i A_{ii}^T + Y_i^T B_{1i} + B_{1i}Y_i + B_{3i}B_{3i}^T & \left[C_i\left(\theta_i\right) Q_i + B_{2i}Y_i\right]^T \\ \left[C_i\left(\theta_i\right) Q_i + B_{2i}Y_i\right] & -\gamma^2 I \end{bmatrix} < 0. \tag{23}$$

Applying the Schur complement formula [18], (23) is equivalent to the following inequality:

$$\begin{aligned} &A_{ii}Q_i + Q_i A_{ii}^T + Y_i^T B_{1i} + B_{1i}Y_i + B_{3i}B_{3i}^T \\ &\quad + \frac{\left[C_i\left(\theta_i\right) Q_i + B_{2i}Y_i\right]^T \left[C_i\left(\theta_i\right) Q_i + B_{2i}Y_i\right]}{\gamma^2} < 0. \end{aligned} \tag{24}$$

If (14) holds, then (24) can be simplified as

$$\begin{aligned} &A_{ii}Q_i + Q_i A_{ii}^T + Y_i^T B_{1i} + B_{1i}Y_i + B_{3i}B_{3i}^T \\ &\quad + \frac{Q_i C_i^T\left(\theta_i\right) C_i\left(\theta_i\right) Q_i + Y_i^T Y_i}{\gamma^2} < 0. \end{aligned} \tag{25}$$

Equation (25) is equivalent to the following inequality:

$$\begin{aligned} &A_{ii}Q_i + Q_i A_{ii}^T - B_{1i}B_{1i}^T + B_{3i}B_{3i}^T \\ &\quad + \frac{Q_i C_i^T\left(\theta_i\right) C_i\left(\theta_i\right) Q_i}{\gamma^2} < 0. \end{aligned} \tag{26}$$

Applying the Schur complement formula again, we obtain.

$$\begin{aligned} &\begin{bmatrix} A_{ii}X_i + X_i A_{ii}^T - \gamma^2\left(B_{1i}B_{1i}^T - B_{3i}B_{3i}^T\right) & X_i C_i^T\left(\theta_i\right) \\ C_i\left(\theta_i\right) X_i & -I \end{bmatrix} \\ &\quad < 0, \end{aligned} \tag{27}$$

where we use a new variable $X_i = \gamma^2 Q_i$, thus concluding the proof. □

Theorem 3 gives one necessary and sufficient condition for the existence of a robust controller when the parameter vector is uncertain.

Now by using that linear matrix inequality (16), we continue to study one special case; that is, matrix $C_i(\theta_i)$ is written as the following special structure:

$$C_i\left(\theta_i\right) = \begin{pmatrix} \theta_i & 0 \end{pmatrix}^T \in R^{n_i \times n_i}. \tag{28}$$

Then the necessary and sufficient condition with respect to this special case can be reformulated as Theorem 4.

Theorem 4. *Consider the parameterized system structure (8), and matrix $C_i(\theta_i)$ is given as (28) and other matrices are known. Assume (14) also holds, and then the following two statements are equivalent:*

(1) *There exists one state feedback controller*

$$u_i(t) = K_i x_i(t) \tag{29}$$

which satisfies $\|T_i(q,\theta_i)\|_\infty < \gamma$ for all $\theta_i \in U_{\theta_i}$.

(2) *There exists a symmetric matrix $X_i \in R^{n_i \times n_i}$ and one scalar $\tau \in R$, $\tau > 0$ such that*

$$\begin{bmatrix} \tau R_i & X_i & \tau R_i \theta_{i0} \\ X_i & -M_i & 0 \\ \tau \theta_{i0}^T R_i & 0 & 1 + \left(\tau \theta_{i0}^T R_i \theta_{i0} - 1\right) \end{bmatrix} > 0, \tag{30}$$

$$M_i = A_{ii} X_i + X_i A_{ii}^T - \gamma^2 \left(B_{1i} B_{1i}^T - B_{3i} B_{3i}^T\right).$$

Proof. Considering system (8) and (28), we continue to compute that

$$C_i(\theta_i) X_i = \begin{pmatrix} \theta_i^T \\ 0 \end{pmatrix} X_i = \begin{pmatrix} \theta_i^T X_i \\ 0 \end{pmatrix}. \tag{31}$$

Substituting (31) into (16), then that linear matrix inequality is rewritten as

$$\begin{bmatrix} A_{ii} X_i + X_i A_{ii}^T - \gamma^2 \left(B_{1i} B_{1i}^T - B_{3i} B_{3i}^T\right) & X_i \theta_i & 0 \\ \theta_i^T X_i & -I & 0 \\ 0 & 0 & 0 \end{bmatrix} < 0. \tag{32}$$

According to the structure of $X_i \theta_i$, we simplify the above (32) as

$$\begin{bmatrix} M_i & X_i \theta_i \\ \theta_i^T X_i & -I \end{bmatrix} < 0. \tag{33}$$

From Schur complement formula, we see that linear matrix inequality (33) is equivalent to the following two linear matrix inequalities:

$$\begin{aligned} M_i &< 0, \\ -1 - \theta_i^T X_i M_i^{-1} X_i \theta_i &< 0. \end{aligned} \tag{34}$$

Rewrite (34) as

$$\begin{pmatrix} \theta_i \\ 1 \end{pmatrix}^T \begin{pmatrix} -X_i M_i^{-1} X_i & 0 \\ 0 & -1 \end{pmatrix} \begin{pmatrix} \theta_i \\ 1 \end{pmatrix} < 0. \tag{35}$$

Similarly the ellipsoidal parameter set U_{θ_i} is rewritten as

$$\begin{pmatrix} \theta_i \\ 1 \end{pmatrix}^T \begin{pmatrix} R_i & -R_i \theta_{i0} \\ -\theta_{i0}^T R_i & \theta_{i0}^T R_i \theta_{i0} - 1 \end{pmatrix} \begin{pmatrix} \theta_i \\ 1 \end{pmatrix} < 0. \tag{36}$$

Applying S-Procedure strategy [18] and combining (35) and (36), there exists one scalar $\tau > 0$, such that

$$\begin{pmatrix} -X_i M_i^{-1} X_i & 0 \\ 0 & -1 \end{pmatrix} - \tau \begin{pmatrix} R_i & -R_i \theta_{i0} \\ -\theta_{i0}^T R_i & \theta_{i0}^T R_i \theta_{i0} - 1 \end{pmatrix} < 0. \tag{37}$$

Rewriting (37), we obtain one simplified form.

$$\begin{pmatrix} -X_i M_i^{-1} X_i - \tau R_i & \tau R_i \theta_{i0} \\ \tau \theta_{i0}^T R_i & -1 - \tau \left(\theta_{i0}^T R_i \theta_{i0} - 1\right) \end{pmatrix} < 0. \tag{38}$$

Applying the Schur complement formula, linear matrix inequality (38) is equivalent to the following two linear matrix inequalities:

$$\begin{aligned} -1 - \tau \left(\theta_{i0}^T R_i \theta_{i0} - 1\right) &< 0, \\ -X_i M_i^{-1} X_i - \tau R_i - \frac{\tau^2 R_i \theta_{i0} \theta_{i0}^T R_i}{-1 - \tau \left(\theta_{i0}^T R_i \theta_{i0} - 1\right)} &< 0. \end{aligned} \tag{39}$$

It means that

$$\begin{aligned} 1 + \tau \left(\theta_{i0}^T R_i \theta_{i0} - 1\right) &> 0, \\ X_i M_i^{-1} X_i + \tau R_i - \frac{\tau^2 R_i \theta_{i0} \theta_{i0}^T R_i}{1 + \tau \left(\theta_{i0}^T R_i \theta_{i0} - 1\right)} &> 0. \end{aligned} \tag{40}$$

Combining (34) and (40) and then using Schur complement formula, we get

$$\begin{bmatrix} \tau R_i - \dfrac{\tau^2 R_i \theta_{i0} \theta_{i0}^T R_i}{1 + \tau \left(\theta_{i0}^T R_i \theta_{i0} - 1\right)} & X_i \\ X_i & -M_i \end{bmatrix} > 0. \tag{41}$$

Because linear matrix inequality (41) is linear with respect to variable X_i and nonlinear of variable τ, rewrite (41) as

$$\begin{aligned} &\begin{bmatrix} \tau R_i & X_i \\ X_i & -M_i \end{bmatrix} \\ &\quad - \begin{bmatrix} \tau R_i \theta_{i0} \\ 0 \end{bmatrix} \frac{1}{1 + \tau \left(\theta_{i0}^T R_i \theta_{i0} - 1\right)} \begin{bmatrix} \tau R_i \theta_{i0} \\ 0 \end{bmatrix}^T > 0. \end{aligned} \tag{42}$$

Applying Schur complement formula again, the result (32) can be obtained, thus concluding the proof. □

As linear matrix inequality (30) is linear with respect to variables X_i, τ, and γ^2, then that minimization performance bound will give a necessary and sufficient condition for the existence of the robust distributed controller. From the robust control theory, we conclude that when the above necessary and sufficient condition is satisfied, then one robust distributed control state feedback controller K_i can be chosen as the following form directly:

$$K_i = -\left(B_{2i}^T B_{2i}\right) B_{1i}^T = -B_{1i}^T, \tag{43}$$

where the second equality holds under the condition of (14).

4. Plug and Play Idea

In this section, we study the plug and play idea and the redesign of new controllers when subsystems are added to or removed from system (8). Note that plugging in and unplugging of subsystems are regarded as offline operation [19].

(1) As a starting point, consider a system composed by subsystems (Σ_i), $i \in M$ with its robust distributed controller u_i, $i \in M$.

Consider the plugging of subsystem (Σ_{M+1}), which is characterized by variables as follows:

$$A_{M+1,M+1}, B_{1,M+1}, B_{2,M+1}, B_{3,M+1}, C_{M+1}, x_{M+1}, u_{M+1}, N_{M+1}, \left(A_{ij}\right)_{j\in N_{M+1}}, \tag{44}$$

into an existing system structure. In order to design controller u_{M+1}, we verify whether (16) in Theorem 3 holds; if it holds, then the robust distributed state feedback controller u_{M+1} can be chosen as form (43). If the above design process stops, we deem that subsystem (Σ_{M+1}) cannot plug in. Set $S_i = \{j : i \in N_j\}$ to be the set of successors to system i, since each subsystem (Σ_j), $j \in S_{M+1}$ has the new neighbour (Σ_{M+1}). When N_j gets larger, the necessary and sufficient condition will be violated. It means that, for each $j \in S_{M+1}$, the controller u_j must be redesigned. Furthermore the addition of system (Σ_{M+1}) triggers the design of controller u_{M+1} and the redesign of controllers u_j, $j \in S_{M+1}$. And the controller redesign does not propagate further in the network system.

(2) When subsystem (Σ_k), $k \in M$ is removed off from the existing system, since, for each $i \in S_k$, the set N_i gets smaller. The size of the ellipsoidal parametric uncertainty set cannot increase and therefore the linear matrix inequality cannot be violated. It means that, for each $i \in S_k$, the controller u_i does not have to be redesigned. Further since, for each system (Σ_j), $j \notin \{k\} \cup S_k$, the set N_j does not change, the redesign of controller u_i is not required.

(3) Generally after combing all above descriptions, one plug and play robust distributed control algorithm is formulated as follows.

Plug and Play Algorithm. Design of controller $u(t)$ for system (1).

Input. $A, B_1, B_2, C(\theta), x(t), y(t), u_\theta$

Output. $u(t)$

(1) Partition the original continuous time linear invariant system as (8) to obtain M subsystems

$$\sum_i, \quad i \in M. \tag{45}$$

(2) Compute matrices and other variables such as $A_{ii}, B_{1i}, B_{2i}, B_{3i}, C_i(\theta_i), x_i(t), y_i(t), u_{\theta_i}$.

(3) Use linear matrix inequality tools from MATLAB 2009 to find one symmetric matrix X_i such that inequality (16) holds.

(4) Find one appropriate state feedback controller $u_i(t)$ as in (43).

(5) Merge the plug and play idea during the above process to verify all M inequalities (16).

(6) Construct the original control input as

$$u(t) = \left(u_1(t) \;\; u_2(t) \;\; \cdots \;\; u_M(t)\right). \tag{46}$$

5. Simulation

In this simulation part, we give one aircraft flutter model parameter identification example to confirm the efficiency of our plug and play robust distributed control strategy.

In the simulation example, we use one flutter mathematical model from [20]. In simulation environment, the input signal is the excited signal chosen by user, output is measured from the point set collected by the accelerometer, the number of sampled points is set $N = 4096$, and sample instant is 1 second. The output and input of the 4096 sampled data are divided into 4 equal data blocks; each data block contains 1024 sample data. The true model matrices are listed as follows.

$$A = \begin{bmatrix} 0 & 1 & 0 \\ -0.3 & 0.4 & -0.2 \\ -0.1 & 0.2 & 0.4 \end{bmatrix},$$

$$B_1 = \begin{bmatrix} 0.8 & 0.17 & 1.09 \end{bmatrix}^T,$$

$$C = \begin{bmatrix} 2 & 1 & 0 \\ 0 & 0 & 0 \end{bmatrix},$$

$$B_2 = \begin{bmatrix} 0 \\ 1 \end{bmatrix}, \tag{47}$$

$$\theta_0 = \begin{bmatrix} 0.5 \\ 0.5 \\ -0.5 \end{bmatrix},$$

$$R = I,$$

$$\gamma = 2,$$

$$\phi_w = 1.$$

U_θ is one guaranteed ellipsoidal parameter uncertain set with probability 95%. To validate the identification result of matrix C, Figure 1 shows the approximation degree between the true system and the identified system. As those two curves approximate to each other very closely, the problem of one $H\infty$ norm with respect to one transfer function less than one given upper bound is equivalent to the problem of designing one robust state feedback controller. From Theorem 3, we see that the above problem is also equivalent to the following

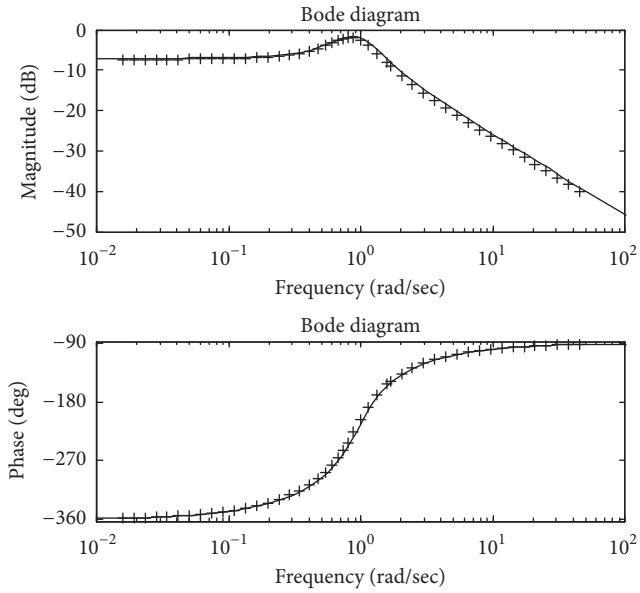

Figure 1: Bode plots compared between the true system and the identified system.

feasible problem with respect to linear matrix inequality. Find one symmetric matrix $X_i \in R^{n_i \times n_i}$, $\tau \in R$, $\tau > 0$ such that

$$\begin{bmatrix} \tau R_i & X_i & \tau R_i \theta_{i0} \\ X_i & -M_i & 0 \\ \tau \theta_{i0}^T R_i & 0 & 1 + \left(\tau \theta_{i0}^T R_i \theta_{i0} - 1\right) \end{bmatrix} > 0, \tag{48}$$

$$M_i = A_{ii} X_i + X_i A_{ii}^T - \gamma^2 \left(B_{1i} B_{1i}^T - B_{3i} B_{3i}^T\right).$$

The above linear matrix inequality can be solved by linear matrix inequality tools from MATLAB 2009; then this robust distributed sate feedback control $K_i = -(B_{2i}^T B_{2i}) B_{1i}^T = -B_{1i}^T$ can achieve the robust stability and performance requirement. To reduce the computational complexity, the plug and play idea is applied in the whole design process.

6. Conclusion

In this short paper, we propose one plug and play robust distributed state feedback control for one kind of continuous linear invariant systems with ellipsoidal parametric uncertain set. After partitioning the original system into some subsystems, we derive one necessary and sufficient condition under which the robust distributed controller exists by using the linear matrix inequality tool for each subsystem. Then we apply the new plug and play idea into the robust control scheme to propose one method-plug and play robust distributed control method. But all the derivations are based on the assumption that the unknown parameter is known in one ellipsoidal set. So when any knowledge of unknown parameter in the state space matrix form is not known a priori, we should apply the input-output data to design one system identification experiment and obtain its parameter estimation. Then the next topic is how to apply the system identification concept into our control strategy.

Competing Interests

The authors declare that there are no competing interests regarding the publication of this paper.

References

[1] S. Riverso, M. Farina, and G. Ferrari-Trecate, "Plug-and-play decentralized model predictive control for linear systems," *IEEE Transactions on Automatic Control*, vol. 58, no. 10, pp. 2608–2614, 2013.

[2] S. Riverso, M. Farina, and G. Ferrari-Trecate, "Plug-and-play model predictive control based on robust control invariant sets," *Automatica*, vol. 50, no. 8, pp. 2179–2186, 2014.

[3] S. Riverso and G. Ferrari-Trecate, "Tube-based distributed control of linear constrained systems," *Automatica*, vol. 48, no. 11, pp. 2860–2865, 2012.

[4] S. Riverso and G. Ferrari-Trecate, "Plug-and-play distributed model predictive control with coupling attenuation," *Optimal Control Applications and Methods*, vol. 36, no. 3, pp. 292–305, 2015.

[5] J. Lavaei and A. G. Aghdam, "Control of continuous time LTI systems by means of structurally constrained controllers," *Automatica*, vol. 44, no. 1, pp. 141–148, 2008.

[6] J. K. Scott, R. Findeisen, R. D. Braatz, and D. M. Raimondo, "Input design for guaranteed fault diagnosis using zonotopes," *Automatica*, vol. 50, no. 6, pp. 1580–1589, 2014.

[7] P. Trodden and A. Richards, "Distributed model predictive control of linear systems with persistent disturbances," *International Journal of Control*, vol. 83, no. 8, pp. 1653–1663, 2010.

[8] R. Scattolini, "Architectures for distributed and hierarchical Model Predictive Control—a review," *Journal of Process Control*, vol. 19, no. 5, pp. 723–731, 2009.

[9] A. Ferramosca, D. Limon, I. Alvarado, and E. F. Camacho, "Cooperative distributed MPC for tracking," *Automatica*, vol. 49, no. 4, pp. 906–914, 2013.

[10] D. M. Raimondo, L. Magni, and R. Scattolini, "Decentralized MPC of nonlinear systems: an input-to-state stability approach," *International Journal of Robust and Nonlinear Control*, vol. 17, no. 5, pp. 1651–1667, 2007.

[11] M. C. Campi and P. R. Kumar, "Learning dynamical systems in a stationary environment," *Systems & Control Letters*, vol. 34, no. 3, pp. 125–132, 1998.

[12] S. Silven, "A neural network based optimization algorithm for multiple targets tracking," *IEEE Journal of Oceanic Engineering*, vol. 37, no. 4, pp. 56–62, 2010.

[13] F. Giulietti, "Dynamics and control issues of formation flight," *Aerospace Science and Technology*, vol. 36, no. 9, pp. 65–71, 2005.

[14] Y. Ben-Asher, S. Feldman, P. Gurfil, and M. Feldman, "Distributed decision and control for cooperative UAVs using ad hoc communication," *IEEE Transactions on Control Systems Technology*, vol. 16, no. 3, pp. 511–516, 2008.

[15] W.-H. Chen, "Nonlinear disturbance observer-enhanced dynamic inversion control of missiles," *Journal of Guidance, Control, and Dynamics*, vol. 26, no. 1, pp. 161–166, 2003.

[16] F. Giulietti, "Dynamics and control of different aircraft formation structures," *Aeronautical*, vol. 108, no. 10, pp. 117–124, 2004.

[17] J. H. Wang, "Fast gradient algorithm in subspace predictive control under fault estimation," *Journal of Shanghai Jiao Tong University*, vol. 47, no. 7, pp. 1015–1021, 2013.

[18] Q. Lan, S. Ding, S. Li, and C. Zhang, "Global decentralised stabilisation for a class of uncertain large-scale feedforward nonlinear systems," *International Journal of Control*, vol. 87, no. 6, pp. 1282–1296, 2014.

[19] Q. Lan, C. Zhang, and S. Li, "Global decentralized stabilization for a class of large-scale feedforward nonlinear systems," in *Proceedings of the American Control Conference (ACC '15)*, pp. 645–650, July 2015.

[20] A. Dankers, P. M. J. Van den Hof, X. Bombois, and P. S. Heuberger, "Identification of dynamic models in complex networks with prediction error methods: predictor input selection," *IEEE Transactions of Automatic Control*, vol. 61, no. 4, pp. 937–952, 2016.

Hindawi Publishing Corporation
Journal of Control Science and Engineering
Volume 2016, Article ID 2625497, 9 pages
http://dx.doi.org/10.1155/2016/2625497

Research Article

On Couple-Group Consensus of Multiagent Networks with Communication and Input Time Delays

Liang-hao Ji and Xin-yue Zhao

Chongqing Key Laboratory of Computational Intelligence, Chongqing University of Posts and Telecommunications, Chongqing 400065, China

Correspondence should be addressed to Liang-hao Ji; lianghao.ji@gmail.com

Received 19 August 2016; Accepted 31 October 2016

Academic Editor: Guanghui Wen

This paper investigated the couple-group consensus problems of the multiagent networks with the influence of communication and input time delays. Based on the frequency-domain theory, some algebraic criteria are addressed analytically. From the results, it is found that the input time delays and the coupling strengths between agents of the systems play a crucial role in reaching group consensus. The convergence of the system is independent of the communication delays, but it will affect the convergence rate of the system. Finally, several simulated examples are provided to verify the validity and correctness of our theoretical results.

1. Introduction

Over the past few years, increasing attention has been paid to the investigation of distributed cooperative control of multiagent networks due to its broad application in many areas, such as distributed sensor networks [1], congestion control in networks [2, 3], and flocking [4, 5]. As a fundamental problem of cooperative control, consensus problem of multiagent networks has become the focus of researchers in many fields. Consensus of multiagent networks usually means a group of agents converging to a consistent state through sharing local communication with their neighbors. Recently, lots of works about consensus have been reported [6–11].

Group consensus is an extended consensus problem, which means that the agents in a network reach more than one consistent state. Namely, some agents in one subgroup can reach a consistent state while there is no consensus among different subgroups of the whole networks.

Recently, many reports about group consensus have been listed, such as, for second-order multiagent networks with time delays, the group consensus problem investigated in [12]. Based on the semitensor product of matrices and the vertex coloring of graphs, the group consensus problem of the multiagent network is discussed [13]. Yi et al. [14] discussed the group consensus issue of linearly coupled multiagent networks, where the relation between Laplacian and number of groups was derived. Based on some assumptions, Tan et al. [15] obtained some sufficient and necessary conditions to guarantee solvability of group consensus problems. Hu et al. [16] studied average-group consensus problems with undirected networks by designing a novel hybrid protocol. In [17], Zhao et al. discussed couple-group consensus problems of second-order multiagent networks with fixed and stochastic switching topologies and provided a sufficient and necessary condition for the mean-square couple-group consensus. In [18], conditions for reaching group consensus with centralized and decentralized event-triggered control were illustrated, respectively. Moreover, pinning control strategies have been introduced for reducing the cost of network control in [19–23]. In [24, 25], Yu and Wang addressed group consensus problems of networks with directed graphs and strongly connected and balanced topology. Furthermore, in [26, 27], Yu and Wang discussed the group consensus problem with communication delays and switching topologies. For the networks with strongly connected and balanced topology, Wang and Uchida [28] investigated the group consensus of multiagent networks with communication delays. Based on the networks with bipartite topology, group consensus of first-order multiagent networks with and without time delays were investigated in [29], respectively. Du et al. [30]

further extended the conclusions in [29] and obtained an upper bound of time delay. Ji et al. [31] considered the group consensus of undirected and connected bipartite graphs, respectively, and proposed a sufficient condition for group consensus. In [32], Lianghao and Xinyue discussed the group consensus problem for second-order multiagent networks with the influence of input and communication time delays.

It is worth noting that the related research works mentioned above either only consider the influence of communication delays or simply discuss the special case that the communication delay is equal to the input delay, such as in [24–27, 29–31]. Meanwhile, most of the works are based on the special topologies [16, 24, 25, 28–31], for instance, undirected, strongly connected, and balanced topologies. As we know, time delays objectively exist in the networks and are usually different. Meanwhile, time delays can degrade or even destroy the stable performance of the complex systems. Inspired by the related works, this paper focuses on discussing the couple-group consensus of multiagent networks under the influence of time delays. The main contributions are listed as follows: firstly, this paper investigated the influence of different time delays for the multiagent networks with the asymmetric topology. By using frequency-domain theory, the criteria which can guarantee the achievement of couple-group consensus are proposed. Secondly, either the algebraic criteria we obtained are less conservative than the findings in related works or the relevant research works can be seen as the special cases of our works.

The rest of the paper is organized as follows. In Section 2, some relevant concepts about graph theory and model formulation are reviewed. In Section 3, the problems of group consensus for multiagent networks with multiple time delays are analyzed. Several numerical experiments are illustrated in Section 4. Finally, some conclusions and future work are drawn.

2. Preliminaries

Based on graph theory, an agent and the information interaction between them in a multiagent networks can be described by $G = (V, E, A)$, where $V = \{v_1, v_2, \ldots, v_N\}$ is node set, $\mathbb{N} = \{1, 2, \ldots, N\}$ denotes node index set, $E \subseteq V \times V$ is the edge set, and $A = \{a_{ij}\} \in \mathbb{R}^{N\times N}$ is the weighted adjacency matrix. The neighbor of node v_i is denoted by $N_i = \{v_j \in V : (v_i, v_j) \in E\}$. For convenience, suppose $a_{ij} > 0$ if $v_j \in N_i$ and $a_{ii} = 0$ for $\forall i \in \mathbb{N}$. The Laplacian matrix of G is denoted by $L = D - A$, where $D = \mathrm{diag}\{d_i,\ i \in \mathbb{N}\}$ and $d_i = \sum_{v_j \in N_i} a_{ij}$.

For first-order multiagent networks, the dynamics of the system can be listed as

$$\dot{x}_i(t) = u_i(t), \tag{1}$$

where $x_i(t), u_i(t) \in \mathbb{R}^k$ denotes the position state and control input of the agent i at time t, respectively. For simplicity, we just only consider the case $x_i(t), u_i(t) \in \mathbb{R}$. When $k > 1$, it is easy to promote the results by applying the Kronecker product.

Next, some related definitions and lemmas will be listed firstly.

Definition 1. For $\forall i, j \in \mathbb{N}$, the first-order multiagent networks (1) can be said to achieve consensus asymptotically if and only if $\lim_{t\to\infty} \|x_i(t) - x_j(t)\| = 0$.

Definition 2 (see [33]). For a bipartite graph $g = (V, E)$ which has the following properties, where V and E denote its vertex and edge sets:

(i) $V_1 \cup V_2 = V$ and $V_1 \cap V_2 = \varnothing$, where V_1 and V_2 are the two vertex subsets;

(ii) $\forall e = (x, y) \in E$, where $x \in V_1$ and $y \in V_2$.

Assumes the topology $G = (V, E, A)$ of order $n + m$ $(n, m > 1)$ consists of two subgroups, $G_1 = (V_1, E_1, A_1)$ and $G_2 = (V_2, E_2, A_2)$, where $V_1 = \{v_1, v_2, \ldots, v_n\}$ and $V_2 = \{v_{n+1}, v_{n+2}, \ldots, v_{n+m}\}$. Then, the set of finite index is defined by $L_1 = \{1, 2, \ldots, n\}$ and $L_2 = \{n + 1, n + 2, \ldots, n + m\}$. In these two subgroups, $N_{1i} = \{v_j \in V_1 : (v_i, v_j) \in E\}$ and $N_{2i} = \{v_j \in V_2 : (v_i, v_j) \in E\}$ represent the neighbor set of node v_i, respectively. Then, we know that $V = V_1 \cup V_2$ and $N_i = N_{1i} \cup N_{2i}$. For convenience, in this paper we only consider the case of two-group consensus problem.

Definition 3. Protocol (1) is said to reach a couple-group consensus asymptotically if the states of agents satisfy

(i) $\lim_{t\to\infty} \|x_i(t) - x_j(t)\| = 0$, $\forall i, j \in L_1$;

(ii) $\lim_{t\to\infty} \|x_i(t) - x_j(t)\| = 0$, $\forall i, j \in L_2$.

Lemma 4 (see [29]). *For a connected bipartite graph G, the rank of $D + A$ is $n - 1$, where D and A are the degree matrix and the adjacency matrix, respectively.*

Lemma 5 (see [34]). *If the graph G contains a globally reachable node, 0 is the simple eigenvalue of its Laplacian matrix.*

Lemma 6 (see [35]). *For $\forall \gamma \in [0, 1)$, if $\omega \in \mathbb{R}$, convex hull $\gamma Co(0 \cup \{E_i(j\omega),\ i \in \mathbb{N}\})$ will not enclose the point $(-1, j0)$, where $E_i(j\omega) = \pi/2T \times e^{-j\omega T}/j\omega$ and T denotes time delay.*

Lemma 7 (see [36]). *For $\omega \in \mathbb{R}$, convex hull $\gamma Co(0 \cup \{E_i(j\omega),\ i \in \mathbb{N}\})$ contains the set of $\bigcup_{i\in\mathbb{N}} G_i$.*

3. Couple-Group Consensus of Multiagent Networks with Multiple Delays

In this section, we illustrate group consensus of multiagent networks with multiple time delays.

3.1. Couple-Group Consensus of Delayed Multiagent Networks with Bipartite Topologies. In [29], group consensus problems

of the multiagent networks with protocol (2) and (3) were discussed and some sufficient conditions which can guarantee the achievement of group consensus were proposed as well:

$$u_i(t) = -\sum_{v_j \in N_i} a_{ij}\left(x_j(t) + x_i(t)\right), \quad i \in \mathbb{N}, \tag{2}$$

$$u_i(t) = -\sum_{v_j \in N_i} a_{ij}\left(x_j(t-\tau) + x_i(t-\tau)\right), \quad i \in \mathbb{N}, \tag{3}$$

where τ denotes the time delay.

Motivated by the related research works, we will discuss the group consensus problem of multiagent networks with different time delays. Consider the following protocol listed as

$$u_i(t) = -\sum_{v_j \in N_i} a_{ij}\left(x_j\left(t - T_{ij}\right) + x_i\left(t - T_i\right)\right), \quad i \in \mathbb{N}, \tag{4}$$

where T_{ij} denotes the communication delay between v_i and v_j and T_i denotes the input delay of v_i. With (4), the closed-loop form of the networks (1) is

$$\dot{x}_i(t) = -\sum_{v_j \in N_i} a_{ij}\left(x_j\left(t - T_{ij}\right) + x_i\left(t - T_i\right)\right), \quad i \in \mathbb{N}. \tag{5}$$

Theorem 8. *$\forall i \in \mathbb{N}$, if $\sum_{v_j \in N_i} a_{ij}T_i < \pi/4$ can be satisfied, system (5) with bipartite topology will achieve couple-group consensus asymptotically.*

Proof. Taking the Laplace transform to (5), we can obtain the characteristic equation as $\det(sI + De^{-sT_{ij}} + Ae^{-sT_i}) = 0$, where I denotes unit matrix, D denotes the degree matrix, and A denotes adjacency matrix. Define $F(s) = \det(sI + De^{-sT_{ij}} + Ae^{-sT_i})$, by the general *Nyquist* stability criterion, it is easy to know that the group consensus of the networks (5) can be achieved if and only if all zeros of $F(s)$ have negative real parts or $F(s)$ has a simple zero at $s = 0$. Therefore, the following two cases are considered, respectively:

(i) When $s = 0$, $F(s) = \det(D + A)$, by Lemma 4, we know that $F(s)$ contains a single zero at $s = 0$.

(ii) When $s \neq 0$, define $P(s) = F(s)/s$, $G(s) = (De^{-sT_{ij}} + Ae^{-sT_i})/s$, then $P(s) = \det(I + G(s))$. It is easy to check that the discussion about the zeros of $F(s)$ is equal to the zeros of $P(s)$. So if all zeros of $P(s)$ have negative real parts, networks (5) will reach group consensus.

Define $s = j\omega$; by the general *Nyquist* stability criterion, it follows that all zeros of $F(s)$ have negative real parts for $\forall \omega \in \mathbb{R}$, if the *Nyquist* curve of the eigenvalue of $G(j\omega)$ does not enclose the point $(-1, j0)$. By the *Gerschgorin* disk theorem, the equivalent of $G(j\omega)$ satisfies

$$\lambda\left(G(j\omega)\right) \in \bigcup_{i \in \mathbb{N}} G_i, \tag{6}$$

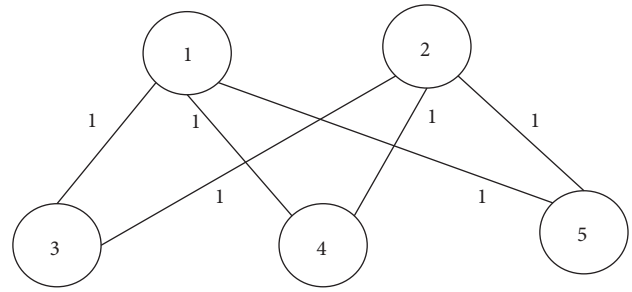

Figure 1: Topology of the multiagent networks (5).

$$G_i = \left\{\zeta : \zeta \in C, \left|\zeta - \sum_{v_j \in N_i} a_{ij}\frac{e^{-j\omega T_i}}{j\omega}\right| \leq \left|\sum_{v_j \in N_i} a_{ij}\frac{e^{-j\omega T_i}}{j\omega}\right|\right\}. \tag{7}$$

From (7), we know that the center of G_i is $G_{i0}(j\omega) = \sum_{v_j \in N_i} a_{ij}(e^{-j\omega T_i}/j\omega)$. Suppose the intersection point W_i connects the center of the disk and the origin point of complex plane. The track of point W_i is $W_i(j\omega) = 2\sum_{v_j \in N_i} a_{ij}(e^{-j\omega T_i}/j\omega)$. Based on Lemma 6, as $W_i(j\omega) = \gamma_i \times E_i(j\omega)$ and $\gamma_i < 1$, we know that $\sum_{v_j \in N_i} a_{ij}T_i < \pi/4$ holds. When $\gamma = \max\{\gamma_i, i \in \mathbb{N}\}$ and $\gamma < 1$, for $\forall i \in \mathbb{N}$, the next equation holds $\gamma \mathrm{Co}(0 \cup \{E_i(j\omega)\}) \supseteq \gamma_i(0 \cup \{E_i(j\omega)\}) = \mathrm{Co}(0 \cup \{W_i(j\omega)\})$. By Lemma 6, noting that $(-1, j0) \notin \gamma \mathrm{Co}(0 \cup \{E_i(j\omega),\ i \in \mathbb{N}\})$ and based on Lemma 7, as $\mathrm{Co}(0 \cup \{W_i(j\omega),\ i \in \mathbb{N}\}) \supseteq \bigcup_{i \in \mathbb{N}} G_i$, then $(-1, j0) \notin \bigcup_{i \in \mathbb{N}} G_i$ holds. Thus, $\lambda(G(j\omega))$ does not enclose the point $(-1, j0)$. That is to say, all zeros of $P(s)$ have negative real parts.

The proof of Theorem 8 is completed. □

Remark 9. When $T_i = T_{ij} = \tau$, that is, all agents have same communication delays and input delays, it is obvious that protocols (3) and (4) are the same. That is to say, protocol (3) is a special form of (4). In [29–31], the cases where the input time delay is identical are discussed respectively. Whereas the time delays of the system including input time delay and communication time delays exist objectively and are usually different from each other, protocol (4) is more general.

Remark 10. Compared with the result in Theorem 8, it is known that the upper bound of time delays derived in [29] is relatively too broad. Meanwhile, according to the results in Theorem 8, it is shown that the group convergence of the networks is related to the input delays and adjacent weights among agents and independent of communication delays.

3.2. Couple-Group Consensus of First-Order Delayed Networks with the Topology Containing a Globally Reachable Node. In [24–27], based on the in-degree balance assumptions (A1) and control algorithm (8), the average-group consensus of multiagent networks with undirected, strongly connected, and balanced topology is explored, respectively.

(A1): $\sum_{j=n+1}^{n+m} a_{ij} = 0, \forall i \in L_1$, and $\sum_{j=1}^{n} a_{ij} = 0, \forall i \in L_2$:

$$u_i(t) = \begin{cases} \sum_{V_j \in N_{1i}} a_{ij}\left(x_j(t) - x_i(t)\right) + \sum_{V_j \in N_{2i}} a_{ij} x_j(t), & \forall i \in L_1 \\ \sum_{V_j \in N_{2i}} a_{ij}\left(x_j(t) - x_i(t)\right) + \sum_{V_j \in N_{1i}} a_{ij} x_j(t), & \forall i \in L_2. \end{cases} \quad (8)$$

Based on (8), Ji et al. [31] addressed multiagent networks (9) with undirected topology and delays:

$$u_i(t) = \begin{cases} \sum_{V_j \in N_{1i}} a_{ij}\left(x_j(t-\tau) - x_i(t-\tau)\right) + \sum_{V_j \in N_{2i}} a_{ij} x_j(t-\tau), & \forall i \in L_1 \\ \sum_{V_j \in N_{2i}} a_{ij}\left(x_j(t-\tau) - x_i(t-\tau)\right) + \sum_{V_j \in N_{1i}} a_{ij} x_j(t-\tau), & \forall i \in L_2, \end{cases} \quad (9)$$

where τ denotes time delay.

Inspired by related research work, group consensus problem of multiagent networks with multiple delays will be discussed. Considering different communication and input delays, group consensus protocol (10) is proposed as

$$u_i(t) = \begin{cases} \sum_{V_j \in N_{1i}} a_{ij}\left(x_j\left(t - T_{ij}\right) - x_i\left(t - T_i\right)\right) + \sum_{V_j \in N_{2i}} a_{ij} x_j\left(t - T_{ij}\right), & \forall i \in L_1 \\ \sum_{V_j \in N_{2i}} a_{ij}\left(x_j\left(t - T_{ij}\right) - x_i\left(t - T_i\right)\right) + \sum_{V_j \in N_{1i}} a_{ij} x_j\left(t - T_{ij}\right). & \forall i \in L_2, \end{cases} \quad (10)$$

With protocol (10), the closed-loop form of the networks (1) is

$$\dot{x}_i(t) = \begin{cases} \sum_{V_j \in N_{1i}} a_{ij}\left(x_j\left(t - T_{ij}\right) - x_i\left(t - T_i\right)\right) + \sum_{V_j \in N_{2i}} a_{ij} x_j\left(t - T_{ij}\right), & \forall i \in L_1 \\ \sum_{V_j \in N_{2i}} a_{ij}\left(x_j\left(t - T_{ij}\right) - x_i\left(t - T_i\right)\right) + \sum_{V_j \in N_{1i}} a_{ij} x_j\left(t - T_{ij}\right). & \forall i \in L_2. \end{cases} \quad (11)$$

Theorem 11. *Based on the in-degree balance conditions (A1), system (11) with the topology containing a globally reachable node can achieve couple-group consensus asymptotically if* $\sum_{k=1,k\neq i}^{m+n} a_{ik} T_i < \pi/4$, $i = 1, 2, \ldots, n+m$, *holds.*

Proof. Taking the Laplace transform to (11), its characteristic equation can be easily obtained as $\det(sI + L(s)) = 0$, where

$$L(s) = \left(l_{ij}(s)\right) = \begin{cases} -a_{ij} e^{-sT_{ij}}, & j \neq i \\ \sum_{k=1,k\neq i}^{m+n} a_{ik} e^{-sT_i}, & j = i. \end{cases} \quad (12)$$

The remainder of the proof process is similar to the proof of Theorem 8, but here we omit it due to the space limitation. □

Remark 12. When $T_i = T_{ij} = \tau$, protocols (9) and (10) are identical. Therefore, the related works in [24–27] can be seen as the special cases of Theorem 11.

Remark 13. From the results in Theorems 8 and 11, it is shown that the achievement of the group consensus of the systems is determined by the input time delays and the coupling weight among the agents. Meanwhile, the node cannot tolerate bigger input delays if it owns a bigger coupling weight.

Corollary 14. *When* $T_i = \tau$, *system (11) with the topology containing a globally reachable node can achieve couple-group consensus asymptotically if assumption (A1) is satisfied and* $\tau < \pi/4d$ *holds, where* $d = \max\{\sum_{k=1,k\neq i}^{m+n} a_{ik}\}$, $i = 1, 2, \ldots, m+n$.

Remark 15. The result in Corollary 14 is a special case of Theorem 11, and it is consistent with the relevant conclusions

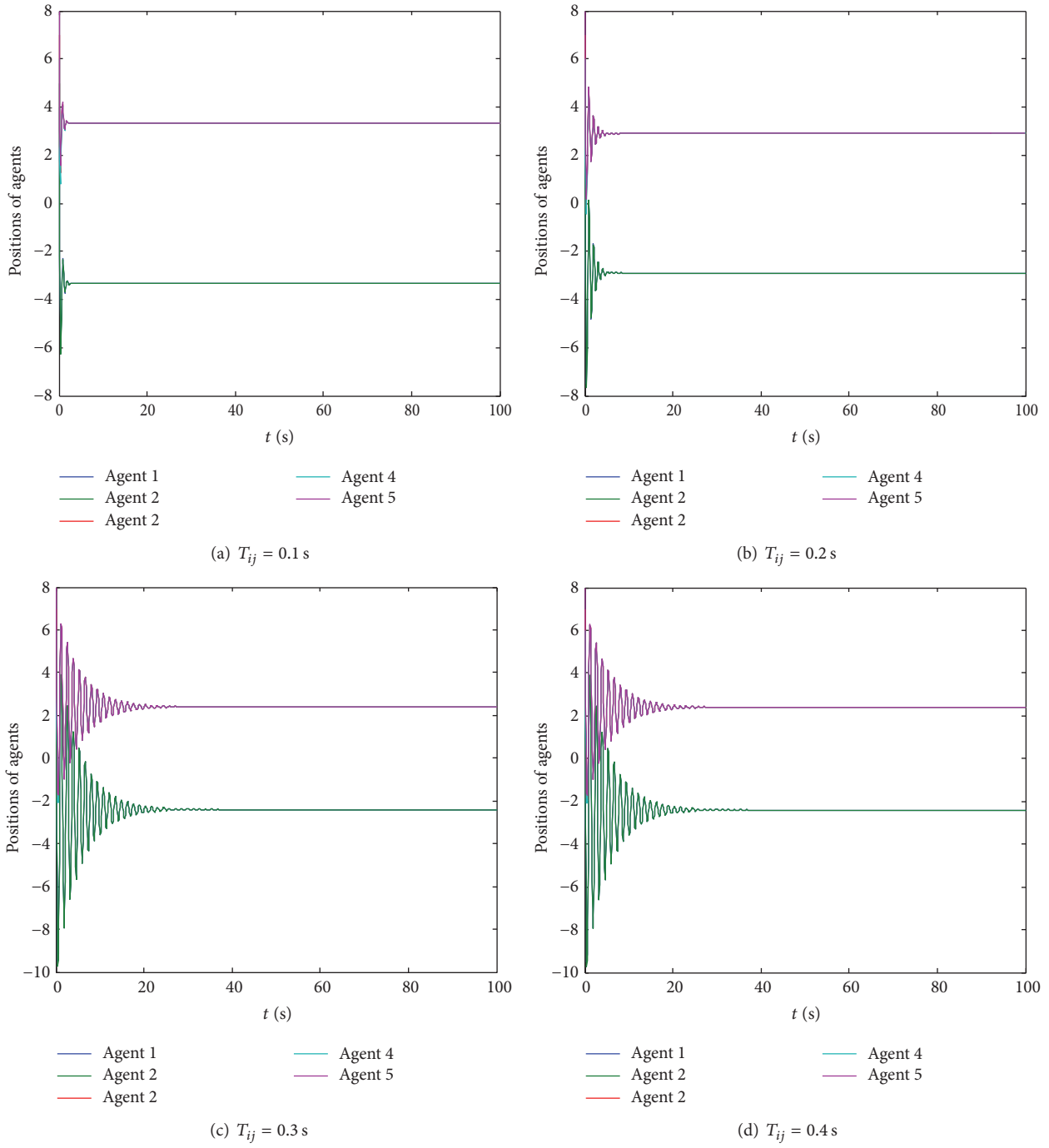

Figure 2: State trajectories of the agents in the networks (5) with delays.

in [31]. Meanwhile, it is shown that the tolerant upper bound of input time delay in the system is determined by the node who owns the max coupling weight.

4. Simulation Examples

In this section, some simulation examples will be given to show the effectiveness and correctness of our findings.

Experiment 1. Suppose the topology of the networks (5) is shown as Figure 1. In Figure 1, nodes v_1, v_2, v_3, v_4, and v_5 belong to the two different subgroups, respectively. In the experiment, initial states of agents are generated from 0 to 10 randomly and the input delays of agents are set as follows: $T_1 = 0.2$ s, $T_2 = 0.2$ s, and $T_3 = T_4 = T_5 = 0.1$ s. It is easy to verify that all input delays satisfy the conditions in Theorem 8. Meanwhile, for simplicity, we only consider the case that the communication time delays among the agents are same and

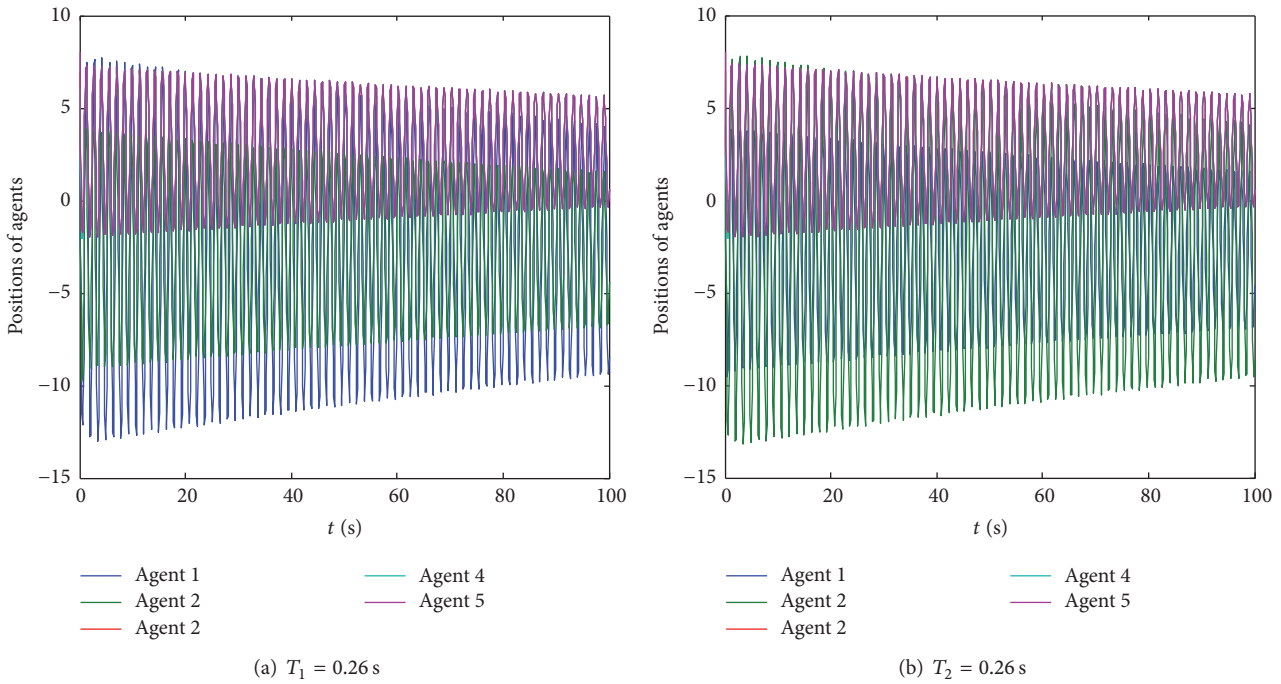

(a) $T_1 = 0.26$ s (b) $T_2 = 0.26$ s

FIGURE 3: State trajectories of the agents in the networks (5) with diverse input delays when $T_{ij} = 0.1$ s.

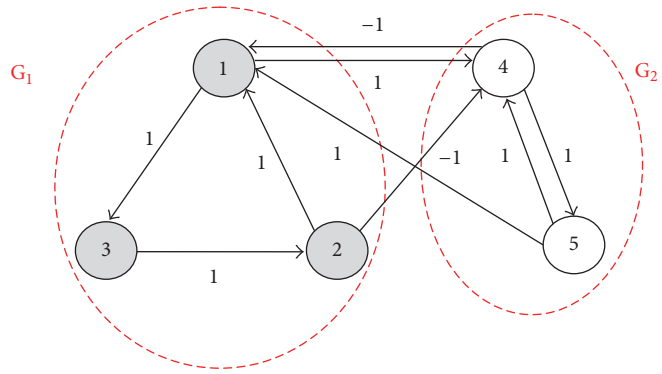

FIGURE 4: The topology of the multiagent networks (11).

set it as $T_{ij} = 0.1, 0.2, 0.3, 0.4$ s, $i, j = 1, 2, 3, 4, 5$, respectively. The trajectories of the agents are shown in Figure 2 for these four cases. According to the results, it is shown that networks (5) can achieve couple-group consensus asymptotically, respectively. At the same time, by comparing the trajectories with different communication delays, it is clear that communication time delays will not affect convergence properties of the networks but can affect the convergence rate of the system. Furthermore, with the decrease of the communication delays, the faster systems will convergence.

From Figure 1, by Theorem 8, the allowed input delays of ν_1 and ν_2 should satisfy $T_i < \pi/12 = 0.26$ s, which means that group consensus of the networks can be achieved. Next, the following two cases are considered and the state trajectories of the networks (5) are shown in Figure 3:

(i) Reset $T_1 = 0.26$ s; input delays of other nodes are not changed.

(ii) Reset $T_2 = 0.26$ s; input delays of other nodes are not changed.

From the results in Figure 3, it is illustrated that networks (5) will not reach couple-group group consensus in these three cases. Therefore, the results of simulation experiments further verity the correctness and effectiveness of the algebraic criteria in Theorem 8.

From Figure 1, it is easy to get its eigenvalues are $0, -2.0, -2.0, -3.0, -5.0$, respectively. Based on the bound of time delays $0 < \tau < (-\pi/2\lambda_m)$ s presented in [29], the bound of time delays presented in [29] has $\tau \in (0, 0.314)$ s. Compared with the results in Figure 3, the upper bound of the time delay is too broader.

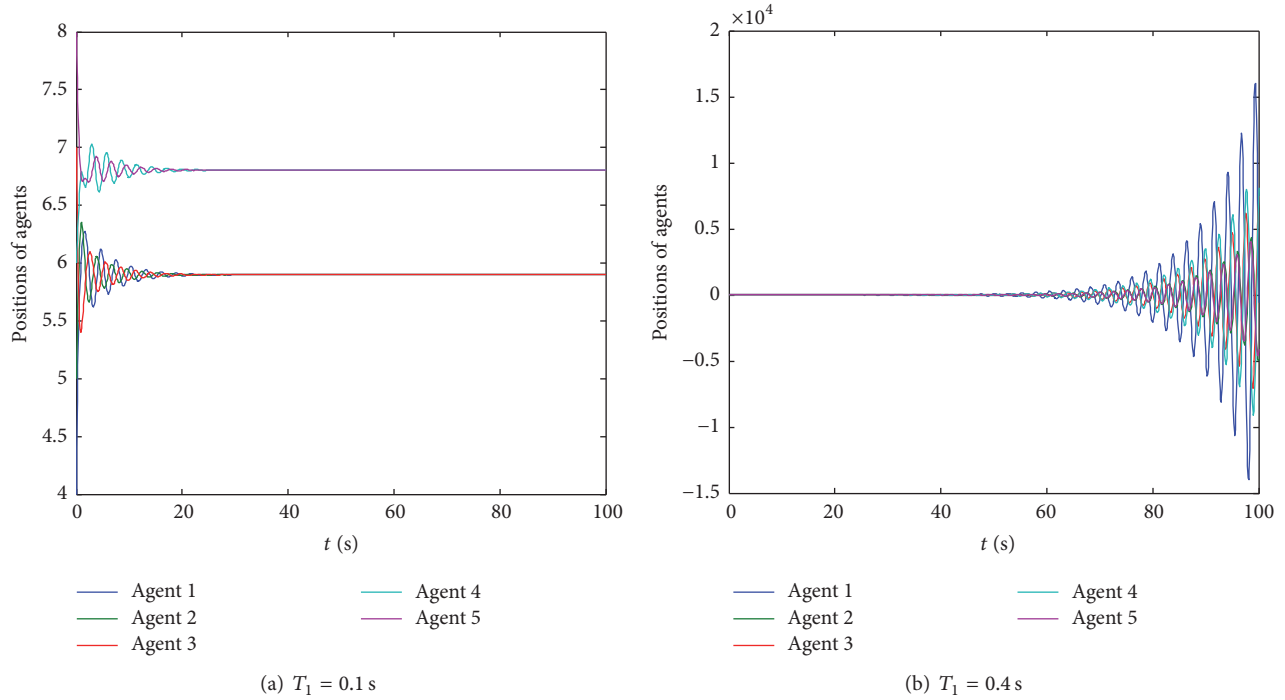

(a) $T_1 = 0.1$ s (b) $T_1 = 0.4$ s

Figure 5: State trajectories of the agents in the networks (11).

Experiment 2. Given the dynamical networks (11) with 5 nodes, the topology and connection weights between nodes are shown in Figure 4. Agents v_1, v_2, and v_3 are in a group while agents v_4 and v_5 are in another group. Meanwhile, the topology of multiagent networks contains a globally reachable node and satisfies the in-degree balance assumption (A1). Similarly, the initial states of agents are generated from 0 to 10 randomly, and communication delay of all agents is set as $T_{ij} = 0.3$ s; input delays of the agents are $T_1 = 0.1$ s, $T_2 = 0.7$ s, $T_3 = 0.2$ s, $T_4 = 0.5$ s, and $T_5 = 0.2$ s. It is easy to verify the conditions in Theorem 11 can be satisfied. The state trajectories of the agents in networks (11) are shown in Figure 5(a); it is clear that the networks can achieve couple-group consensus.

Next, the upper bound of time delay presented in Theorem 11 will be checked. To node v_1, it has $\widetilde{d}_1 = 2$ according the topology shown in Figure 4. By Theorem 11, the input delay of node v_1 should satisfy $T_1 < \pi/8$ s. If set $T_1 = 0.4$ s, obviously, the condition in Theorem 11 is not satisfied. In the case of communication and input delays of other nodes keeping unchanged, described in Figure 5(b), couple-group consensus will not be achieved.

Experiment 3. Based on the Experiment 2, the validity of Corollary 14 will be verified here. From Corollary 14, we can get $\tau < \pi/8$ s. So the following two cases are considered: $\tau = 0.35$ s and $\tau = 0.4$ s. The trajectories of the agents are shown in Figure 6, respectively. The results illustrate that the couple-group consensus of the system can be achieved if the conditions in Corollary 14 are satisfied.

5. Conclusion

This paper investigated the couple-group consensus problem of multiagent networks with time delays. By applying the theory of frequency-domain, some criteria are derived which can guarantee the realization of group consensus. Meanwhile, the upper bounds of input time delays that the systems can be tolerant are proposed analytically as well. From the results, it is shown that both the input delays and the coupling weights between the agents play an important part in the achievement of group consensus. However, communication delays just only affect the convergence rate of networks. Thus, convergence performance of the system can be improved by reducing the communication time delays.

Competing Interests

All authors declare they have no competing interests.

Acknowledgments

This work was supported by the Natural Science Foundation Project of Chongqing Science and Technology Commission under Grant no. cstc2014jcyjA40047 and in part by the Scientific and Technological Research Program of Chongqing Municipal Education Commission under Grant no. KJ1400403 and in part awarded by State Scholarship Fund of China Scholarship Council.

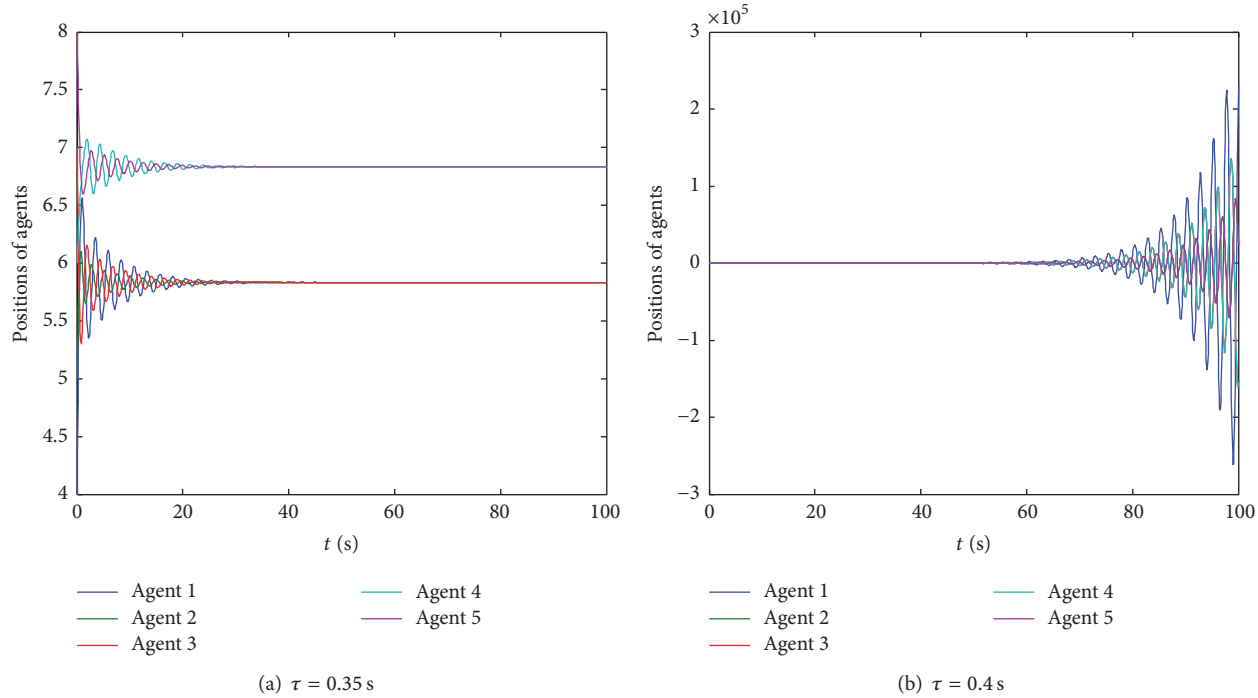

(a) $\tau = 0.35$ s (b) $\tau = 0.4$ s

FIGURE 6: State trajectories of the agents in the networks (11) when $T_i = \tau$.

References

[1] H. Shi, L. Wang, and T. Chu, "Swarming behavior of multi-agent systems," *Journal of Control Theory and Applications*, vol. 2, no. 4, pp. 313–318, 2004.

[2] A. Ghaffari, "Congestion control mechanisms in wireless sensor networks: a survey," *Journal of Network and Computer Applications*, vol. 52, pp. 101–115, 2015.

[3] C. Sergiou, V. Vassiliou, and A. Paphitis, "Hierarchical Tree Alternative Path (HTAP) algorithm for congestion control in wireless sensor networks," *Ad Hoc Networks*, vol. 11, no. 1, pp. 257–272, 2013.

[4] Z. C. Li and X. P. Xue, "Cucker-Smale flocking under rooted leadership with free-will agents," *Physica A. Statistical Mechanics and Its Applications*, vol. 410, pp. 205–217, 2014.

[5] S. Martin, "Multi-agent flocking under topological interactions," *Systems & Control Letters*, vol. 69, no. 1, pp. 53–61, 2014.

[6] W. W. Yu, G. R. Chen, and M. Cao, "Some necessary and sufficient conditions for second-order consensus in multi-agent dynamical systems," *Automatica*, vol. 46, no. 6, pp. 1089–1095, 2010.

[7] X. J. Wu and H. T. Lu, "Outer synchronization of uncertain general complex delayed networks with adaptive coupling," *Neurocomputing*, vol. 82, pp. 157–166, 2012.

[8] Z. J. Tang, T. Z. Huang, J. L. Shao, and J. P. Hu, "Consensus of second-order multi-agent systems with nonuniform time-varying delays," *Neurocomputing*, vol. 115, pp. 169–177, 2012.

[9] B. Liu, X. L. Wang, H. S. Su, Y. P. Gao, and L. Wang, "Adaptive second-order consensus of multi-agent systems with heterogeneous nonlinear dynamics and time-varying delays," *Neurocomputing*, vol. 118, pp. 289–300, 2013.

[10] H. Yan, Y. Shen, H. Zhang, and H. Shi, "Decentralized event-triggered consensus control for second-order multi-agent systems," *Neurocomputing*, vol. 133, pp. 18–24, 2014.

[11] T. C. Zhang and H. Yu, "Average consensus for directed networks of multi-agent with time-varying delay," *Computer Science*, vol. 6145, pp. 723–730, 2010.

[12] D. M. Xie and L. Teng, "Seconde-order group consensus for multi-agent systems with time delays," *Neurocomputing*, vol. 153, pp. 133–139, 2015.

[13] Y. Z. Wang, C. H. Zhang, and Z. B. Liu, "A matrix approach to graph maximum stable set and coloring problems with application to multi-agent systems," *Automatica*, vol. 48, no. 7, pp. 1227–1236, 2012.

[14] J.-W. Yi, Y.-W. Wang, and J.-W. Xiao, "Reaching cluster consensus in multi-agent systems," in *Proceedings of the 2nd International Conference on Intelligent Control and Information Processing (ICICIP '11)*, pp. 569–573, Harbin, China, July 2011.

[15] C. Tan, G. P. Liu, and G. R. Duan, "Group consensus of networked multi-agent systems with directed topology," *IFAC Proceedings Volumes*, vol. 44, no. 1, pp. 8878–8893, 2011.

[16] H.-X. Hu, L. Yu, W.-A. Zhang, and H. Song, "Group consensus in multi-agent systems with hybrid protocol," *Journal of the Franklin Institute*, vol. 350, no. 3, pp. 575–597, 2013.

[17] H. Y. Zhao, J. H. Park, and Y. L. Zhang, "Couple-group consensus for second-order multi-agent systems with fixed and stochastic switching topologies," *Applied Mathematics and Computation*, vol. 232, pp. 595–605, 2014.

[18] H. W. Ma, D. R. Liu, D. Wang, F. X. Tan, and C. Li, "Centralized and decentralized event-triggered control for group consensus with fixed topology in continuous time," *Neurocomputing*, vol. 161, pp. 267–276, 2015.

[19] X. Liu and T. Chen, "Cluster synchronization in directed networks via intermittent pinning control," *IEEE Transactions on Neural Networks*, vol. 22, no. 7, pp. 1009–1020, 2011.

[20] H. Su, Z. Rong, M. Z. Q. Chen, X. Wang, G. Chen, and H. Wang, "Decentralized adaptive pinning control for cluster synchronization of complex dynamical networks," *IEEE Transactions on Cybernetics*, vol. 43, no. 1, pp. 394–399, 2013.

[21] G. Wen, W. Yu, J. Wang, D. Xu, and J. Cao, "Distributed node-to-node consensus of multi-agent systems with time-varying pinning links," *Neurocomputing*, vol. 149, pp. 1387–1395, 2015.

[22] X. F. Liao and L. H. Ji, "On pinning group consensus for dynamical multi-agent networks with general connected topology," *Neurocomputing*, vol. 135, pp. 262–267, 2014.

[23] L. Ji, Q. Liu, and X. Liao, "On reaching group consensus for linearly coupled multi-agent networks," *Information Sciences*, vol. 287, pp. 1–12, 2014.

[24] J. Y. Yu and L. Wang, "Group consensus of multi-agent systems with undirected communication graph," in *Proceedings of the Asian Control Conference*, Beijing, China, 2009.

[25] J. Yu and L. Wang, "Group consensus of multi-agent systems with directed information exchange," *International Journal of Systems Science*, vol. 43, no. 2, pp. 334–348, 2012.

[26] J. Y. Yu and L. Wang, "Output feedback stabilization of networked control systems via switched system approach," *International Journal of Control*, vol. 82, no. 9, pp. 1665–1677, 2009.

[27] J. Y. Yu and L. Wang, "Group consensus in multi-agent systems with switching topologies and communication delays," *Systems & Control Letters*, vol. 59, no. 6, pp. 340–348, 2010.

[28] M. H. Wang and K. Uchida, "Cluster Consensus of Multi-agent system with communication delay," in *Proceedings of the International Conference on Control Automation and Systems*, Gwangiu, Korea, October 2013.

[29] Q. Wang, Y. Z. Wang, and R. M. Yang, "The design and analysis of group-consensus protocol for a class of multi-agent systems," *Control and Decision*, vol. 28, no. 3, pp. 369–373, 2013.

[30] X. Y. Du, Y. Z. Wang, and Q. Wang, "Weighted group-consensus analysis of multi-agent systems with and without time-delay network," in *Proceedings of the 34th Chinese Control Conference (CCC '15)*, pp. 6900–6905, Hangzhou, China, July 2015.

[31] L.-H. Ji, X.-F. Liao, and Q. Liu, "Group consensus analysis of multi-agent systems with delays," *Acta Physica Sinica*, vol. 61, no. 22, Article ID 220202, 2012.

[32] J. Lianghao and Z. Xinyue, "Group consensus of second-order multi-agent networks with multiple time delays," in *Proceedings of the International Conference on Applied Mathematics, Simulation and Modelling (AMSM '16)*, pp. 437–441, Beijing, China, May 2016.

[33] C. Godsil and G. Royle, *Algebraic Graph Theory*, vol. 207 of *Graduate Texts in Mathematics*, Springer, New York, NY, USA, 2001.

[34] W. Ren and R. W. Beard, "Consensus seeking in multiagent systems under dynamically changing interaction topologies," *IEEE Transactions on Automatic Control*, vol. 50, no. 5, pp. 655–661, 2005.

[35] Y. Tian and H. Y. Yang, "Stability of distributed congestion control with diverse communication delays," *Intelligent Control and Automation*, vol. 2, pp. 1438–1442, 2004.

[36] H.-Y. Yang, S.-W. Tian, and S.-Y. Zhang, "Consensus of multi-agent systems with heterogeneous delays and leader-following," *Acta Electronica Sinica*, vol. 39, no. 4, pp. 872–876, 2011.